Modeling and Control of Batch Pulsed Top-spray Fluidized bed Granulation

PhD Thesis

Huolong Liu

This thesis is submitted in partial fulfillment of the requirements of De Montfort University for the award of Doctor of Philosophy

June 2014

Faculty of Health and Life Sciences

De Montfort University

Leicester

I dedicate this thesis to my grandmother

Mrs Xiuzhen Wei

Contents

Declaration

I declare that the word described in this thesis is original work undertaken by myself for the Doctor of Philosophy degree, at the Pharmacy School, Faculty of Healthy and Life Sciences, De Montfort University, Leicester, United Kingdom.

No part of the material described in this thesis has been submitted for the award of any other degree or qualification in this or any other university or college of advanced education.

Huolong Liu

Abstract

In this thesis, a thorough study of the batch top-spray fluidized bed granulation was carried out including experimental study, population balance model (PBM), computational fluid dynamic (CFD) study and control strategy development.

For the experimental study, the influence variables of pulsed frequency, binder spray rate and atomization pressure of a batch top-spray fluidized bed granulation process were studied using the Box-Behnken experimental design method. Different mathematical models were developed to predict the mean size of granules, yield, relative width of granule distribution, Hausner ratio and final granule moisture content. Validation experiments have shown the reliability and effectiveness of using the Box-Behnken experimental design method to study a fluidized bed granulation process.

The one-dimensional population balance models (ODPBMs) have been developed to model a pulsed top-spray fluidized bed granulation, linking the operating factors of the pulsed frequency, the binder spray rate, and atomization air pressure with the granule properties to predict granule growth behavior at different operating conditions. A multi-stage open optimal control strategy based on the developed ODPBMs was proposed to reduce the model and process mismatch through adjusting the trajectory of the evolution of the granule size distribution at predefined sample intervals. The effectiveness of the proposed modeling and multi-stage open optimal control strategy has been validated by experimental and simulation tests.

In addition, an Eulerian-Eulerian two-fluid model (EETFM) was developed to describe the gas-particle two-phase flow in the fluidized bed granulator. By computational fluid dynamic analysis, it has been proven that the fluidized bed granulation system is not homogeneous, based on which a two-compartmental population balance model (TCPBM) was developed to describe the particle growth in the fluidized bed granulation. Validation experiments have shown the effectiveness and superior accuracy of the TCPBM comparing with the ODPBM in predicting the final particle size distribution.

Publications

Journal publications

[1] **Huolong Liu**, Ke Wang, Walkiria Schlindwein, Mingzhong Li, Using the Box-Behnken experimental design to optimize operating parameters in pulsed spray fluidized bed granulation. International Journal of Pharmaceutics, 2013. 448(2): p. 329-338.

[2] **Huolong Liu**, Mingzhong Li, Population balance modelling and multi-stage optimal control of a pulsed spray fluidized bed granulation. International Journal of Pharmaceutics, 2014. 468(1-2): p. 223-233.

[3] **Huolong Liu**, Mingzhong Li, Two-compartmental population balance modeling of a pulsed spray fluidized bed granulation based on computational fluid dynamics (CFD) analysis. International Journal of Pharmaceutics, 2014. 475(1–2): p. 256-269.

[4] **Huolong, Liu**, Mingzhong Li, Computational Fluid Dynamics (CFD) study of the influence of particle size and inlet air velocity on the gas-solid flow pattern in a small-scale fluidized bed granulator. Publication in preparation.

Conference publications

[1] **Huolong Liu**, Mingzhong Li, Box-Behnken design for the optimization of operation variables of a small-scale top-spray fluidized bed granulation, Proceeding 6th International Granulation Workshop, Sheffield, UK, 26th -28th June 2013.

[2] **Huolong Liu**, Mingzhong Li, Population balance modeling and control strategy development for a lab-scale batch pulsed spray fluidized bed granulation, Proceeding

2014 APS Pharmsci Conference, Hatfield, UK, 8th -10th 2014.

[3] **Huolong Liu**, Modeling and control of batch pulsed top-spray fluidized bed granulation based on one-dimensional population balance model. Proceeding 12th UK Particle Technology Forum, 16th-17th September, 2014, Manchester Conference Centre, Manchester, UK.

Oral presentations

[1] **Huolong Liu**, Population balance modeling and multi-stage optimal control of a pulsed spray fluidized bed granulation, Doctoral Training Programme presentation, Hawthorn Building, De Montfort University, Leicester, UK, 22th May 2014.

[2] **Huolong Liu**, Modeling and control of batch pulsed top-spray fluidized bed granulation based on one-dimensional population balance model, 12th UK Particle Technology Forum 2014, Manchester Conference Centre, Manchester, 17th September, 2014.

Acknowledgements

I would like to express my sincere appreciation to my supervisors Dr Mingzhong Li, Dr Walkiria Schlindwein and Dr. Michael Goodman for their invaluable advice and skillful supervision throughout my PhD study. Your profound knowledge, creativeness, encouragement and unfaltering patience provide me courage in completing my PhD research. Your pursuit of truth and endless enthusiasm for research inspire me deeply.

I am very grateful to all technicians in the faculty of Health and Life Sciences who provide me technical support and equipment support for my experiments.

I would also like to thank all my colleagues in Health and Life Science Faculty, for their valuable suggestions and discussions, for their encouragement and support, and for the productive working environment.

In addition, I would like to thank the Graduate School Office at De Montfort University for the outstanding management.

Finally, I wish particularly to thank my beloved parents, my dearest brother for their endless love, caring and encouragement throughout my entire life. I am also thankful to my girlfriend for her patience, love, and understanding.

List of figures

List of tables

Abbreviations and symbols

Abbreviations

API	active pharmaceutical ingredient
CFD	computational fluid dynamic
CQAs	critical quality attributes
CPPs	critical process parameters
CS	control space
DEM	discrete element model
DoE	design of experiment
DDPM	dense discrete phase model
DPM	discrete phase model
DQMOM	direct quadrature method of moment
DS	design space
EETFM	Eulerian-Eulerian two fluid model
EKEK	equipartition of kinetic energy kernel
ETMK	equipartition of translational momentum kernel
FBRs	fluidized bed reactors
HPMC	hydroxy propyl methyl cellulose
ICH	International Conference on Harmonization
KTGF	kinetic theory of granular flow
MAs	material attributes
MC	Monte Carlo
MCC	microcrystalline cellulose
MCPBM	multi-compartmental population balance model
MZPBM	multi-zonal population balance model
MPC	model predictive control
ODEs	ordinary differential equations
ODPBM	one-dimensional population balance model
PBEs	population balance equations

PBMs	population balance models
PD	Product-Difference
PID	proportional-integral-derivative control
PL	positive large
PM	positive medium
PS	positive small
PSD	particle size distribution
QbD	quality by design
QbT	quality by testing
QMOM	quadrature method of moment
QTPP	quality target product profile
RSM	response surface methodology
RW	relative width of granule distribution
SMM	standard method of moment
SQMOM	sectional quadrature method of moment
SSEs	sum of square errors
Stv	stokes number
TCPBM	two-compartmental population balance model
VOF	volume-of-fluid
ZR	zero

Symbols

A_h	surface area (m^2)
A_i	area of the *ith* cell (m^2)
$b(L\|\lambda)$	length based fragment size distribution (m^{-1})
B	nucleation rate ($s^{-1}m^{-1}$)
C_D	drag coefficient
C_μ,$C_{1\varepsilon}$,$C_{2\varepsilon}$	coefficients in turbulence model
d_{pi}	geometrical mean of *ith* size interval
$d_{p,m}$	particle mean diameter (μm)
d_s	particle diameter (m)

D_{10},D_{90}	granule size at 10% and 90% cumulative particle size distribution
$\overline{D}$	mass mean diameter (μm)
$\overline{D}_m$	desired mean diameter (μm)
e_s	particle-particle collision restitution coefficient
f_i	mass fraction of *ith* size interval
$\vec{F}_{lift,q}$	lift force of phase q (N)
$\vec{F}_q$	external body force of gas phase q (N)
$\vec{F}_{vm,q}$	virtual mass force of phase q (N)
g_0	radial distribution function
$\vec{g}$	gravitational acceleration (ms^{-2})
G	particle growth rate (ms^{-1})
$G_{k,g}$,$G_{k,mix}$	production of turbulent kinetic energy
h_{max}	maximum bed height particles can explore
h_{min}	minimum bed height particles can explore
I_{2D}	the second invariant of the deviatoric stress tensor
$\bar{\bar{I}}$	identity matrix
k	turbulence kinetic energy tensor
k_q	turbulence kinetic energy tensor of phase q
k_{Θ_s}	diffusion coefficient for granular energy
K_{ps}	interaction force coefficient between phase p and s (kgm^2s^{-1})
l	particle size (μm)
L_{mf}	the bed height at minimum fluidization velocity (m)
L_i	abscissas of the quadrature approximation (m)
m_k	*kth* moment of number density (m^k)
$\dot{m}_{gs}$	mass transfer from gas to solid (kgs^{-1})
$\dot{m}_{sg}$	mass transfer from solid to gas (kgs^{-1})
n	particle number density (m^{-1})
$n_{d,inlet}$, $n_{d,outlet}$	particle number density inlet and outlet of drying zone (m^{-1})
n_d	particle number density in drying zone (m^{-1})
n_{eq}	total number of size intervals

n_s	particle number density in spraying zone (m^{-1})
$n_{s,inlet}$,$n_{s,outlet}$	particle number density inlet and outlet of spraying zone (m^{-1})
n_p	total number of phases
n_s	number of solid phases
n_spe	number of species
N_d	grid number on the surface particle flow downward
N_i	number of particles in *ith* size interval
N_q	order of the quadrature approximation
N_u	grid number on the surface particle flow upward
p	pressure (chapter 2), parameter in aggregation kernel (chapter 4)
p_s	solid phase pressure (Pa)
ΔP	pressure drop (Pa)
q	parameter in breakage kernel
r	ratio of the upper and lower bounds of a size interval
R	particle volume flow rate ($m^3 s^{-1}$)
Re_s	particles Reynolds number
$S(\lambda)$	length based breakage kernel (s^{-1})
S_d	breakage kernel in drying zone (s^{-1})
S_q	mass source term for phase q (kgs^{-1})
S_0	breakage kernel constant ($m^{-q} s^{-1}$)
$S_{0,d}$	breakage kernel constant in drying zone (s^{-1})
t_c	circulation time (s)
u	particle size (μm)
$\vec{U}_g$	phase-weighted gas velocity
$\vec{U}_l$	phase-weighted velocity of phase l
$\vec{U}_q$	phase-weighted velocity of phase q
$v_{a,inlet}$	inlet air velocity ($m^3 s^{-1}$)
$v_d(y)$	time-averaged downward particle velocity at bed height y (ms^{-1})
$v_u(y)$	time-averaged upward particle velocity at bed height y (ms^{-1})
v_y	solid Y velocity (ms^{-1})

$\vec{v}_g$	gas phase velocity (ms^{-1})
$\vec{v}_{mix}$	mixture velocity (ms^{-1})
$\vec{v}_q$	velocity vector of phase q (ms^{-1})
$\vec{v}_s$	solid phase velocity (ms^{-1})
$v_s^{'}$	solid phase fluctuating velocity (ms^{-1})
V_d	total particle volume in drying zone (m^3)
V_s	total particle volume in spraying zone (m^3)
V_t	total particle volume in granulator (m^3)
w_i	weights of the quadrature approximation
x_{1_min},x_{1_max}	lower and upper constraints of pulsed frequency
x_{2_min},x_{2_max}	lower and upper constraints of binder spray rate ($gmin^{-1}$)
x_{3_min},x_{3_max}	lower and upper constraints of atomization pressure (psi)
X_1	pulsed frequency
X_2	binder spray rate ($gmin^{-1}$)
X_3	atomization pressure (psi)
Y_1	mean size of final granules (μm)
Y_2	yield of final granules
Y_3	relative width of final granule distribution
Y_4	Hausner ratio
Y_5	Moisture content at 30% of binder solution sprayed
Y_6	Moisture content at 70% of binder solution sprayed
Y_7	Moisture content at 100% of binder solution sprayed

Greeks

α	portion of entire particle volume in spraying zone
α_g	volume fraction of gas phase
α_q	volume fraction of phase q
α_s	volume fraction of solid phase
$\beta(L,\lambda)$	length based aggregation kernel (s^{-1})
β_s	aggregation kernel in spraying zone (s^{-1})

β_0	aggregation rate constant ($m^{-p}s^{-1}$)
$\beta_{0,s}$	aggregation rate constant in spraying zone ($m^{-3}s^{-1}$)
γ	adjusting parameter in control
γ_{Θ_s}	collisional dissipation of energy (m^2s^{-2})
ε	turbulence dissipation rate (m^2s^{-3})
ε_{mf}	the bed voidage at minimum fluidization velocity
ε_q	turbulence dissipation rate of phase q (m^2s^{-3})
η	effectiveness factor
θ	angle of internal friction (degree)
λ_s	solid bulk viscosity (Pas)
μ_g	viscosity of gas phase (Pas)
μ_s	solid shear viscosity (Pas)
$\mu_{s,col}$	solid collisional viscosity (Pas)
$\mu_{s,fin}$	solid frictional viscosity (Pas)
$\mu_{s,kin}$	solid kinetic viscosity (Pas)
$\mu_{t,g}$	frictional viscosity of gas phase (Pas)
$\mu_{t,m}$	frictional viscosity of system m (Pas)
ρ_g	gas density (kgm^{-3})
ρ_m	density of system m (kgm^{-3})
ρ_{mix}	density of mixture system (kgm^{-3})
ρ_q	density of phase q (kgm^{-3})
ρ_s	solid density (kgm^{-3})
$\hat{\rho}_q$	effective density of phase q (kgm^{-3})
σ_k,σ_ε	granular kinetic theory parameter (Pas)
$\bar{\bar{\tau}}_g$	gas phase stress strain tensor (Pa)
τ_s	particulate relaxation time (s)
$\bar{\bar{\tau}}_s$	solid phase stress strain tensor (Pa)
Θ	system parameters
Θ_s	granular temperature (m^2s^{-2})
φ_{ps}	dissipation of granular energy resulting from fluctuation in

	particle velocity from phase *p* to phase *s*
Ψ	physical property parameters of powder mixtures

Subscripts

g	gas phase
s	solid phase
p, *q*	phase *p*, *q*

Chapter 1 Introduction

1.1 Fluidized bed spray granulation

Granulation is the process of agglomerating fine powder materials to give larger granules, including dry granulation and wet granulation, of which wet granulation, by adding a binder solution to powders, is one of the most common ways to produce granules. The wet granulation can be achieved in a range of different processing equipment including drums, pans, fluidized beds, and high shear mixers, which are summarized in Figure 1.1. It is an important process in a range of industries including agricultural chemicals, pharmaceuticals, mineral processing, food, and detergents.

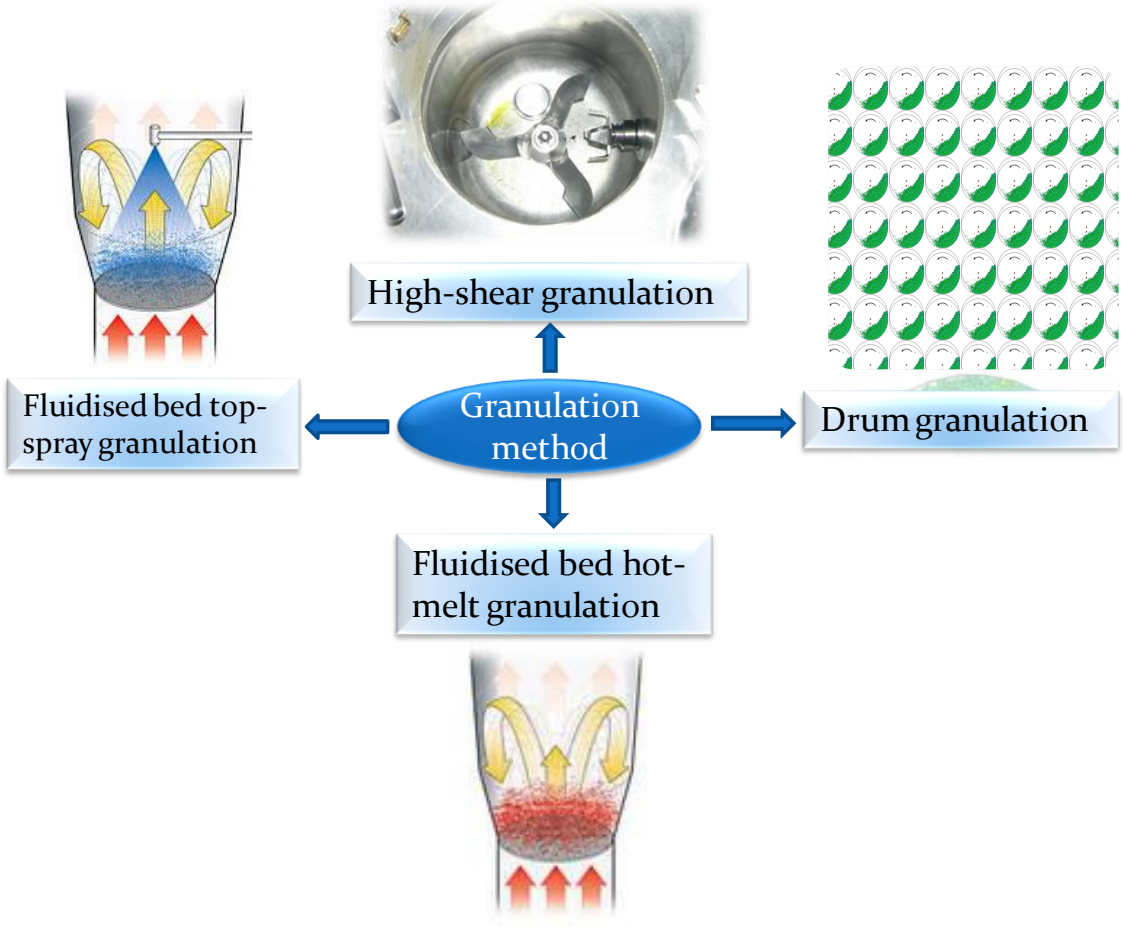

Figure 1.1 Summary of wet granulation methods

Of the wet granulation methods shown in Figure 1.1, fluidized bed spray granulation is well known method to produce granules by spraying binder solution over the solid powder in a fluidized bed. A main advantage of this technique is that several steps can be completed, compared with other methods, in the same piece of equipment including pre-blending of the solid powder, granulation with a suitable liquid binding agent, followed by drying of the granules to a predetermined moisture content level. In addition, this technique also provides various advantages, i.e. well materials mixing, high heat and mass transfer rates, uniform binder distribution, and fine particle control. Due to the interests above, fluidized bed spray granulation is extensively adopted in the pharmaceutical, food and chemical industries and has a long history more than 40 years. The initial investigation of the fluidized bed spray granulation began from Wurster in his work on air suspension coating [1]. In the following decades, fluidized bed spray granulation was investigated widely and developed quickly [2-5].

To start with, it is necessary to have a basic knowledge of the definition: fluidization. A definition utilized by Khoshtaghaza and Chayjan [6] is that fluidization is an operation that suspends solid particles in a gas. Generally, four stages are identified in the process of fluidizing a bed of solid particles based on the velocity of gas flow through the bed: fixed bed, expanded bed, bubbling bed, and pneumatically conveying. When a gas is passed through a bed of solid particles at a low velocity, the gas liquid first percolates through the void spaces between the particles and this is called the fixed bed. When the fluidizing air velocity is increased, particles begin to vibrate and an insignificant increase in the void fraction in the bed is then observed [7]. This is the expanded bed and at this stage, the bed height becomes higher but still has a similar performance with the fixed bed. During this period, when the weight of the bed is counterbalanced by the frictional force of the upward flowing gas, the velocity is called the minimum fluidization velocity (u_{mf}). As the fluidizing velocity increased continuously, the bubble formation and transportation state occurs. Another classification method is proposed by Geldart [8] to characterize fluidization behavior, focusing on the physical properties of the particle. In the Geldart classification method, four distinct groups of particles (group A: aeratable materials, group B: sand-like solids, group C: cohesive and fine powders, group D: spoutable large particles) are identified, which can result

different performance of fluidization.

The fluidized bed spray granulation is a complicated process involving multiple process variables and several simultaneous rate processes. According to the position of the spray nozzle, three patterns of the fluidized bed granulation are characterized: top spray, bottom spray and tangential spray, of which the top-spray granulation is the most commonly used method where binder solution is sprayed from a nozzle positioned above the fluidized bed [9, 10]. Usually, fluidized bed granulators can be divided into batch operating mode and continuous mode, of which the batch mode is popularly used (Figure 1.2). For batch mode fluidized bed granulation, powder is initially charged into the fluidized bed with air being forced into the granulator from a distributor at the bottom of the bed. A mesh keeps powder from leaving at the bottom, while filters at the top of the column allow air to pass, but keep solid particles from leaving. These filters are periodically shaken to dislodge any particles and to return them back to the fluidized bed. Once the powder is fluidized and mixed, a binder agent is pumped and subsequently atomized into fine droplets by nozzles positioned in the top of the fluidized bed before being added to the powder. Nucleation and agglomeration process occur subsequently with the addition of the binder. Once the granules are grown to the desired size, the binder addition is terminated and the granules are then allowed to dry by continuously fluidizing hot air into the bed.

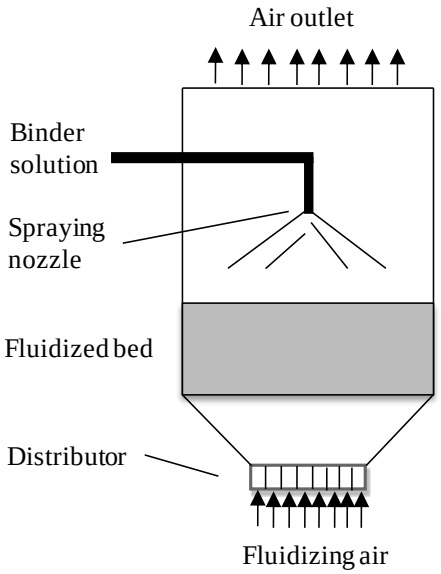

Figure 1.2 Batch mode top-spray fluidized bed granulator

1.2 Research aim and objectives

The aim of the proposed research project is to develop accurate mathematical models to predict the evolution of granule size and granule size distribution (GSD) in a top-spray fluidized bed granulation process and to design control strategies to minimize time and effort to achieve the desired granule properties. It is expected that the batch pulsed top-spray granulation can be better understood.

The specific objectives of this research are briefly listed as follows:

Objective 1: Review the background, mechanism, experimental study, modeling approach and control strategy of fluidized bed spray granulation and give a comprehensive literature review.

Objective 2: Design experiments using Box-Behnken experimental design method to investigate the influence of three operating parameters: pulsed frequency, binder spray rate, and atomization pressure on the final granule properties. Especially, study the capability of the pulsed binder spray in controlling fluidized bed spray granulation.

Objective 3: Develop a one-dimensional population balance model (ODPBM) to predict the evolution of granule size and granule size distribution. Propose a multi-stage optimal control strategy to control the fluidized bed granulation process. Validate both process model and control strategy using experiments and simulations.

Objective 4: Study the influence of particle size and inlet air velocity on the gas-solid fluid dynamics within the fluidized bed granulator using computation fluid dynamics (CFD) simulation and finally determine the solid flow pattern.

Objective 5: Develop a multi-compartmental population balance model (MCPBM) to simulate the fluidized bed spray granulation process, in which the fluidized bed granulator is divided into different zones according to the hydrodynamics study using computation fluid dynamics (CFD) simulation, as described in Figure 1.3. Apply homogeneous ODPBM on each zone and obtain exchange and local zone information from CFD simulation. Apply the proposed multi-stage optimal control on the new

developed MCPBM and validate the MCPBM and control strategy using experiments and simulations.

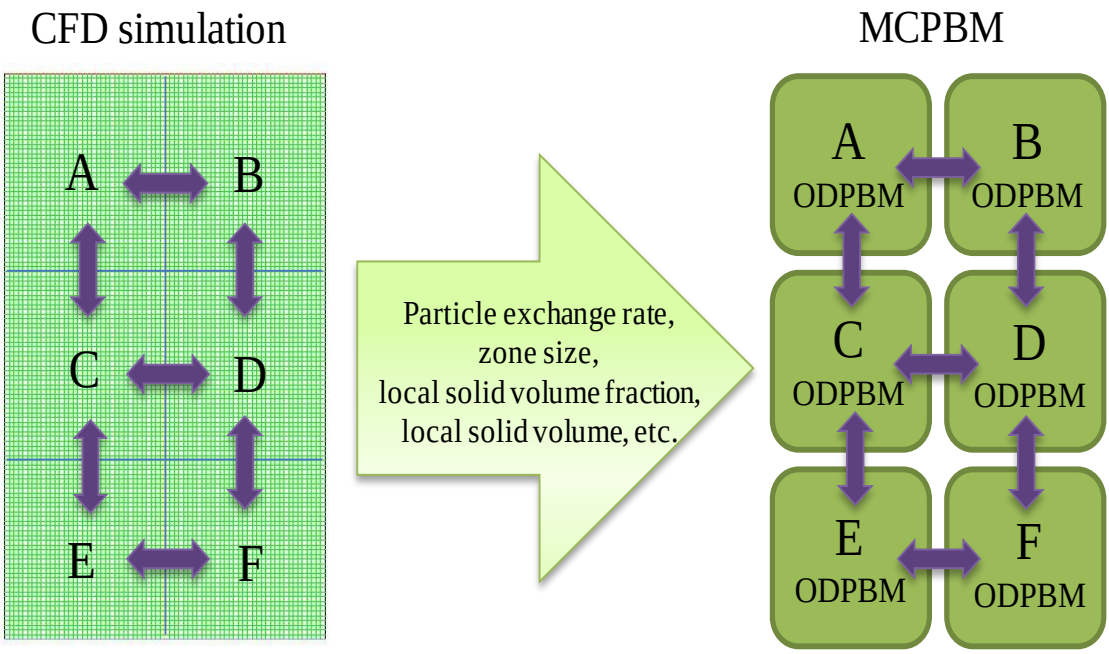

Figure 1.3 Structure of multi-compartment population balance model (MCPBM)

1.3 Novelty of research

The main novelties of this thesis are described as follows:

- One-dimensional population balance model (ODPBM) from real operating conditions to final granule properties;
- Design experiments using Box-Behnken experimental design method;
- Develop mathematical relationship between fluidization level and inlet air velocity;
- Develop two-compartmental population balance model (TCPBM) based on computational fluid dynamics (CFD) analysis;
- Model-based multi-stage optimal control strategy.

A detailed introduction of the novelties is given in Table 1.1.

Table 1.1 Detailed introduction of novelties in this study

novelty	Traditional	Current study
One-dimensional PBM	PBM in terms of aggregation and breakage kernels	PBM in terms of real operating conditions
Experiments design	Comparison experiments by changing specified condition	Box-Behnken experimental design method
Inlet air velocity adjust	By experience	Accurately adjust by developed mathematical model
Compartments division of TCPBM	By experiments results or experience	By fluid dynamics analysis using CFD simulation
Control strategy	Online real-time control	Multi-stage optimal control

1.4 Thesis structure

This thesis includes 8 chapters:

Chapter 1 gives a basic introduction of the research background and the objectives of the work. An outline of this thesis is given in chapter 1.

Chapter 2 presents the detailed literature review regarding the research field. This includes the granulation mechanism, experimental work, existing model for the fluidized bed granulation and published control methodology.

Chapter 3 introduces the experiments carried out in the work. The materials, equipment, and experiment method will be introduced in this chapter. In addition, the processing of the end granules and measurement and sampling of granules is also explained in this chapter.

In chapter 4, the experiment data are analyzed and discussed to study the influence of the operating conditions of pulsed frequency, binder spray rate and atomization pressure. Mathematical models between the end granule properties, such as mean size, yield of granules, relative width of final granule distribution, and the operating conditions were developed to understand the granulation process. The effect of operating condition interaction was also studied, and the designed space is determined based on applying

constraints on the mean size of granules.

In chapter 5, a process model for the spray fluidized bed granulation process based on the one-dimensional population balance model (ODPBM) has been developed. The developed PBMs have linked the key binder solution spray operating factors of the binder spray rate, atomizing air pressure and pulsed frequency of spray with the granule properties to predict granule growth behavior in the pulsed spray fluidized bed granulation process at. A multi-stage open optimal control strategy based on the developed PBMs was proposed to reduce the model mismatch, in which through adjusting the trajectory of the evolution of the granule size to determine the optimal operating variable.

Chapter 6 investigates the multiphase flow dynamics within the spray fluidized bed granulator modeled based on the granulator equipment in our lab using the Computational Fluid Dynamics (CFD) software ANSYS Fluent 13.0. Three dimensional simulations were carried out to study the influence of particle size and inlet air velocity on the fluid dynamics. Finally, a mathematical model describing the relationship between particle circulation time and particle size and inlet air velocity was developed. Based on the fluid dynamic study, the granulator domain was divided into different compartments, which is assumed as homogeneous for the multi-compartment modeling study.

In chapter 7, a two-compartment PBM (TCPBM) model is developed. The same control strategy developed in chapter 5 was applied on the proposed TCPBM. The TCPBM was compared with the one-dimensional PBM (ODPBM) model, which has shown that the TCPBM is more superior in predicting the final particle size distribution.

Chapter 8 summarizes the research results and objectives obtained in this study. In addition, further work that can be carried or modified based on this study is described in this chapter.

Chapter 2 Literature review

2.1 Chapter overview

In this chapter, a brief and systematic literature review of the spray fluidized bed granulation is presented. To start with, the knowledge of granulation mechanisms including nucleation, growth and consolidation, attrition and breakage are briefly introduced, which gives a detailed understanding of the granulation process. Then, in order to understand the mechanisms happen during the granulation, the experimental studies up to date are reviewed mainly from two aspects: influence of process-related parameters and effect of binder and material properties. The modeling investigation of fluidized bed granulation including population balance modeling (PBM) and computational fluid dynamics (CFD) are subsequently summarized, which replenish the knowledge of fluidized bed granulation. The study of control of fluidized bed granulation process is also illustrated. Finally, the application of quality by design (QbD) concept recently to study the fluidized bed granulation is presented. As an important parameter to control the granulation process, the binder solution pulsed spraying is especially introduced at the end of present chapter.

2.2 Granulation mechanism

Thorough understanding of the hydrodynamics and the mechanism prevailing in the granulation process is necessary for understanding the process and further modelling and control. The mechanism of granulation process has been extensively studied. To date, several literature reviews focusing on fluidized bed granulation have been published [11-15]. A review critically evaluating the current understanding of the three key areas of wet granulation processes: wetting and nucleation, consolidation and growth, and breakage and attrition was provided by Iveson et al. [11]. Bouffard et al. [12] provided an overview of process-related variables and physicochemical properties in fluidized bed granulation and discussed their influence on granulation mechanism. The breakage behaviors in granulation were reviewed from the process scale down to the single granule scale by Reynolds et al. [16], with large amount of experimental and

modeling results discussed. Basically, the mechanisms of granulation are often distinguished as nucleation, growth and consolidation, and breakage and attrition [11], which may happen simultaneously in the granulation process.

2.2.1 Nucleation

Nucleation means the formation of the initial nuclei by clumping primary particles together after bringing liquid binder into contact with dry powder. As an important stage of the granulation, nucleation plays a crucial role as the initial nuclei size distribution obtained will influence the resulting granule size distribution and the need to study nucleation mechanism has been identified [17, 18]. To date, there are several publications focusing on the nucleation mechanisms [19-22].

Nucleation occurs when the binder droplet penetrates the powder mass and nucleates particles in its immediate vicinity to form a granule nucleus. This process is mainly influenced by the ability of the liquid binder to spread over the solid surface. Through extensively experimental studies, two distinct nucleation mechanisms (Figure 2.1): immersion mechanism and distribution mechanism, depending on the ratio of particle size to droplet size were proposed by Schaefer and Mathiesen [19].

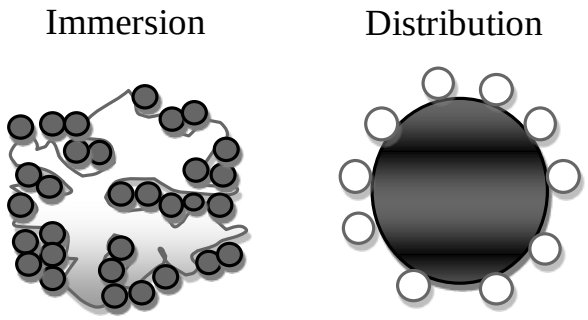

Figure 2.1 Nucleation mechanisms

In the distribution mechanism, binder is distributed on the surface of the powder particles, and the formation of nuclei occurs by coalescence between the wetted particles [23]. In the immersion mechanism where the binder droplet size is larger than the size of the powder particles, the primary particles are captured on the surface of the

binder droplet and are subsequently immersed. Therefore, the factors that can contribute to small binder droplet size, such as low binder viscosity and high impeller speed (in high-shear granulation), will promote the distribution nucleation mechanism [21]. On the other hand, large initial binder droplet size, high binder viscosity and low impeller speed promote the immersion mechanism.

2.2.2 Growth and consolidation

Granule growth occurs when particles come into contact and stick together in a granulation process, of which two distinct growth mechanisms (Figure 2.2) can be distinguished: layering and coalescence [11], according to the colliding particle size.

Layering refers to the coalescence between one large granule and many small particles, or the sticking of fine particles onto the surface of large pre-existing granules [13, 24]. In wet granulation, the fluidized particles are wetted with a liquid layer on the surface. When the fine particles and fragments formed by breakage collide with large granules, they will stick on the surface of large granules. Therefore, the layering is mainly determined by the existence of liquid layer on the large granule surface. It is often induced by rolling action and is a mean of granule growth that creates hard, compact granules.

The coalescence happens when two nearly equally sized wet granules collide and are bounded by a liquid bridge formed between the two particles which becomes a solid bridge during the subsequent drying period. According to the dependency of coalescence on deformability of the colliding granules, two types of coalescence can be concluded: non-deformable coalescence and deformable coalescence. Non-deformable coalescence takes place frequently when the impact velocities are very small or the granules are extremely rigid, relatively little permanent deformation occurs during granules collision. In a fluidized bed spray granulation process, this type coalescence often occurs during the initial nucleation period and later stages when the compact forces are relatively gentle and granules have become rigid enough after consolidation, respectively.

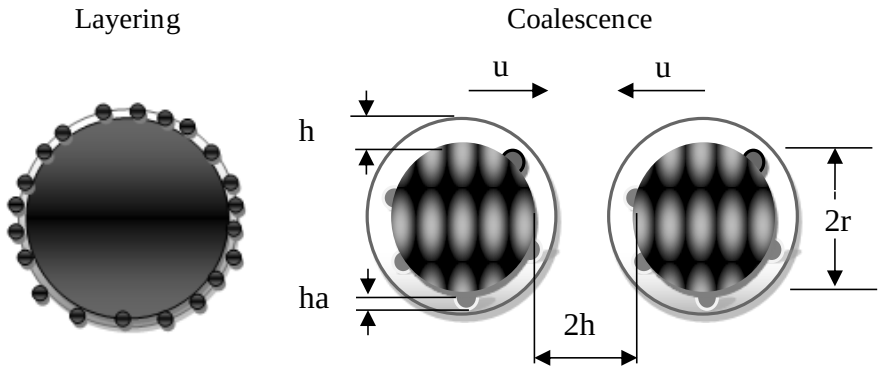

Figure 2.2 Particle growth mechanisms

There are many coalescence models available in literature describing the coalescence mechanisms, which include a variety of formulation and process parameters, such as the mechanical properties of the granules, the properties of the liquid binder, and the granule collision velocity. Basically, these models consider whether the particle rebound or stick together during their collision [11, 25-27]. In these models, the coalescence happens if the particles do not possess sufficient kinetic energy to rebound. For example, Ennis et al. [25] studied the non-deformable coalescence by considering the colliding of two solid particles both of which were surrounded by a thin viscous binder layer. In their model, the viscous force was considered, then, coalescence happened successfully only if the kinetic energy of particles was totally dissipated by the viscous dissipation in the binder layer. During the rebounding stage, the liquid bridge was assumed to rapture at the same distance at which the two binder layers first contacted (i.e. 2h, Figure 2.2). A dimensionless binder stokes number (Stv) has been used to determine whether coalescence between two particles occurs, which is a measure of the ratio of granule collision kinetic energy to the viscous dissipation brought about by interstitial binder.

Granule consolidation occurs when collision happens between granules, between granules and wall or between granules and impellers in high shear granulator. Consolidation can reduce granules size and porosity, squeeze out entrapped air or even squeeze liquid binder to the granule surface. Granules with high porosity are weak and friable, whereby those with lower porosity are strong to resist breakup. Hence, consolidation has an effect on the mechanical properties of granules. Because granule

yield stress generally increases as granule porosity decreases [28], consolidation decreases the amount of deformation when two granules collide, which decreases the likelihood of coalescence. However, consolidation also increases the pore saturation, and this in turn increases granule plasticity and the availability of liquid binder at the granule surface, both of which will contribute to coalescence. Therefore, how the consolidation will influence the granule growth may be probably determined by the formulation and binder properties.

As a complex process in granulation, consolidation can be affected by several variables: binder content, binder viscosity, binder surface tension, particle size, and operating conditions [29-34]. Three forces are often utilized to analyse the consolidation process: capillary force, viscous force, and friction force. Interestingly, the effects of viscosity and liquid content are highly interactive. Increasing binder content reduces inter-particle friction due to lubrication but increases viscous forces since there is more binder to be squeezed between particles as they rearrange. Therefore, Increasing the liquid content increases the degree of consolidation when lower viscosity binder is used [32], and as high viscosity binder is used the effect of binder content on consolidation reverses. Decreasing binder surface tension is found to increase the rate of consolidation, but to decrease the extent of consolidation [29]. The rate of consolidation decreases as particle size decreases. As the particle size decreases, the capillary, viscous force in liquid binder and friction forces between granules which resist to granule deformation all increase [29]. In addition, the effect of equipment type or equipment speed on consolidation have also been studied by some researchers in pan granulation [33] and high shear mixer [34].

2.2.3 Attrition and breakage

Attrition and breakage means the wet granules breakage in the granulation process and the attrition in drying process [11]. As an important process in granulation, breakage and attrition of granules can influence the final granule size distribution. From the product quality perspective, they help to improve granule homogeneity and flowability [35]. Hence, a good knowledge of breakage and attrition can well contribute to the design and modeling of the granulation system, as well as control of granulation.

However, wet granules breakage and dry granules attrition in granulator is less well understood than coalescence [36-39].

Wet granule breakage is the process by which granules, comprising liquid binder and primary particles, are broken up into smaller granules. The literature on identifying and quantifying the breakage kinetics during fluidized bed granulation is extremely limited [39-41]. A granule will breakage if the external stress during an impact exceeds the intrinsic strength of the granule [41]. In a wet granule, a granule yield strength mainly depends on the liquid bridges forces, which are in turn made up of capillary forces, viscous forces and frictional forces [42]. Therefore, all the factors that have effect on the granule yield strength and external dynamic energy will influence the breakage behavior, such as the formulation properties and operating conditions. The formulation properties including the binder viscosity, binder saturation, and binder surface tension as well as primary particle size have been shown to have a large influence on the granule breakage behavior [29, 35, 38, 43]. The extent of breakage is found to decrease with the increase of binder saturation, binder viscosity, and binder surface tension, and increase with primary particle size [38]. The operating conditions, such as impact velocity and angle, are also studied, in which a high extent of breakage was reported with high impact velocity [37, 44-47].

Attrition is caused by normal forces of small magnitude mainly happening in the drying process, by which the sharp edges and surface asperities are removed and fine dust is formed. Granule shape also becomes more spherical and smoother due to attrition [48]. Formation of fines by attrition is actually an important parameter because it can affect flowability of the granule product. Although unwanted size reduction of pharmaceutical granules during fluidized bed granulation drying [49] or high shear granulation [35] has been reported, attrition has received relatively little attention.

2.3 Experimental study

In order to well understand the complex mechanisms happened during the granulation process, experimental design becomes an effective method and many research results based on experimental study have been published [12, 50-64]. It has been shown that

the granulation results can be significantly influenced by operating parameters such as inlet air relative humidity, binder feed rate, fluidizing air velocity, inlet air temperature, spray atomizing pressure, and granulation time. In addition, both primary powder properties and the binder properties have a great effect on the quality of final product, especially on the granule size distribution.

2.3.1 Effect of process-related variables

2.3.1.1 Variables related to fluidization

Fluidizing air relative humidity

The inlet air relative humidity is known to have an effect on agglomerate growth and the particle size of the end product, and has been addressed by a number of researchers. It has been found that larger granules are formed as relative humidity of inlet air increases during granulation [50-54], because the water evaporation capacity of the inlet air is decreased and the formation of liquid and solid bridges is increased. The relative air humidity is also found to influence the granule growth and the mixing behaviour by influencing the inter-particle cohesion when it exceeds a critical value [50, 54]. Besides, the relative humidity has an effect on the minimum fluidization velocity (U_{mf}), which shows a proportional increase with relative humidity of inlet air. Experiments focusing on the effect of relative air humidity on final granule size were also carried out and the results indicated that the relative humidity had a positive linear contribution to the final granule size [51-53]. By using a humidifying system, the relative air humidity is available to be controlled to avoid improper granulation modes [65]. The bed temperature increases with the relative air humidity because of the high heat capacity of high relative air humidity, and the final moisture content is found to increase when the humidity content of air [66].

Fluidizing air velocity

Fluidizing inlet air velocity is an important operating parameter affecting both fluidization hydrodynamics and granule growth, and it plays a key role in producing high powder mixing uniformity. Fluidizing inlet air velocity can affect the granulation

behavior and final granule size distribution by affecting the drying capacity [54]. At the initial stage of the granulation, it is reported that higher air velocity produces a higher growth rate because of the higher frequency and energy of collisions between granules, while larger granules were finally obtained from lower fluidizing air velocity due to the small shear force provided by the lower fluidizing air velocity [12]. Besides, the higher fluidizing gas velocity was found to reduce operation efficiency, and agglomerates fraction [12]. Increasing fluidizing air velocity was found to produce a smaller granule size [12, 54], and the granules obtained at low gas velocity were less friable than those produced at high gas velocity [54, 67]. If the fluidizing air velocity is lower than some critical value, defluidization can happen [54]. In addition to the effect on growth rate, Tan et al. [55] reported a narrower granule size distribution produced by increasing fluidizing air velocity. In another study [68], the effect of fluidizing air velocity on bed humidity was studied, which has found that the bed humidity decreased with increasing air flow rate.

Fluidizing air temperature

Inlet air temperature is a key parameter affecting the fluid bed temperature and moisture evaporation [50, 53, 56, 57]. Higher inlet air temperature can dry the wet granules quickly and makes a lesser granulation time. The bed temperature is found to be dependent on the inlet air temperature and the granule diameter decreased when fluidising air temperature was increased [53, 56]. The inlet temperature was also found to affect the granule growth [50], and it was observed experimentally that at lower temperature, the granules grew to their final size faster than those of higher temperature. In addition, the inlet air temperature has an influence on bed humidity [68]. The higher the inlet air temperature is, the lower the bed humidity is because of the faster evaporation rate. The inlet air temperature is pointed as an important parameter for controlling the fluidized bed granulation process due to its influence on the bed moisture content [57].

2.3.1.2 Variables related to binder spraying

Atomizing pressure

In the fluidized bed granulation, binder solutions are sprayed into the solid bed through an atomizer in order to produce evenly fine droplets. Thus, the atomizing pressure plays a really important role in the granulation. The atomizing pressure influences the angle of sprayed liquid jet and the speed and diameter of the sprayed liquid droplets [56]. As the atomizing air pressure increased, smaller value of the jet angle, the liquid droplets diameter and higher value of the droplets speed are obtained, leading to reduction of the final granule size [12, 51, 56]. As mentioned before, two nucleation mechanisms were classified as: the immersion mechanism and the distribution mechanism according to the droplet and particle size ratio [55]. Therefore, the atomizing pressure has a significant effect on the granulation process through influencing the droplet size. The effect of binder droplet size on granulation mechanisms was also investigated extensively [12, 55, 61-64]. Droplet size was found to impact the nucleation mechanism and the granule growth [61]. A larger droplet size may promote the granule growth because of a higher liquid saturation in the agglomerate surface due to the immersion nucleation. With increasing the droplet size, the granules become more spherical and dense [62]. However, if the binder to solid content ratio is constant, larger droplet size is found to produce a large fraction of un-granulated fines [63]. The results obtained by Tan et al. [55] demonstrated that the droplet size can influence the growth rate of different granulation stage: the smaller droplets was prone to promote a faster initial growth while the larger droplets seemed to induce a faster secondary growth stage.

Liquid binder feed rate

The binder spray rate is one of the most widely studied parameters, which can affect granule size, bed moisture content and product quality [57]. Generally, increasing the binder spray rate enhances granule growth and produces granules with larger mean size [12, 52, 56, 58-60]. The granule growth increases with the higher binder spray rate because of its significant enhancement on droplet size and moisture content [68]. However, the binder spray rate was reported to have no influence on the granule growth rate when it was lower than a critical value [54]. This phenomenon can be interpreted that lower binder spray rate has too smaller influence on the relative humidity to affect the granule growth. In another literature [56], it was reported the liquid feed rate

influenced both the angle of the sprayed jet and the droplets size, and changed the drying conditions within the fluidized bed. When the liquid feed rate increased, the liquid jet angle and the diameter of the liquid droplets increased therefore it was more difficult to dry the granules.

Granulation time

As expected, longer granulation time produces larger granules. With increasing granulation time, the mass of un-granulated particles decreases. It is observed that the mass fraction of large size granules increased initially, while the mass fraction of larger granules decreases at the later stage of granulation [62]. This indicates the phenomenon of breakage of large unconsolidated granules. In addition, it has been reported that at the early stage of granulation process, the growth rate of the granules is higher [69].

Spray nozzle position

The influence of the atomizer position has been studied, and it is found that decreasing the height of the spraying nozzle gives rise to an increase of mean granule size and a decrease of friability of the granules [54, 60]. This phenomenon can be explained by the fact that when nozzle is located at lower position, the distance of the droplet traveling to meet particle becomes shorter, which decreases the probability of the spray evaporation and enhances the binder potential to wet the particles. However, a lower position of the spray nozzle may cause the clogging due to the sub-merge by fluidizing particles. Therefore, it is recommended that an appropriate height of the spraying nozzle is that the tip of the nozzle coincides with the surface of the packed bed [54].

2.3.2 Effect of binder and material properties

There are several physicochemical variables of the binder and material properties that affect the granulation process. The most regularly studied variables include primary powder particle size, wettability of the liquid on solid, solubility [54, 56, 61, 62, 70-73] and binder properties of binder concentration, viscosity [54, 56, 61-64, 69, 71, 73].

2.3.2.1 Effect of powder properties

The properties of the primary material have an important effect on the granulation process and final granule properties. Usually, the most frequently studied powder properties include primary powder particle size, wettability of the binder liquid on solid, solubility, and particle shape factor [57].

It was shown that as the primary mean particle size decreased, the particle growth rate increased, and the final granule mean size decreased [54, 61, 62]. An increasing growth rate is observed when the solubility of primary powder increases [56, 70, 71]. The particle surface wettability can be indicated by the contact angle between the binder droplet and solid particle and the experiments results show that the agglomeration kinetics becomes more important as the contact angle decreases [54, 62, 72, 73]. Furthermore, when the contact angle is similar, the growth is determined by the particle shape factor with larger shape factor causing slow growth [54, 73].

2.3.2.2 Effect of binder properties

During the granulation process, liquid binder is sprayed into the powder in the bed, and particles are bonded with the liquid bridge. Therefore, the properties of binder have a key influence on granulation. The most important binder properties include the binder viscosity, binder concentration, and the binder content.

Generally, the growth rate, maximum median granule diameter, and the final granule porosity are found to increase as the binder concentration increases [54, 56, 61, 64, 69, 71, 73]. The low viscosity binder is proved to promote the granulation and the growth rate [69], due to the high probability of viscous binders being forced to the surface during collision. The percentage of un-granulated fines is found to decrease with increasing the binder content and granule growth also depended on the binder content [62, 69]. However, Ansari and Stepanek [63] have proved that the mean size of pure granules (excluding the un-granulated fines) is independent on the binder content, instead of on the droplet size. Besides, there should be a limitation for the binder content, above which the over-wetting or defluidization could occur [74].

2.4 Population balance modeling

2.4.1 Population balance equation

In order to develop a better design method and tight control strategy, an accurate mathematical model of the fluidized bed granulation process is needed. The population balance model (PBM) has been used for describing the change of particle size distribution of fluidized bed granulation in a large number of works for decades [39, 67, 75-85]. To date, several literature reviews have been published [13, 86-88].

A general length-based population balance equation in batch mode that describes the rate of change in particle length number density function n(t,L) is given as follows [89, 90]:

$$\frac{\partial n(t,L)}{\partial t} = B(t,L) \quad \text{Nucleation}$$

$$-\frac{\partial}{\partial L}(G(t,L)n(t,L)) \quad \text{Growth}$$

$$+\frac{L^2}{2}\int_0^L \frac{\beta\left(t,\left(L^3-\lambda^3\right)^{\frac{1}{3}},\lambda\right)}{\left(L^3-\lambda^3\right)^{\frac{2}{3}}} n\left(t,\left(L^3-\lambda^3\right)^{\frac{1}{3}}\right) n(t,\lambda)d\lambda - n(t,L)\int_0^\infty \beta(t,L,\lambda)n(t,\lambda)d\lambda$$

Aggregation

$$+\int_L^\infty S(t,\lambda)b(t,L|\lambda)\, n(t,\lambda)d\lambda - S(t,L)n(t,L) \quad \text{Breakage}$$

(2.1)

Where, $n(t,L)$ is the number density function in terms of the particle diameter L, $\beta(t,L,\lambda)$ is the length-based aggregation kernel that describes the frequency that particles with diameter L and λ collide to form a particle of volume $L^3+\lambda^3$, $b(t,L|\lambda)$ is the fragments distribution function that describe the frequency of formation of particles of diameter L from the breakup of particle of diameter λ, $S(t,L)$ is the length-based breakage selection rate that is the frequency of disruption of a particle of diameter L,

$B(t, L)$ is nucleation rate, and $G(t, L)$ is the growth rate.

The terms on the right hand side of equation (2.1) have different meanings as follows (the number corresponds to the terms):

(1) The appearance of new particles of diameter L because of nucleation.
(2) The birth of particle of diameter L due to the growth of smaller particles.
(3) The birth of particles of diameter L due to aggregation of two smaller particles of diameter $(L^3 - \lambda^3)^{\frac{1}{3}}$ and λ.
(4) The death of particles of diameter L due to aggregation of particle of diameter L and particle of any diameter λ.
(5) The birth of particle of diameter L due to the breakage of larger particles of diameter λ.
(6) The death of particle of diameter L due to breakage.

2.4.2 Nucleation kernel

Up to date, a limited number of nucleation kernels have been proposed based on the mechanism of nucleation discussed in section 2.2.1. For population balance model, a brief summary of the nucleation kernels is given in Table 2.1. A nucleation kernel based on the immersion nucleation mechanism is proposed [91, 92] and should be very popular in population balance formulating. In this kernel, the binder droplet size is bigger than the particle size and one droplet can form one nucleus. When the spray droplets dry entirely before they hit any other particles, they do not contribute to growth, but to nucleation [82].

Table 2.1 Summary of nucleation kernels in literature

Nucleation kernel	Comments	reference
$B = A_0 Q e^{\lambda/RT}$ $\lambda = \begin{cases} W_A - W_{CL}, & D_d \approx D_p \\ W_A - W_{CS}, & D_d \gg D_p \end{cases}$	A_0: adjustable parameter, Q: liquid binder spray rate, R: ideal gas constant, T: operating temperature, λ is the spreading coefficient, W_A:work of adhesion. W_{CS}, W_{CL}: works of cohesion for a solid and liquid, respectively. Suitable for immersion mechanism nucleation.	[91, 92]

$B(t, L_0) = \frac{b\Phi}{\frac{1}{6}\pi L_0^3}\delta(L - L_0)$	b: spray fraction contribute to nucleation, Φ: spray solute volume flow, L_0: nuclei size, δ: Dirac delta function	[82]

2.4.3 Growth kernel

In fluidized bed granulation, the growth of the particles is mainly caused by the layering mechanism. However, during the fluidized bed granulation, aggregation of particles is considered as dominated process and the growth is rarely studied by researchers, hence, it is usually not included in population balance modeling of granulation process. To the author's knowledge, there is only one growth kernel applied for the population balance modeling of the fluidized bed spray granulation [82], given as follows:

$$G = \frac{2(1-b)\Phi}{\pi \int_0^\infty nL^2 dL} \tag{2.2}$$

Where, b is the spray binder fraction that contributes to nucleation, Φ is spray solute volume flow, L is the particle diameter.

2.4.4 Aggregation kernel

Aggregation kernel is a measure of the successful coalescence frequency between particles. The aggregation kernel can mainly be determined by two factors: collision frequency of particles, and collision efficiency [13, 93]. The collision frequency function mainly deals with how many collisions the granules of a specific size are exposed to per unit time and the collision efficiency function deals with whether collision will cause coalescence or rebound.

For last decades, aggregation kernel is investigated extensively and kernels of different forms are given in literatures [24, 76, 78, 80, 94-100]. A summary of the proposed aggregation kernels is presented in Table 2.2.

For simplicity, size-independent aggregation kernel is proposed and applied [95, 100]. Some empirical kernels are proposed to study the particle size-dependent coalescence and have been very popular for a long time [80, 94, 96, 98, 99]. Recently, some theoretical kernels which can be used to study the hydrodynamics in the fluidized bed

granulator becomes more and more popular, such as the equipartition of kinetic energy kernel (EKEK) and equipartition of translational momentum kernel (ETMK) [24, 89]. In addition, some kernels based on the coalescence theory, are developed to describe whether the two colliding particles can coalescence [76, 78, 97, 101].

Table 2.2 A summary of proposed aggregation kernels in the literature

Models	Comments	References
$\beta = \beta_0$	Size-independent kernel, β_0: constant.	Kapur and Fuerstenau [95]
$\beta = \beta_0 \frac{(u+v)^a}{(uv)^b}$	Empirical kernel, β_0: coaleacence rate constant, depending on process-realated variables, such as moisture content, material properties, *u*, *v*: particle volume.	Kapur [94]
$\beta = \beta_0 \frac{(u^{2/3}+v^{2/3})}{1/u+1/v}$	Empirical kernel, *u*, *v*: particle volume, β_0: determined from experimental data.	Sastry [96]
$\beta = \alpha(u+v)$	Empirical kernel, *u*, *v*: particle volume, α: constant.	Golovin [99]
$\beta = \alpha \frac{(u-v)^2}{(u+v)}$	Empirical kernel, *u*, *v*: particle volume, α: constant.	Golovin [99]
$\beta = \begin{cases} k_1, t < t_s \\ k_2(u+v), t > t_s \end{cases}$	Theoretical kernel, k_1, k_2: constant, t_s: switching time, *u*, *v*: particle volume.	Adetayo et al. [76]
$\beta = \begin{cases} k, w < w^* \\ 0, w > w^* \end{cases}$ $w = \frac{(u+v)^a}{(uv)^b}$	Theoretical kernel, k, a, b: constants, *u*, *v*: particle volume, w^*: critical average granule volume.	Adetayo and Ennis [97]
$\beta = \beta_0(1/u+1/v)^{1/2}(u^{1/3}+v^{1/3})^2$ $\beta = \beta_0\left(u^{-1/3}+v^{-1/3}\right)(u^{1/3}+v^{1/3})$	Empirical kernel, *u*, *v*: particle volume, β_0: determined from experimental data..	Friedlander [102]
$\beta = \beta_0 \int_{-\infty}^{St^*} f(\Phi, t) d\Phi$	Empirical kernel, where, $St^* = \alpha_1(1 + e^{t-\alpha_2})$, $f(\Phi, t)$ is the discrete probability density function, α_1, α_2: constants, β_0: determined from experimental data.	Cryer [80]

$\beta = \begin{cases} \beta_1 & Types\ I\ and\ II\ without\ permanent\ deformation \\ \beta_2 & Type\ II\ with\ permanent\ deformation\ rebound \\ 0 & \end{cases}$	Theoretical kernel, β_1, β_2: constants, The aggregation kernel is different constant according to the coalescence type.	Liu and Litster [78]
$\beta = \beta_0(t)(l_i + l_j)^2\sqrt{\frac{1}{l_i^3} + \frac{1}{l_j^3}}$ $\beta = \beta_0(t)(l_i + l_j)^2\sqrt{\frac{1}{l_i^6} + \frac{1}{l_j^6}}$	Theoretical kernel, Where, $\beta_0(t) = \psi g_{ij}\sqrt{\frac{3\theta_s}{\rho}}$, θ_s: granular temperature, g_{ij}: particle radial distribution, ρ: particle density, ψ: successful factor for aggregation.	Hounslow [89], Goldschmidt [24]
$\beta = \beta_0(t)(l_i + l_j)^3$ $\beta_0(t) = \beta_A + \beta_B(t - 480)$	Empirical kernel, l_i, l_j: particle diameter, β_A, β_B: constant, large-large particle collision is favored.	Hounslow [89]
$\beta = \begin{cases} k_1 & stage\ I \\ k_2(u * v) & stage\ II \end{cases}$	Theoretical kernel, k_1, k_2: constants, u, v: particle volume.	Papiya Roy et al. [101]

2.4.5 Breakage kernel

A breakage kernel includes the breakage selection rate, which represents the particle fraction breakup per unit time, and the fragments size distribution function, which describes the distribution of the fragments from the breakage of parent particles.

2.4.5.1 Breakage selection rate

Comparing with aggregation, breakage in the fluidized bed granulation received less research. Based on the theory for particle breakage described in the section 2.2.3, several models for breakage selection rate have been proposed [67, 81, 89] and summarized in Table 2.3.

Table 2.3 Breakage selection rates in literature

Models	Comments	References
$S(t, l) = S_0$	Constant breakage selection rate, S_0: constant.	Tan et al. [67]
$S(t, l) = S_0 l^q$	Proportional to the granule size to the power q, S_0: constant, l: particle diameter.	Tan et al. [81], Kumar et al. [100], Soos et al. [103]
$S(t, l) = S_A exp(-\frac{t-480}{20})$	Time-dependent selection rate, S_A: constant.	Hounslow et al. [89]

$S(t,l)=\left(\frac{4}{15\pi}\right)^{\frac{1}{2}}Gexp(-\frac{B}{G^2l})$	*B*: adjustable parameter, *G*: shear rate, l: particle diameter.	Soos, Sefcik et al. [103]

Among the above kernels, the exponential breakage is the most popular and implemented by most researchers [89, 90, 103]. Through the analysis, the size and time independent breakage selection rate is shown to be very effective [67, 81]. In addition, the powder law kernel is another choice of breakage selection model being frequently used [81, 100, 103].

2.4.5.2 Fragments size distribution function

Similarly, for the fragments size distribution function, a summary is given in Table 2.4. From the fragments size distribution function, fragmentation and uniform breakage are found to be frequently used function [81, 90]. Recently, several combination forms of fragment distributions are also proposed and applied into the fluidized bed granulation [81, 89]. In addition to the empirical models, some breakage selection functions that can account for process or material properties to determine breakage rate have also been developed [41, 104].

Table 2.4 Fragments size distribution functions in literature

Models	Comments	References
$b(L,\lambda)=N_b(\lambda)f_0(L)$ $f_0(x)=\frac{1}{\sqrt{2\pi}\sigma_0}exp\left[-\frac{(x-\bar{l}_0)^2}{2\sigma_0^2}\right]$	Fragmentation, the granules break up into primary particles, where $N_b(\lambda)$ is the number of fragments and $f_0(L)$ is the primary particle size distribution. λ and L are particle diameters before and after breakage (the same symbol is used in the following kernels).	Tan et al. [81]
$b(L,\lambda)=f_0(L)+f_0\left(\sqrt[3]{\lambda^3-L^3}\right)$ $f_0(x)=\frac{1}{\sqrt{2\pi}\sigma_0}exp\left[-\frac{(x-\bar{l}_0)^2}{2\sigma_0^2}\right]$	Attrition breakage, a single particle of size comparable to primary particles is formed and the original granule very slightly reduced in size.	Tan et al. [81]
$b(L,\lambda)=\frac{6L^2}{\lambda^3}$	Uniform binary breakage, fragments of any size can be formed.	Tan et al. [81]
$b(L,\lambda)=0.484b_{f,1}(L,\lambda)+0.516b_{f,2}(L,\lambda)$	Two kinds of fragments are formed, where, $b_{f,1}$, $b_{f,2}$ both have following form but	Hounslow et al. [89], Tan et al.

	different mean size $\bar{l}_{gv}$: $b_f(x,l) = \left(\frac{l}{x}\right)^3 \frac{\frac{1}{x\sqrt{\pi/2}ln\sigma_g} exp\left[-\left(\frac{ln\, x/\bar{l}_{gv}}{\sqrt{2}ln\sigma_g}\right)^2\right]}{1+erf\left[\frac{ln\, x/\bar{l}_{gv}}{\sqrt{2}ln\sigma_g}\right]}, \bar{l}_{gv}$ and σ_g are needed to fit.	[81]
$b(L,\lambda) = zf_0(L)\frac{\lambda^3}{\lambda_0(\lambda_0^2+3\sigma_0^2)} + (1-z)\frac{6L^2}{\lambda^3}$	Two kinds of fragments are formed, z is the fraction of granules to form small fragments, while $(1-z)$ shows the remaining portion of granules to form two random fragments, σ_0: standard deviation of the primary particle size distribution.	Tan et al. [81]

2.4.6 Numerical Solutions of population balance model

Due to the complexity of the structure of the population balance equation, obtaining the analytical solution of population balance equations (PBEs) becomes nearly impossible but only for several specific cases with the most idealized situations. Therefore, numerical methods are often utilized to solve a population balance equation and there exist many numerical methods in the literature as attempts to solve different types of the population balance equations. Usually, these numerical methods can be mainly divided into three categories: discrete method, method of moments, and Monte Carlo (MC) method. To date, several review literatures of available numerical methods are presented [88, 105, 106].

2.4.6.1 Discrete method

The discrete method is to approximate the particle size distribution through discretizing the internal coordinate of particles into a set of classes. On every size interval, the population balance equation is solved. In the open literature, several studies focusing on the application of discrete method into particulate process are published [89, 106-110].

A classical discrete method to solve the population balance equation [89, 107], is presented as:

$$\frac{dN_i}{dt} = B_0\delta(L_i - L_0)$$ Nucleation

$$+\frac{2G}{(1+r)L_i}\left(\frac{r}{r^2-1}N_{i-1} + N_i - \frac{r}{r^2-1}N_{i+1}\right)$$ Growth

$$+N_{i-1}\sum_{j=1}^{i-2} 2^{j-i+1}\beta_{i-1,j}N_j + \frac{1}{2}\beta_{i-1,i-1}N_{i-1}^2 - N_i\sum_{j=1}^{i-1} 2^{j-i}\beta_{i,j}N_j - N_i\sum_{j=i}^{n_{eq}}\beta_{i,j}N_j$$

Aggregation

$$-S_iN_i + \sum_{j=i}^{n_{eq}} b_{i,j}S_jN_j$$ Breakage

(2.3)

Where, N_i represents the number of particles in the size range of (L_i, L_{i+1}), also called discrete number density, and n_{eq} is the total number of intervals, r is the ratio of the upper and lower limits of size for any size interval: $r = \frac{L_{i+1}}{L_i}$ and $\beta_{i,j}$ is the coalescence kernel between particles from *ith* and *jth* size interval, and S_i is the selection rate for interval i and $b_{i,j}$ is the number of fragments from interval j that are assigned to interval i.

Normally, a geometric ratio of $r = \sqrt[3]{2}$ was used to discretize the particle size [89, 111]. However, finer grid of particle size is needed to satisfy the prediction accuracy of particle size distribution. Lister et al. [108] extended the discrete method of Hounslow to a more general form through constructing a geometric series with the ratio of particle volume $\frac{V_{i+1}}{V_i} = 2^{1/q}$ with an adjustable factors q (q is an integer, positive number). Therefore, more particle size intervals can be obtained through increasing the value of q. But, the high accuracy by a finer grid comes companied with a high computation cost. To avoid the limitation of grid, the fixed pivot technique and moving pivot technique that can adopt arbitrary grid are proposed by Kumar & Ramkrishna [109, 110], which can guarantee conservation of any two required integral properties of the distribution and has been validated to be excellent in predicting pure breakage.

In discrete method, the population balance equation is solved on every individual size

interval. Therefore, an advantage of this technique is that the approach directly presents the result of the particle size distribution. On the other hand, in order to achieve an excellent accuracy, a large number of intervals are needed, which means a disadvantage of huge computation cost, especially for cases with wide particle size distribution.

2.4.6.2 Method of moment

The method of moment is a technique to solve the population balance in terms of moment, which is defined as:

$$m_k(t) = \int_0^{+\infty} n(L;t)\, L^k dL \tag{2.4}$$

Where, *k* is the order of the moment and *n* is the length number density in terms of particle size *L*.

The concept of solving the population balance equation using moment method has been firstly proposed by Hulburt and Katz [112]. By multiplying L^k and integrating for *L*, the population balance equation is transferred into the form of moment. The general population balance equation in terms of particle length is given as follows:

$$\frac{dm_k(t)}{dt} = B_0 0^k \qquad \text{Nucleation}$$

$$+ \int_0^{\infty} kL^{k-1} G(t,L) n(t,L) dL \qquad \text{Growth}$$

$$+ \frac{L^2}{2} \int_0^{\infty} L^k \int_0^{L} \frac{\beta\left(t,(L^3-\lambda^3)^{\frac{1}{3}},\lambda\right)}{(L^3-\lambda^3)^{\frac{2}{3}}} n\left(t,(L^3-\lambda^3)^{\frac{1}{3}}\right) n(t,\lambda) d\lambda\, dL$$

$$- \int_0^{\infty} L^k n(t,L) \int_0^{\infty} \beta(t,L,\lambda)\, n(t,\lambda) d\lambda dL \qquad \text{Aggregation}$$

$$+ \int_0^{\infty} L^k \int_0^{\infty} S(t,\lambda) b(t,L|\lambda) n(t,\lambda)\, d\lambda dL - \int_0^{k} L^k S(t,L) n(t,L) dL \qquad \text{Breakage}$$

(2.5)

Where, $n(t,L)$ is the number density function in terms of the particle diameter L, $\beta(t,L,\lambda)$ is the coalescence kernel, while $S(t,L)$ and $b(t,L|\lambda)$ are breakage selection rate function and fragments size distribution function, respectively. $G(t,L)$ is the size dependent growth rate, and B_0 is the nucleation rate.

If the equation (2.5) is solved directly, this is called standard method of moment (SMM) [113-117]. Comparing with discrete method, the main advantage of the SMM is that the number of moments required is very small, however, the closure problem of the equation in terms of moment can only be solved for some size-independent growth rates and aggregation kernels while for any breakage kernels impossible [118]. In fact, it is only in above cases that the SMM formulation of the problem can be expressed in terms of a closed set of kernels. Based on this situation, the quadrature method of moment (QMOM) is proposed by McGraw [118] for modeling the size evolution and has been developed by a lot of researchers [90, 119-124]. In this method, a quadrature approximation is employed:

$$m_k = \int_0^{+\infty} n(L) L^k dL \approx \sum_{i=1}^{N_q} w_i L_i^k \tag{2.6}$$

Where, weights (w_i) and abscissas (L_i) are used to approximate the moments and are determined through a Product-Difference (PD) algorithm from the lower-order moments. Through equation (2.6), it can be seen that $2N_q$ moments are needed to calculate the weights and abscissas. After the QMOM is used, the following population balance equation is given [90, 121]:

$$\begin{aligned}
&\frac{\partial m_k}{\partial t} = B_0 0^k && \text{Nucleation}\\
&+k \sum_{i=1}^{N_q} w_i L_i^{k-1} G(L_i) && \text{Growth}\\
&+\frac{1}{2}\sum_{i=1}^{N_q} w_i \sum_{j=1}^{N_q} w_j \left(L_i^3 + L_j^3\right)^{\frac{k}{3}} \beta(L_i, L_j) - \sum_{i=1}^{N_q} L_i^k w_i \sum_{j=1}^{N_q} w_j \beta(L_i, L_j) && \text{Aggregation}\\
&+\sum_{i=1}^{N_q} w_i S(L_i) \int_0^{\infty} L^k b(L, L_i) dL - \sum_{i=1}^{N_q} w_i L^k S(L_i) && \text{Breakage}
\end{aligned} \tag{2.7}$$

Where, N_q is the number of nodes of the quadrature approximation, while the other variables have the same meaning with equation (2.5).

In fact, the particle size distribution can also be obtained by the QMOM method, through doing the reconstruction from the moments. Assuming the particle size

distribution is given as:

$$n(l) = exp\left(\sum_{i=0}^{N-1} A_i l^i\right) \tag{2.8}$$

Where, N is the number of moments used to do reconstruction. Then, the coefficient A_i can be calculated by equating the moments to the moments calculated using equation (2.8) as follows:

$$m_k = \int_0^{\infty} l^k exp\left(\sum_{i=0}^{N-1} A_i l^i\right) d(l), \quad k = 0,1,\dots,N-1 \tag{2.9}$$

The QMOM method provides an attractive alternative to the SMM method for size dependant growth, aggregation and breakage. Rather than an exact particle size distribution, QMOM gives a series of N_q weights and N_q abscissas that can be calculated from the first 2N lower order moments. Its advantage is that there are fewer variables to lead to a small computation cost [90]. However, there are two main disadvantages of QMOM: (1) if applied to multivariate distributions it loses simplicity and efficiency, and (2) by tracking only the moments of the size distribution, it does not represent realistically poly-disperse systems with strong coupling between the internal coordinates and phase velocities [120]. To solve these problems, the direct quadrature method of moment (DQMOM) was proposed by Marchisio et al. [120] by tracking directly the variables appearing in the quadrature approximation, rather than tracking the moments of the particle size distribution. Both the QMOM and DQMOM methods have a drawback that a full reconstruction of distribution is not possible. Using the sectional quadrature method of moment (SQMOM) developed by Attarakih and co-workers [125], the reconstruction problems can be well addressed. In this technique, the particle distribution is divided into sections where the classical QMOM method is applied. Therefore, the SQMOM assembles the advantages of both the SQMOM and QMOM methods.

2.4.6.3 Monte Carlo method

The Monte Carlo (MC) method is a numerical simulation technique for solving problems by means of stochastic sampling [126]. This technique is generally applied to

analyze physical systems where experiment is difficult or where population balance equations cannot be solved [127]. As an alternative to solve population balance equation, Monte Carlo approach can be applied to the particulate system [126, 128].

Usually, two general categories of Monte Carlo methods can be distinguished: time-driven MC method [128-130] and event-driven MC method [131-133]. A big difference between the two types of MC method is whether the time-step is chosen before the event. In the former approach, a time interval is initially defined and Monte Carlo is used to decide which or how many events will be realized within the time-step [128, 130]. By contrast, in event-driven MC method, the time between events is calculated on the basis of the known event probability. Therefore, this method does not need explicit time discretization and has advantage that the time step can adjust itself to the rate of the process.

The Monte Carlo methods can also be classified by whether the total volume or particle number is constant in the simulation: constant-volume MC method [132] and constant-number MC method [134-136]. In the constant volume MC method, when a sufficient number of simulation particles is used, this method is validated to have capability to well minimize statistical errors [132]. However, if the simulation volume is kept constant, in the simulation total particle number will increase or decrease, which obviously influence the accuracy of the Monte Carlo method and the computation time. To solve this problem, the constant number MC method is developed [134-136], in which, the number of particle is kept constant. This technique amounts to expanding or contracting the physical volume represented by the simulation so as to continuously maintain a reaction volume that contains constant number of particles [134].

Comparing with discrete method, the MC method can well deal with the following problems: (1) there is no information about the history of each particle, (2) when multidimensional systems have to be dealt with, the sectional representation results in very complex algorithm [132]. Another obvious advantage is that discretization is unnecessary since a sample of the population is simulated explicitly. However, if high accuracy is needed, the simulation number should be increased, which may also result in high computation cost.

2.5 Combination of computational fluid dynamic (CFD) and PBM for study of fluidized bed granulation

2.5.1 Hydrodynamics study

Although a large number of experimental studies have been carried out regarding the quantification of gas and particle flow regime identification for different process parameters and physical properties, the complex hydrodynamics of the fluidized bed granulation are not well understood due to complicated phenomena such as particle-particle, particle-droplet and particle-bubble interactions. Recently, with the development of high speed computers, the computational fluid dynamics (CFD) was reported as an emerging technique and holds great potential in providing detailed information of the complex gas-solid fluid dynamics [137-141].

In general, there are two different categories of CFD models used for simulating the gas-particle fluid dynamics within fluidized bed granulator: the Eulerian model and the Lagrangian models.

The Eulerian-Eulerian multiphase flow model considers each phase as separate interpenetrating and interacting continua in the shared computational domain using modified Navier-Stokes equation, while the volume of each phase cannot be occupied by another phase. In this scheme, the solid particles are generally considered to be identical having a representative diameter and density. The interaction forces between the phases are simulated as source terms in the equations describing each separate phase. The advantage of this approach is that full-scale process simulation with high solid loading can be performed, since the computational cost is not expensive and two-way coupling is relatively easy to implement. As a result, the CFD simulation based on the Eulerian-Eulerian framework is popularly adopted to perform gas-solid multiphase flow investigation of the fluidized bed granulator [140-144].

A disadvantage is particle-particle interaction must be modeled through an averaged solid-stress applied to the dispersed phase. To describe the particulate phase stress in the Eulerian-Eulerian approach, the kinetic theory of granular flow (KTGF) has been used

[145-147], which was developed to model the motion of a dense collection of nearly elastic spherical particles [148, 149]. The application of kinetic theory to model the motion of a dense collection of nearly elastic spherical particles is based on an analogy to the kinetic theory of dense gas. A granular temperature is defined to represent the specific kinetic energy of the velocity fluctuation or the translational fluctuation energy resulting from the particle velocity fluctuations. In granular flow, particle velocity fluctuations about the mean are assumed to result in collisions between particles being swept along together by the mean flow. The granular particle temperature equation can be expressed in terms of production of fluctuation by shear, dissipation by kinetic and collisional shear flow, dissipation due to inelastic collision with molecules, and dissipation due to interaction with the fluid [150].

The Lagrangian model solves equations of motion for each particle taking into account particle-particle collisions and the forces acting on the particle by the gas, which allows the effects of various particle properties on the motion of fluid to be studied and attracted lots of researches' attention [151-156]. However, due to the velocity and corresponding trajectory are solved for each individual particle, the computation cost of Lagrangian model is intensive. Due to computational limitations, the Lagrangian model is still not possible to track more than about a million particles within reasonable simulation time, even though recent advances in computation seem to be very promising [157]. Therefore, when the number of particles is large, as is the case in fluidized beds, the computational requirements can force the Eulerian-Eulerian models to be preferred selection.

2.5.2 Eulerian-Eulerian multi-phase flow model (EEMFM)

The general Eulerian-Eulerian multi-phase flow model utilized to simulate granular flow in a fluidized bed granulator and constitutive equations are presented in this section.

2.5.2.1 Governing equations

As described early, an Eulerian-Eulrian model considers each phase as interpenetrating

continua and the volume of each phase cannot be occupied by another phase, which introduces the concept of phasic volume fraction, denoted as α_q. The sum of the space fraction occupied by each of the phase equals one. The phasic volume fraction equation is given by:

$$\sum_{q=1}^{n\_p} \alpha_q = 1 \tag{2.10}$$

Where n_p represents the total number of phases and α_q represents the volume fraction of each phase, q (q=g, gas phase and q=s, solid phase).

The effective density of phase q is

$$\hat{\rho}_q = \alpha_q \rho_q \tag{2.11}$$

Where ρ_q is the physical density of phase q.

The Eulerian-Eulerian model allows for incorporation of multiple secondary solids phases. The conservation of mass and momentum are satisfied, respectively, for each phase. Thus, the Eulerian-Eulerian model solves a set of n continuity and momentum equations, which forces this approach to be one of the most complex and computation costing multiphase model.

Conservation of mass

The continuity equation for phase q is

$$\frac{\partial(\alpha_q \rho_q)}{\partial t} + \nabla \cdot \left(\alpha_q \rho_q \vec{v}_q\right) = \sum_{p=1}^{n\_p} \left(\dot{m}_{pq} - \dot{m}_{qp}\right) + S_q \tag{2.12}$$

Where n_p is the number of phases and $\dot{m}_{pq}$ characterizes the mass transfer form phase p to phase q, and $\dot{m}_{qp}$ characterizes the mass transfer from phase q to phase p. S_q means a mass source term for phase q, which is zero by default.

For a batch mode fluidized bed granulation with no mass transfer between gas and solid, the continuity equations for phase q (q=g for gas phase, q=s for solid phase) can be

written as

$$\frac{\partial(\alpha_q \rho_q)}{\partial t} + \nabla \cdot \left(\alpha_q \rho_q \vec{v}_q\right) = 0 \tag{2.13}$$

Conservation of momentum

The momentum balance equations for the gas phase can be written as:

$$\frac{\partial(\alpha_g \rho_g \vec{v}_g)}{\partial t} + \nabla \cdot \left(\alpha_g \rho_g \vec{v}_g \vec{v}_g\right) = -\alpha_g \nabla p + \nabla \cdot \bar{\bar{\tau}}_g + \alpha_g \rho_g \vec{g} +$$

$$\sum_{s=1}^{n\_s}\left(K_{gs}\left(\vec{v}_s - \vec{v}_g\right) + \dot{m}_{sg}\vec{v}_{sg} - \dot{m}_{gs}\vec{v}_{gs}\right) + \left(\vec{F}_g + \vec{F}_{lift,g} + \vec{F}_{vm,g}\right) \tag{2.14}$$

Where n_s represents the number of solid phases. The first term on the left hand side of equation (2.14) means the unsteady acceleration and the second term represents the convective acceleration of the flow. The first term on the right hand of momentum equation accounts for pressure changes, where p is the pressure shared by all phases. The second term on the right hand side is stress-strain tensor term, given by

$$\bar{\bar{\tau}}_g = \alpha_g \mu_g \left(\nabla \vec{v}_g + \nabla \vec{v}_g^T\right) \tag{2.15}$$

Where μ_g is the viscosity of gas phase g. The bulk viscosity of a fluid is a measure of the difference between the thermodynamic mechanical pressures and for a Newtonian fluid (e.g. air), the bulk viscosity is set to zero in what is referred to as the Stokes' assumption. $\nabla \vec{v}_g^T$ is the transpose of the velocity gradient, and $\bar{\bar{I}}$ is the identity matrix. The third term on the right hand side of equation (2.14) means the effect of gravitational force. The fourth term includes the interaction force between gas and solid phase, and effect of mass transfer between phases. The final term on the right hand side includes an external body force $\vec{F}_g$, a lift force, $\vec{F}_{lift,g}$, and a virtual mass force, $\vec{F}_{vm,g}$.

For the study in this thesis, there are one gas phase and one solid phase, and the mass transfer terms, external body force, lift force, and virtual mass force terms are all zero, simplifying the momentum equation for the gas phase to the following form:

$$\frac{\partial(\alpha_g\rho_g\vec{v}_g)}{\partial t} + \nabla\cdot\left(\alpha_g\rho_g\vec{v}_g\vec{v}_g\right) = -\alpha_g\nabla p + \nabla\cdot\bar{\bar{\tau}}_g + \alpha_g\rho_g\vec{g} + K_{gs}\left(\vec{v}_s - \vec{v}_g\right) \quad (2.16)$$

The conservation of momentum for the s^{th} solid phase is given

$$\frac{\partial(\alpha_s\rho_s\vec{v}_s)}{\partial t} + \nabla\cdot(\alpha_s\rho_s\vec{v}_s\vec{v}_s) = -\alpha_s\nabla p - \nabla p_s + \nabla\cdot\bar{\bar{\tau}}_s + \alpha_s\rho_s\vec{g} +$$

$$\sum_{p=1}^{n\_p}\left(K_{ps}\left(\vec{v}_p - \vec{v}_s\right) + \dot{m}_{ps}\vec{v}_{ps} - \dot{m}_{sp}\vec{v}_{sp}\right) + \left(\vec{F}_s + \vec{F}_{lift,s} + \vec{F}_{vm,s}\right) \quad (2.17)$$

Where, p_s is the s^{th} solid phase pressure, K_{ps} is the interaction force coefficient between the gas phase or solid phase p and the s^{th} solid phase. All other terms have similar definitions as those in equation (2.14). For study in this thesis, there is a single solid phase and no mass transfer between gas and solid phase, the solid phase momentum equation simplifies to the following form

$$\frac{\partial(\alpha_s\rho_s\vec{v}_s)}{\partial t} + \nabla\cdot(\alpha_s\rho_s\vec{v}_s\vec{v}_s) = -\alpha_s\nabla p - \nabla p_s + \nabla\cdot\bar{\bar{\tau}_s} + K_{gs}\left(\vec{v}_g - \vec{v}_s\right) + \alpha_s\rho_s\vec{g} \quad (2.18)$$

Where, the solid-phase stress tensor is given by:

$$\bar{\bar{\tau}}_s = \alpha_s\mu_s(\nabla\vec{v}_s + \nabla\vec{v}_s^T) + \alpha_s(\lambda_s - \frac{2}{3}\mu_s)\nabla\cdot\vec{v}_s\bar{\bar{I}} \quad (2.19)$$

2.5.2.2 Kinetic theory of granular flow (KTGF)

The multi-phase flow model requires constitutive equations to describe the rheology of the solid phase. When the particle motion is dominated by collision interaction in sufficiently dense suspensions, the concepts from fluid kinetic theory can be introduced to describe the effective stresses in the solid phase resulting from particle streaming collision contribution. Equivalent to the thermodynamic temperature for gases, the granular temperature can be introduced as a measure for the energy of the fluctuating velocity of the particles [158]. The granular temperature for solid phase *s*, Θ_s is defined as

$$\Theta_s = \frac{1}{3}\overline{v_s' v_s'} \quad (2.20)$$

Where v_s' is the particle fluctuating velocity of s^{th} solid phase.

A transport equation of granular temperature for the s^{th} solid phase is proportional to the kinetic energy of the random motion of the particles. The transport equation derived from kinetic theory according to Ding and Gidaspow's model [159] is give as follows:

$$\frac{3}{2}\left[\frac{\partial(\alpha_s\rho_s\Theta_s)}{\partial t}+\nabla\cdot(\alpha_s\rho_s\vec{v}_s\Theta_s)\right]=\left(-p_s\bar{\bar{I}}+\bar{\bar{\tau}}_s\right):\nabla\vec{v}_s-\nabla\cdot\left(k_{\Theta_s}\nabla\Theta_s\right)-\gamma_{\Theta_s}+\varphi_{ps} \quad (2.21)$$

Where $\left(-p_s\bar{\bar{I}}+\bar{\bar{\tau}}_s\right):\nabla\vec{v}_s$ is the generation of energy by the solid stress tensor, $k_{\Theta_s}\nabla\Theta_s$ represents the diffusion of energy, with the diffusion coefficient for granular energy k_{Θ_s} is given by Syamlal et al. [160], which is also used in the CFD study of this thesis:

$$k_{\Theta_s}=\frac{15\rho_s d_s\alpha_s\sqrt{\pi\Theta_s}}{4(41-33\eta)}\left[1+\frac{12}{5}\eta^2(4\eta-3)g_0\alpha_s+\frac{16}{15\pi}(41-33\eta)\eta g_0\alpha_s\right] \quad (2.22)$$

Where,

$$\eta=\frac{1}{2}(1+e_s) \quad (2.23)$$

Where e_s is the coefficient of restitution for particle collision.

An alternative expression of the diffusion coefficient for granular energy is developed by Gidaspow et al. [161]:

$$k_{\Theta_s}=\frac{150\rho_s d_s\sqrt{\pi\Theta_s}}{384(1+e_s)g_0}\left[1+\frac{6}{5}(1+e_s)g_0\alpha_s\right]^2+2\rho_s d_s\alpha_s^2(1+e_s)g_0\sqrt{\frac{\Theta_s}{\pi}} \quad (2.24)$$

The collisional dissipation of energy, γ_{Θ_s}, represents the rate of energy dissipation within the s^{th} solid phase due to collisions between particles. This term is modeled using the correlation by Lun et al. [162], which is utilized in the CFD study of this thesis:

$$\gamma_{\Theta_s}=\frac{12(1-e_s^2)g_0}{d_s\sqrt{\pi}}\rho_s\alpha_s^2\Theta_s^{1.5} \quad (2.25)$$

An alternative option of γ_{Θ_s} is developed by Gidaspow et al. [158] and given as

$$\gamma_{\Theta_s} = 3(1-e_s^2)^2\alpha_s^2\rho_s g_0\Theta_s\left(\frac{4}{d_s}\sqrt{\frac{\Theta_s}{\pi}} - \nabla\cdot\vec{v}_s\right) \quad (2.26)$$

The transfer of the kinetic energy of random fluctuation in particle velocity from the s^{th} solid phase to the p^{th} fluid or solid phase is represented by φ_{ps}

$$\varphi_{ps} = -3K_{ps}\Theta_s \quad (2.27)$$

In this thesis, an algebraic equation, which comes from a simplified complete granular temperature transport equation by neglecting convection and diffusion terms, is utilized as follows [160]:

$$0 = \left(-p_s\bar{\bar{I}} + \bar{\bar{\tau}}_s\right):\nabla\vec{v}_s - \gamma_{\Theta_s} + \varphi_{ps} \quad (2.28)$$

2.5.2.3 Constitutive equations

Solid pressure

For granular flows in the compressible regime, i.e. where the solid volume fraction is less than it maximum allowed value, a solid pressure is calculated independently and used for the pressure gradient term ∇p_s in the momentum conservation equation (2.17). The solid pressure represents the particle normal forces due to particle-particle interaction, which is composed of a kinetic term and a collisional term. The kinetic term represents the influence of particle translation, whereas the collisional term accounts for the momentum transfer by collision between particles. The solid pressure is given as follows:

$$p_s = \alpha_s\rho_s\Theta_s[1 + 2g_0\alpha_s(1+e_s)] \quad (2.29)$$

The above solid pressure (equation (2.29)) is selected in the CFD study of this thesis, while there exist other formulations [160]

$$p_s = 2g_0\alpha_s^2(1+e_s)\rho_s\Theta_s \quad (2.30)$$

And [163]

$$p_s = \alpha_s \rho_s \Theta_s \left[(1 + 4 g_0 \alpha_s) + \frac{1}{2} \left[(1 + e_s)\left(1 - e_s + 2\mu_{fric}\right) \right] \right] \tag{2.31}$$

Solid bulk viscosity

The solid bulk viscosity accounts for the resistance of the granular particles to compression and expansion. It has the following form from Lun et al. [162] and used in this thesis:

$$\lambda_s = \frac{4}{3} \alpha_s \rho_s d_s g_0 (1 + e_s) \sqrt{\frac{\Theta_s}{\pi}} \tag{2.32}$$

Radial distribution function

The radial distribution function, g_0 is a correction factor that modifies the probability of collision between particles when the solid granular phase become dense. This function may also be interpreted as the non-dimensional distance between spheres:

$$g_0 = \frac{s + d_p}{s} \tag{2.33}$$

Where *s* is the distance between particles. From equation (2.33) it can be seen that for a dilute solid phase $s \to \infty$, therefore $g_0 \to 1$. In the dense solid phase where $s \to 0$, $g \to \infty$. In the literature, there are several formulations for the radial distribution function as follows and equation (2.34) is utilized in the CFD study of this thesis.

For case with one solid phase, use [164]

$$g_0 = \left[1 - \left(\frac{\alpha_s}{\alpha_{smax}} \right)^{1/3} \right]^{-1} \tag{2.34}$$

For case with more than one solid phase

$$g_{0,ll} = \left[1 - \left(\frac{\alpha_s}{\alpha_{smax}} \right)^{1/3} \right]^{-1} + \frac{1}{2} d_l \sum_{k=1}^{N} \frac{\alpha_k}{d_k} \tag{2.35}$$

Where

$$\alpha_s = \sum_{k=1}^{N} \alpha_k \tag{2.36}$$

And *k* is solid phase only.

Another formulation developed by [165]

$$g_{0,ll} = \frac{1}{\left(1-\frac{\alpha_s}{\alpha_{smax}}\right)} + \frac{3}{2} d_l \sum_{k=1}^{N} \frac{\alpha_k}{d_k} \tag{2.37}$$

Also available [163]

$$g_{0,ll} = \frac{1+2.5\alpha_s+4.59\alpha_s^2+4.52\alpha_s^3}{\left(1-\left(\frac{\alpha_s}{\alpha_{smax}}\right)^3\right)^{0.678}} + \frac{1}{2} d_l \sum_{k=1}^{N} \frac{\alpha_k}{d_k} \tag{2.38}$$

The following equation [160] is available

$$g_{0,kl} = \frac{1}{(1-\alpha_s)} + \frac{3\left(\sum_{k=1}^{N} \frac{\alpha_k}{d_k}\right)}{(1-\alpha_s)^2 (d_l+d_k)} d_k d_l \tag{2.39}$$

Solid shear stresses

The solid stress tensor contains shear and bulk viscosities arising from particle momentum exchange due to translation and collision. A frictional component of viscosity can be included to account for the viscous-plastic transition that occurs when particle of a solid phase reach the maximum solid volume fraction. The solid shear stress includes collisional part, kinetic parts and frictional part as follows:

$$\mu_s = \mu_{s,col} + \mu_{s,kin} + \mu_{s,fri} \tag{2.40}$$

The collisional part of the shear viscosity is modeled as [160, 161]

$$\mu_{s,col} = \frac{4}{5} \alpha_s \rho_s d_s g_0 (1 + e_s) \sqrt{\frac{\Theta_s}{\pi}} \tag{2.41}$$

Two kinds of kinetic viscosity expressions are summarized as follows[160, 161]:

$$\mu_{s,kin} = \frac{\alpha_s \rho_s d_s \sqrt{\Theta_s \pi}}{6(3-e_s)} \left[1 + \frac{2}{5}(1+e_s)(3e_s-1)\alpha_s g_0\right] \quad (2.42)$$

$$\mu_{s,kin} = \frac{10\rho_s d_s \sqrt{\Theta_s \pi}}{96\alpha_s g_0 (1+e_s)} \left[1 + \frac{4}{5}\alpha_s g_0 (1+e_s)\right]^2 \quad (2.43)$$

The frictional viscosity is calculated as follows:

$$\mu_{s,fri} = \frac{p_s sin\theta}{2\sqrt{I_{2D}}} \quad (2.44)$$

Where, θ is the angle of internal friction and I_{2D} is the second invariant of the deviatoric stress tensor.

In the CFD study of this thesis, the combination of equation (2.41), (2.43) and (2.44) are used.

2.5.2.4 Gas-solid interaction

It can be seen in equation (2.16) and (2.18) that momentum exchange between gas and solid phase is based on the gas-solid interaction force coefficient K_{gs}. The gas-solid momentum exchange coefficient K_{gs} can be written in general form as:

$$K_{gs} = \frac{\alpha_s \rho_s f}{\tau_s} \quad (2.45)$$

Where f is defined depending on the different exchange-coefficient models, and τ_s is the particulate relaxation time and is defined as

$$\tau_s = \frac{\rho_s d_s^2}{18\mu_g} \quad (2.46)$$

Where d_s is the diameter of particles of phase *s*.

Teaters [166] presented a detailed summary of various drag model that are popular used for predicting gas-solid interactions which is given in Table 2.5. In this thesis, the momentum transfer between the gas and solid phases is described by the empirical drag law developed by Gidaspow et.al [158].

Table 2.5 Drag model correlations [166]

Drag model	K_{gs}	C_D
Richardson-Zaki [167]	$\frac{\rho_s \alpha_g g}{v_{r,s} \alpha_s^{n-1}}$	
Wen-Yu [168]	$\frac{3}{4} C_D \frac{\alpha_s \alpha_g \rho_g \lvert \vec{v}_s - \vec{v}_g \rvert}{d_s} \alpha_g^{-2.65}$	$\frac{24}{\alpha_g Re_s}\left[1 + 0.15\left(\alpha_g Re_s\right)^{0.687}\right]$
Gibilaro et al. [169]	$\left[\frac{17.3}{Re_s} + 0.336\right] \frac{\rho_g}{d_s} \lvert \vec{v}_s - \vec{v}_g \rvert \alpha_s \alpha_g^{-1.8}$	
Syamlal-O'Brien [170]	$\frac{3\alpha_s \alpha_g \rho_g}{4 \mathrm{v}_{\mathrm{r,s}}^2 d_s} C_D \left(\frac{Re_s}{v_{r,s}}\right) \lvert \vec{v}_s - \vec{v}_g \rvert$	$\left(0.63 + \frac{4.8}{\sqrt{\frac{Re_s}{v_{r,s}}}}\right)^2$
Arastoopour et al. [171]	$\left[\frac{17.3}{Re_s} + 0.336\right] \frac{\rho_g}{d_s} \lvert \vec{v}_s - \vec{v}_g \rvert \alpha_s \alpha_g^{-2.8}$	
Di Felice [172]	$\frac{3}{4} C_D \frac{\alpha_s \rho_g \lvert \vec{v}_s - \vec{v}_g \rvert}{d_s} \alpha_g^{-x}$	$\left(0.63 + \frac{4.8}{\sqrt{Re_s}}\right)^2$
Gidaspow [158]	$\begin{cases} \frac{3}{4} C_D \frac{\alpha_s \alpha_g \rho_g \lvert \vec{v}_s - \vec{v}_g \rvert}{d_s} \alpha_g^{-2.65}, & \alpha_g > 0.8 \\ 150 \left(\frac{\alpha_s (1-\alpha_g) \mu_g}{\alpha_g d_s^2}\right) + 1.75 \left(\frac{\rho_g \alpha_s \lvert \vec{v}_s - \vec{v}_g \rvert}{d_s}\right), & \alpha_g \le 0.8 \end{cases}$	$\frac{24}{\alpha_g Re_s}\left[1 + 0.15\left(\alpha_g Re_s\right)^{0.687}\right]$
Koch et al. [173]	$\frac{3}{4} C_D \frac{\alpha_s \alpha_g \rho_g \lvert \vec{v}_s - \vec{v}_g \rvert}{d_s}$	$12 \frac{\alpha_g^2}{Re_{s,r}} \mathrm{F}$
Zhang-Reese [174]	$\begin{cases} \frac{3}{4} C_D \frac{\alpha_s \rho_g}{d_s} \left[\lvert \vec{v}_s - \vec{v}_g \rvert^2 + \frac{8T}{\pi}\right]^{0.5} \alpha_g^{-2.65}, & \alpha_s \ge 0.8 \\ 150 \frac{\alpha_s^2 \mu_g}{\alpha_g d_s^2} + 1.75 \frac{\alpha_s \rho_g}{d_s} \left[\lvert \vec{v}_s - \vec{v}_g \rvert^2 + \frac{8T}{\pi}\right]^{0.5}, & \alpha_s < 0.8 \end{cases}$	$\left(0.28 + \frac{6}{\sqrt{Re_s}} + \frac{21}{Re_s}\right)$

2.5.2.5 Turbulence model

In general, there are three turbulent models: $k-\varepsilon$ model, $k-\omega$ model and Reynolds stress model (RSM). For the first two models, there are three kinds of methods for modeling turbulence in multiphase flow: mixture turbulence model, dispersed turbulence model and turbulence model for each phase, while within the context of RSM, only two turbulence options are provided. The three kinds of $k-\varepsilon$ model are summarized in this section, among which the $k-\varepsilon$ mixture turbulence model is utilized in this thesis.

$k-\varepsilon$ mixture turbulence model

The mixture turbulence model represents the first extension of the single-phase $k-\varepsilon$ model and it is applicable when phase separate and the density ratio between phases is close to 1. In these cases, using mixture properties and mixture velocities is sufficient to capture important features of the turbulent flow. The transport equations for *k* and *ε* are written as follows:

$$\frac{\partial}{\partial t}(\rho_{mix}k) + \nabla\cdot(\rho_{mix}\vec{v}_{mix}k) = \nabla\cdot\left(\frac{\mu_{t,mix}}{\sigma_k}\nabla k\right) + G_{k,mix} - \rho_{mix}\varepsilon \tag{2.47}$$

$$\frac{\partial}{\partial t}(\rho_{mix}\varepsilon) + \nabla\cdot(\rho_{mix}\vec{v}_{mix}\varepsilon) = \nabla\cdot\left(\frac{\mu_{t,mix}}{\sigma_\varepsilon}\nabla\varepsilon\right) + \frac{\varepsilon}{k}(C_{1\varepsilon,mix}G_{k,mix} - C_{2\varepsilon,mix}\rho_{mix}\varepsilon) \tag{2.48}$$

Where the mixture density and velocity, ρ_{mix} and $\vec{v}_{mix}$are computed from

$$\rho_{mix} = \sum_{i=1}^{n_{spe}}\alpha_i\rho_i \tag{2.49}$$

$$\vec{v}_{mix} = \frac{\sum_{i=1}^{n\_spe}\alpha_i\rho_i\vec{v}_i}{\sum_{i=1}^{n\_spe}\alpha_i\rho_i} \tag{2.50}$$

Where, n_spe is the number of species.

The turbulent viscosity, $\mu_{t,mix}$ is computed from,

$$\mu_{t,mix} = \rho_{mix}C_\mu\frac{k^2}{\varepsilon} \tag{2.51}$$

And the production of turbulent kinetic energy, $G_{k,mix}$, is computed from

$$G_{k,mix} = \mu_{t,mix}(\nabla\vec{v}_{mix} + (\nabla\vec{v}_{mix})^T):\nabla\vec{v}_{mix} \tag{2.52}$$

$k-\varepsilon$ dispersed turbulence model

The dispersed turbulence model is the appropriate model when the concentrations of the secondary phase are dilute. In this case, inter-particle collision are negligible and the dominate process in the random motion of the secondary phases is the influence of the primary-phase turbulence. This model is applicable when there is clearly one primary

continuous phase and the rest are dispersed dilute secondary phases. Turbulent predictions are obtained from the modified $k-\varepsilon$ model for gas phase:

$$\frac{\partial}{\partial t}\left(\alpha_g \rho_g k_g\right) + \nabla \cdot \left(\alpha_g \rho_g \vec{U}_g k_g\right) = \nabla \cdot \left(\alpha_g \frac{\mu_{t,g}}{\sigma_k} \nabla k_g\right) + \alpha_g G_{k,g} - \alpha_g \rho_g \varepsilon_g + \alpha_g \rho_g \Pi_{k_g} \tag{2.53}$$

$$\frac{\partial}{\partial t}\left(\alpha_g \rho_g \varepsilon_g\right) + \nabla \cdot \left(\alpha_g \rho_g \vec{U}_g \varepsilon_g\right) = \nabla \cdot \left(\alpha_g \frac{\mu_{t,g}}{\sigma_\varepsilon} \nabla \varepsilon_g\right) + \alpha_g \frac{\varepsilon_g}{k_g}\left(C_{1\varepsilon} G_{k,g} - C_{2\varepsilon} \rho_g \varepsilon_g\right) + \alpha_g \rho_g \Pi_{\varepsilon_g} \tag{2.54}$$

Where Π_{k_g} and Π_{ε_g} represent the influence of the dispersed phases on the continuous gas phase, and $G_{k,g}$ is the production of turbulent kinetic energy. $\vec{U}_g$ is the phase-weighted gas velocity.

$k-\varepsilon$ per phase turbulence model

This turbulence model solves a set of k and ε transport equations for each phase and is appropriate for case that the turbulence transfer among the phases plays a dominate role. A disadvantage of this turbulence model is computationally intensive.

Turbulence prediction for phase q are obtained from

$$\frac{\partial}{\partial t}\left(\alpha_q \rho_q k_q\right) + \nabla \cdot \left(\alpha_q \rho_q \vec{U}_q k_q\right) = \nabla \cdot \left(\alpha_q \left(\mu_q + \frac{\mu_{t,q}}{\sigma_k}\right) \nabla k_q\right) + \left(\alpha_q G_{k,q} - \alpha_q \rho_q \varepsilon_q\right) + \sum_{l=1}^{N} K_{lq}\left(C_{lq} k_l - C_{ql} k_q\right) - \sum_{l=1}^{N} K_{lq}\left(\vec{U}_l - \vec{U}_q\right) \cdot \frac{\mu_{t,l}}{\alpha_l \sigma_l} \nabla \alpha_l + \sum_{l=1}^{N} K_{lq}\left(\vec{U}_l - \vec{U}_q\right) \cdot \mu t,q \alpha q \sigma q \nabla \alpha q$$

(2.55)

$$\frac{\partial}{\partial t}\left(\alpha_q \rho_q \varepsilon_q\right) + \nabla \cdot \left(\alpha_q \rho_q \vec{U}_q \varepsilon_q\right) = \nabla \cdot \left(\alpha_q \frac{\mu_{t,q}}{\sigma_\varepsilon} \nabla \varepsilon_q\right) + \frac{\varepsilon_q}{k_q}\Big[\left(C_{1\varepsilon} \alpha_q G_{k,q} - C2\varepsilon \alpha q \rho q \varepsilon q + C3\varepsilon l{=}1NKlqClqkl - Cqlkq - l{=}1NKlqUl - Uq \cdot \mu t,l \alpha l \sigma l \nabla \alpha l + l{=}1NKlqUl - Uq \cdot \mu t,q \alpha q \sigma q \nabla \alpha q\right.$$

(2.56)

2.5.3 Coupled CFD-PBM model

Usually, the assumption of a spatially homogeneous (well-mixed) system is employed in development of population balance models. However, since powder characteristics and essential hydrodynamics and kinetic parameters regarding the size enlargement process are changing with time and position in the fluidized bed, the population balance model based on homogeneity cannot be applied for the whole fluidized bed granulation process and be applied for a priori design and scale-up of fluidized bed granulation process [24]. For instance, wetting of the particles is usually limited to a certain portion (i.e. 30%) of the fluidized bed and as a result, fluidizing gas velocity and particle properties with respect to different zones or regions of the fluidized bed granulator would be different [56, 175, 176].

In order to rigorously account for particle-related phenomena (e.g. agglomeration and breakage), the population balance model (PBM) must be solved along with the continuity and momentum balance equations, which gives huge potential of the combined CFD-PBM research. The solid volume fraction, particle velocity and temperature calculated from the Navier-Stokes transport equations by CFD are used to solve the PBM, because they are related to the particle growth, aggregation, and breakage [177, 178]. Once the population balance equations are solved, results of PBM can be used to calculate the Sauter mean diameter to further modify the gas-solid interaction in the multiphase flow model and hence update the information of solid volume fraction, particle velocity, and temperature for PBM. Recently, some hybrid CFD models have been developed to describe gas-solid flow field, as well as the particle population balance equation for particle size distribution (PSD) in fluidized bed reactors, which is called CFD-PBM coupled models [15, 179-183]. Notably, Fan et. al. [180, 181] started to use the CFD-PBM coupled models to simulate poly-disperse gas-solid fluidized bed reactors (FBRs). In their work, the quadrature method of moments (QMOM) and direct quadrature method of moments (DQMOM) were used to solve the PBM, and they were implemented in a multi-fluid model to simulate poly-disperse gas-solid FBRs. Rajniak's work [15] presented an direct comparison between the CFD-PBM coupled model and homogeneous PBM, in which the QMOM is employed to

solve the CFD-PBM coupled model and homogeneous PBM.

However, this CFD-PBM coupled model has the same disadvantage as the CFD model of expensive computational time and, due to the complex fluid dynamics of spray fluidized bed granulation, attempts to incorporate the PBM into multi-fluid model to describe the evolution of the particle size distribution in a fluidized bed granulator are still very limited.

2.5.4 Multi-compartmental PBM model

Based on the analysis above, CFD simulations present huge advantages on predicting the multiphase flow hydrodynamics of fluidized bed granulation, while they have the main problems of expensive computation cost and no continuous model output, which are essential for model based system control. For example, it has been reported that to compute 30s in real time for the precipitation process, the fully coupled CFD-PBM simulation takes nearly 60 days and simulation relying on frozen flow field obtained by switching off flow and turbulence equations after reaching quasi-steady state requires about 21 minutes. Hence, the multi-compartmental PBM model emerges as potential to reduce computational time and to be applied for control, in the mean time, considering local hydrodynamics of different region of fluidized bed granulator. In the multi-compartmental PBM model, the fluidized bed granulator is divided into different compartments according the gas-solid fluid dynamics study. Each region is assumed as homogeneous, based on which the one-dimensional PBM is implemented on each region to predict the local particle growth and particle size distribution evolution, considering particles communicating between neighbor regions. The number of regions is determined by experimental measurement, CFD simulation or empirical experience.

Until now, only very limited literatures could be found about the multi-compartmental PBM study, especially on the application of spray fluidized bed granulation [184-186]. Tuichiuli et al. [185] divided the fluidized bed granulator into three different zones: wetting-active zone, isothermal zone and hear transfer zone by experimental measurement of the bed humidity. A two-zone PBM was developed in their work by considering particle layering growth and agglomeration in the wetting-active zone and

only particle exchange happened in the other two zones. A two-compartmental PBM study of bottom-spray wurster fluidized bed granulation was carried out by Matthias et al. [184] considering particle growth in the spray compartment. Mubashir et al. divided the fluidized bed granulator into two compartments: spraying zone and dying zone. A fundamental study of the two-compartmental PBM model was carried out by considering particle agglomeration happening on the spraying zone and comparison was done between the one-compartment PBM and two-compartmental PBM. However, all the local gas-particle fluid dynamics and particle communicating of above study are based on empirical equation and so far, to the author's knowledge, no multi-compartmental research combined with CFD simulation has been found on the study of spray fluidized bed granulation.

2.6 Control of fluidized bed granulation

Fluidized bed granulation is a complex interaction process, which is affected by a large number of factors: operating variables, material properties and equipment parameters. Any subtle change of these variables may give rise to huge deterioration in final granules quality and result in energy and material waste. Therefore, accurate control strategy is required to improve the quality of final granules and consistency of granulation process. The necessarity of tight control for granulation process has been identified [57, 187].

While many papers focusing on the modelling of the granulation system, the literature in the field of control of fluidized bed spray granulation process is somewhat limited. One of the most important issues for the effective control of granulation process is the development of fast and reliable measurement techniques for characterization of the particulate system. Usually, particle size, size distribution, and shape of granules are the most frequently used objective variables, of which, however, the direct measurement is very difficult. Hence, some indirect monitoring parameters have been adopted as the indicators of particle characteristics, such as moisture content [188, 189], and power consumption [57]. Although the measurement of moisture or power consumption is a reliable method to monitor the granule growth indirectly, it is susceptible to the disturbance in powder properties and the operating conditions. However, the emergence

of the imaging process system effectively solved this problem and the particle characteristics can be considered as objective variables directly [190, 191].

Basically, the control strategies of granulation process can be divided into two categories: model based control [192-194] and un-model based control [188, 190, 191], which are distinguished with whether an accurate mathematical model is needed.

2.6.1 Model based control

In order to accurately control the granulation process, in some cases, the mathematical models are needed, of which model predictive control has been suggested by Gatzke and Doyle [192] and has been used most frequently. Model predictive control (MPC), also referred to as moving horizon control or receding horizon control, has become an attractive control strategy in fluidized bed granulation, which is based on a family of MPC algorithms in which models are utilized to predict the future system response. At each control interval an MPC algorithm attempts to optimize future plant behavior by computing a sequence of future manipulated variable adjustments. The first control move of calculated optimal inputs is then sent into the plant, and the entire calculation is repeated at subsequent control intervals. According to the model, two kinds of model predictive control strategies are distinguished: linear MPC [192-194] and non-linear MPC [195], of which linear MPC is used most popularly.

For the linear MPC, in the area of top spray fluidized bed granulation, there are very few applications in open literature [192-194]. In these linear MPC applications, an empirical, linear model obtained by fitting to process data is implemented to calculate the optimal control horizon of the input variables. Because of the complex nonlinearity of the population balance model, to date, there are very limited literatures of nonlinear MPC utilizing population balance model [195]. In these works mentioned above, the most common manipulated variable is binder flow rate, and the objective variables are bulk density, particle size distribution, and control effort. In real systems, some process output has constraints and some control objectives are much more important than other objectives, which can be solved by introducing the soft output constraint and prioritized control objectives [192]. The main advantage of model predictive control is that it can

accommodate with multivariable input-output systems and systems with process constraints. For the complex systems that the mathematical model is difficult to extract, the application of model predictive control is impossible.

2.6.2 Un-model based control

Besides the model-based control strategy, there are a number of practical control schemes in the granulation area, which do not rely on mathematical models. Recently, the development of intelligent methods makes them possible to be used in modelling and controlling the complex granulation systems, for example, fuzzy logic [188, 190, 191]. In addition, there are several works presenting the application of simple feedback control, such as PID control, in fluidized bed granulation [194].

Fuzzy logic control of fluidized bed granulation

The fuzzy logic control is to calculate the manipulated variables through a fuzzy logic algorithm to achieve the control objective. For the objective variable of granule size, a control system using fuzzy logic is designed and implemented to control granule growth in the fluidized bed granulation [190, 191]. In this control system, the image processing system was used for direct monitoring of number median granule size with high accuracy. For the fuzzy controller, there are two input variables: (1) deviation between desired granule size and measured value, and (2) the changing rate of this deviation. The IF-THEN algorithm is used and the result of fuzzy reasoning is used to control the output power of liquid feed pump, considering four fuzzy variables: ZR (zero), PS (positive small), PM (positive medium) and PL (positive large). The selection of the moisture content of granules during fluidized bed granulation as the objective variable has also been successfully implemented using the fuzzy logic controller [188].

Simple feedback control

With the development of measurement techniques, information about the particle distribution can be obtained on-line and sent back quickly, which is really a key factor of feedback control. To date, there are several applications about feedback control [189, 196]. Mont et al. [196] developed a feedback control strategy to control the level of

binder dilution in a continuous binder-agglomeration process using image processing system. In another application [189], the IR moisture sensor is successfully utilized to continuously measure the granule moisture content for feedback in fluidized bed granulation. Besides, a PID controller is also implemented into a granulation system to compare with the model predictive control results [194].

2.7 Quality by design (QbD) application to study fluidized bed granulation

2.7.1 QbD implementation

The pharmaceutical industry is encouraged within Quality by Design (QbD) to apply science-based manufacturing principles to assure quality not only of new but also of existing processes, including the fluidized bed granulation. Due to the intrinsic variability and complexity, successful applications of QbD on the fluidized bed granulation process are still limited [51, 197-199]. A basic regime map of quality by design (QbD) is given in Figure 2.3.

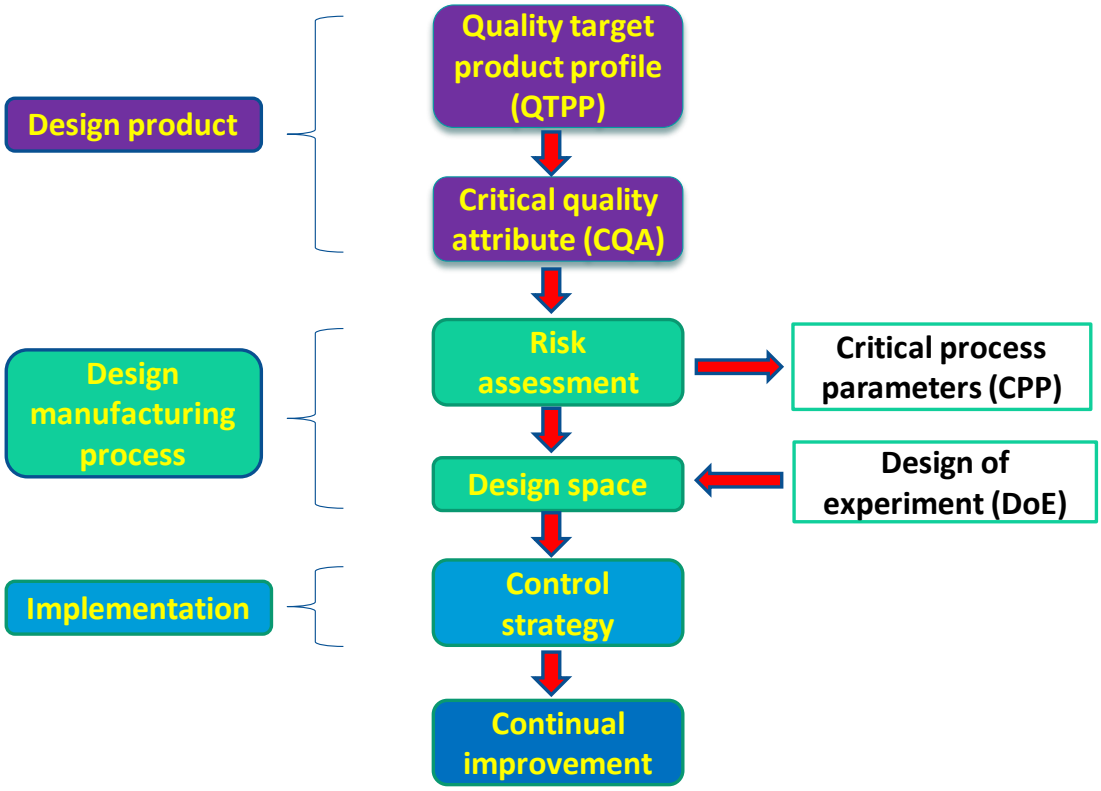

Figure 2.3 Regime map of quality by design (QbD)

The first is to define the quality target product profile (QTPP) while the second is to make sure critical quality attributes (CQA). QTPP is the basic point in the design of product. It describes the criteria that ensures the quality, safety, and efficacy of the product and usually includes intended use, dose, strength, dosage form, and route of administration. For the granulation process, the desired tablet or granule dissolution profile can be defined as the quality target product profile. CQAs identify what is drug product attributes which are critical to the patient. For the granulation process, CQAs include the mean size of granules, granule size distribution, flowability, yield of final granules and granule moisture content, etc. Material attributes (MAs) include the binder type, binder concentration and viscosity, primary material size and density, primary material solubility, etc.

After determination of CQAs, a suitable strategy is applied to control these attributes. Risk management is one of the most common and accepted strategies in this regard. Application of risk management shall be done at sequential steps as initial risk assessment followed by appropriate justification and risk reduction. There are several different kinds of risk assessment methods, among which the fish bones method behaves as the most regular. The purpose of risk assessment is to find the critical process parameters (CPPs) which have large influence on the CQAs. For the fluidized bed granulation process, the important influencing factors mainly come from several aspects, such as equipment-related parameters, environment conditions, operating conditions, material properties, and mankind factors.

To improve process knowledge, statistical design of experiments (DoE) is a valuable tool to establish in mathematical form the relationships between Critical Process Parameters (CPPs) and Critical to Quality Attributes (CQAs). A main purpose of the DoE is to discover the design space (DS). A definition of design space from the document ICH Q8 is “the multidimensional combination and interaction of input variables (e.g. material attributes) and process parameters that have been demonstrated to provide assurance of quality”. A range for each process parameter and their combinations can be defined, in which the desired CQAs values are achieved. Also, a range for the quality of raw materials that affect the CQAs can also be defined. All

likely combinations of raw material attributes and process parameters that need to be realized by the process, to ensure that the CQAs stay within the required ranges, can be called the Design Space (DS) of the process. After the DS is determined, the control strategy can be developed for the granulation process introduced in chapter 4 [200] and further the control space (CS) can be determined.

2.7.2 Role of model in Process understanding by QbD

In the pharmaceutical industry, historically very conservative in technological aspects, there has been an effort to promote technological advances and increase process flexibility, if one can demonstrate enhanced process understanding, to assure products of better quality. One of these initiatives is known as Quality by Design (QbD). Quality by Design (QbD) was firstly introduced to the pharmaceutical industry in 2006 by the International Conference on Harmonization (ICH) Q8 guidance [201]. In the ICH Q8 (R2) guidance [202], QbD is defined as "a systematic approach to development that begins with predefined objectives and emphasizes product and process understanding and process control, based on sound science and quality risk management." This framework represents a move away from the traditional approach in the industry of "quality by testing" (QbT). QbD is a comprehensive approach targeting all phases of drug discovery, manufacture, and delivery. The aim is to improve the quality and reduce the costs of medicines for consumers. It has been recognized that a consistent and well-controlled granulation process in a fluidised bed processor requires a thorough understanding of the complex influence of various factors on critical granule attributes and identification of the design space, as opposed to the traditional reliance on operator experience. For pharmaceutical manufacturing processes, QbD could well be paraphrased as the application of fit-for-purpose engineering models to the design and scale-up of active pharmaceutical ingredient (API) production and dosage form manufacturing processes. The goal is to improve product quality and process efficiency.

Process characterization under QbD involves three key steps: first, a risk assessment is performed to identify the relevant CPPs and CMAs; second, design of experiments (DoE), so that the effects of CPPs and CMAs on CQAs can be quantified and third, the results are analyzed to generate accurate models, relating each CQA with the relevant

CPP/CMA, which are used to generate the design space. In the case of top-spray fluidized bed granulation, theoretical models often comprise two types: empirical model from operating to granule properties used for analysis influence of operating conditions on granules properties, and mechanical model from operating conditions to granule size distribution by population balance model used to analysis the particle formation and breakage mechanisms during granulation. Particularly for the last two steps of QbD shown in Figure 2.3, appropriate mathematical modeling tools are necessary to work through these steps. The benefit of using mathematical modeling during pharmaceutical development should be seen as reduced experimentation and reduced developmental resources. Accordingly, modeling would be the tool that allows both to guide smart decisions about the fit-for-purpose experimentation and to provide increased process understanding by formalizing in mathematical terms the relationships between variables [203]. On the other hand, mathematical modeling can be considered as important PAT tool. As a consequence, models can be used to support development activities, in order to accelerate the lunch of new products in the market, but also to improve the productivity and to control the product quality in manufacturing environment [203].

2.7.3 Design of experiments (DoE)

Design of experiments which is one of key elements of the Quality by Design principle has been used to study a fluidized bed granulation process [65, 197, 204]. Use of design of experiments allows for testing a large number of factors simultaneously and precludes the use of a huge number of independent runs when the traditional step-by-step approach is used. Systematic optimization procedures can be carried out by selecting an objective function, finding the most important or contributing factors and investigating the relationship between responses and factors. Currently there are very few studies using a design of experimental approach to investigate a pulsed spray fluidized bed granulation process, in particular, the effect of pulsed frequency on the granule properties and its interaction with other process parameters.

Basically, there are two kinds of DoE: screening DoE and optimization DoE. Screening DoE aims to identify the CPPs and CQAs together with a deeper understanding of the process, which can be considered as part of risk analysis. Optimization DoE aims to

determine the ranges of operating parameters for design space and considers more complex situations, such as the quadratic terms of variables, comparing with screening DoE.

Full factorial design

A full factorial design contains all possible combinations of a set of factors. This is the most fool proof design approach, but it is also the most costly in experimental resources. In full factorial designs, you perform an experimental run at every combination of the factor levels. The sample size is the product of the numbers of levels of the factors. For example, a factorial experiment with a two-level factor, a three-level factor, and a four-level factor has 2 x 3 x 4 = 24 runs. Full factorial designs are the most conservative of all design types. There is little scope for ambiguity when you are willing to try all combinations of the factor settings. Unfortunately, the sample size grows exponentially in the number of factors, so full factorial designs are too expensive to run for most practical purposes.

Fractional factorial design

This design method could be utilized for fitting the process model which includes the interactions terms and linear terms. Fractional factorial designs are expressed using the notation l^{k-p}, where l is the number of levels of each factor investigated, k is the number of factors investigated, and p describes the size of the fraction of the full factorial used. Formally, p is the number of generators, assignments as to which effects or interactions are confounded, i.e., cannot be estimated independently of each other. A design with p such generators is a $1/l^p$ fraction of the full factorial design. For example, a 2^{5-2} design is 1/4 of a two level, five factor factorial design. Rather than the 32 runs that would be required for the full 2^5 factorial experiment, this experiment design requires only eight runs. In practice, one rarely encounters $l > 2$ levels in fractional factorial designs, since response surface methodology is a much more experimentally efficient way to determine the relationship between the experimental response and factors at multiple levels.

Response surface methodology (RSM)

Response surface methodology (RSM) is one of the popular methods in design of experiments, which involves the use of different types of experimental designs to generate polynomial mathematical relationships and mapping of the response over the experimental domain to select the optimal process parameters [205]. This design method includes three kinds of central composite designs and Box-Behnken designs (Figure 2.4), which can be applied for the third model to give an optimum point of the variables to the response.

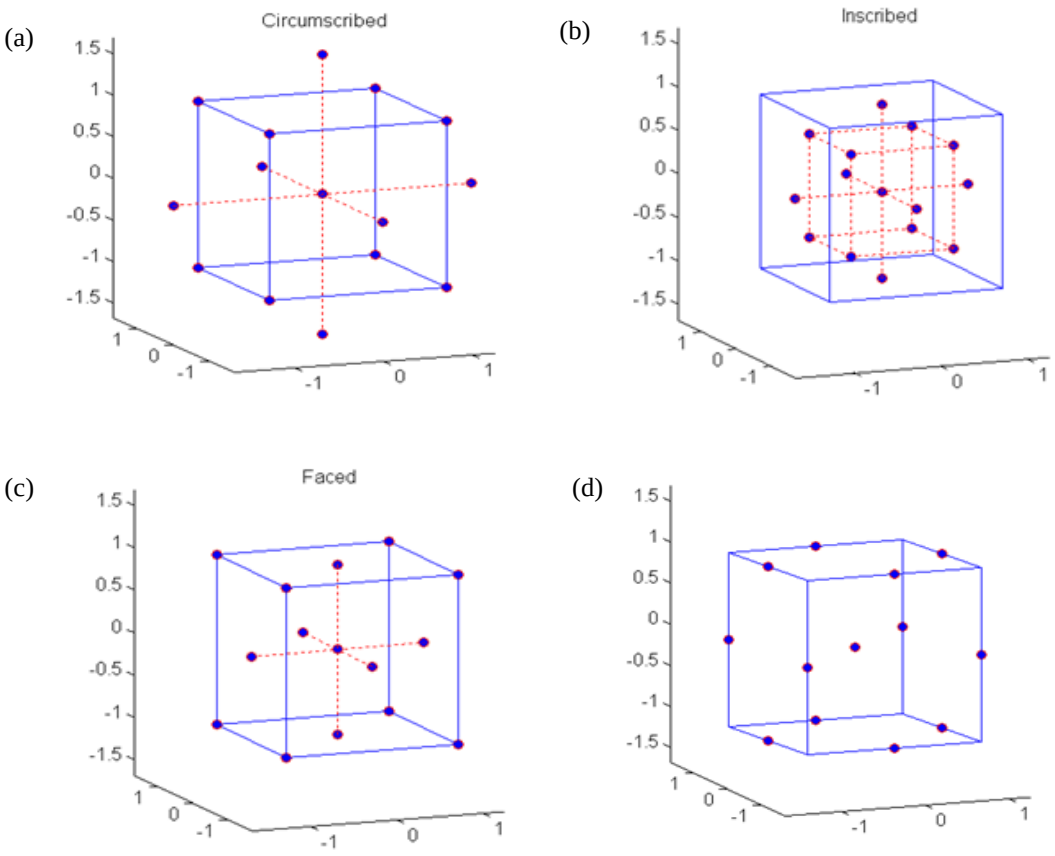

Figure 2.4 Response surface methodology methods. (a) Circumscribed design (b) Inscribed design (c) Faced design (d) Box-Behnken design

Box-Behnken statistical design is one type of RSM designs, which is an independent, rotatable or nearly rotatable, quadratic design having the treatment combinations at the midpoints of the edges of the process space and at the centre [206, 207]. Box-Behnken

experimental design was used to optimize and evaluate main effects, interaction effects and quadratic effects of the process variables on the quality of granules. A significant advantage of Box-Behnken statistical design is that it is a more cost-effective technique, which requires fewer experimental runs and less time for optimization of a process, compared with other techniques such as central composite design, 3-level factorial design and D-optimal design.

For the response surface methodology involving Box-Behnken design, a total of 15 experiments were designed for three factors at three levels of each parameter shown in Table 2.6.

Table 2.6 Experiment table by the Box-Behnken experimental design

Run	Independent variables (levels)			
	Mode	X_1	X_2	X_3
1	−−0	-1	-1	0
2	−0−	-1	0	-1
3	−0+	-1	0	1
4	−+0	-1	1	0
5	0−−	0	-1	-1
6	0−+	0	-1	1
7	000	0	0	0
8	000	0	0	0
9	000	0	0	0
10	0+−	0	1	-1
11	0++	0	1	1
12	+−0	1	-1	0
13	+0−	1	0	-1
14	+0+	1	0	1
15	++0	1	1	0

This design is equal to the three replicated centre points and the set of points lying at the midpoint of each surface of the cube defining the region of interest of each parameter, as described by the red points in Figure 2.4 (d). The non-linear quadratic model generated by the design is given as

$$Y = b_0 + b_1X_1 + b_2X_2 + b_3X_3 + b_{12}X_1X_2 + b_{13}X_1X_3 + b_{23}X_2X_3 + b_{11}X_1^2 + b_{22}X_2^2 + b_{33}X_3^2 \quad (2.57)$$

where, *Y* is a measured response associated with each factor level combination; b_0 is an intercept; b_1 to b_{33} are regression coefficients calculated from the observed experimental values of *Y*; and X_1, X_2 and X_3 are the coded levels of independent variables. The terms X_1X_2, X_1X_3, X_2X_3 and X_i^2 (*i=1, 2, 3*) represent the interaction and quadratic terms, respectively.

2.8 Study of pulsed top-spray fluidized bed granulation

In fluidized bed granulation, it would be not easy to control the granule size directly because of difficulty in in-line particle size determination. The moisture content in the bed is the key parameter to control because it is the most critical factor influencing overall process performance [57]. In order to control the moisture content in the bed, the binder spray rate is often adjusted during the granulation process. Recently it has been found that a pulsed spray has more potential for controlling the granulation process to determine the quality of final product and to target the end particle size in fluidized bed granulation [50-52].

During the fluidized bed granulation, the liquid binder is sprayed into the bed by an atomizer in two modes: continuous spraying and pulsed spraying. Continuous spraying is to spray the binder solution into the fluidizing bed continuously from the beginning of experiment, which is utilized for most of the experimental study of fluidized bed granulation. Pulsed spraying is to interrupt the binder feed in a regular sequence during the spraying phase, which makes the powder materials in the fluidized bed undergoing intermittent drying and wetting, resulting in a better control of the humidity within the granulation chamber.

A spray cycle includes two stages: a spraying phase in which the pump is turned on to spray the binder solution on the bed for a predetermined time and a pulsed phase in which the pump is turned off to stop spraying the binder solution for a predetermined time. The previous spray cycle ends and the next one starts again. Repeated spray cycles

make the spray pulsed. In a spray circle, the ratio of the pulsed and spraying time is called pulsed frequency, which is normally controlled by a computer in experiments. For example, a pulsed frequency is zero, showing that the binder solution is sprayed continuously, and the pulsed frequency is 1, indicating that the binder solution is sprayed for half spray circle and stops for another half circle.

For the literature, until now, only very limited publications could be found on the investigation of influence of pulsed spraying [50-52]. It was found that shorting the spraying period affected the bed moisture level but did not influence the growth rate and final granule size when the amount of granulation liquid was constant [50]. It was found that the pause time of liquid feed can be used to compensate the change of liquid feed rate and inlet air humidity, in order to maintain the median granule size [52]. It was also indicated that the liquid feed pulsing decreased the median granule size clearly and broadened the size distribution slightly when the liquid feed rate and relative humidity were constant, which may be explained by the attrition of granules during the pulsed spraying time [52]. All above experiments are based on varying pulsed frequency. In another study using fixed pulsed frequency [51], it was found that by varying the spray circle, it is also possible to control granule nucleation and growth. Through above analysis, it can be seen clearly that the pulsed binder spray is a useful tool to achieve the targeted final product size and is a straightforward tool in process control of the fluidized bed granulation

2.9 Chapter conclusions

In this chapter, a full literature review of the study of fluidized bed granulation is presented. At the beginning, the granulation mechanisms are introduced. Subsequently, the experimental study is summarized, including the influence of process-related parameters and material-related properties. The modelling studies of the fluidized bed granulation process are presented from two aspects: population balance modelling and computational fluid dynamics modelling. The limited study of the coupled CFD-PBM model is also investigated and the multi-compartmental PBM is introduced. The control study and application of quality by design (QbD) study of fluidized bed granulation were summarized. Finally, the pulsed binder spray in literature was summarized.

Chapter 3 Experimental study of pulsed spray fluidized bed granulation

3.1 Chapter overview

In this thesis, the purpose of experiments is to study the influence of three operating parameters of spray pulse frequency, binder spray rate and atomization pressure on the final granule properties, such mean size, flowability, and particle yield.

In this chapter, all the experiments carried out in this thesis are introduced, including the materials, experimental apparatus, operating method, and end granules properties characterization. 15 experiments are designed using the Box-Behnken experimental design method and 4 validation experiments are also carried out to validate the developed mathematical models. Three operating parameters of spray pulsed frequency, binder spray rate and atomization pressure are selected to investigate their influence on the final granule properties.

3.2 Materials and methods

3.2.1 Materials

The powder used for granulation was microcrystalline cellulose (MCC) supplied by (Blackburn Distributions Ltd, UK). The size distribution of the primary particles ranged from 150-180 μm. HPMC (Hydroxy Propyl Methyl Cellulose, methocel A 15 LV) was used as the binder. The concentration of the binder solution was 6% w/w that was prepared by adding HPMC to deionised water under constant stirring. The solution was allowed to sit overnight to allow hydration and degassing. For each granulation experiment, 46.5g of MCC and 3.5g of dry binder HPMC corresponding to 58.33g of the binder solution were used. The binder to powder ratio was 7.5% (w/w).

Microcrystalline cellulose is a very frequently used pharmaceutical excipient in the wet granulation process. Firstly, MCC allows dilution to be distributed evenly through the wet granulation process. In addition, tablet or granules made up of MCC excipient has

been found to disintegrate relatively easy, which provides the possibility of rapid dissolution tablet dosage form. In particular, MCC has excellent compactibility, which can contribute to the strength and robustness of a tablet dosage form. In the meantime, it should be mentioned that the compactibility of MCC could be changed by the granulation operating factor and the amount of binder. Normally, the active pharmaceutical ingredient (API) and excipient should be included simultaneously in the formulation of granulation. However, in this study, only the MCC is used in the fluidized bed granulation, because only the physical properties of granules need to be measured, such as the granule size distribution, granule mean size, or granule moisture. Therefore, it is impossible to measure properties of API using the granulation experiments in this study, such as the dissolution test.

3.2.2 Experimental equipment

Granulation experiments were carried out in a lab-scale batch fluidized bed granulator (MP-Micro ™, GEA Process Engineering Ltd, UK). The schematic diagram for the experimental setup can be seen in Figure 3.1.

The product chamber is a conical cylinder made from Perspex. The height of the container is 30 cm with inner diameters of 4.97 cm and 7.48 cm at the bottom and top. The air distributor is a 4500 mesh stainless steel plate at the bottom of the product container. The inlet air was preheated at a constant temperature of 40 °C by an electrical heater before entering the bed for each experiment. The binder spray nozzle was a movable, internal mixing two-fluid spray nozzle (GEA Niro, NTF-I- 50/50) and was placed at 16.2 cm above the distributor plate. Spray from the nozzle was in a downward direction and counter current to the fluidizing air flow. The binder was drawn from a reservoir of HPMC solution using a peristaltic pump. The total amount of binder solution withdrawn for each experiment was constant at 58.33g corresponding 7.5%w/w of the dry binder and powder rate.

Although the fluidized bed granulator used in this study is small-scale, the purpose-designed equipment can bring all the flexibility of a full-size production fluid bed granulator to the laboratory bench up. Firstly, it can perform the drying mixing and

liquid addition. Further, during the granulation process, the particle size can be enhanced as the binder sprayed. In addition, this equipment can be used for the spray coating and granule drying. In particular, the most important advantage of a small-scale granulator is material saving, especially for expensive API, and easy sampling and measurement.

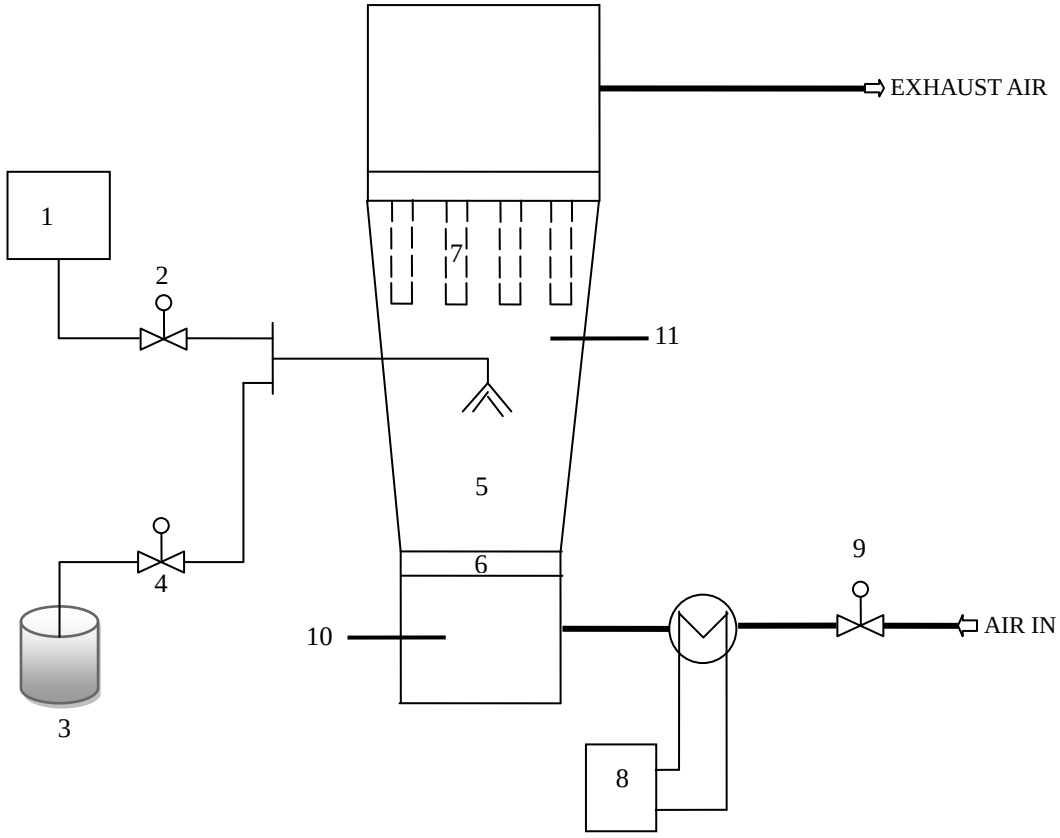

1. Air compressor
2. Atomizating pressure regulator
3. Binder solution container
4. Binder flow rate regulator
5. Product container
6. Air distributor (orifice plate)
7. Back blow filter
8. Heater controller
9. Inlet air velocity regulator
10. Inlet air temperature probe
11. Outlet air temperature probe

Figure 3.1 Top-spray fluidized bed granulator setup

3.2.3 Sampling and granule size measurement

For each experiment, samples of 5 g were taken at three different points of 30%, 70% and 100% of the granulation time for granule characteristics analysis.

Final granule size distribution was determined by the sieve analysis method. A set of sieves (150, 180, 250, 355, 500, 710, 1000, and 2000 um) in combination with the Retsch AS 200 sieve shaker (RETSCH, Germany) was used for size distribution analysis. Before the particle size analysis, final granules were dried in an oven at 60°C for 24 hours. The dried granules were transferred to the pre-weighed sieves and allowed to shake at amplitude of 1 mm for 10 minutes. The sieves were then reweighted to determine the weight fraction of granules retained on each sieve. These weights were converted in mass percentage.

The mean diameter and relative width of granule distribution are calculated according to the following equations

$$\text{Mean diameter:} \qquad \overline{D} = \frac{\sum_i f_i d_{pi}}{\sum_i f_i} \tag{3.1}$$

$$\text{Relative width of granule distribution: } RW = \frac{D_{90} - D_{10}}{\overline{D}} \tag{3.2}$$

where $\overline{D}$ is the mean diameter of final granules; d_{pi} is the geometrical mean of sieve band i; D_{10} and D_{90} are granule sizes at 10% and 90% percentages from the mass cumulative particle size distribution; RW is the relative width of granule distribution.

The yield of granules between 250 and 1000 μm was obtained by emulating of the mass percentage from the sieves of 250, 355, 500, 710 and 1000 μm based on the final granule size distribution.

3.2.4 Granule physical property characterization

The granules were analyzed for bulk and tapped densities and Hausner ratio.

Bulk and tapped densities

Granules were gently poured into a 250 *ml* graduated cylinder. The granule weight and volume were measured to calculate the bulk density. Using an automatic tapping density tester, the cylinder was tapped 2000 times and the new volume was read to calculate the tapped density.

Hausner ratio

Hausner ratio is calculated using the bulk and tapped densities to describe the granules flowability according to the equation as follows [208]:

$$Hausner\ ratio = \frac{Tapped\ density}{Bulk\ density} \tag{3.3}$$

Moisture content

In this study, a Halogen Moisture Analyzer (HB43-S Mettler Toledo) was used to measure moisture content of the granules after the samples were taken. This moisture analyzer can be used for measuring the moisture content of almost any substance. The thermogravimetric principle was applied by the halogen moisture analyzer. The working theory is: at the beginning of the measurement, the weight of the sample was determined, the moisture analyzer then quickly heated the sample by the integral halogen heating module to let the moisture vaporize. As the samples was heated, the moisture analyzer continually measures the weight of the sample and obtained the moisture reduction. Once drying process has been completed, the weight reduction of sample is obtained as the final result of moisture content.

3.3 Experimental design

3.3.1 JMP software

In this study, the Box-Behnken experimental design, response surfaces and analysis were all carried out using JMP 11 software (SAS, SAS Institute, Cary, NC, USA).

JMP is a powerful and interactive data visualization and statistical analysis tool, which can be utilized to learn more about the data by performing analyses and interacting with the data using data tables, graphs, charts, and reports. During last decades, JMP has been adopted by more and more researchers to perform a wide range of statistical analyses and modeling. In addition, JMP has become popular to the business analyst who wants to quickly uncover trends and patterns in data. Generally, JMP can mainly work on the following aspects (see JMP website):

- Create interactive graphs and charts to explore your data and discover relationships.
- Discover patterns of variation across many variables at once.
- Explore and summarize large amounts of data.
- Develop powerful statistical models to predict the future.

One of the most important application areas of JMP is design of experiment (DoE), which is powerful, elegant, and cost-effective statistical methods comparing with traditional costly and time-consuming trial-and-error searches. JMP offers powerful capabilities for design of experiment and analysis. Design of experiment in JMP is centered around factors, responses, a model, and runs, which helps you determine how the responses were influenced by factors. In addition to a complete library of classical DOE designs (classical screening (fractional factorial), response surface, full factorial, nonlinear and mixture designs, as well as advanced designs), JMP also offers an innovative custom design capability that tailors experimental design to specific situations. Once the data has been collected, JMP streamlines the analysis and model building so you can easily see the pattern of response, identify active factors and optimize responses. Also, JMP is the only software that implements definitive screening designs, which is the most important new class of designs in the past two decades and were used to efficiently and reliably separate the vital few factors that have a substantial effect from the trivial many that have negligible impact.

3.3.2 Box-Behnken experimental design

The aim of this chapter is to investigate the effect of spray operating parameters including the pulsed frequency, binder spray rate and spray atomization pressure on the quality of granules such as granule size, granule yield and moisture content and to explore the inter-relationship of these three spray operating parameters. In this chapter, the Box-Behnken experimental design was used to obtain a design of space which determined the operating ranges of different process parameters for achieving the desired quality of granules. A 3-factor, three-level design was used because it was suitable for exploring quadratic response surfaces and constructing second order polynomial models for optimization. The independent factors and dependent responses used in this design are listed in Table 3.1. The low, medium and high levels of each

independent factor were selected based on the results from the preliminary experiments.

Table 3.1 Variables and levels in the Box-Behnken experimental design

In dependent variables	Levels		
	Low (-1)	Medium (0)	High (1)
X_1: pulsed frequency	0	0.5	1
X_2: Binder spray rate (g/min)	0.9	1.2	1.5
X_3: Atomization pressure (psi)	10	15	20
Dependent responses	Constraints		Optimum
Y_1: Mean size of final granules $\overline{D}$ (μm)	$300 \leq Y_1 \leq 500$		
Y_2: Yield of final granules	$85\% \leq Y_2$		Maximum
Y_3: Relative width of final granule distribution			
Y_4: Hausner ratio	$Y_4 \leq 1.25$		
Y_5: Moisture content at 30% of binder solution sprayed			
Y_6: Moisture content at 70% of binder solution sprayed			
Y_7: Moisture content at 100% of binder solution sprayed			

As described in chapter 2.7, using Box-Behnken experimental design, 15 experiments were designed for the three involved factors at three levels of each parameter, given in Table 3.3 together with the 7 dependent responses. Three replicated experiments at center points are designed to validate the experiment repeatability. The Box-Behnken experimental design, response surfaces and analysis were all carried out using JMP 11 software (SAS, SAS Institute, Cary, NC, USA).

3.3.3 Validation experiments design

In order to validate the RSM results, further four experiments in which all of operating parameters were in the ranges of the design space have been carried out. The same materials and operating method were used in the validation experiments. Table 3.2 shows the operating conditions, the experimental and predicted values of all the response variables and their percentage errors.

Table 3.2 Validation results for FBG process

Operating conditions (X_1:X_2:X_3)	Response variable	Experimental value (y)	Model prediction ($\hat{y}$)	Percentage of prediction error ($\frac{\lvert y-\hat{y}\rvert}{y}$%)
(0.4;1.4;12)	*Mean granule size Y_1(um)*	506.00	494.93	2.19
	Granule yield Y_2(%)	89.34	88.79	0.62
(0.6;1.3;14)	*Mean granule size Y_1(um)*	426.96	421.80	1.21
	Granule yield Y_2(%)	83.64	85.59	2.33
(0.8;1.2;17)	*Mean granule size Y_1(um)*	386.53	375.55	2.84
	Granule yield Y_2(%)	84.97	88.64	4.32
(0.9;1;20)	*Mean granule size Y_1(um)*	342.42	323.34	5.57
	Granule yield Y_2(%)	91.01	98.68	8.43

3.3.4 Pulsed top-spray fluidized bed Granulation

Recently a pulsed spray has been found to be a great potential for controlling a granulation process [14, 52, 209]. During the spraying phase the liquid feed is interrupted in regular sequences to allow drying and rewetting of the granules, resulting in a better control of the humidity within the granulation chamber. In this study, the length of a spray cycle is kept constant at 2 minutes, in which the ratio of the pulsed and spraying time is called pulsed frequency and is altered automatically by a computer. For example, a pulsed frequency is zero, indicating that the binder solution is sprayed continuously, and the pulsed frequency is 1, showing that the binder solution is sprayed for 1 minute and stops for another 1 minute. In this study, the range of pulsed frequency from 0 to 1 was investigated, which was based on the preliminary experiments. During the pulsed phase the pump was switched off while keeping the atomization pressure to prevent clogging of the nozzle and irregularities in the level of fluidization. The liquid feed rate during the spray phase and atomization pressure during granulation were kept constant, which were set at the beginning of each experiment. The granulation liquid was at ambient room temperature.

The inlet air velocity was not part of investigation in this study. Although the inlet air velocity has a profound effect on the granulation process, its key function is to provide

good mixing of the primary particles [54, 55, 209]. A high fluidization velocity would have resulted in entrainment of particles and too low a fluidized velocity would have resulted in a fast collapse of the fluidized bed by insufficient mixing. During the granulation process, the mass and moisture content of the processed powders vary, resulting in a risk over-fluidization in dry conditions and insufficient fluidization in wet conditions if the inlet air velocity is kept constant. In order to keep same level of fluidization during granulation, the inlet fluidizing air velocity was adjusted manually in real time between 0.6 m^3/h and 2 m^3/h in each experiment in this study.

The inlet air was at ambient relative humidity as an uncontrolled variable and the range of the inlet air humidity was from 30% to 55%.

After granulation, the final wetted granules were dried in an oven at 60°C for 24 hours for analysis.

3.4 Results and discussion

3.4.1 Overview of results

In this section, the experiment results were discussed and analyzed. The Box-Behnken design was applied in this study to optimize the fluidized bed granulation process with constraints on the mean particle size, yield and Hausner ratio. The aim of the granulation process optimization was to determine the design space of process operating parameters of pulsed frequency, binder spray rate and atomization pressure to obtain a mean granule size between 300 to 500 μm with a minimum 85% yield of granule sizes between 250 and 1000 μm. These specifications were obtained from the preliminary experimentation. The observed responses for the 15 runs are already given in Table 3.3. Ten batches showed the mean size of granules within the desired range of 300 to 500 μm. The range of mean size Y_1 for all batches was from 290 μm to 734 μm. the maximum yield Y_2 was 97.3% for the batch 14 and minimum yield was just 70.65% for the batch 1. The range of the relative width of granule distribution Y_3 showed a big variation from 0.74 to 1.29. The range of Hausner ratios for all batches varied from 1.11 to 1.28. The moisture contents of final granules at different batches changed

significantly from 18.2% to 40.05%. All the experiments particle size distribution including validation experiments are plotted in mass fraction in appendix A.1.

Table 3.3 The Box-Behnken experimental design and responses

Run	Independent variables				Dependant variables						
	Mode	X_1	X_2	X_3	Y_1	Y_2	Y_3	Y_4	Y_5	Y_6	Y_7
1	−−0	0	0.9	15	526	70.65	1.29	1.20	22.19	32.03	36.49
2	−0−	0	1.2	10	734	87.56	0.81	1.18	15.78	24.19	25.47
3	−0+	0	1.2	20	429	89.66	1.01	1.27	24.18	35.05	38.71
4	−+0	0	1.5	15	579	96.79	0.80	1.19	21.01	29.23	30.48
5	0−−	0.5	0.9	10	449	89.85	1.13	1.25	17.02	28.29	29.58
6	0−+	0.5	0.9	20	290	90.74	0.74	1.26	21.06	28.09	26.78
7	0	0.5	1.2	15	401	84.23	1.05	1.27	21.08	32.6	35.65
8	0	0.5	1.2	15	391	88.33	1.03	1.28	20.44	31.64	33.49
9	0	0.5	1.2	15	419	83.29	1.13	1.28	25.04	34.54	40.05
10	0+−	0.5	1.5	10	489	90.50	0.99	1.27	22.17	32.79	35.31
11	0++	0.5	1.5	20	381	95.00	0.88	1.25	19.5	27.43	27.76
12	+−0	1	0.9	15	335	92.15	0.84	1.11	18.34	26.84	26.94
13	+0−	1	1.2	10	558	79.20	1.24	1.25	19.74	29.82	31.36
14	+0+	1	1.2	20	396	97.30	0.77	1.22	16.79	23.21	18.20
15	++0	1	1.5	15	450	86.63	1.16	1.23	23.36	35.76	39.22

3.4.2 Fitting data to model

Using a fitted full quadratic model in equation (2.57), a response surface regression analysis for each of responses Y_1, Y_2, and Y_3 was performed using the JMP 11 software. Table 3.4 shows the values calculated for the coefficients and *P*-values. Using a 5% significance level, a factor is considered to affect the response if the coefficients differ from zero significantly and the *P*-value is less than 0.05 (p<0.05). Therefore, the regression models of Y_1, Y_2, and Y_3 can be simplified by including only statistically significant coefficients shown in Table 3.4. Positive sign of a coefficient in front of a factor in the polynomial equation represents that the response increases with the factor. A negative sign means that the response and factors have reciprocal relation. Coefficients with higher order terms or more than one factor term in the regression equation represent quadratic relationships or interaction terms, indicating nonlinear

relationship between the response and factors.

Table 3.4 Regression coefficients and associated probability values (*P*-value) for Responses of Y_1, Y_2, and Y_3

Term	Mean size of final granules Y_1		Yield of final granules Y_2		Relative width of final granule distribution Y_3	
	Coefficient	*P*-value	Coefficient	*P*-value	Coefficient	*P*-value
Constant	403.67	<.0001	85.28	<.0001	1.07	<.0001
X_1	-66.13	0.0043*	1.33	0.4186	0.01	0.6423
X_2	37.37	0.0379*	3.19	0.0877	-0.02	0.4394
X3	-91.75	0.0010*	3.20	0.0872	-0.10	0.0126*
$X_1 * X_2$	15.50	0.4486	-7.92	0.0138*	0.20	0.0024*
$X_1 * X_3$	35.75	0.1165	4.00	0.1193	-0.17	0.0054*
$X_2 * X_3$	12.75	0.5290	0.90	0.6895	0.07	0.1079
$X_1 * X_1$	97.92	0.0041*	-0.91	0.6984	-0.01	0.7509
$X_2 * X_2$	-29.08	0.1985	2.18	0.3704	-0.04	0.3906
$X_3 * X_3$	27.67	0.2178	4.06	0.1269	-0.10	0.0436*
Regression equation	$Y_1 = 403.67 - 66.13X_1 + 37.37X_2 - 91.75X_3 + 97.92X_1^2$		$Y_2 = 85.28 - 7.92X_1X_2$		$Y_3 = 1.07 - 0.10X_3 + 0.20X_1X_2 - 0.17X_1X_3 - 0.10X_3^2$	
R-square	*0.958067*		*0.86379*		*0.941784*	
Prob>F of ANOVA	*0.006**		*0.0895*		*0.0131**	

It is clearly indicated that all three factors of the pulsed frequency (X_1), binder spray rate (X_2) and atomization pressure (X_3) have significant effects on the mean size of granules. The atomization pressure X_3 has negative effects on the mean size of granules while the binder spray rate (X_2) has positive effects. As expected, increasing the binder spray rate resulted in an increase of the mean size of granules and increasing the atomization pressure resulted in a decrease of the granule size, all of which have already been reported in literatures by several researchers [12, 54, 56]. These can be explained that the high spray rate promotes granule growth via excessive liquid supply while lower atomization pressure promotes granule growth via large droplet size. It seemed that there was no interaction effect of the spray rate and atomization pressure on the mean granule size because the interaction term can be neglected in the model, which is

consistent with those reported in the literatures [12, 54, 55]. When a pulsed mode is used during granulation, the pulsed frequency has profound effects on the mean size of granules shown in the regression equation in Table 3.4. It had both direct negative and positive quadratic effects on the mean size. Interestingly, there was no interaction effect of the pulsed frequency with either the spray rate or atomization pressure on the mean size of granules. The result can be seen as the strong evidence to support previous finding that the pulsed spray was a potential for controlling a granulation process [14, 52, 209]. Therefore, when a pulsed mode is used during granulation, more choices are available to control the granule size. However, care has to be taken when the pulsed frequency is chosen for controlling the granule size due to the nonlinear quadratic relation in the regression mode. More discussion will be given in the next section of contour plot analysis. There was no direct effect from either three of operating factors on the yield of final granules Y_2 which was determined by the interaction effect of the pulsed frequency (X_1) and binder spray rate (X_2). From the regression equation, it was evident that only the atomization pressure (X_3) had direct negative and quadratic effects on the relative width of granule distribution Y_3. The interaction effect of X_1 and X_2 was favorable for increasing the relative width of size distribution while the interaction effect of X_1 and X_3 could reduce the size distribution.

The R-square value of model fit and Prob>F value of analysis of variance were also shown in Table 3.4. R-square is a statistical measure of how close the data are to the fitted regression line. It is also known as the coefficient of determination, or the coefficient of multiple determination for multiple regression. The definition of R-square is fairly straight-forward, which is the percentage of the response variable variation that is explained by a linear model. R-square is always between 0 and 100%. 0% indicates that the model explains none of the variability of the response data around its mean. 100% indicates that the model explains all the variability of the response data around its mean. In general, the higher the R-square value, the better the model fits your data. From Table 3.4, it can be seen that all the R-square values are close to 1, which means the fitted models for Y_1, Y_2, Y_3 can well fit the experiment data. Probability of obtaining (by chance alone) an F value greater than the one calculated if, in reality, there is no difference in the population group means. Observed significance probabilities of 0.05 or less are

often considered evidence that there are differences in the group means. From Table 3.4, it can be seen that the P-value for model Y_1 and Y_3 are smaller than 0.05, while P-value for model Y_2 are obviously larger than 0.05. This indicated the model Y_2 cannot perfectly well fit the experiment date.

Table 3.5 shows the values calculated for the coefficients and *P*-values for the regression models of the moisture contents at different granulation times of 30%, 70% and 100% of binder solution sprayed. At the beginning of granulation up to 30% of the total binder sprayed, the moisture content of granules was affected mainly by interaction term of the pulsed frequency (X_1) and the atomization pressure (X_3). It was surprised that the bind spray rate had no significant effect on the moisture content of granules at the beginning of granulation. After that, the moisture content of granules was determined by the interaction effects of the pulsed frequency (X_1) with both the binder spray rate (X_2) and the atomization pressure (X_3) and also by the quadratic term of the atomization pressure. The similar regression models at 70% and 100% of binder solution sprayed in Table 3.5 were obtained, indicating that the dynamic equilibrium state had been established after 30% of the binder solution sprayed. All the R-square values for model Y_5, Y_6, and Y_7 are close to 0.9, which are accepted for model fitting. However, none of the P-value of analysis of variance for model Y_5, Y_6, and Y_7 is smaller than 0.05, which reflected the weakness of the model fitted on fitting the experimental data.

Repeatability of the process was studied by examining the results of the experiments 7, 8, and 9. With the exclusion of moisture content of granules, values of the other dependent responses were similar, indicating good repeatability in the experiments. The deviation of moisture content of granules in the three replicated centre points could be caused by many factors, such as variations in the inlet flow velocity, granule sampling and size measurement, in particular, the inlet air relative humidity. In this study the inlet air relative humidity was uncontrolled and changed significantly from minimum 30% to 55% among different experiments. It was concluded that the inlet air relative humidity was the main factor contributing to the variation of the moisture content of granules. However, it was surprised that the other dependent responses, in particular mean

granule size, were not affected by variation of the inlet air relative humidity. It was contradictive to the reported finding that the inlet air relative humidity was critical importance during the fluidized bed granulation process, which can increase the moisture level of granules to improve the granule plasticity, leading to slightly larger granules [12]. Further research is therefore needed to study this issue.

Table 3.5 Regression coefficients and associated probability values (*P*-value) for Responses of Y_5, Y_6, and Y_7

Term	Moisture content at 30% Y_5		Moisture content at 70% Y_6		Moisture content at 100% Y_7	
	Coefficient	*P*-value	Coefficient	*P*-value	Coefficient	*P*-value
Constant	22.19	<.0001	32.93	<.0001	36.40	<.0001
X_1	-0.62	0.3600	-0.61	0.4690	-1.93	0.1756
X_2	0.93	0.1894	1.24	0.1701	1.62	0.2419
X3	0.85	0.2223	-0.16	0.8415	-1.28	0.3419
$X_1 * X_2$	1.55	0.1332	2.93	0.0446*	4.57	0.0458*
$X_1 * X_3$	-2.84	0.0220*	-4.37	0.0106*	-6.60	0.0124*
$X_2 * X_3$	-1.68	0.1102	-1.29	0.2935	-1.19	0.5228
$X_1 * X_1$	-0.89	0.3692	-1.52	0.2409	-2.27	0.2632
$X_2 * X_2$	-0.07	0.9383	-0.44	0.7166	-0.85	0.6582
$X_3 * X_3$	-2.18	0.0604	-3.34	0.0331*	-5.69	0.0250*
Regression equation	$Y_5 = 22.19 - 2.84X_1X_3$		$Y_6 = 32.93 + 2.93X_1X_2 - 4.37X_1X_3 - 3.34\,X_3^2$		$Y_7 = 36.40 + 4.57X_1X_2 - 6.60X_1X_3 - 5.69X_3^2$	
R-square	*0.85505*		*0.881604*		*0.884915*	
Prob>F of ANOVA	*0.1022*		*0.0662*		*0.0622*	

3.4.3 Response contour plots

The relationship between the dependent and independent variables was further elucidated using response contour plots, which are very useful to study the effects of two factors on the response at one time when the third factor is kept at a constant level. Here the main focus was to study the effect of the pulsed frequency, binder spray rate, atomization pressure and their interactions on the responses of the mean size of final granules, yield of final granules, relative width of granule distribution and moisture contents.

The effect of X_1 and X_2 and their interaction on the mean size of final granule (Y_1) at low, medium and high levels of X_3 is given in Figure 3.2. It is clearly shown that the relationships among the three variables are non-linear because of the curved contour lines. At three different levels of atomization pressure, it was found that at a fixed spray rate increasing pulsed time within a spray circle resulted in a reduced mean particle size. At a fixed pulsed frequency, increasing spray rate resulted in increased mean particle size. In the contour plots shown in Figure 3.2, the white areas show the operating spaces which can granulate the required mean particle size in the range of 300 um to 500 um. It is shown that the operating ranges of the pulsed frequency and spray rate for required mean particle size increased significantly with increasing the atomization pressure.

At low level of the atomization pressure, the operating space only covers small ranges of X_1 and X_2. From the contour plot shown in Figure 3.2(a), it is indicated that the most effective operating variable to control granule size is the pulsed frequency in which a wide range of granule size can be produced from around 450μm to 700μm and the granule size was almost independent on the spray rate. Research has shown that the ratio of droplet size/particle size is the main factor to determine nucleation mechanism of granulation [61]. At a low atomization pressure, large binder droplets were produced, which can cause immersion of the solid particles in the liquid binder. This can not only enhance particle agglomeration and growth but also cause oversetting of the bed surface, resulting in formation of large lumps and defluidization. In order to lower the moisture content of the bed and increase mixing, the best way to control granule size was to pulse the binder spay to dry the wet granules to a required level of moisture content. Therefore the mean size of granules was affected significantly by the pulsed frequency X_1 and was unaffected by the spray rate X_2.

At the medium and high levels of atomization pressure, the binder droplets were smaller than the particles so that the distribution nucleation mechanism was dominant in the fluid bed granulation, in which nuclei were formed by collisions between the surface-wetted powder particles. Because both the pulsed frequency and spray rate affected the wetting profiles of the particles, the mean size of granules was determined by the combination effect of the two factors. It can also be seen that the operating ranges of X_1

and X_2 increase significantly with increasing the atomization pressure.

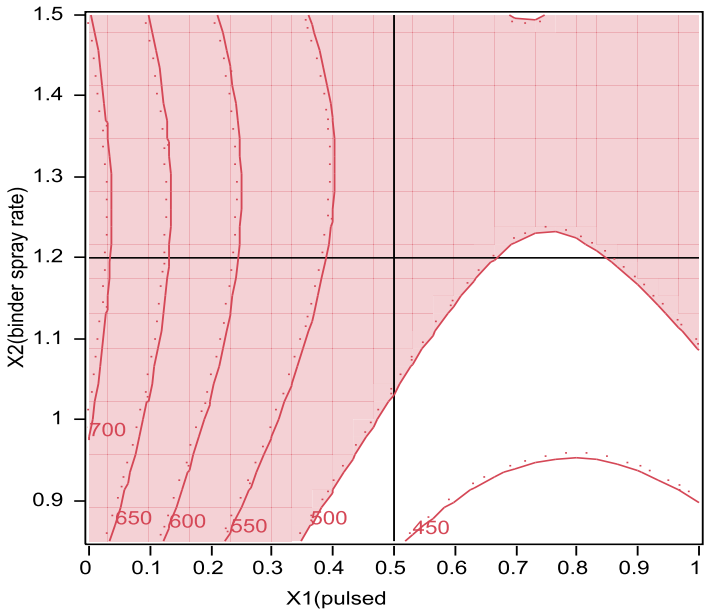

(a)

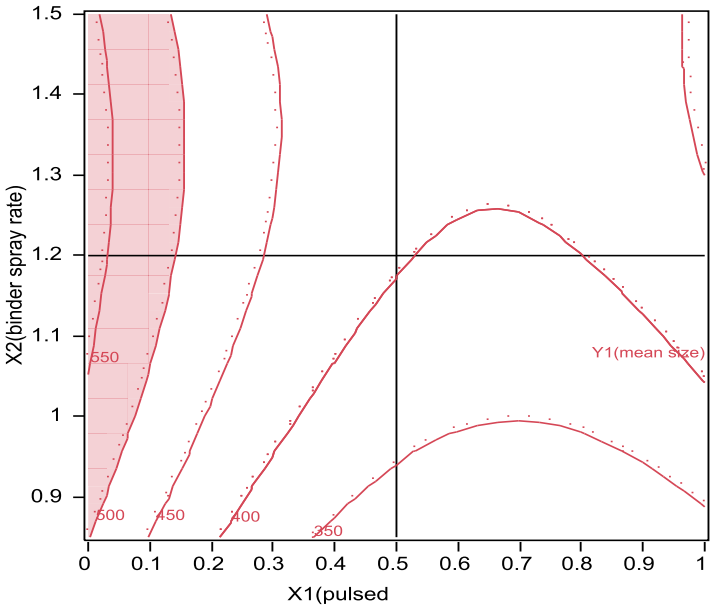

(b)

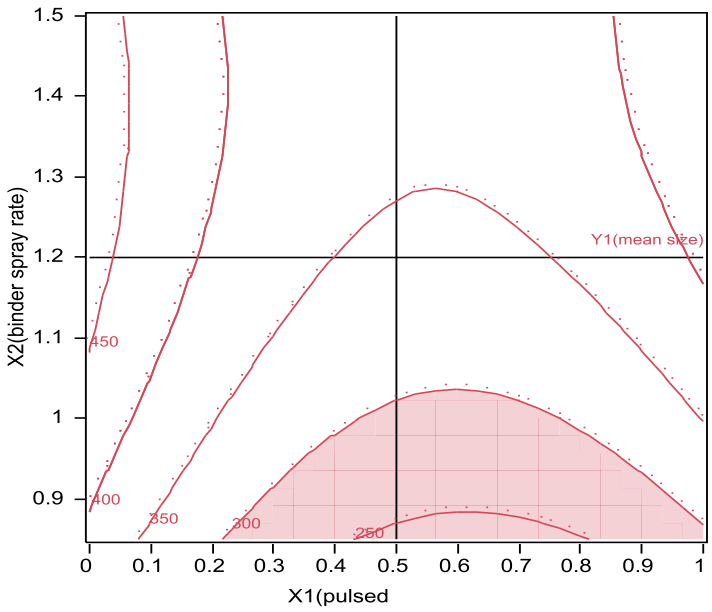

(c)

Figure 3.2 Response contour plots showing effect of pulsed frequency (X_1) and binder spray rate (X_2) on mean size of final granules (Y_1) (a) at low level of atomization pressure (X_3); (b) at medium level of atomization pressure (X_3); (c) at high level of atomization pressure (X_3)

The main effect of the independent variables on the dependent variable Y_1 is summarized using a Pareto chart and interaction plot in Figure 3.3. From the interaction plots, it is shown that at a high level of the pulsed frequency, the mean granulate size remained constant with changes in the spray rate and atomization pressure. The mean granule size showed significant change by changing the pulsed frequency within the whole ranges of spray rate and atomization pressure. The mean granule size decreased with increasing the atomization pressure. The standardized Pareto chart for Y_1 depicts the main effect of the independent variables on the mean granule size in fluidized bed granulation. The length of each bar in the graph indicates the effect of these factors and the level of their effects on the response. From Figure 3.3(a), it can be inferred that factors X_3, X_1, X_2, and X_1^2 have significant effects on the mean granule size. The most significant factor was the atomization pressure and the next two most significant factors were the quadratic term of X_1^2 and direct term of X_1. Therefore the complex effects of the pulsed frequency on the mean size of granules should be studied thoroughly to achieve desired granule size.

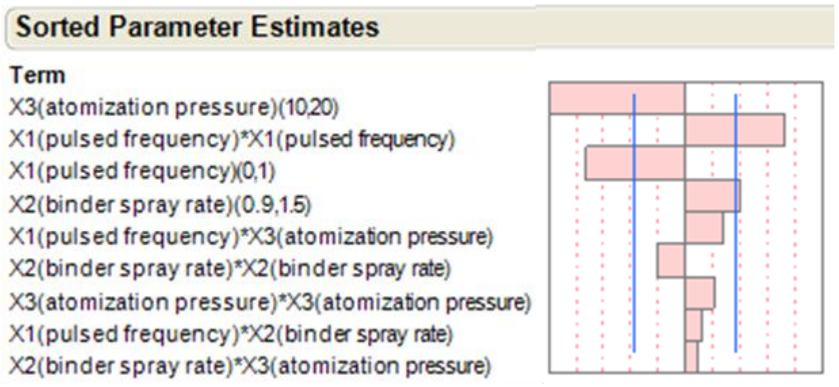

(a)

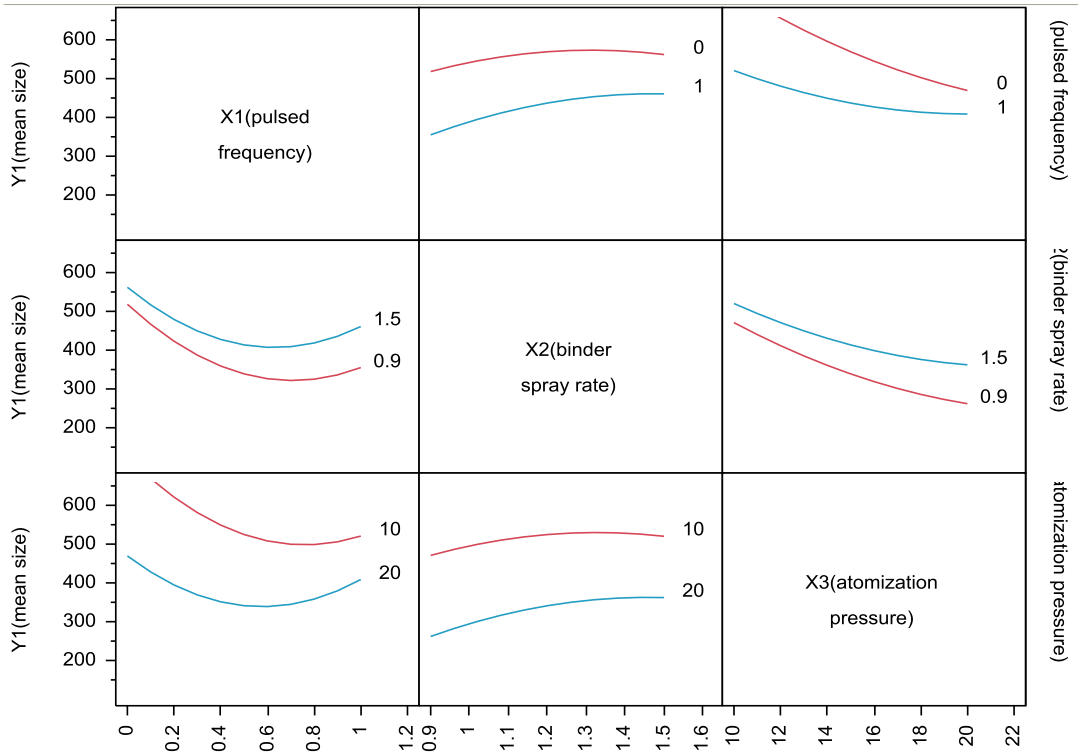

(b)

Figure 3.3 Effects of independent variables on the mean particle size Y_1: (a) standard Pareto chart showing the effects of independent variables and their combined effects on the mean size of granules; (b) interaction plot showing the quadratic effects of interactions between factors on the mean size of granules

The effect of X_1 and X_2 and their interaction on the granule yield (Y_2) at low, medium and high levels of atomization pressure X_3 is given in Figure 3.4. It is shown that with increasing atomization pressure, operating ranges of parameters of X_1 and X_2 to achieve the desired granule yield (Y_2) of 85% increased. Generally at fixed atomization pressure and spray rate, increasing the pulsed frequency in a spray circle resulted in a reduced

yield. The reason could be due to attrition of granule surfaces during the pulsed phase resulting in more fines which were out of desired range of granules [52].

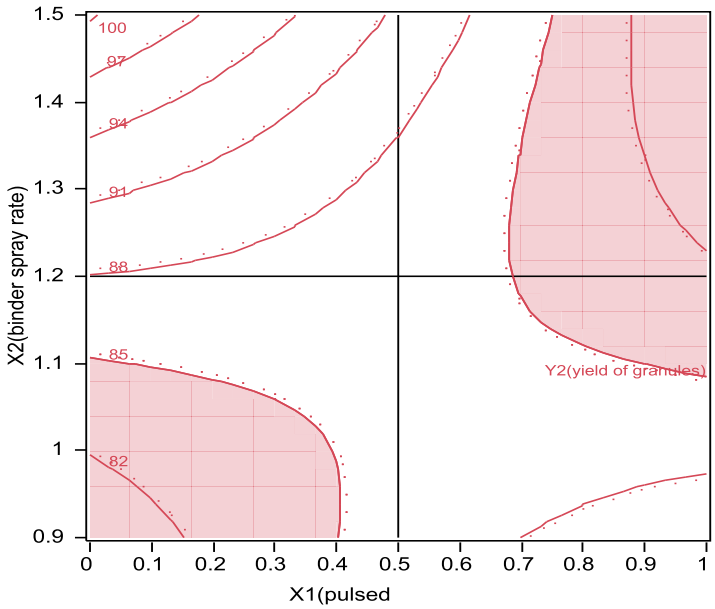

(a)

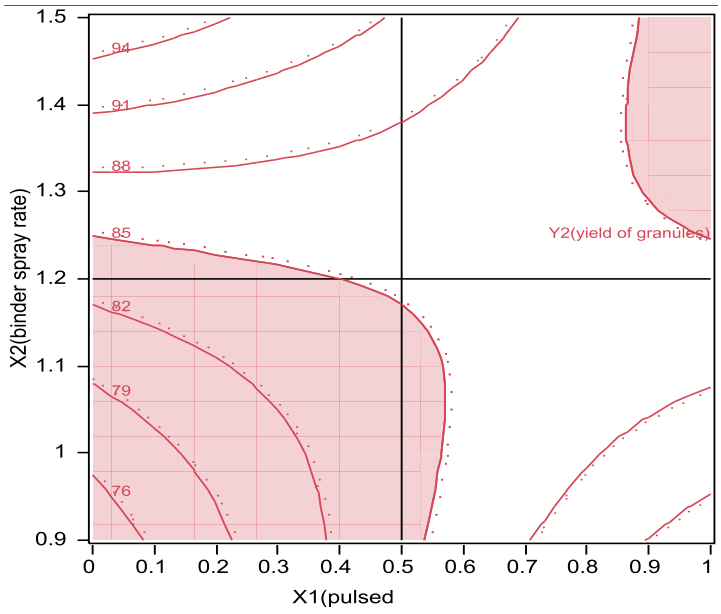

(b)

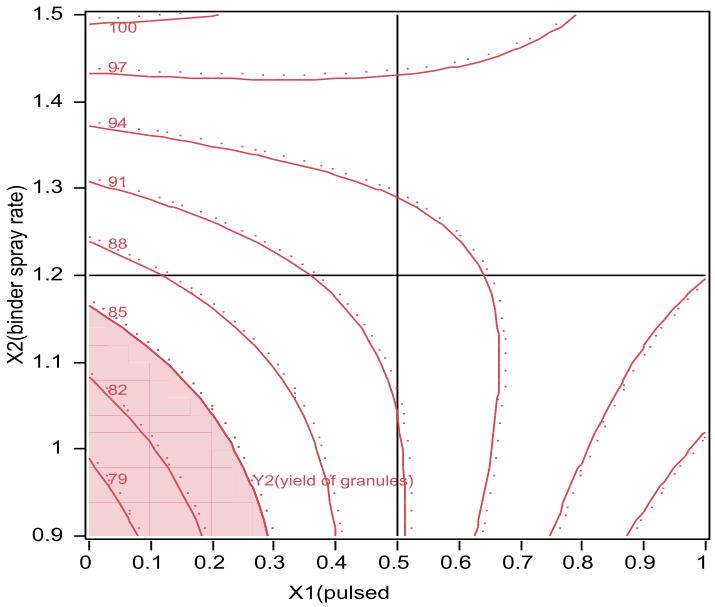

(c)

Figure 3.4 Contour plots showing effect of pulsed frequency (X_1) and binder spray rate (X_2) on final granule yield (Y_2): (a) at low level of atomization pressure; (b) at medium level of atomization pressure; (c) at high level of atomization pressure

The main effect of the independent variables on the dependent variable Y_2 is summarized using a Pareto chart and interaction plot in Figure 3.5. Regarding the interaction plot, it is shown that at low level of the atomization pressure, the granule yield remained constant with changes of the pulsed frequency and spray rate. It is observed that there is a strong nonlinear relationship between factors of X_1 and X_2. Factors X_2 and X_3 have almost a linear relationship. From Figure 3.5(a), it is inferred that the interaction term X_1X_2 is the only significant factor to achieve a higher yield rate.

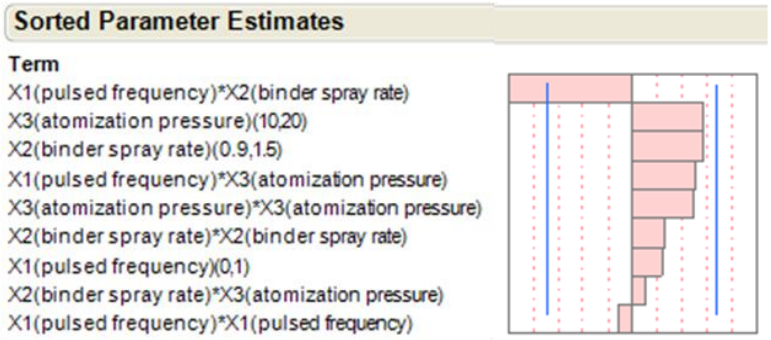

(a)

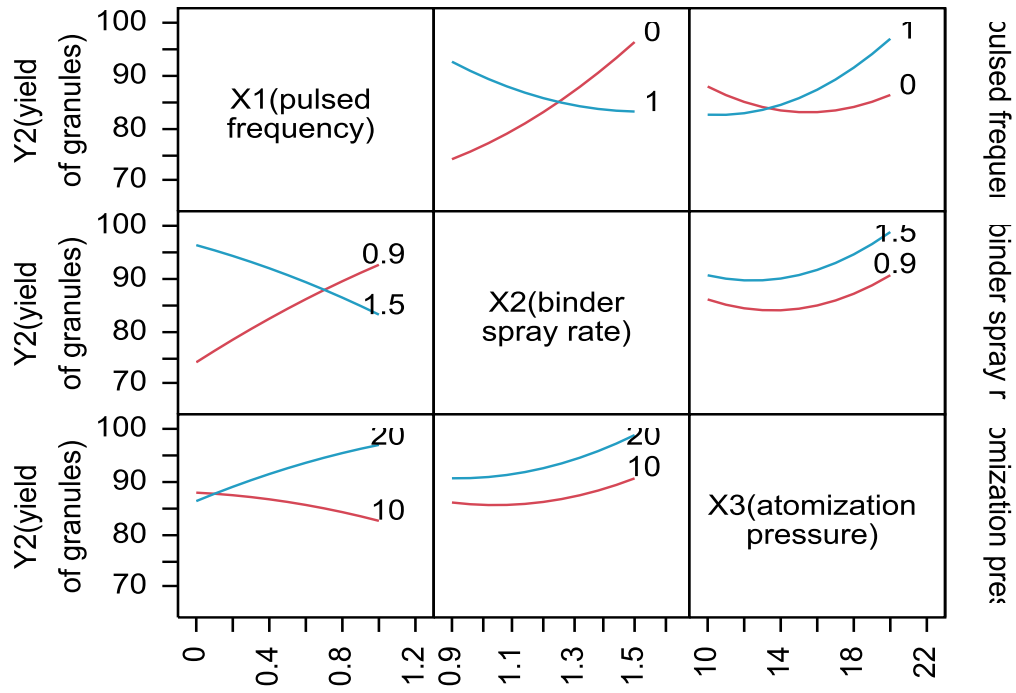

(b)

Figure 3.5 Effects of independent variables on the granule yield Y_2: (a) standard Pareto chart showing the effects of independent variables and their combined effects on the granule yield; (b) interaction plot showing the quadratic effects of interactions between factors on the granule yield

Moisture content of granules is very important, which impacts not only nucleation and growth of granules, but also causes uneven mixing in the bed. If moisture content of granules is high, larger lumps can be formed so that they decrease the mixing and cause further overwetting and defluidization. In order to avoid defluidization in this study, the air flow rate was adjusted to keep the granule flow pattern consistent during granulation.

As granulation proceeded agglomerates became larger and more influential for the air flow. The effect of X_1 and X_2 and their interaction on the moisture content of final granules (Y_7) at low, medium and high levels of atomization pressure X_3 is given in Figure 3.6. All three operating parameters are very much inter-related and have profound effects on the moisture content of granules. Previous studies have shown that the moisture content of granules was affected by not only operating parameters but also by other factors such as the inlet air relative humidity and inlet velocity [12, 14, 52]. In this work, the inlet air relative humidity was uncontrolled varying from 30% to 55%.

Therefore a large model prediction error was observed. In order to predict the moisture content of granules accurately, it would be necessary to include more factors, in particular the inlet air humidity in the model. From Figure 3.6, a clear trend of effect of the pulsed frequency on the moisture content of granules was observed at medium and high levels of the atomization pressure, showing that increasing the pulsed frequency resulted in a reduced moisture content of the granules.

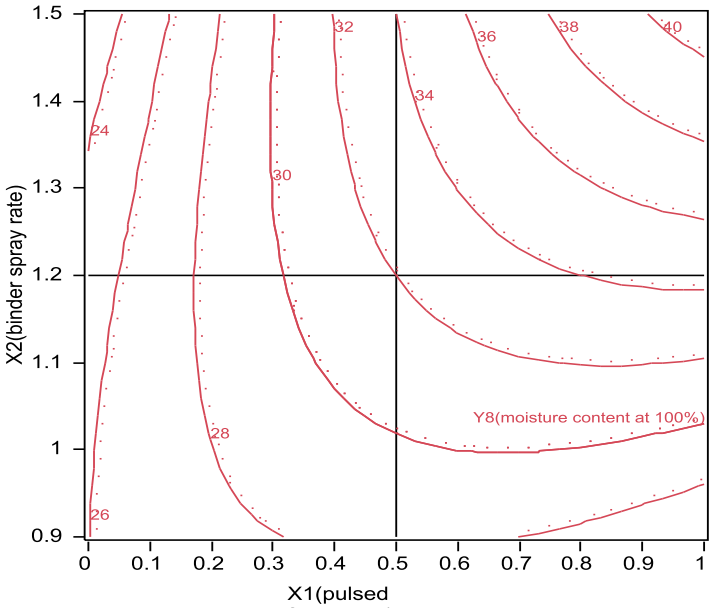

(a)

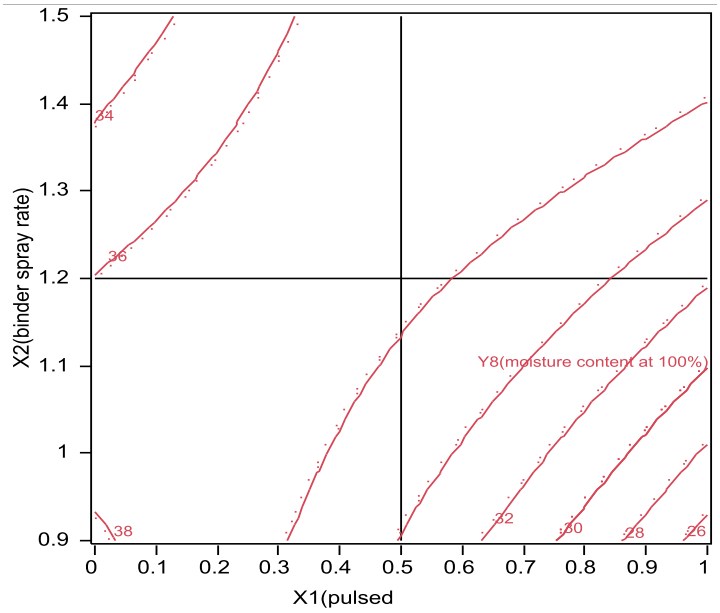

(b)

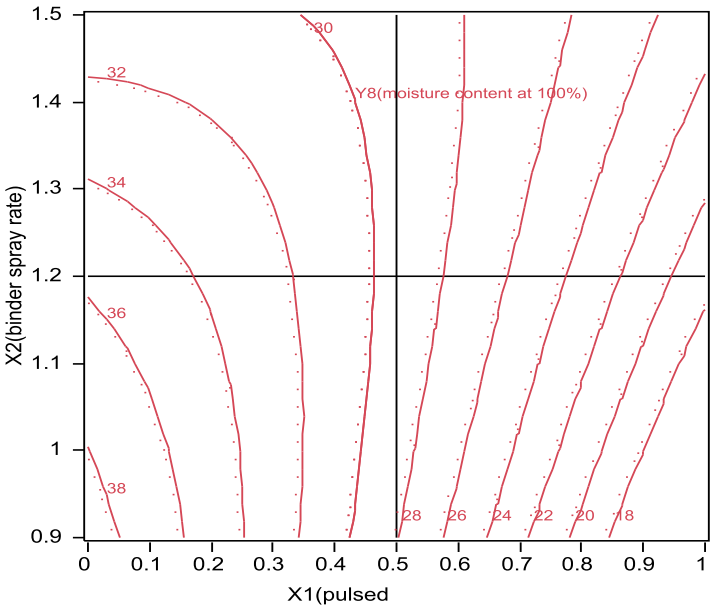

(c)

Figure 3.6 Contour plots showing effect of pulsed frequency (X_1) and binder spray rate (X_2) on moisture content of granules (Y_7): (a) at a low level of atomization pressure; (b) at a medium level of atomization pressure; (c) at a high level of atomization pressure

3.4.4 Determination of a design space

Based on the response surface models, a design space of the FBG process can be defined, in which the final granule quality can be ensured. The design space should define the ranges of the operating parameters of the pulsed frequency, binder spray rate and atomization pressure. The key quality attributes considered in the study were the mean size of final granules Y_1 and granule yield Y_2. The design space of the operating variables of the pulsed frequency X_1, binder spray rate X_2, and atomization pressure X_3 were determined based on applying constraints on the mean size of granules Y_1 ($300 \leq Y_1 \leq 500$) and the granule yield Y_2 ($Y_2 \geq 85\%$). The white areas in Figure 3.7 show the operating ranges of the pulsed frequency X_1 and binder spray rate X_2 at three different levels of the atomization pressure. It is clearly shown that the operating ranges of X_1 and X_2 increase significant with increase of the atomization pressure.

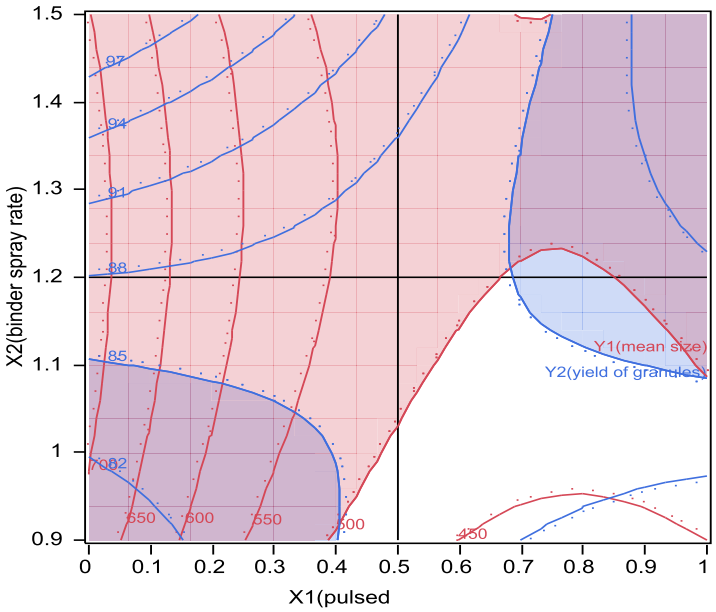
X2(binder spray rate)
X1(pulsed
Y1(mean size)
Y2(yield of granules)
97
94
91
88
85
82
650
600
550
500
450
1.5
1.4
1.3
1.2
1.1
1
0.9
0
0.1
0.2
0.3
0.4
0.5
0.6
0.7
0.8
0.9
1

(a)

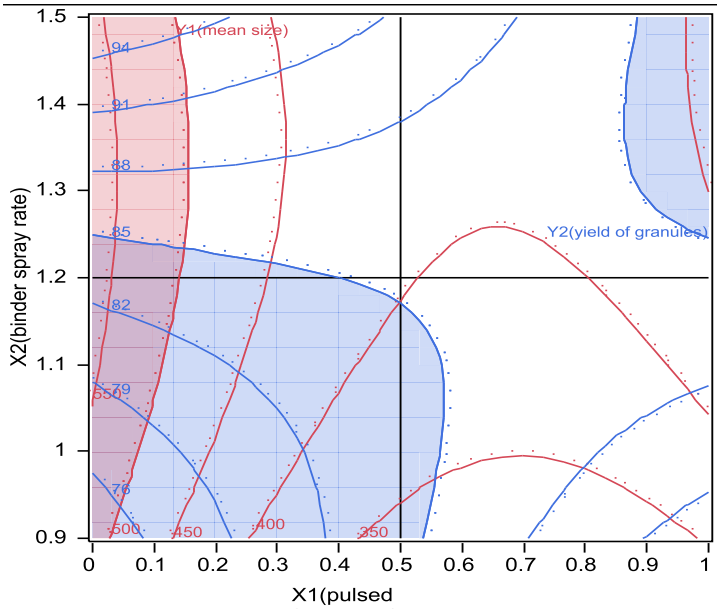
X2(binder spray rate)
X1(pulsed
Y1(mean size)
Y2(yield of granules)
94
91
88
85
82
79
76
550
500
450
400
350
1.5
1.4
1.3
1.2
1.1
1
0.9
0
0.1
0.2
0.3
0.4
0.5
0.6
0.7
0.8
0.9
1

(b)

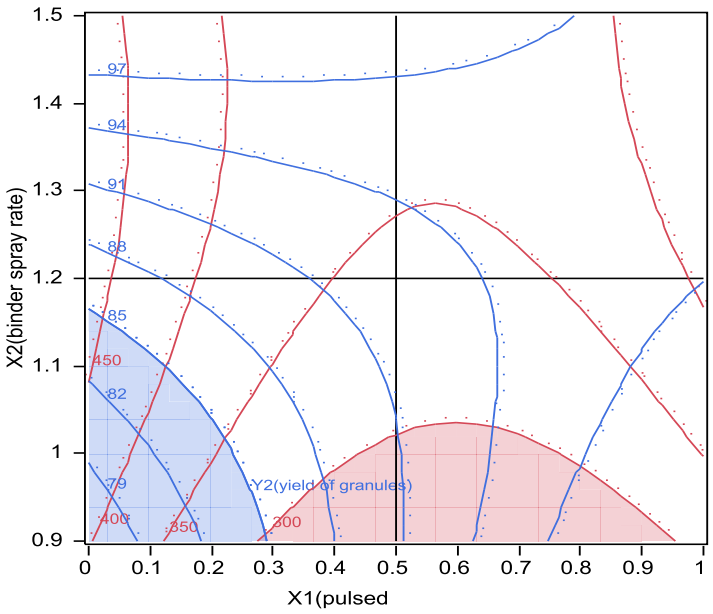

(c)

Figure 3.7 Design space for the FDG process: (a) operating ranges of pulsed frequency and binder spray rate at low level of atomization pressure; (b) operating ranges of pulsed frequency and binder spray rate at medium level of atomization pressure; (c) operating ranges of pulsed frequency and binder spray rate at high level of atomization pressure

3.4.5 Validation for process model

In order to validate the RSM results, further four experiments in which all of operating parameters were in the ranges of the design space have been carried out. The operating conditions, the experimental and predicted values of all the response variables and their percentage errors were already shown in Table 3.6. From the results, it is shown that the prediction error between the experimental values of the responses and those of the anticipated values was small, varying between 1.21% and 5.57% for Y_1 and between 0.62% and 8.43% for Y_2.

Table 3.6 Validation results for FBG process

Operating conditions (X_1:X_2:X_3)	Response variable	Experimental value (y)	Model prediction ($\hat{y}$)	Percentage of prediction error ($\frac{\lvert y-\hat{y}\rvert}{y}$%)
(0.4;1.4;12)	*Mean granule size Y_1(um)*	506.00	494.93	2.19
	Granule yield Y_2(%)	89.34	88.79	0.62
(0.6;1.3;14)	*Mean granule size Y_1(um)*	426.96	421.80	1.21
	Granule yield Y_2(%)	83.64	85.59	2.33
(0.8;1.2;17)	*Mean granule size Y_1(um)*	386.53	375.55	2.84
	Granule yield Y_2(%)	84.97	88.64	4.32
(0.9;1;20)	*Mean granule size Y_1(um)*	342.42	323.34	5.57
	Granule yield Y_2(%)	91.01	98.68	8.43

3.4.6 Other granule physical properties

Hausner ratio

Hausner ratio gives a measure of the packing of the granules and it also provides an indication of the granule flow behavior. Hausner ratio tends to be big with smaller granules because of high surface to mass ratio resulting in greater cohesiveness and greater bulk density. Hausner ratio was highly correlated with granule size shown in Figure 3.8, indicating that the Hausner ratio decreases with increasing granule size. Values of Hausner ratio less than 1.25 indicate good flow [208]. Based on the experimental data except for run 12 whose Hausner ratio was abnormal, a regress model between Hausner ratio and granule size can be obtained as y=-0.0001x+1.2819, which means that granule sizes larger than 300 μm can result in acceptable Hausner ratio of 1.25.

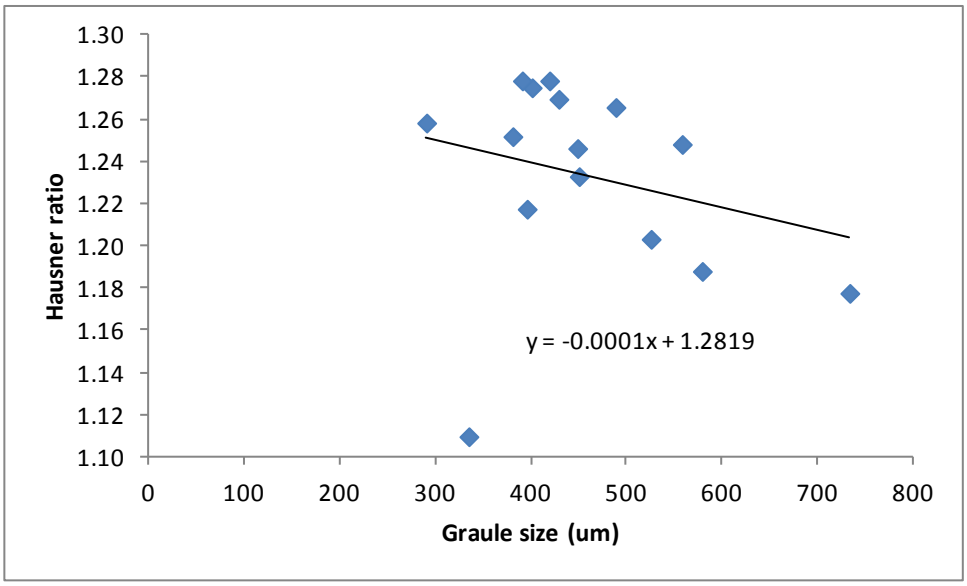

Figure 3.8 Hauser ratio as a function of granule size

Relationship between the final granule moisture content and mean size

Figure 3.9 shows the relationship between the mean size of final granules and moisture content, indicating that there is not direct link between them. In previous studies [14, 52], it has been shown that the granule size increases proportionally with the powder bed moisture content. On the other hand the similar result as that of this study has also been observed by other researchers [12, 209], in which no influence of the humidity on the growth curve of the granules was seen. A possible explanation could be that because the change of the granule moisture content was slow compared to the mixing rate in this study the granule size was determined by the latter factor of mixing affecting the growth and nucleation mechanisms in the bed. In this study, the mixing level was kept constant during granulation by adjusting the inlet fluidizing air velocity so that the moisture content of granules did not affect the growth of granules.

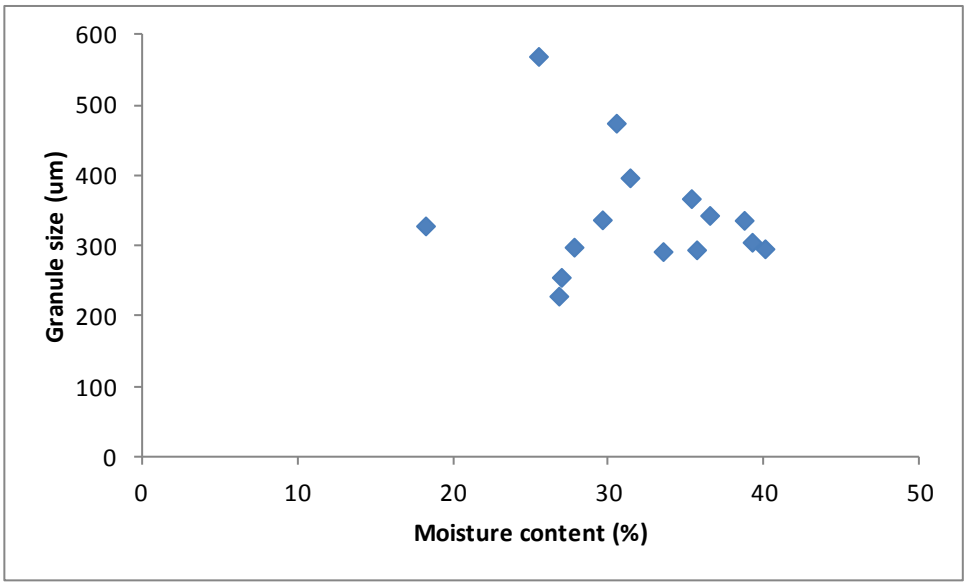

Figure 3.9 Relationship between mean size of final granules and moisture content

3.5 Chapter conclusions

In this chapter, all the experiments carried in this work was introduced, including the materials, experimental apparatus, operating method, sampling and final granule properties characterization. The influence factors of pulsed frequency, binder spray rate and atomization pressure of the top-spray fluidized bed granulation process were studied using the Box-Behnken experimental design method. Different mathematical models were developed to predict the mean size of granules, yield, relative width of granule distribution and final granule moisture content. The study has supported the theory that the granule size can be controlled through the liquid feed pulsing [14, 52, 209]. However, care has to be taken when the pulsed frequency is chosen for controlling the granule size due to the nonlinear quadratic relation in the regression model. The design space of the ranges of operating parameters has been determined based on constraints of the mean size of granules Y_1 ($300 \leq Y_1 \leq 500$) and granule yield Y_2 ($Y_2 \geq 85\%$). High degree of prediction obtained from validation experiments has shown the reliability and effectiveness using the Box-Behnken experimental design method to study the fluidized bed granulation process.

Chapter 4 Population balance modeling and multi-stage optimal control of a pulsed spray fluidized bed granulation

4.1 Chapter overview

The primary aim of this chapter was to develop a process model which can link the key binder solution spray operating factors of the binder spray rate, atomizing air pressure and pulsed frequency of spray with the granule properties to predict granule growth behavior in a pulsed spray fluidized bed granulation process. The model will be then used to design the control strategies to operate the pulsed spray fluidized bed granulation under more optimal conditions to achieve the desired quality of the end granules. The model was based on the one-dimensional discretized population balance model (PBM) of the fluidized bed to describe the changes of granule size by assuming that aggregation and breakage were key mechanisms in the granulation process. Through selecting the appropriate kernels of the aggregation and breakage processes in which the spray operating factors were built, the model can predict evolution of the granule size and distribution at different binder spray operating conditions with accuracy. After the process was developed, based on which a multi-stage open optimal control strategy was proposed to achieve the desired mean size of the end granules. In the method the optimal operating variables related to the binder spray, including the spray rate of binding liquid, atomizing air pressure and pulsed frequency of spray, were determined through adjusting the trajectory of the evolution of the granule size distribution at predefined sample intervals.

4.2 Population balance model

The full population balance model considering nucleation, growth, aggregation and breakage was already introduced in chapter 2 and given in equation (2.1) and equation (2.3) in continuous and discretization form, respectively. In this chapter, only the aggregation and breakage were simultaneously considered in the PBM, which means equation (2.1) and (2.3) only consider the aggregation and breakage terms. The population balance model will not be rewritten here and the equation (2.3) mentioned in

this chapter means the equation (2.3) only considering aggregation and breakage terms.

In this work, the group of ordinary differential equations in equation (2.3) was solved by the ode45 solver in MATLAB based on the following assumptions: (a) every particle is a sphere; (b) the size of granules in a particular size class is represented by the left edge of the size interval; and (c) the relative growth rate is uniform for each particle within the same volume interval.

4.2.1 Selection of aggregation model

An aggregation model can generally be split into two parts as [16, 210]

$$\beta(t, l, \mu) = \beta_0(t, \Theta, \Psi)\beta^*(l, \mu) \tag{4.1}$$

where $\beta_0(t, \Theta, \Psi)$ is the granulation rate constant, which incorporates various system parameters Θ, such as the binder spray and fluidization operating conditions for a top spray fluidized bed granulator, and nonequipment parameters Ψ, such as physical properties of the powder mixtures. The second term $\beta^*(l, \mu)$ expresses the influence of granule size on the likelihood of aggregation.

Based on our previous study of a top spray fluidized bed granulator, it was shown that the quality of end granules was affected significantly by the binder solution spray conditions [198]. Therefore, for the given materials and formulation, the granulation rate constant β_0 should be a function of the binder solution spray conditions of the pulsed frequency x_1, binder spray rate x_2 and atomization pressure x_3, which can be represented as a non-linear quadratic model as

$$\beta_0(x_1, x_2, x_3) = b_0 + b_1x_1 + b_2x_2 + b_3x_3 + b_{12}x_1x_2 + b_{13}x_1x_3 + b_{23}x_2x_3 + b_{11}x_1^2 + b_{22}x_2^2 + b_{33}x_3^2 \tag{4.2}$$

where b_0, b_1……, b_{33} are constants.

There are many empirical or semi-empirical mathematical models proposed for the second term of $\beta^*(l, \mu)$ and a general expression can be described as [211],

$$\beta^*(l,\mu) = (l+u)^p \tag{4.3}$$

where p is the order of the kernel. The order of the kernel enables the aggregation to become size independent if $p=0$ or to follow Smoluchowski's shear kernel if $p=3$.

All constants b_0, b_1 ……, b_{33} and p in the aggregation model will be determined through fitting the experimental datasets, which will be detailed in section 4.2.3.

4.2.2 Selection of breakage model

A breakage selection function can also be described as the following two parts [81, 211],

$$S(t,l) = S_0(t,\Theta,\Psi)S^*(l) \tag{4.4}$$

Where $S_0(t,\Theta,\Psi)$ is the breakage selection rate constant, which incorporates various system parameters Θ and physical property parameters Ψ of powder mixture. The second term $S^*(l)$ is the size dependence of the selection rate.

Similar as the granulation rate constant β_0, the breakage selection rate constant can be represented as a non-linear quadratic model of the binder solution spray conditions of the pulsed frequency x_1, binder spray rate x_2 and atomization pressure x_3, detailed as

$$S_0(x_1,x_2,x_3) = c_0 + c_1x_1 + c_2x_2 + c_3x_3 + c_{12}x_1x_2 + c_{13}x_1x_3 + c_{23}x_2x_3 + c_{11}x_1^2 + c_{22}x_2^2 + c_{33}x_3^2 \tag{4.5}$$

Where c_0, c_1……, c_{33} are constants.

The size dependence of the selection rate $S^*(l)$ is assumed as

$$S^*(l) = l^q \tag{4.6}$$

Where q is the order of the kernel, which enables the breakage to become size independent if $q=0$ or to be proportional to the particle volume if $q=3$.

The breakage kernel $b(l|\mu)$ describes the formation of fragments of diameter l from the breakage of particles of diameter μ. In this study, it is assumed that any size of fragment

is equally probable and the total volume of the fragments formed equals the volume of the selected breakage of particle of diameter μ. Therefore the breakage kernel $b(l|\mu)$ is described as

$$b(l|\mu) = \frac{6l^2}{\mu^3} \tag{4.7}$$

All constants c_0, c_1……, c_{33} and q in the breakage model will be determined from the experiments detailed in section 4.2.3.

4.2.3 Determination of the parameters of aggregation and breakage models

In order to predict the evolution of granule size distribution under different operating conditions of the binder solution spray in a top spray fluidized bed granulation process, a best fit approach is adopted, in which the set of parameters used in the PBM is the best prediction for the experimental data of dynamics of granulation processes in chapter 3. In this work, the granule size distribution was chosen as the criterion for the dynamics of granulation. Details of the modeling approach used in this work are illustrated in Figure 4.1. In the algorithm, the first step is to define the kinetics of aggregation and breakage mechanisms in the PBM by setting one of combinations of $p \in \{0, 1,2,3\}$ and $q \in \{0,1,2,3\}$. In the second step, the granulation rate $\beta_{p,q,0,k}$ and breakage selection rate $S_{p,q,0,k}$ constants for each experimental data set $k = 1,2, \dots, n$ are determined by minimizing the following cost function of the sum of square errors (SSE) of the particle size distribution through an iterative optimal algorithm for a given p and q,

$$\min_{\beta_{p,q,0,k},S_{p,q,0,k}} \left\{ SSE\left(p, q, \beta_{p,q,0,k}, S_{p,q,0,k}\right) = \right.$$
$$twtiwiVNt,i-VNt,ip,q,\beta p,q,0,k,Sp,q,0,k\,2 \tag{4.8}$$

where w_t and w_i are the optional weights of each size class over time and size, $N_{t,i}$ is the measured number of granules in the size range of (L_i, L_{i+1}) at time t and $V\left(N_{t,i}\right)$ is the normalized volume fraction of particles $N_{t,i}$, and $\widehat{N}_{t,i}$ is the predicted number based on $\beta_{p,q,0,k}$and $S_{p,q,0,k}$ and $V\left(\widehat{N}_{t,i}\right)$ is the normalized volume fraction of particles $\widehat{N}_{t,i}$. In

this study, we only considered the end granule size distribution and therefore both of w_t and w_i were set as 1.

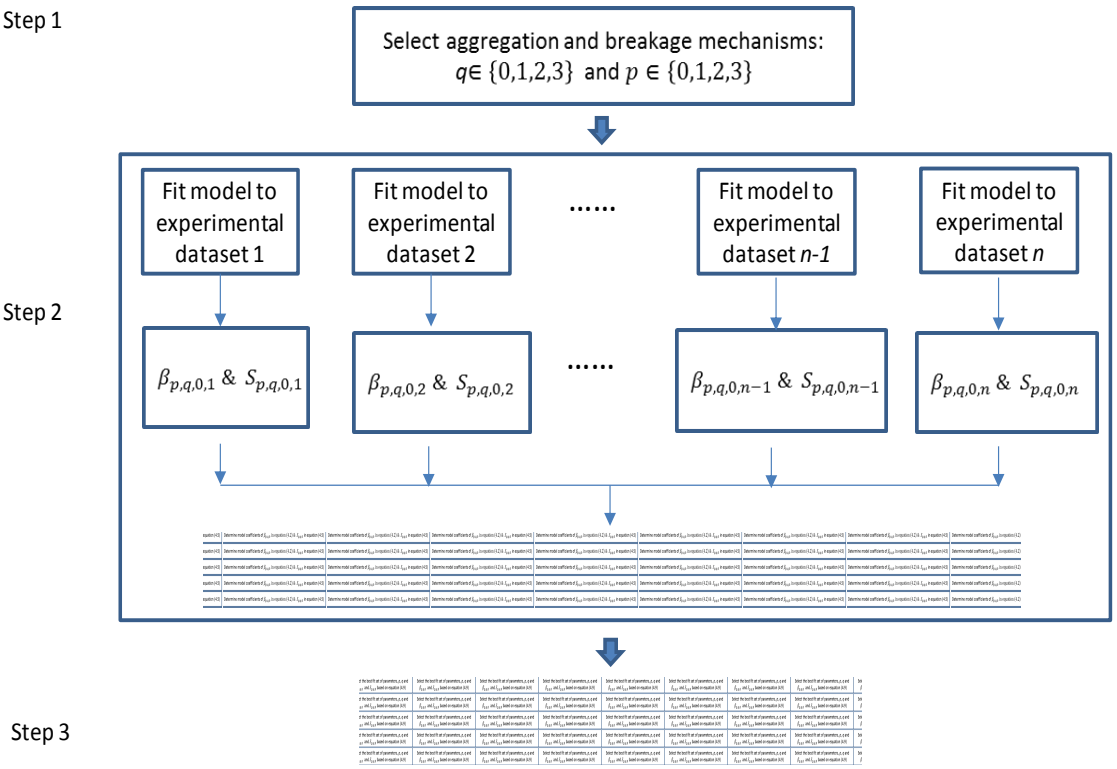

Figure 4.1 Schematic diagram of modeling approach to determine the optimal set of parameters for PBM

For each experimental dataset the aggregation rate constant $\beta_{p,q,0,k}$ and breakage selection rate constant $S_{p,q,0,k}$ were determined by optimizing the objective function in equation (4.8) using the iterative optimization method provided by the optimization Toolbox in MATLAB in this work. The population balance model is solved using the MATLAB function 'ode45', which is a variable-step solver. The function of 'lsqcurvefit', which solves nonlinear curve-fitting (data-fitting) problems in least-squares sense in equation (4.8), is used to determine the aggregation rate and breakage selection rate constants. When the 'lsqcurvefit' is used to solve a nonlinear programming problem, it is normally difficult to find the global optimal point because of the nonconvex or non-smooth of the process model. Hence, a multi-starting-point optimization technique is utilized. This is achieved by repeating the optimization randomly starting from a feasible solution space and then finding the best solution. The

limitation lies in the ability to adequately search the entire feasible region of the parameter space. It is noted that no guarantee can be made on local or global optimality of the resulting solution, especially for very complex process model. In this work, the solution searched by setting 20 starting points demonstrated good optimality when comparing with the experimental results. In the optimization method, the maximum iteration and desired error limitation were set as 500 and 1×10^{-8}. The commercial software MATLAB (2011b) on a 2 GHz Intel Four Core processor desktop computer with 4 GB RAM using a XP platform was used in computation.

Once the best fit parameters of $\beta_{p,q,0,k}$ and $S_{p,q,0,k}$ for each of experimental dataset were obtained at the given aggregation kernel p and breakage kernel q , the process model parameters of $\beta_{p,q,0}(x_1, x_2, x_3)$ and $S_{p,q,0}(x_1, x_2, x_3)$ linking the binder solution spray operating parameters in equations (4.2) and (4.5) can be obtained using JMP 11 software (SAS, SAS Institute, Cary, NC, USA).

Finally the best fit set of parameters, p, q and $\beta_{p,q,0}$ and $S_{p,q,0}$ in the PBM in equation (2.3) is obtained based on the minimal prediction error given by

$$optmal\left\{p, q, \beta_{p,q,0}(x_1, x_2, x_3),\ S_{p,q,0}(x_1, x_2, x_3)\right\} =$$

$$\min_{p,q}\left\{\sum_{k=1}^{n}\sum_{t} w_t \sum_{i} w_i \left(V\left(N_{t,i}\right) -\right.\right.$$

$$VNt,ip,q,\beta p,q,0,kx1,x2,x3,Sp,q,0,kx1,x2,x32 \qquad (4.9)$$

where n is the total number of experiments.

4.3 PBM based multi-stage optimal strategy to determine the optimal operating conditions of binder solution spray

For a continuous fluidized bed granulation process, a closed-loop control strategy can be implemented through on-line adjusting the operating factors, such as the solid feed rate and binder spray rate, to achieve the desired granule size distribution and consistent quality based on the process model and different control strategies [193, 194, 212-214].

However, there are more challenges on implementation of a closed-loop strategy to adjust the operating factors of a batch fluidized bed granulation process in real time. For a batch fluidized bed granulation, the process is inherently unstable, very sensitive to its bed humidity, large delay and short processing time. Any change of the binder spray operating conditions during a fluidized bed granulation process could pose the danger of overwetting of the particles, leading to a non-retrievable bed collapse. Additionally, on-line measurements of critical parameters of granules during fluidized bed granulation, in particular granule size and size distribution, is still challenging and problematic even though significant progress has been made over past few years [215]. Therefore, the best way to control a fluidized bed granulation process is to set the operating conditions right from the beginning of the operation. In this chapter, a multi-stage open optimal control strategy was proposed to achieve the desired mean size of the end granules. In the method the optimal operating variables related to the binder spray, including the spray rate of binding liquid, atomizing air pressure and pulsed frequency of spray, were determined through adjusting the trajectory of the evolution of the granule size distribution at predefined sample intervals.

Based on the developed model of a pulsed spray fluidized bed granulation process in Section 4.2, the optimal operating conditions of the binder solution spray can be determined, with the aim of obtaining the end granules with the desired properties, such as mean size, size distribution and yield of final granules. To simply the problem, the mean size of the end granules was considered as the sole objective of optimization in this study. Therefore, the optimal operating conditions of the binder solution spray, including the pulsed frequency x_1, binder spray rate x_2 and atomization pressure x_3, can be determined by solving the following optimization problem as

$$\min_{x_1,x_2,x_3}\left\{J=\left(\overline{D}_m-\widehat{D}_m\left(t_f\right)\right)^2\right\} \tag{4.10}$$

Subject to:

(a) $\frac{\partial n(t,l)}{\partial t}=f(x_1,x_2,x_3,t)$ given by the PBM in equations (2.3) and (4.1)-(4.9)

(b) Operating range of pulsed frequency x_1 as $x_{1\_min}\le x_1\le x_{1\_max}$

(c) Operating range of binder spray rate x_2 as $x_{2\_min} \leq x_2 \leq x_{2\_max}$

(d) Operating range of atomization pressure x_3 as $x_{3\_min} \leq x_3 \leq x_{3\_max}$

Where $\overline{D}_m$ is the desired mean diameter of end granules; t_f is the granulation completion time at which a fixed amount of binder solution has been sprayed; $\widehat{D}_m(t_f)$ is the mean size of the end granules given by

$$\widehat{D}_m(t_f) = \sum_{i=1}^{n_{max}} V\left(\widehat{N}_i(t_f)\right) d_{pi} \tag{4.11}$$

Where $V\left(\widehat{N}_i(t_f)\right)$ is the volume fraction of end granules at size interval $i = 1, 2, \ldots, n_{max}$, $\widehat{N}_i(t_f)$ is the number of end granules in the *i*th size interval calculated by the PBM in equation (2.3), and d_{pi} is the geometrical mean of the size interval $i = 1, 2, \ldots, n_{max}$.

This is an open-loop optimization problem in which the trajectory of the mean granule size evolution is determined to achieve the desired mean diameter of end granules. The same optimization method for the modeling development in section 4.2 was used for determination of the optimal settings of the pulsed frequency x_1, binder spray rate x_2 and atomization pressure x_3. It is well known that the drawback of an open-loop optimization problem is that it relies on accuracy of the process model. For a batch top-spray fluidized bed granulation process it is undoubted that there exists the model mismatch between the developed PBM and actual granulation process. Hence, a multi-stage optimization strategy has been developed, shown in Figure 4.2. At the beginning of the granulation process, the optimal settings of the pulsed frequency x_{1_0}, binder spray rate x_{2_0} and atomization pressure x_{3_0} is determined based on the desired end mean size $\overline{D}_m(t_f)$ and PBM, and the trajectory of the mean granule size evolution is given in the Figure 4.2. Due to the model mismatch, it is expected that the actual mean size of end granules is $\widehat{D}_{pm\_0}(t_f)$ which is significantly different from the desired value of $\overline{D}_m(t_f)$. If the granule size distribution is available through an on-line particle sizer at a sampling time t_1, the optimal settings of the binder solution spray can be adjusted through a new optimal search at a new initial process point $\widehat{D}_{pm\_1}(t_1)$ based on a

modified objective function in which the model mismatch $\Delta\overline{D}_c(t_1) = \widehat{D}_{pm\_1}(t_1) - \widehat{D}_{mm\_1}(t_1)$ can been compensated as

$$\min_{x_1,x_2,x_3}\left\{J = \left(\overline{D}_m - \gamma * \Delta\overline{D}_c(t_1) - \widehat{D}_m(t_f)\right)^2\right\} \tag{4.12}$$

where γ is an adjusting parameter, which was set at 1 in this work. Therefore, the adjusted optimal settings of the pulsed frequency x_{1_1}, binder spray rate x_{2_1} and atomization pressure x_{3_1} can be determined and the 1st adjusted trajectory of the mean granule size evolution is shown in Figure 4.2. Depending on the availability of the on-line granule size distribution measurements, the same approach can be used at another sampling time t_2 shown in Figure 4.2. By utilizing this approach, the desired mean size of end granules can be achieved.

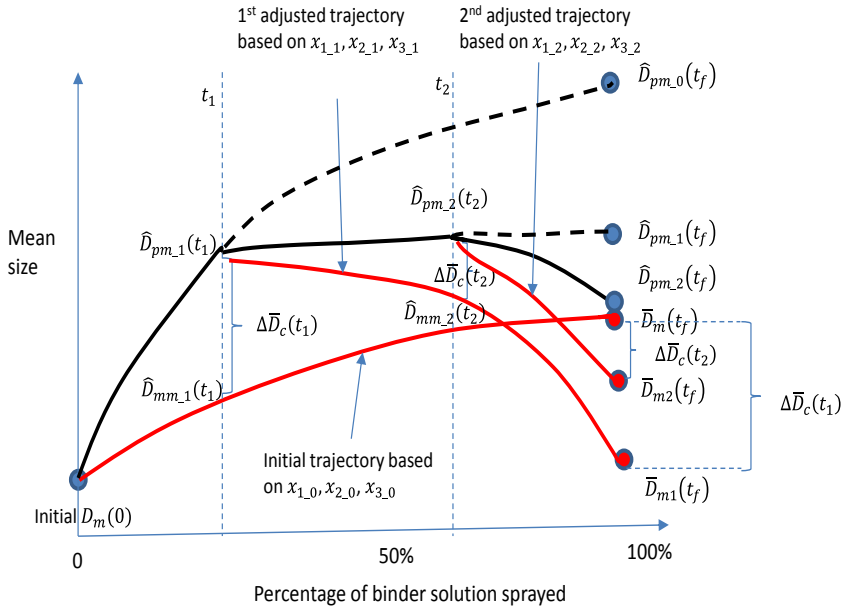

$\overline{D}_m(t_f)$: desired mean size

$\overline{D}_{m1}(t_f)$: adjusted desired mean size based on size measurement at t_1

$\overline{D}_{m2}(t_f)$: adjusted desired mean size based on size measurement at t_2

$\widehat{D}_{pm\_0}(t_f)$: actual mean size based on initial optimization

$\widehat{D}_{pm\_1}(t_f)$: actual mean size adjusted based on size measurement at t_1

$\widehat{D}_{pm\_2}(t_f)$: actual mean size adjusted based on size measurement at t_2

Figure 4.2 Multi-stage optimal control strategy

4.4 Experimental data processing

Final granule size distribution was determined by the sieve analysis method. A set of

sieves (150, 180, 250, 355, 500, 710, 1000, and 2000 um)

The experiments results obtained in chapter 3 were used in the modeling work of this chapter. However, in order to carry out the modeling work in section 4.2, the raw data from sieving based on the volume fraction have to be first transferred into a standard number-based datasets using a series of size intervals with $r = \frac{L_{i+1}}{L_i} = \sqrt[3]{2}$, where L_{i+1} and L_i are the upper and lower boundaries of *i*th size interval, required by solving the discretized PBM in equation (2.3) proposed by Hounslow et al [89, 107]. An assumption used in the transformation is that the particles volume is normally distributed within each size interval of the initial set of sieves: 150-180, 180-250, 250-355, 355-500, 500-710, 710-1000, 1000-2000 μm. After transformation, the size range used in the modelling work was from 150 μm to 2400 μm which was divided into 12 intervals as: 150-189, 189-238, 238-300, 300-378, 378-476, 476-600, 600-756, 756-952, 952-1200, 1200-1512, 1512-1905, 1905-2400 μm. At the beginning of the simulation, all initial particles were defined to have a diameter of 150 μm in the first size interval and total number of particles was 5.8475×10^7 corresponding to the total number of primary particles used in the experiments.

4.5 Results and discussion

4.5.1 Determination of PBMs for a pulsed top spray fluidized bed granulation

A PBM based process model has been developed based on the experimental data obtained in section 4.4 using the proposed method in section 4.2 to predict the evolution of granule size in a pulsed spray fluidized bed granulation process at different operating conditions of the binder solution spray.

The kernel orders of p in the aggregation model and q in the breakage model indicate the mechanisms of evolution of the granules during granulation. If values of p and q are 0, it indicates that aggregation and breakage of the granules are size independent and while as if values of p and q are 1, 2, or 3, it shows that the aggregation and breakage of granules are dependent on granules' length, surface area or volume. In total 16 combinations of p and q have been tested to investigate the mechanisms of granulation

in a pulsed spray fluidized bed granulation process in this work. For each combination of p and q, the granulation rate constant $\beta_{p,q,0,k}$ and breakage selection rate constant $S_{p,q,0,k}$ for each experimental dataset were determined based on the cost function in equation (4.8). Subsequently the parameters of non-linear quadratic models of the granulation rate constant $\beta_{p,q,0}$ in equation (4.2) and breakage selection rate constant $S_{p,q,0}$ in equation (4.5) which link the operating factors of the binder spray rate, atomizing air pressure and pulsed frequency of spray were determined. The SSE of the end granule size distribution between the experimental data and model predictions can be calculated for each combination of p and q in equation (4.9) and the relative magnitude of the SSEs in volume fraction for all combinations of the aggregation and breakage kernels is shown in Figure 4.3. It is clearly indicated that the PBMs show good predictions when the breakage kernel q is zero, indicating the breakage of granules was size independent during granulation. Among them, the best fitted PBM is $p=3$ and $q=0$, indicating the aggregation of granules was dependent on the granule volume following the Smoluchowski's shear kernel. Studies of aggregation and breakage kernels in fluidized bed granulation have indicated that they were closely correlated with the mixing properties of a fluidized bed, such as Stokes number [16, 80]. In the study, the experiments were carried out at the same level of fluidization during granulation for each granulation experiment. Therefore, the Stakes number was kept constant over the whole granulation process. It was not surprising that the breakage kernel was constant [16]. Aggregation kernel was dependent the volume of granules which was the same as the previous study for the best predictive PBM [80]. Table 4.1 shows the best two PBMs obtained from the mathematical fitting. From the R-Square of sum of fit and P-value of ANOVA, it can be seen all the aggregation models and breakage models of p=2, q=0 and p=3, q=0 can well fit the original kernel constants, which also means these model can be trusted in following work.

Table 4.1 Fitted aggregation and breakage models

	Model 1 (*p=3, q=0*)				Model 2 (*p=2, q=0*)			
	Aggregation model		Breakage model		Aggregation model		Breakage model	
	$\beta(x_1, x_2, x_3, l, \mu) = \beta_0(x_1, x_2, x_3)(l + \mu)^3$		$S(x_1, x_2, x_3, l) = S_0(x_1, x_2, x_3)$		$\beta(x_1, x_2, x_3, l, \mu) = \beta_0(x_1, x_2, x_3)(l + \mu)^2$		$S(x_1, x_2, x_3, l) = S_0(x_1, x_2, x_3)$	
Terms of non-linear quadratic model	$\beta_0(x_1, x_2, x_3)$		$S_0(x_1, x_2, x_3)$		$\beta_0(x_1, x_2, x_3)$		$S_0(x_1, x_2, x_3)$	
	Coefficient	P-value	Coefficient	P-value	Coefficient	P-value	Coefficient	P-value
Constant	5.55×10^{-1}	0.0006	4.57×10^{-4}	0.1594	3.80×10^{-4}	0.0023	1.29×10^{-3}	0.0096
x_1	-3.34×10^{-1}	0.0006	-2.12×10^{-4}	0.2668	-2.33×10^{-4}	0.0023	-2.99×10^{-4}	0.1832
x_2	1.09×10^{-1}	0.0567	-2.50×10^{-4}	0.1995	2.31×10^{-5}	0.5956	-3.49×10^{-4}	0.1315
x_3	-9.94×10^{-2}	0.074	-3.87×10^{-5}	0.8284	-1.04×10^{-4}	0.052	-1.32×10^{-4}	0.5246
$x_1 * x_2$	8.80×10^{-2}	0.2174	6.39×10^{-4}	0.0445	1.74×10^{-4}	0.0294	1.25×10^{-3}	0.006
$x_1 * x_3$	1.48×10^{-2}	0.8222	-1.63×10^{-4}	0.5261	-7.20×10^{-5}	0.2672	-7.27×10^{-4}	0.0449
$x_2 * x_3$	1.67×10^{-2}	0.799	2.02×10^{-5}	0.9363	2.40×10^{-5}	0.6943	1.16×10^{-4}	0.6892
${x_1}^2$	2.34×10^{-1}	0.0154	1.63×10^{-4}	0.5435	2.10×10^{-4}	0.0172	2.05×10^{-4}	0.5034
${x_2}^2$	-1.05×10^{-2}	0.8775	1.94×10^{-5}	0.941	-3.58×10^{-5}	0.5773	-2.41×10^{-4}	0.4356
${x_3}^2$	-8.44×10^{-2}	0.2501	-4.57×10^{-4}	0.1267	-9.10×10^{-5}	0.1896	-7.64×10^{-4}	0.0437
R-square	0.945896		0.754751		0.92987		0.895353	
Prob>F ANOVA	0.0111		0.2878		0.0203		0.0504	

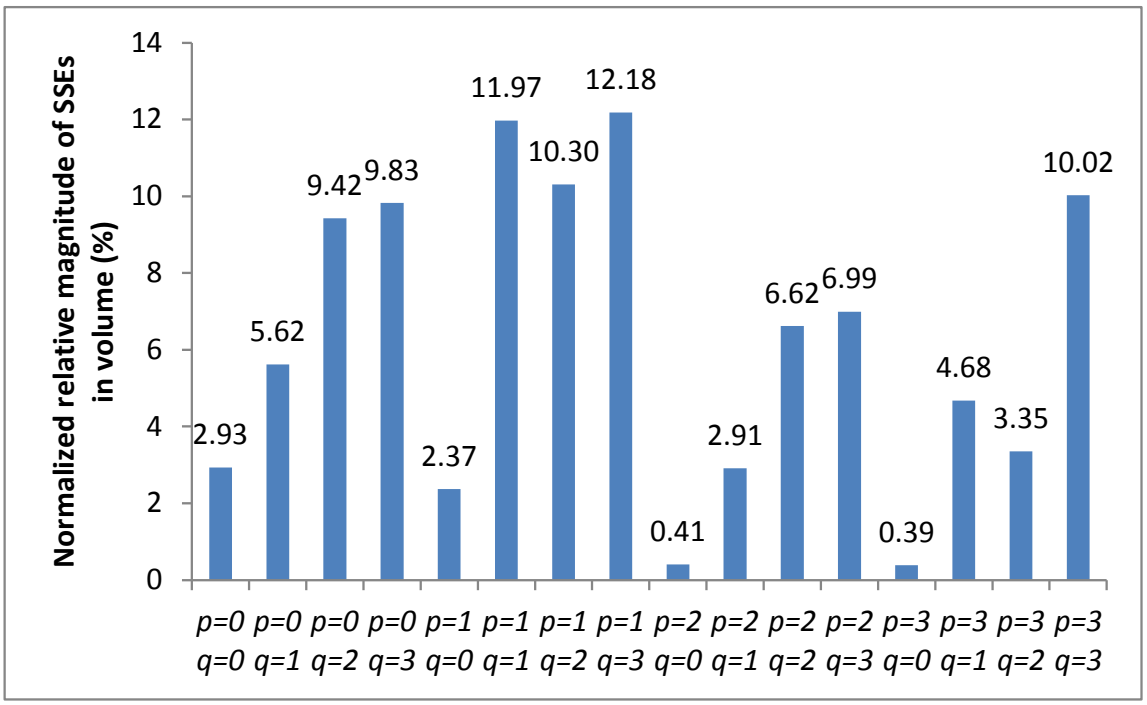

Figure 4.3 Comparison of SSEs for different aggregation and breakage kernels

Figure 4.4 shows the comparison of the final granule size distributions between the experimental data and predictions by the two best PBMs with the kernel orders of $p=3$ and $q=0$ and the kernel orders of $p=2$ and $q=0$. Generally the PBM model can predict the end granules with reasonable accuracy at different operating conditions except for experiments 2 and 4 for the PBM with the kernel orders of $p=3$ and $q=0$ and experiments 13 and 14 for the PBM with the kernel orders of $p=2$ and $q=0$. The discrepancy of the model predictions and experiments is caused by many factors, such as random errors in sampling and granule size measurement. A relative small number of the experimental data set for development of the regression models of $\beta_{p,q,0}$ and $S_{p,q,0}$ is another factor, leading to significant errors in prediction for some data points, in particular, at the boundaries of operating ranges of the parameters. Experiments 7-9 were three replicated experiments carried out at the middle points of the binder spray operating parameters. It is clearly shown that the PBM can predict the end granule size distribution accurately for those three experiments shown in Figure 4.4. Comparison of the mean size of end granules between experiments and PBM predictions is given in Figure 4.4(c), indicating that the mean size of the end granules can be predicted by the PMB with the kernel orders of $p=3$ and $q=0$ accurately.

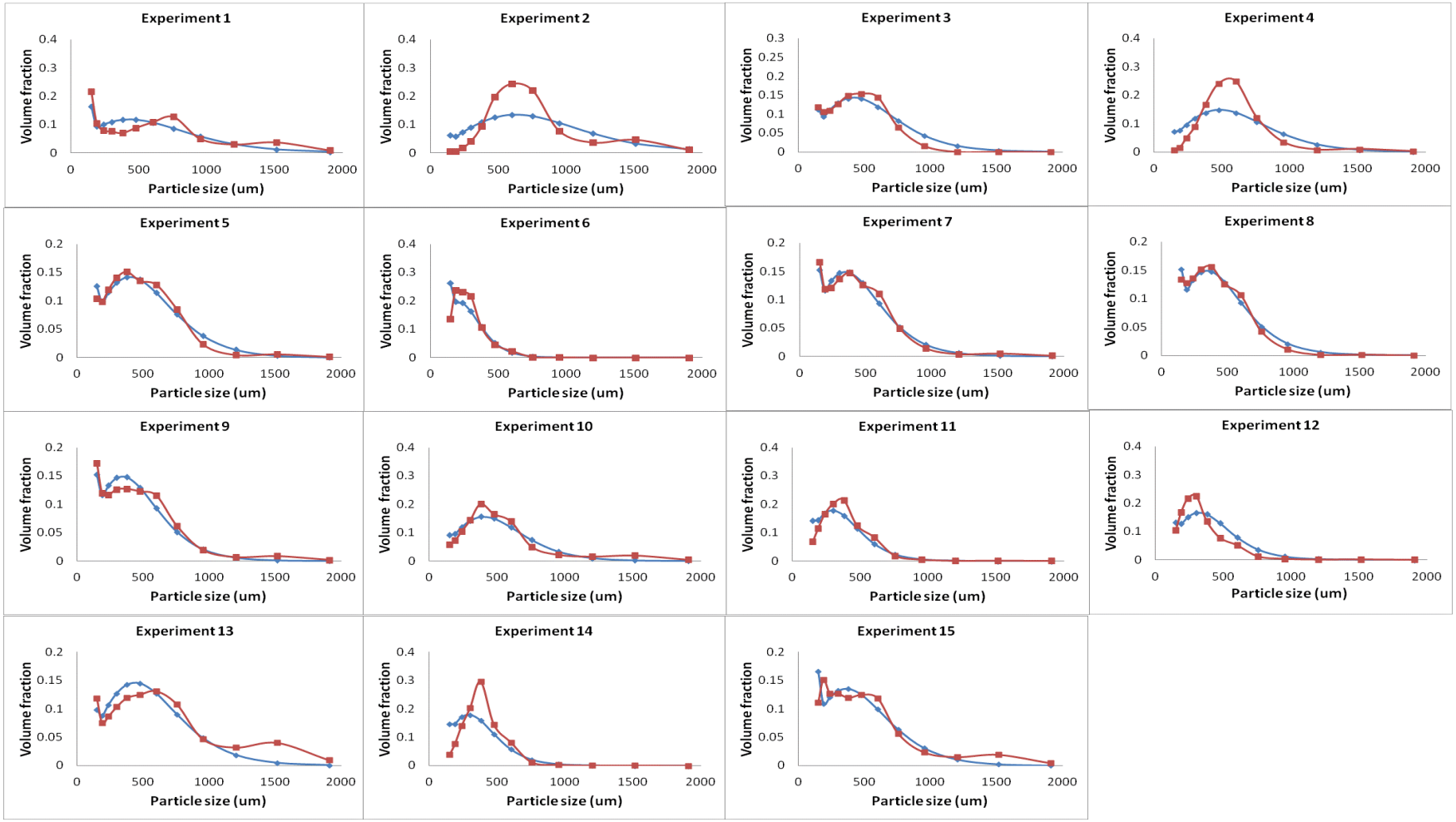
Experiment 1
Experiment 2
Experiment 3
Experiment 4
Experiment 5
Experiment 6
Experiment 7
Experiment 8
Experiment 9
Experiment 10
Experiment 11
Experiment 12
Experiment 13
Experiment 14
Experiment 15
Volume fraction
Particle size (um)

(a)

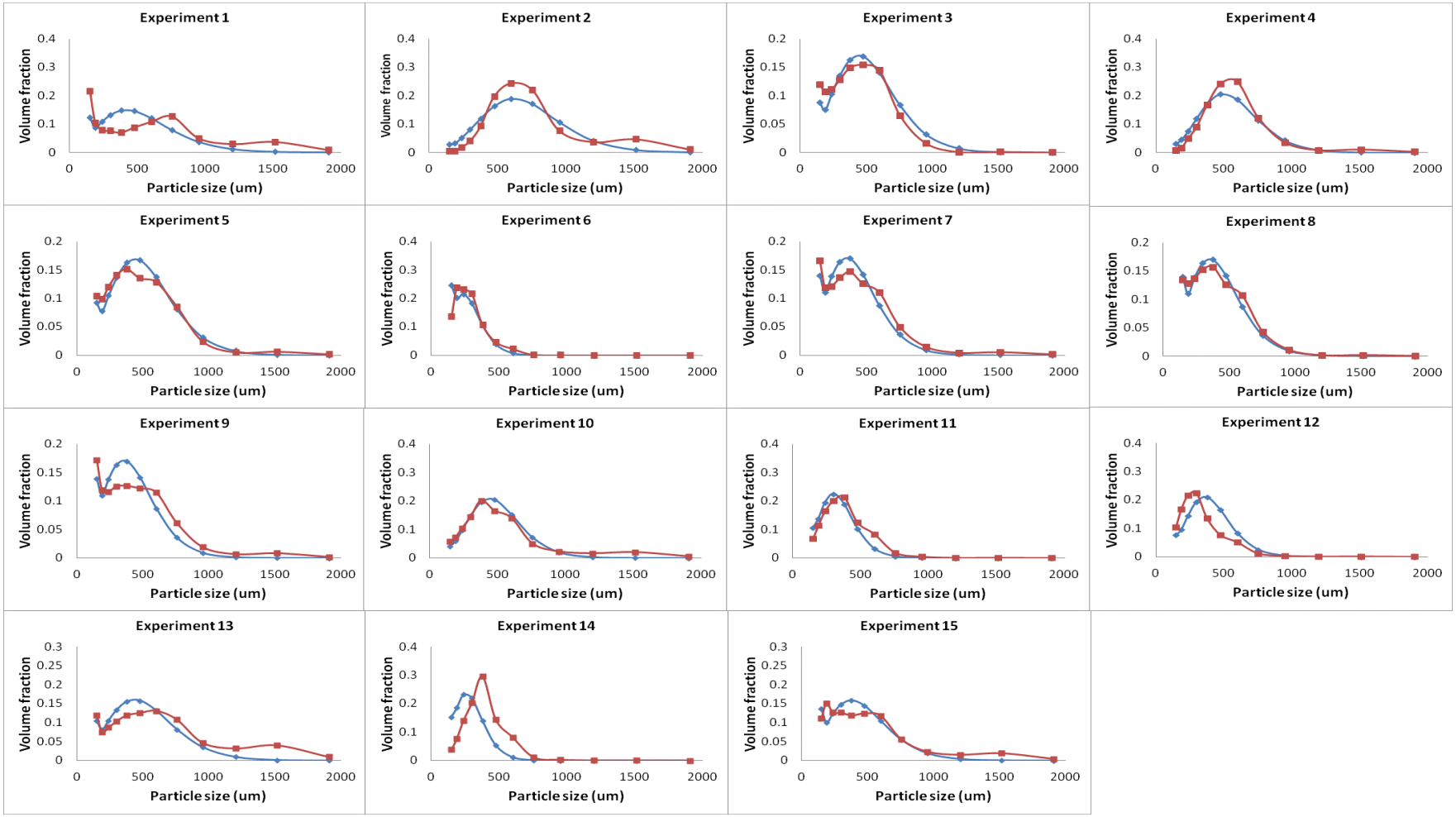
Experiment 1
Experiment 2
Experiment 3
Experiment 4
Experiment 5
Experiment 6
Experiment 7
Experiment 8
Experiment 9
Experiment 10
Experiment 11
Experiment 12
Experiment 13
Experiment 14
Experiment 15
Volume fraction
Particle size (um)

(b)

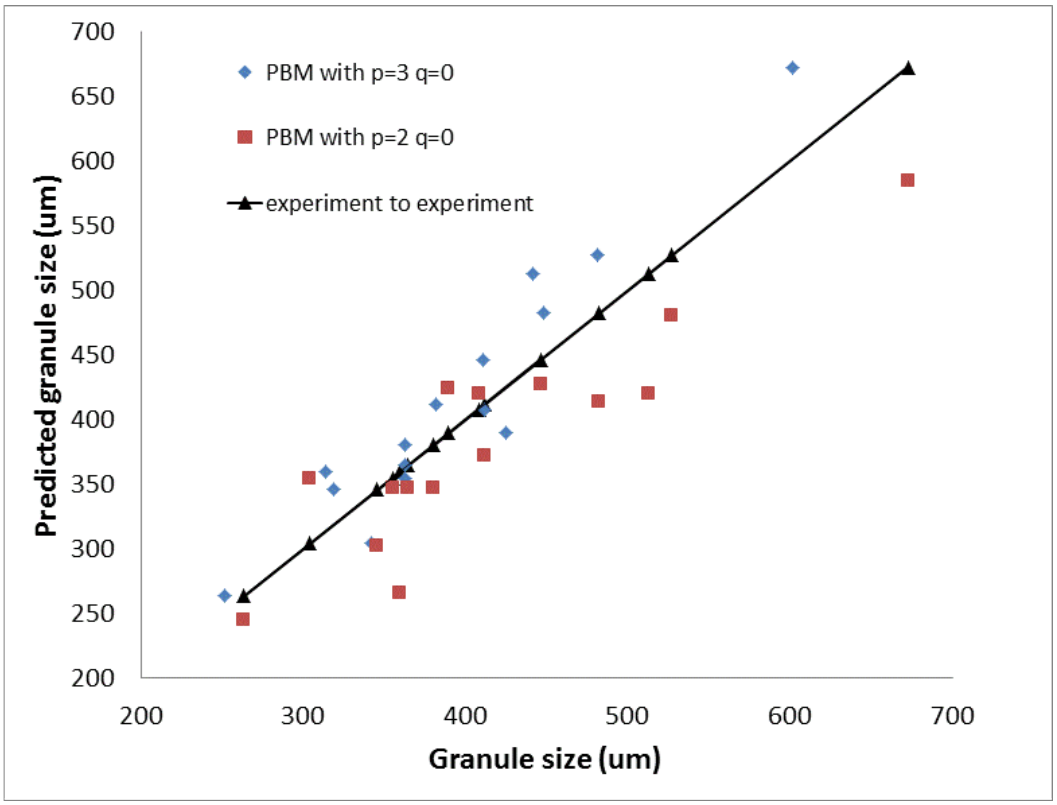

(c)

Figure 4.4 Comparison of experimental data with the predictions by the PBMs (red square: experimental data; blue diamond: prediction value): (a) the kernel orders of *p=3* and *q=0*; (b) Kernel order of *p=2*; and *q=0*; (c) mean size.

In order to validate the developed PBM models, two further experiments in which all of operating parameters were away from the boundaries from the previous study were selected to compare the model predictions [198]. Figure 4.5 shows the validation results of evolution of granule distribution predicted by the developed PBMs with the experiment results at the operating conditions of x_1*=0.2,* x_2 *= 0.33,* x_3 *= -0.2,* corresponding the actual operating conditions of 0.6 of the pulsed frequency of spray, 1.3 g/min of spray rate of binding liquid, and 14 psi of atomizing air pressure. Generally both of the developed PBMs can track the evolution of the granules at different times with accuracy shown in Figure 4.5. The predicted errors decreased significantly with increasing the spray time because that the PBMs were developed based on the end granule size distributions. In order to reduce the discrepancy between the model and experimental results at different spray times, more intermediate granules size

distributions should be included in equation (4.8) to obtain the optimal granulation rate and breakage selection rate constants. Based on the prediction error curve in Figure 4.5(d), it is shown that the PBM with the kernel orders of $p=2$ and $q=0$ had better predictions for the granules at 30% and 70% of binder sprayed times compared with those predicted the PBM with the kernel orders of $p=3$ and $q=0$.

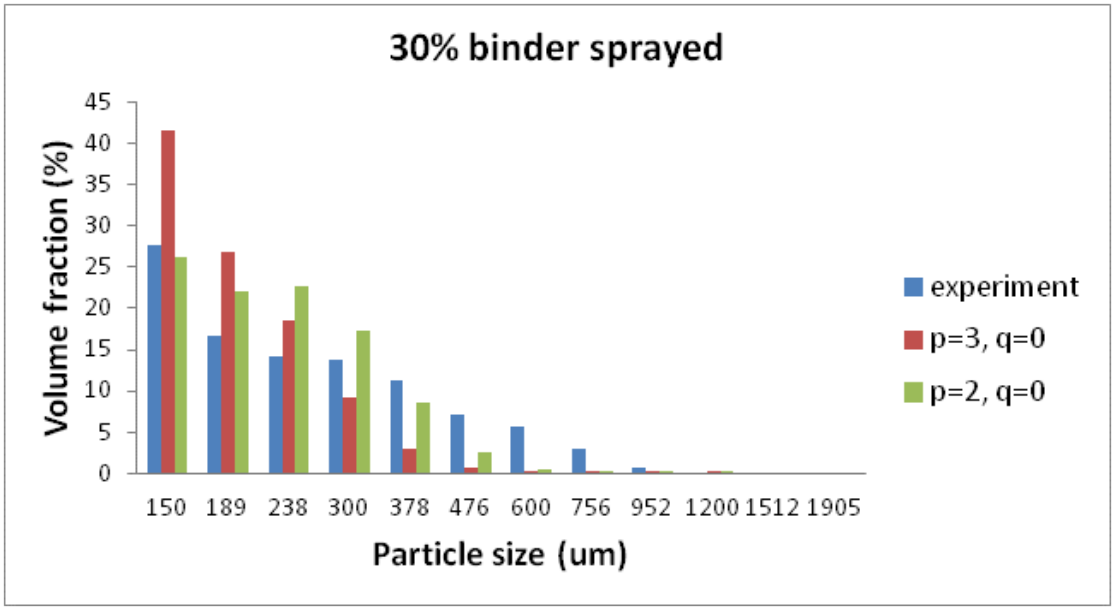

(a)

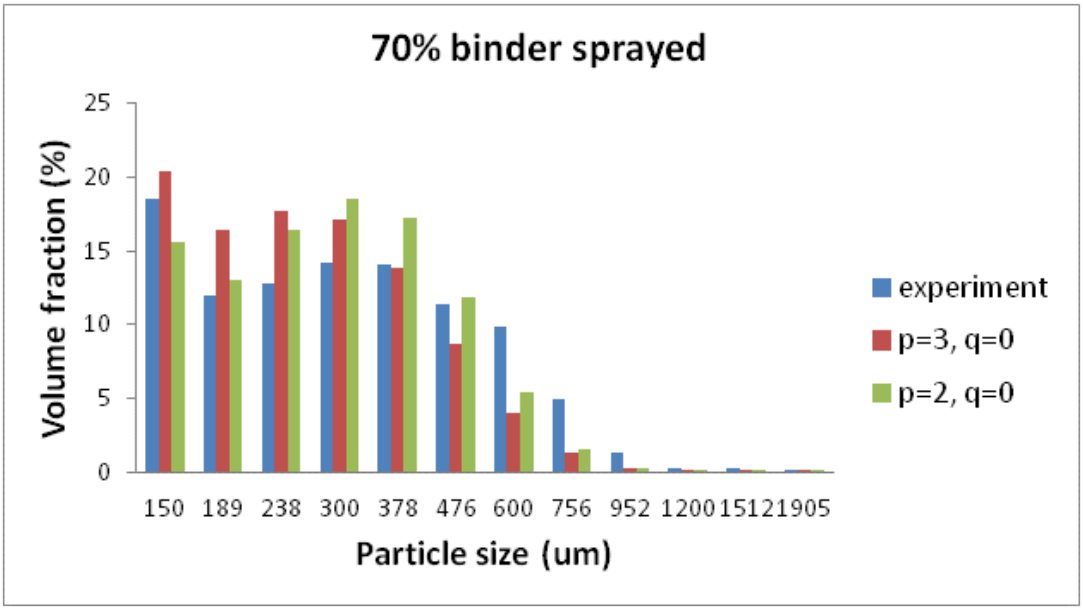

(b)

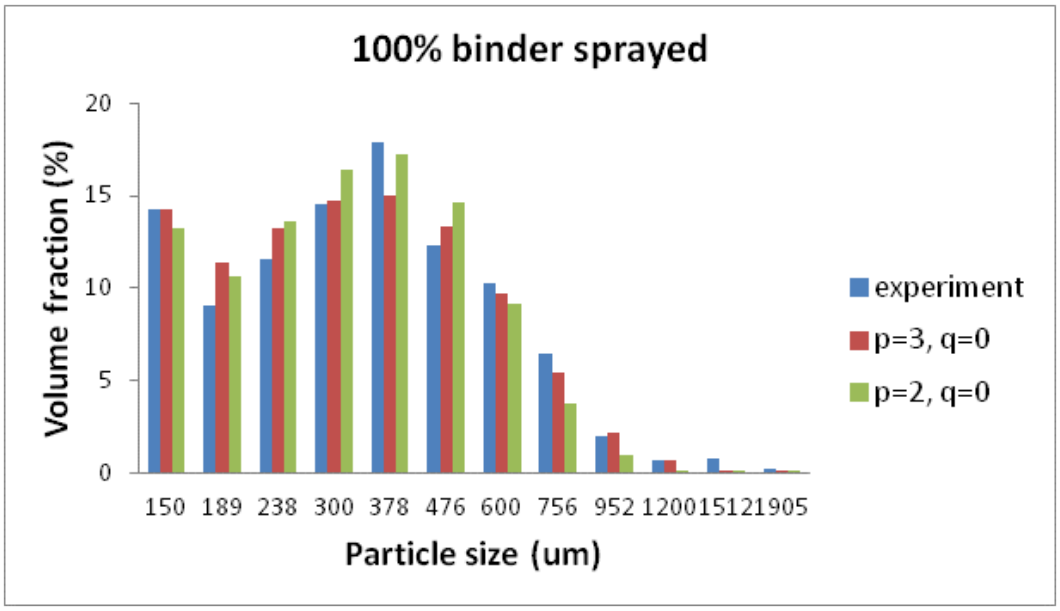

(c)

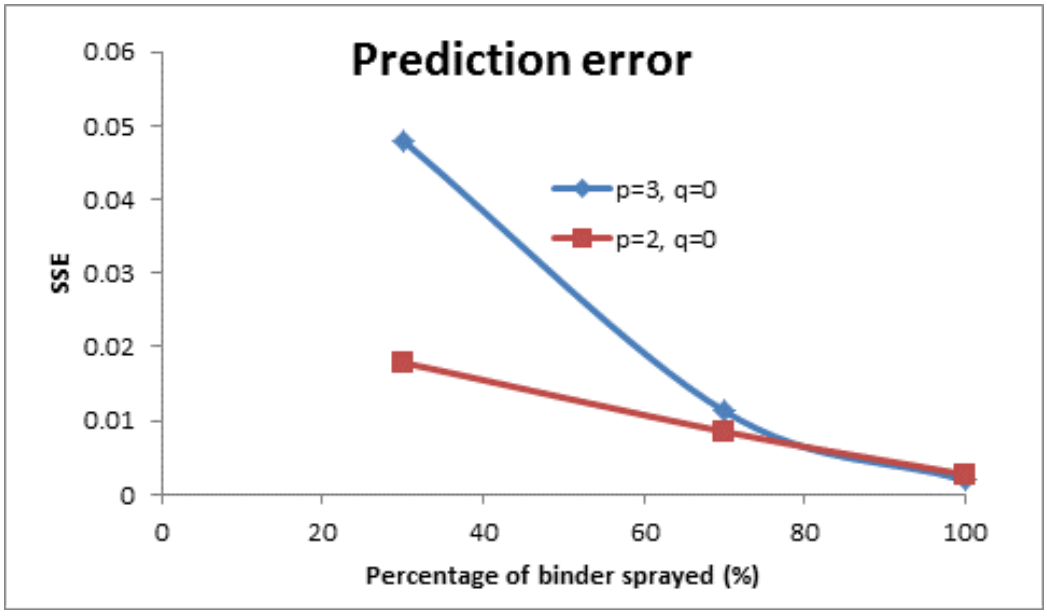

(d)

Figure 4.5 Validation of predictions of granule distribution by the PBMs with the kernel orders of $p=3$ and $q=0$ and the kernel order of $p=2$and $q=0$ at the operating condition of $x_1=0.2$; $x_2=0.333$; $x_3=-0.2$: (a) at 30% binder sprayed; (b) at 70% binder sprayed; (c) at 100% binder sprayed; (d) evolution of prediction errors.

Figure 4.6 shows the validation experiment at another operating condition of $x_1=0.6$,

$x_2=0$, $x_3=0.4$, corresponding the actual operating conditions of 0.8 of the pulsed frequency of spray, 1.2 g/min of spray rate of binding liquid, and 17 psi of atomizing air pressure. A similar trend of the model predictions can be found as that of the first validation data: the model prediction errors decreased significantly with increasing the granulation time. However, the PBM with the kernel orders of $p=3$ and $q=0$ has shown significantly better prediction than that with the kernel orders of $p=2$ and $q=0$ at 70% and 100% of bind sprayed times. Therefore, it would be important to consider both of model development and validation experimental data for selection of the best PBM.

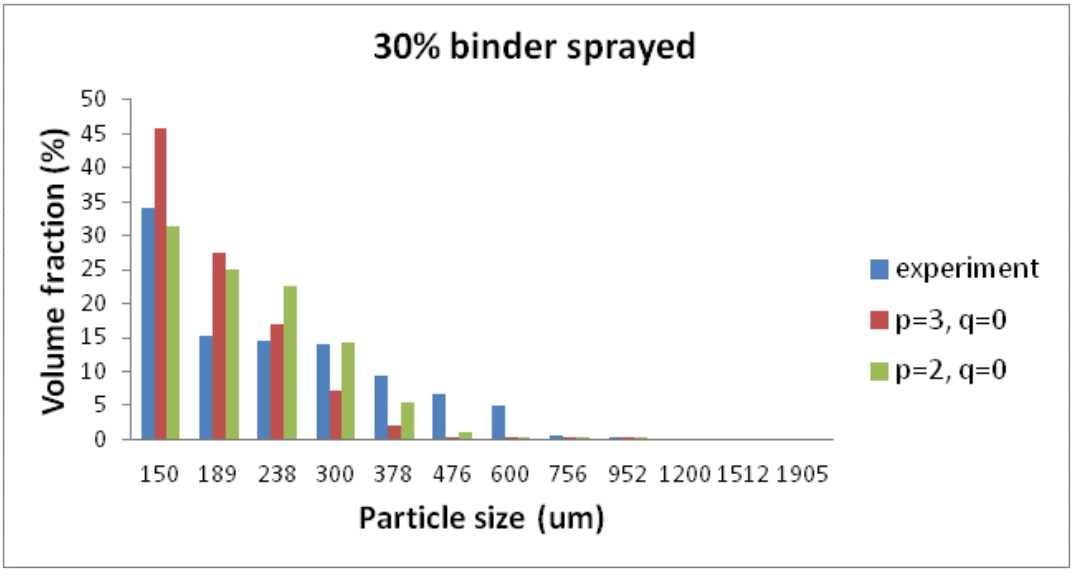

(a)

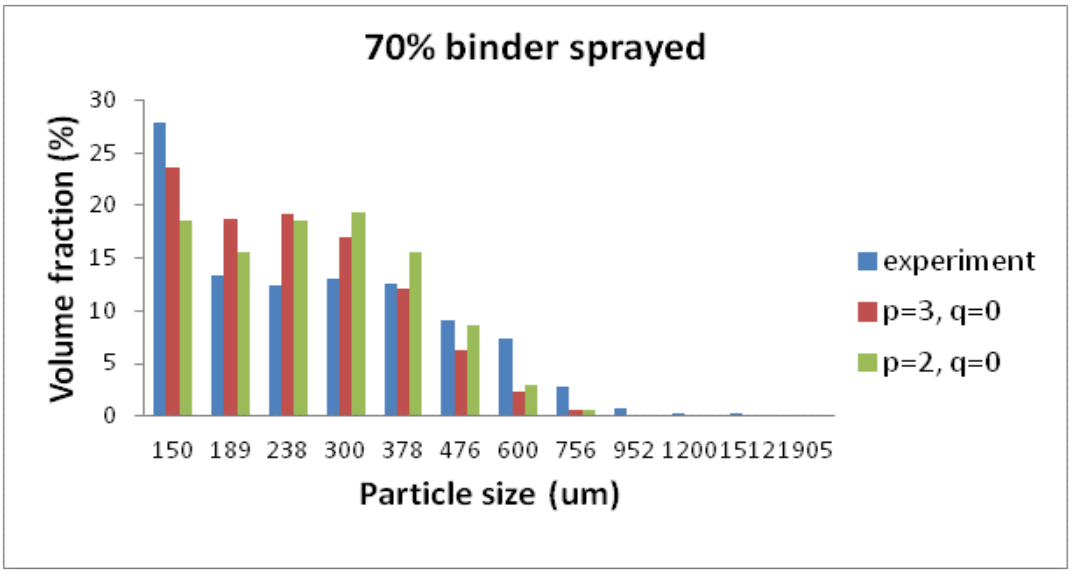

(b)

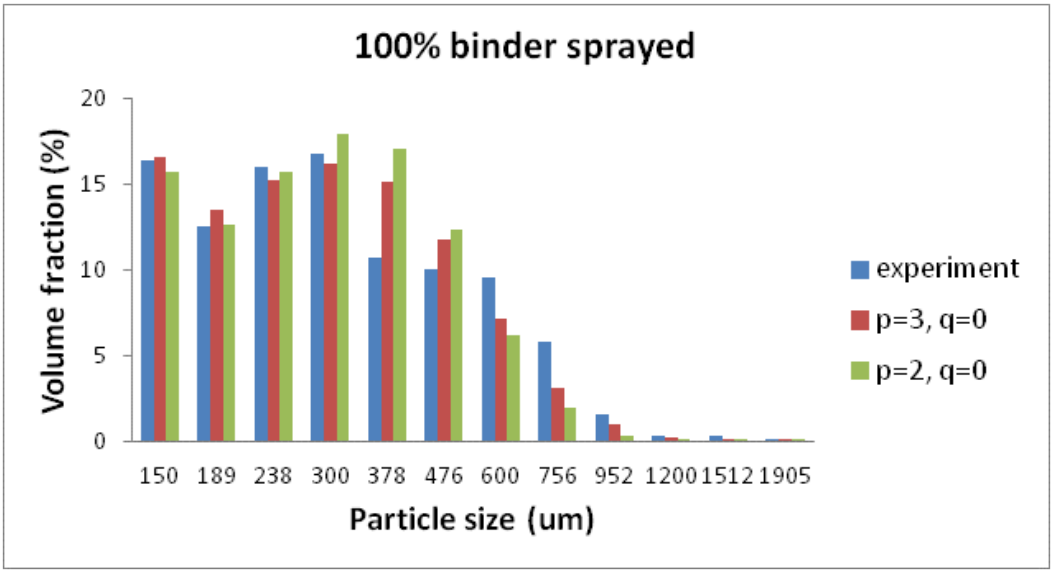

(c)

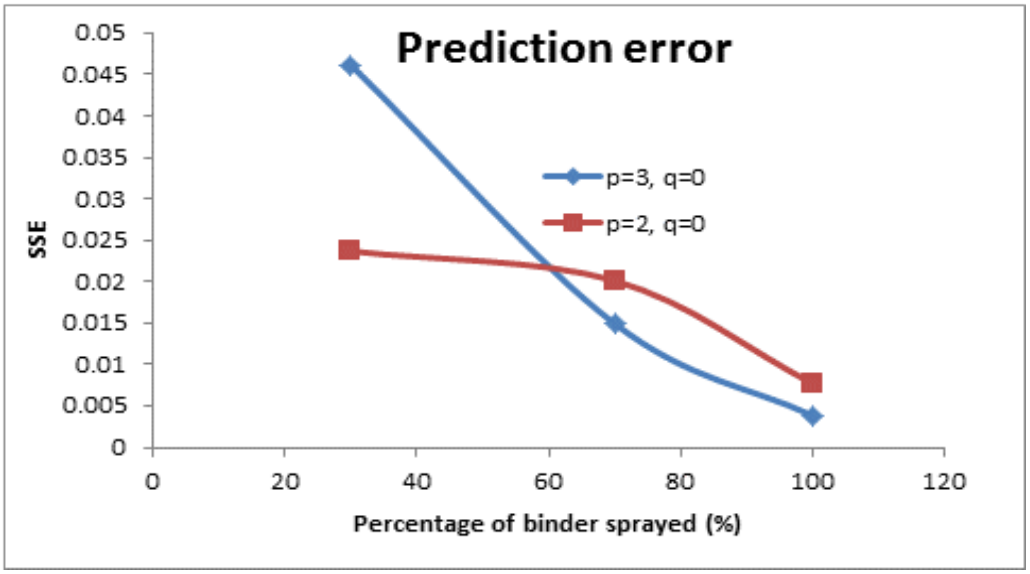

(d)

Figure 4.6 Validation of predictions of granule distribution by the PBMs with the kernel orders of *p=3* and *q=0* and the kernel order of *p=2* and *q=0* at the operating condition of x_1*=0.6;* x_2 *= 0;* x_3 *= 0.4*: (a) at 30% binder sprayed; (b) at 70% binder sprayed; (c) at 100% binder sprayed; (d) evolution of prediction errors.

4.5.2 Multi-stage optimal control of a pulsed top spray fluidized bed granulation

The optimization strategy to determine the optimal operating conditions of binder

solution spray was applied to a simulation of a pulsed top spray fluidized bed granulation process. The granulation process was simulated by the developed PBM with the kernel orders of $p=3$ and $q=0$ given in Table 4.1. The process model used for determination of the optimal operating conditions of binder solution spray was a simplified process model in which coefficients are only statistically significant in the models of the granulation rate and breakage selection rate constants. In this study, using a 5% significance level, a factor is considered to affect the response if the coefficients differ from zero significantly and the *P*-value is less than 0.05 ($p<0.05$) shown in Table 4.1. Therefore in the process model the granulation rate constant is given by

$$\hat{\beta}_0(x_1, x_2, x_3) = 5.55 \times 10^{-1} - 3.34 \times 10^{-1}x_1 + 1.09 \times 10^{-1}x_2 - 9.94 \times 10^{-2}x_3 + 2.34 \times 10^{-2}x_1^2 \quad (4.13)$$

and the breakage selection rate constants is given by

$$\hat{S}_0(x_1, x_2, x_3) = 4.57 \times 10^{-4} + 6.39 \times 10^{-4}x_1x_2 \quad (4.14)$$

Comparison of evolution of the granule mean sizes of granulation process and its process model at different operating conditions of binder spray is given in Figure 4.7. It is shown that at the center of each operating variable the process model can predict the granule process accurately in Figure 4.7(a). The significant discrepancy between the outputs of the granulation process and its process model can be found when the operating variables are away from its center as shown in Figures 4.7(b) and 4.7(c).

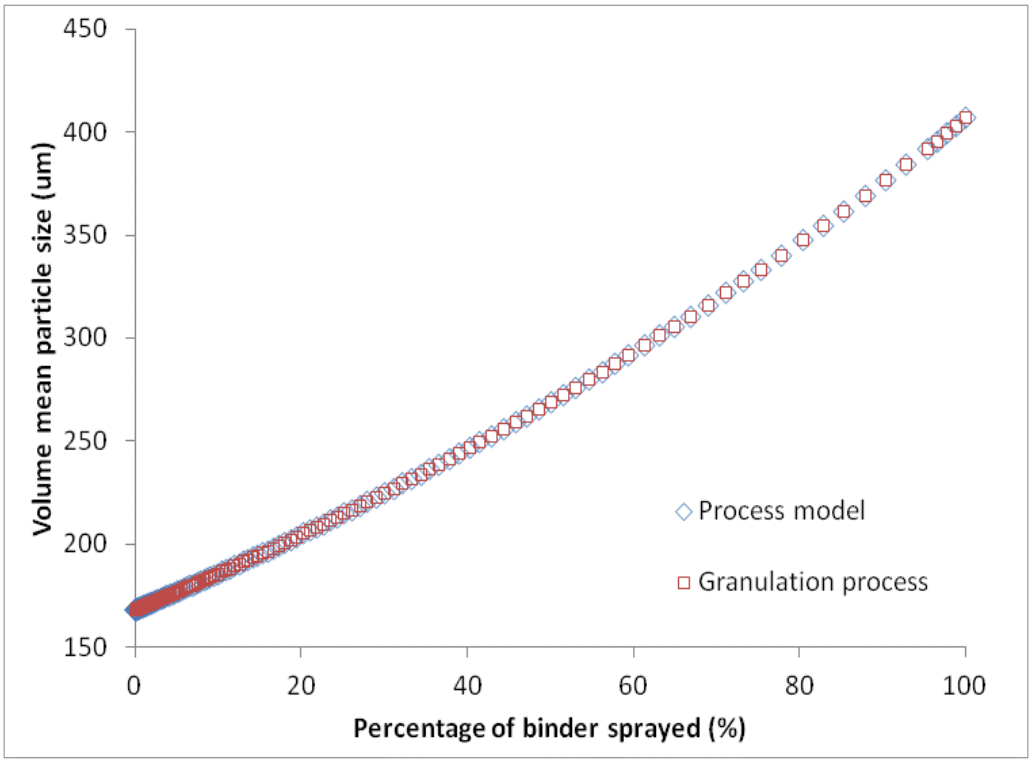
450
400
350
300
250
200
150
Volume mean particle size (um)
0
20
40
60
80
100
Percentage of binder sprayed (%)
Process model
Granulation process

(a)

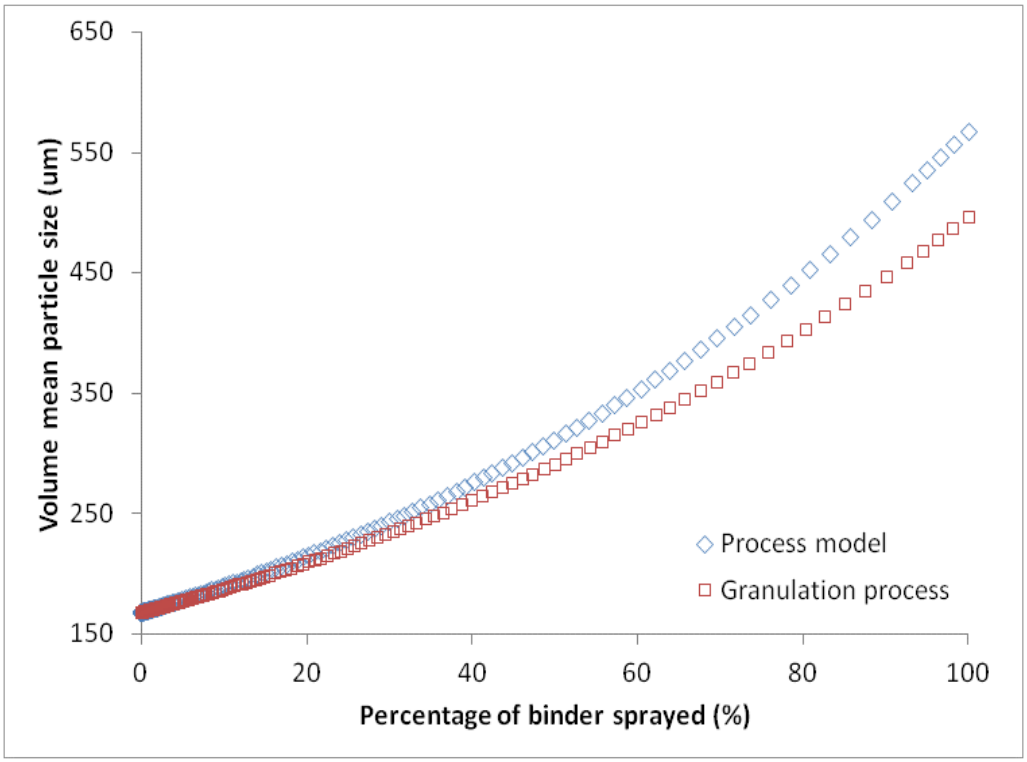
650
550
450
350
250
150
Volume mean particle size (um)
0
20
40
60
80
100
Percentage of binder sprayed (%)
Process model
Granulation process

(b)

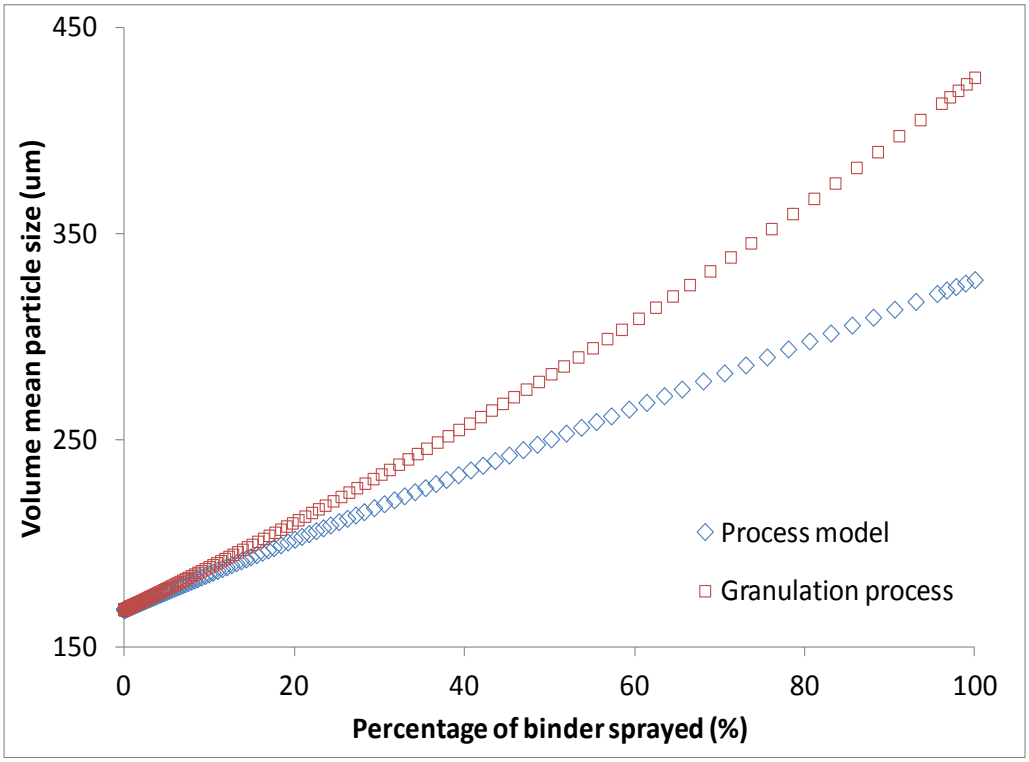

(c)

Figure 4.7 Comparison of evolution of the granule mean sizes of granulation process and process model at random operating conditions: (a) x1=0, x2=0, x3=0; (b) x1=-1, x2=0.5, x3=0.8; (c) x1=1, x2=1, x3=0.2.

In this study, the aim of the granulation control is to increase the powder size from its initial mean size of 150 μm to a desired end mean size of 600 μm. Figure 4.8 shows evolution of mean granule sizes in the simulated granulation process under different operating conditions of binder solution spray obtained by different stages of optimization, including one stage, two stages and three stages. The colored curves in Figures 4.8(a)-(c) show the trajectories of evolution of mean granule size at different stages of optimization obtained by the process model given by equations (4.13) and (4.14), respectively. All the black curves in Figure 4.8(a)-(c) show the evolution of actual mean granule sizes under those operating conditions. It can be seen that based on one stage optimization method the end mean granule size of 549 μm is significantly smaller than the desired value of 600μm due to the mismatch of the actual process and the developed process model. Based on the measured granule size distribution at 50% of binder sprayed, the model mismatch can be compensated through adjusting the desired end mean granule size in the new costing function in equation (4.12) to determine a new

trajectory (green color curve) shown in Figure 4.8(b). It is shown that the difference between the end mean granule size and the desired granule size based on two-stage optimization is reduced significantly to 26 μm from 51 μm based on one-stage optimization. For a three-stage optimization, the end mean granule size is nearly same as the desired mean size. The operation variables of the binder solution spray obtained by the different stages of optimization are also given in Figure 4.8(a)-(c).

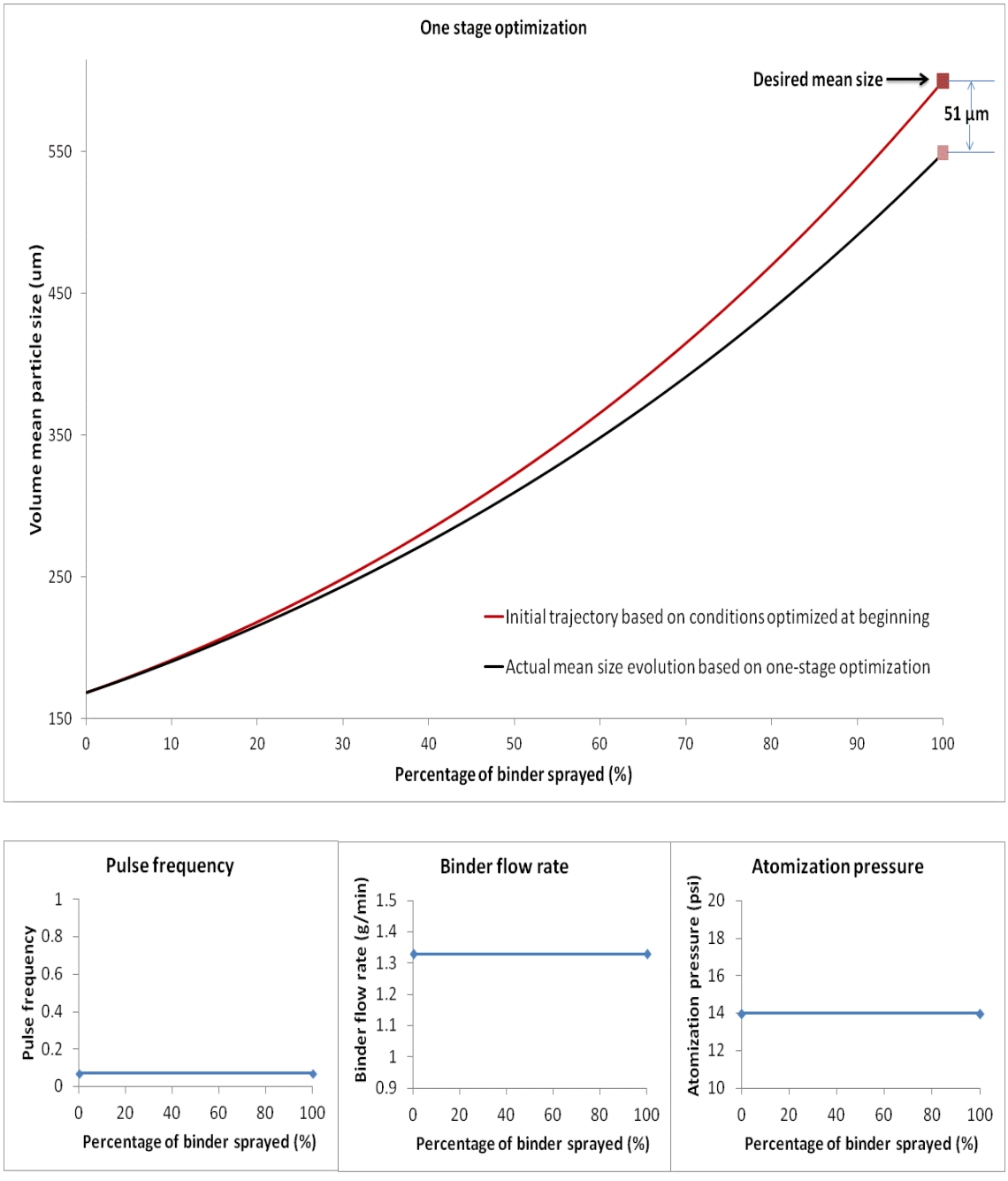

(a)

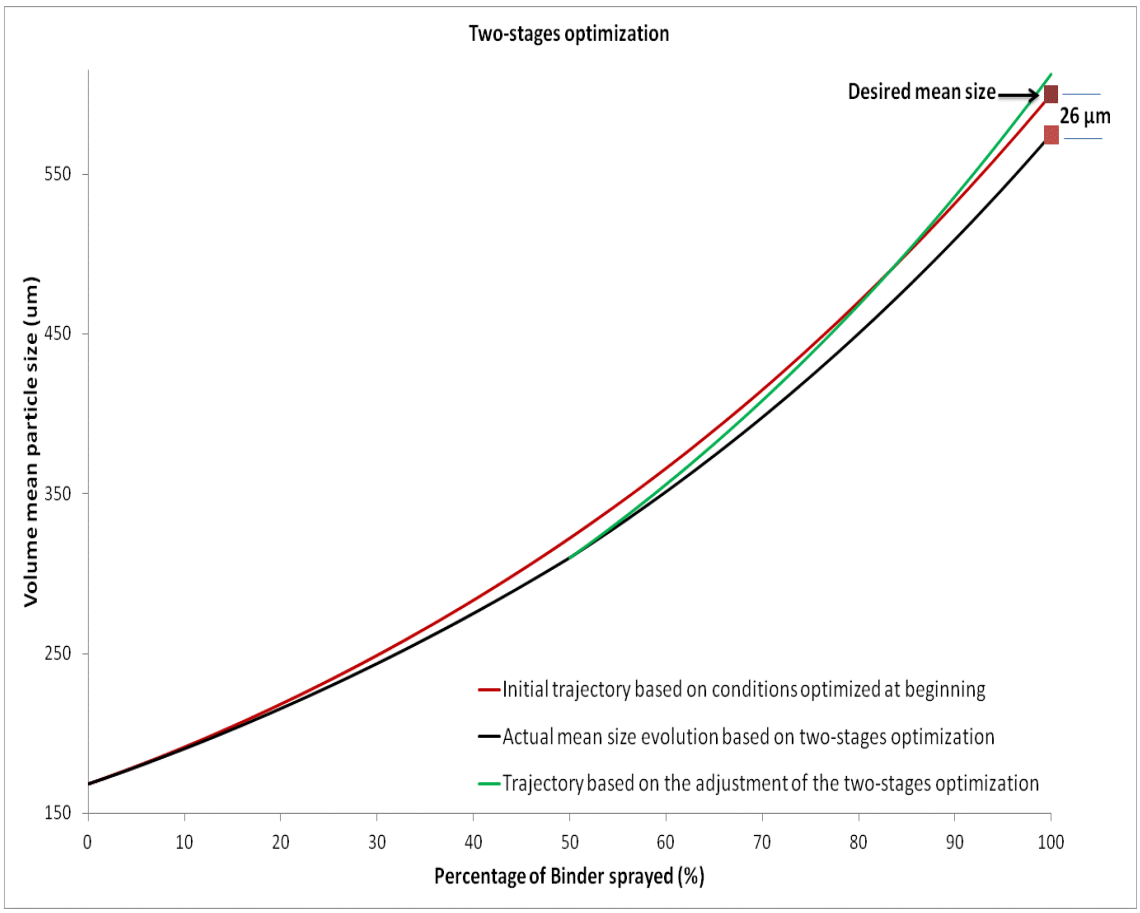
Two-stages optimization
Desired mean size
26 µm
Volume mean particle size (um)
550
450
350
250
150
0
10
20
30
40
50
60
70
80
90
100
Percentage of Binder sprayed (%)
Initial trajectory based on conditions optimized at beginning
Actual mean size evolution based on two-stages optimization
Trajectory based on the adjustment of the two-stages optimization

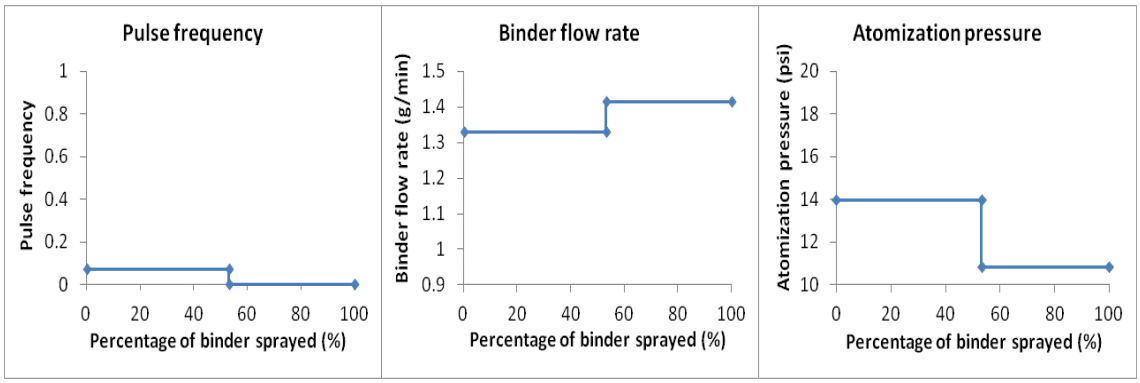
Pulse frequency
Pulse frequency
1
0.8
0.6
0.4
0.2
0
0
20
40
60
80
100
Percentage of binder sprayed (%)
Binder flow rate
Binder flow rate (g/min)
1.5
1.4
1.3
1.2
1.1
1
0.9
0
20
40
60
80
100
Percentage of binder sprayed (%)
Atomization pressure
Atomization pressure (psi)
20
18
16
14
12
10
0
20
40
60
80
100
Percentage of binder sprayed (%)

(b)

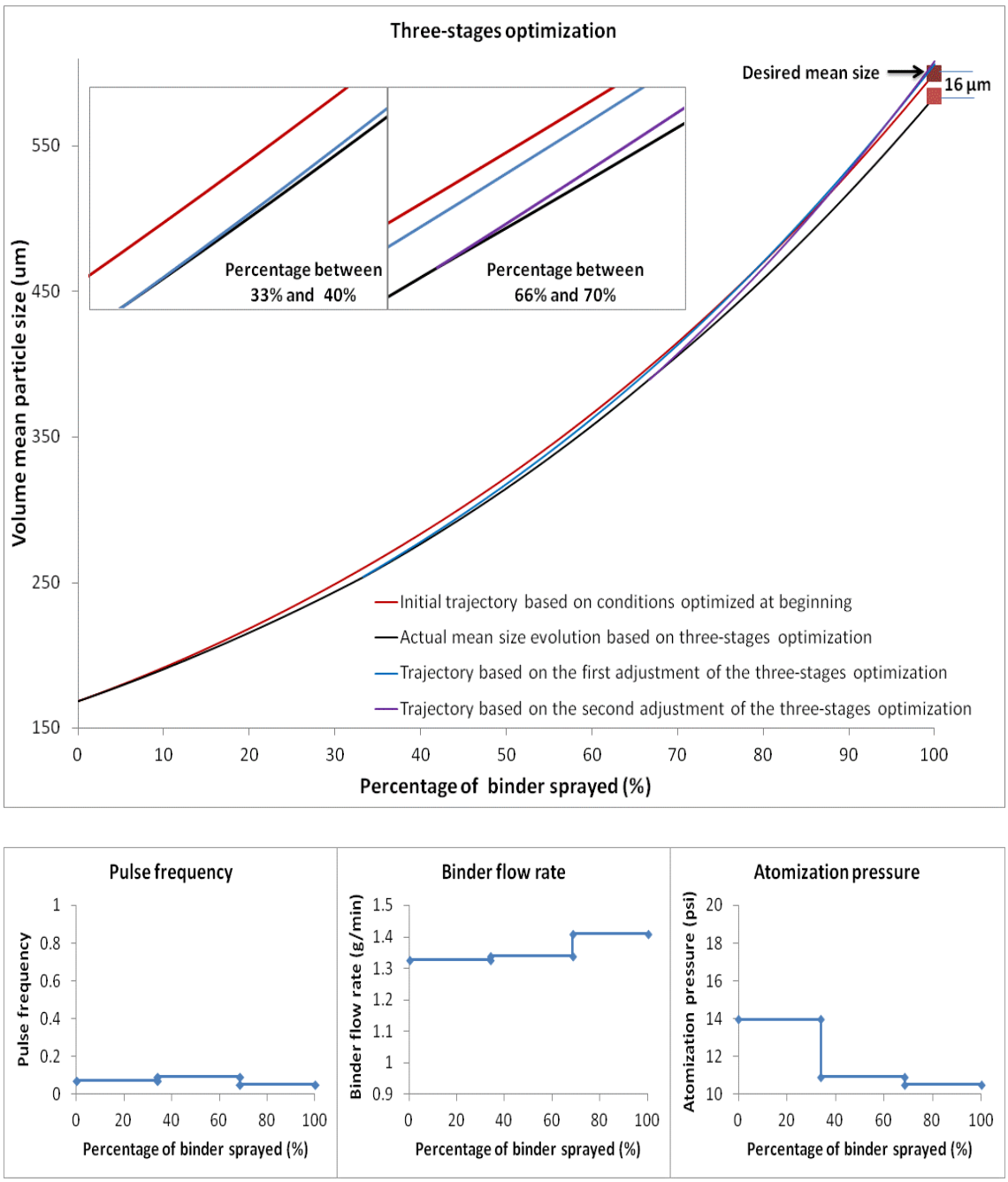

(c)

Figure 4.8 Actual mean size evolution and size trajectory using different stages of optimization and optimal operating conditions: (a) one-stage optimization results; (b) two-stages optimization results; (c) three-stages optimization results.

4.6 Chapter Conclusions

In this chapter, a pulsed top-spray fluidized bed granulation was modeled by one-

dimensional population balance models (ODPBM). The developed PBMs have linked the key binder solution spray operating factors of the binder spray rate, atomizing air pressure and pulsed frequency of spray with the granule properties to predict granule growth behavior in a pulsed spray fluidized bed granulation process at different operating conditions. It has been found that the aggregation of granules was volume dependent and breakage of the granules was size independent in a pulsed top-spray fluidized bed granulation process. Experimental validation has shown that the developed PBMs with both the kernel orders of $p=3$ and $q=0$ and the kernel orders of $p=2$ and $q=0$ can predict the evolution of granule size distribution with accuracy.

The developed PBMs have been used to design the control strategies to operate the pulsed spray fluidized bed granulation under more optimal conditions to achieve the desired quality of the end granules. In this work, a multi-stage open optimal control strategy was proposed, in which through adjusting the trajectory of the evolution of the granule size distribution at predefined sample intervals, to determine the optimal operating variables related to the binder spray including the spray rate of binding liquid, atomizing air pressure and pulsed frequency of spray. Simulated results have shown that the proposed multi-stage open optimal control strategy can effectively reduce the effects of the model mismatch and provide an effective tool to determine the optimal operating variables for a pulsed spray fluidized bed granulation process.

Chapter 5 Three-dimensional computational fluid dynamics (CFD) study of the gas-solid circulation pattern in a fluidized bed granulator

5.1 Chapter overview

In this chapter, the particle-gas two-phase fluid dynamics within top-spray fluidized bed granulator was studied by the commercial computational fluid dynamics (CFD) software ANSYS Fluent 13.0. The fluid dynamic characteristics of fluidized bed granulation process were studied by changing the particle size and inlet air velocity. CFD simulations were designed by a two-factors three-levels full factorial experimental design. The influence of particle size and inlet air velocity on the particle circulation pattern was investigated and a mathematical relationship between the particle circulation time with particle size and inlet air velocity was developed in this chapter.

5.2 CFD software packages

5.2.1 ANSYS ICEM CFD

The basic flowchart of a CFD simulation is pre-processing, calculation and post-processing. The prerequisite for pre-processing is to create the geometry and to generate the mesh, both of which, in this work, are completed using the powerful commercial software ANSYS ICEM CFD 13.0 (Ansys Inc., US).

ANSYS ICEM CFD provides advanced geometry acquisition, mesh generation, and mesh optimization tools to meet the requirement for integrated mesh generation for today's sophisticated analyses. ANSYS ICEM CFD can provide wide range of tools for both creating new geometry and manipulating existing geometry. Different formats of geometry can be transported into ANSYS ICEM CFD, such as geometry generated by a commercial CAD design package, 3rd party universal database, scan data or point data. Beginning with a robust geometry module which supports the creation and modification of points, curves and surfaces, ANSYS ICEM CFD's open geometry database offers the

flexibility to combine geometric information in various formats for mesh generation. The resulting structured or unstructured meshes, topology, inter-domain connectivity and boundary conditions are then stored in a database where they can easily be translated to input files formatted for a particular solver. Generally, ANSYS ICEM CFD's mesh generation tools offer the capability to parametrically create meshes from geometry in numerous formats:

- Multiblock structured
- Unstructured hexahedral
- Unstructured tetrahedral
- Cartesian with H-grid refinement
- Hybrid meshes comprising hexahedral, tetrahedral, pyramidal and/or prismatic elements
- Quadrilateral and triangular surface meshes

In the present work, the truncated conical 50 gram/batch lab scale fluidized bed granulator with inner-diameter 4.97 cm at the bottom and 7.48 cm at the top and height of 30 cm is modeled and meshed in ANSYS ICEM CFD 13.0. The granulator model is created in three dimensional and meshed into 'O' type unstructured hexahedrons, which is detailed shown in Figure 5.1.

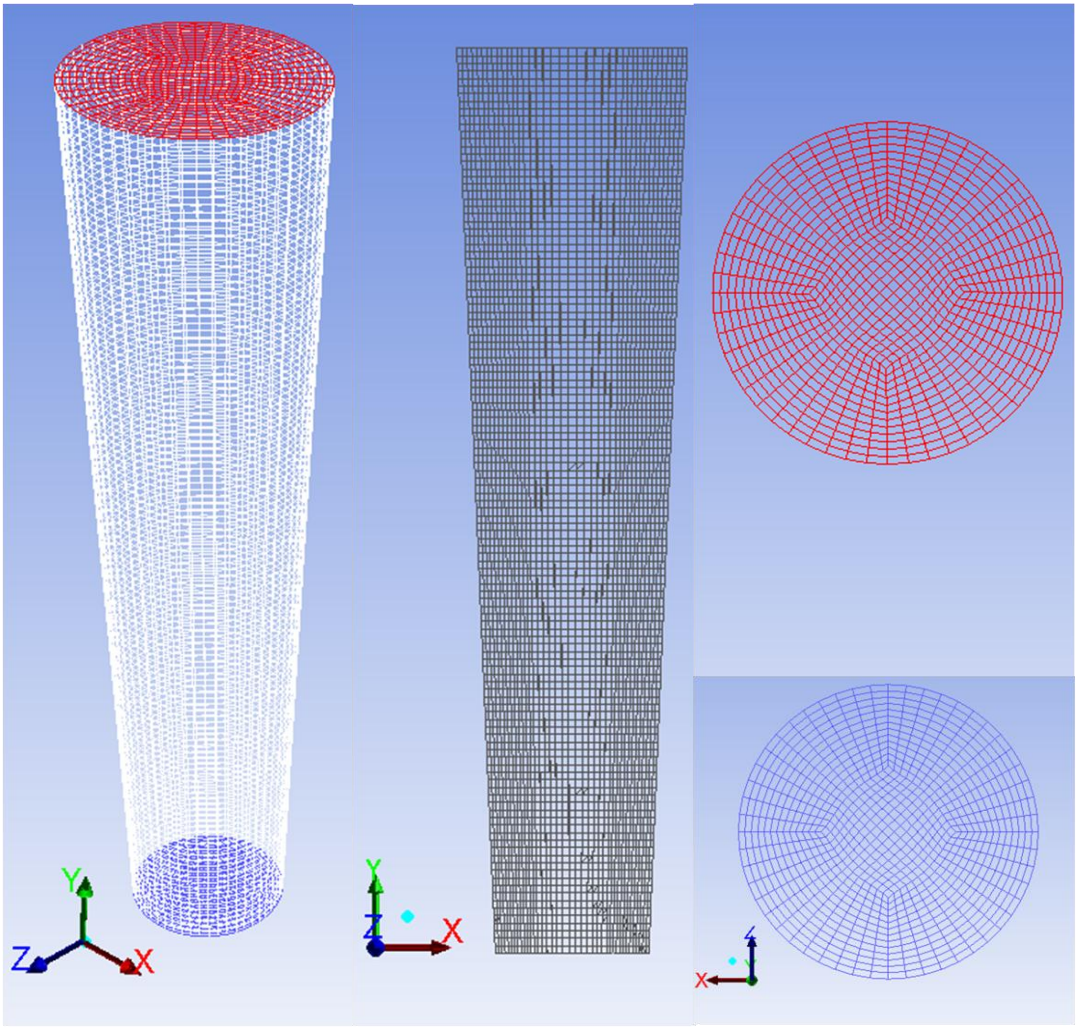

(a) (b) (c)

Figure 5.1 The geometry and mesh strategy of the fluidized bed granulator: (a) the fluidized bed granulator overview; (b) the X-Y cross-sectional plane; (c) the inlet (blue) and outlet (red) cross-sectional plane.

5.2.2 ANSYS Fluent

In this work, both procedures of calculation and post-processing of the CFD simulation for gas-solid two-phase flow hydrodynamics within the top-spray fluidized bed granulator are performed utilizing the commercial software package ANSYS Fluent 13.0 (Ansys Inc., US). Fluent is a state-of-the-art computer program for modelling fluid flow and heat transfer in complex geometries. Generally, the Fluent solver has the following modelling capabilities:

- Flow problems in 2D/3D
- Steady-state and transient flow
- Incompressible and compressible flows
- Heat transfer
- Chemical species mixing and reaction
- Free surface and multiphase models
- Lagrangian trajectory calculation
- Cavitation model
- Phase change model
- Porous media
- Inertial and non-inertial, multiple reference frames
- Dynamic mesh model
- Material property database
- Extensive customization capability via user-defined functions
- Population balance module

Regarding simulating multiphase flow, actually, several kinds of CFD software could be considered, such as Fluent, CFX, COMSOL, MFIX, and Star-CD, among which ANSYS Fluent is leading in multiphase modelling. Its powerful capabilities allow engineers to gain insight into equipment that is often difficult to probe. ANSYS Fluent can also be utilized to capture the interaction between multiple fluid phases, such as gases and liquids, dispersed particles and droplets.

Different group of models are provided by ANSYS Fluent for multiphase flows. The volume-of-fluid (VOF) model is offered for immiscible multiphase flows. The discrete phase model (DPM) can be used for multiphase applications such as spray dryers, liquid fuel sprays. For flows with denser droplets or particulates concentration, ANSYS Fluent offers the dense DPM (DDPM) model. Furthermore, ANSYS Fluent discrete element particles model (DEM) can be used to track the collisions between solids particles.

Recently, ANSYS Fluent was popularly used for modelling fluidized bed granulation or fluidisation. A large number of research articles have been published in recent years on

the application of ANSYS Fluent in analysis of fluidized bed granulation and fluidization [141, 143, 144, 146, 177, 216-220].

5.3 CFD modeling strategy

An Eulerian-Eulerian two-fluid model (EETFM) which considers the conservation of mass and momentum for the gas and particle phases [221] is utilized to model the fluidized bed granulation in this chapter, which was already introduced in chapter 2.5.2 and was summarized together with the closure equations in Table 5.1. The standard $k-\varepsilon$ model was considered to describe the turbulence inside the fluidized bed granulator, where the kinetic theory of granular flow was employed to close the momentum balance equation for the solid phase. The finite volume approach by a commercial CFD software package ANSYS Fluent 13.0 (Ansys Inc., US) was used for solving the set of governing equations in Table 5.1 in a 3-D domain comprising all the interior volume of the conical product chamber in the fluidized bed granulator in double precision mode. The phase coupled SIMPLE algorithm was used for the pressure-velocity coupling, in which the coupling terms were solved implicitly to form part of the solution matrix. First order upwind schemes in both space and time were used for the solution of the equations. The transient simulation mode is selected and a time step of 1×10^{-4}s with maximum 200 iterations per time step is utilized to ensure adequate convergence. The convergence criterion was set to 1×10^{-3} for the relative error between two successive iterations for each scaled residual component.

Table 5.1 Models used for CFD simulations

Continuity equation	Gas: $\frac{\partial(\alpha_g\rho_g)}{\partial t}+\nabla\cdot\left(\alpha_g\rho_g\overrightarrow{v_g}\right)=0$ Solid: $\frac{\partial(\alpha_s\rho_s)}{\partial t}+\nabla\cdot(\alpha_s\rho_s\overrightarrow{v_s})=0$
Momentum equation	Gas: $\frac{\partial(\alpha_g\rho_g\overrightarrow{v_g})}{\partial t}+\nabla\cdot\left(\alpha_g\rho_g\overrightarrow{v_g}\overrightarrow{v_g}\right)=-\alpha_g\nabla p+\nabla\cdot\overline{\overline{\tau_g}}+K_{gs}\left(\overrightarrow{v_s}-\overrightarrow{v_g}\right)+\alpha_g\rho_g\vec{g}$ Solid: $\frac{\partial(\alpha_s\rho_s\overrightarrow{v_s})}{\partial t}+\nabla\cdot(\alpha_s\rho_s\overrightarrow{v_s}\overrightarrow{v_s})=-\alpha_s\nabla p-\nabla p_s+\nabla\cdot\overline{\overline{\tau_s}}+K_{gs}\left(\overrightarrow{v_g}-\overrightarrow{v_s}\right)+\alpha_s\rho_s\vec{g}$

	Stress tensors: $\bar{\bar{\tau}}_g = \alpha_g \mu_g \left(\nabla \vec{v_g} + \nabla \vec{v_g}^T\right)$ $\bar{\bar{\tau}}_s = \alpha_s \mu_s \left(\nabla \vec{v_s} + \nabla \vec{v_s}^T\right) + \alpha_s (\lambda_s - \frac{2}{3}\mu_s) \nabla \cdot \vec{v_s} \bar{\bar{I}}$
Gas solid drag model [222]	$k_{gs} = \frac{3}{4} C_D \frac{\alpha_s \alpha_g \rho_g \left\vert \vec{v_s} - \vec{v_g} \right\vert}{d_s} \alpha_g^{-2.65} \quad for\ \alpha_g > 0.8$ $k_{gs} = 150 \frac{\alpha_s^2 \mu_g}{\alpha_g d_s^2} + 1.75 \frac{\alpha_s \rho_g \vert \vec{v_s} - \vec{v_g} \vert}{d_s} \quad for\ \alpha_g \leq 0.8$ Where, $C_D = \frac{24}{\alpha_g Re_s} \left[1 + 0.15 \left(\alpha_g Re_s\right)^{0.687}\right]$ $Re_s = \frac{\rho_g d_s \vert \vec{v_s} - \vec{v_g} \vert}{\mu_g}$
Solid pressure [223]	$p_s = \alpha_s \rho_s \Theta_s [1 + 2 g_0 \alpha_s (1 + e_s)]$
Bulk viscosity	$\lambda_s = \frac{4}{3} \alpha_s \rho_s d_s g_0 (1 + e_s) \sqrt{\frac{\Theta_s}{\pi}}$ $\Theta_s = \frac{1}{3} \overline{v_s' v_s'}$
Radial distribution function [223]	$g_0 = \left[1 - \left(\frac{\alpha_s}{\alpha_{smax}}\right)^{1/3}\right]^{-1}$
Kinetic theory of granular flow model [159] [224] [223]	$\frac{3}{2}\left[\frac{\partial (\alpha_s \rho_s \Theta_s)}{\partial t} + \nabla \cdot (\alpha_s \rho_s \vec{v_s} \Theta_s)\right] = \left(-p_s \bar{\bar{I}} + \bar{\bar{\tau}}_s\right) : \nabla \vec{v_s} - \nabla \cdot \left(k_{\Theta_s} \nabla \Theta_s\right) - \gamma_{\Theta_s} - \varphi_{gs}$ $k_{\Theta_s} = \frac{15 \rho_s d_s \alpha_s \sqrt{\pi \Theta_s}}{4(41 - 33\eta)} \left[1 + \frac{12}{5} \eta^2 (4\eta - 3) g_0 \alpha_s + \frac{16}{15\pi} (41 - 33\eta) \eta g_0 \alpha_s\right]$ $\eta = \frac{1}{2}(1 + e_s)$ $\gamma_{\Theta_s} = \frac{12(1 - e_s^2) g_0}{d_s \sqrt{\pi}} \rho_s \alpha_s^2 \Theta_s^{1.5}$ $\varphi_{gs} = -3 K_{gs} \Theta_s$
Simplified KTGF	$0 = \left(-p_s \bar{\bar{I}} + \bar{\bar{\tau}}_s\right) : \nabla \vec{v_s} \left(-p_s \bar{\bar{I}} + \bar{\bar{\tau}}_s\right) : \nabla \vec{v_s}$
Solid dynamic	$\mu_s = \mu_{s,col} + \mu_{s,kin} + \mu_{s,fri}$

viscosity [222] [225]	$\mu_{s,col} = \frac{4}{5}\alpha_s\rho_s d_s g_0(1+e_s)\sqrt{\frac{\Theta_s}{\pi}}$ $\mu_{s,kin} = \frac{10\rho_s d_s\sqrt{\Theta_s\pi}}{96\alpha_s g_0(1+e_s)}\left[1+\frac{4}{5}\alpha_s g_0(1+e_s)\right]^2$ *(Gidaspow)* $\mu_{s,fri} = \frac{p_s sin\theta}{2\sqrt{I_{2D}}}$ *(Schaeffer's)*
Turbulence model	$\frac{\partial}{\partial x}(\rho_m k) + \nabla\cdot(\rho_m k\overrightarrow{v_m}) = \nabla\cdot\left(\frac{\mu_{t,m}}{\sigma_\varepsilon}\nabla k\right) + G_{k,m} - \rho_m\varepsilon$ $\frac{\partial}{\partial x}(\rho_m\varepsilon) + \nabla\cdot(\rho_m\varepsilon\overrightarrow{v_m}) = \nabla\cdot\left(\frac{\mu_{t,m}}{\sigma_\varepsilon}\nabla\varepsilon\right) + \frac{\varepsilon}{k}(C_{1\varepsilon}G_{k,m} - C_{2\varepsilon}\rho_m\varepsilon)$ $\rho_m = \sum_{i=1}^{N}\alpha_i\rho_i$ $\overrightarrow{v_m} = \frac{\sum_{i=1}^{N}\alpha_i\rho_i\overrightarrow{v_i}}{\sum_{i=1}^{N}\alpha_i\rho_i}$ $\mu_{t,m} = \rho_m C_\mu\frac{k^2}{\varepsilon}$ $G_{k,m} = \mu_{t,m}(\nabla\overrightarrow{v_m} + (\nabla\overrightarrow{v_m})^T):\nabla\overrightarrow{v_m}$

In each CFD simulation of a fluidized bed, particles were assumed to be spherical and monodispersed. Particle diameter differs with simulations between 164 μm and 500 μm, which were the geometric mean of the initial primary particles in the experiments and desired final mean particle size, respectively. Based on the experiments, it was found that the bed height of initial primary MCC particles of 46.5g packed was around between 8 and 9 cm. In order to simulate the experiments accurately, the initial solid particle packed bed height was patched as 8.75 cm in the CFD simulations and the particle volume fraction was set as 0.5273 based the ratio of the volume of the actual primary particles used in the experiments and the volume of the initial bed patched in the simulations.

For the boundary conditions in a simulation, the distributor was modeled as a porous plate placed at the bottom of the conical product chamber in which the uniform air was

injected into the bed. The particles were not allowed to penetrate the distributor. The superficial inlet-velocity range was between 0.6 m^3/h and 1.8 m^3/h. The pressure-outlet boundary condition was set on the top of the granulator which was assumed to have a constant static atmospheric pressure as a reference operating pressure. No-slip wall condition was set for both air and solid, which means no momentum waste happening when the air and solid colliding with the wall. The restitution coefficient was set as 0.9 for the particles in the simulations. Configuration of the simulated fluidized bed and its boundary conditions are shown in Figure 5.2 and the details of parameters used the simulations are given in Table 5.2.

Table 5.2 All the parameters used in the CFD simulation

Property	Value
Gas density (kg/m^3)	1.225
Gas viscosity ($kg/(m.s)$)	1.7894×10^{-5}
Solid particle density (kg/m^3)	450
Superficial inlet velocity (m^3/h)	0.6, 1.2, 1.8
Particle diameter (μm)	164, 332, 500
Initial solid packing	0.5273
Initial bed height (cm)	8.75
Restitution coefficient	0.9
Time step (s)	0.0001
Convergence criteria	1.0×10^{-3}
Operating pressure (Pa)	101325
Maximum iterations every step	200

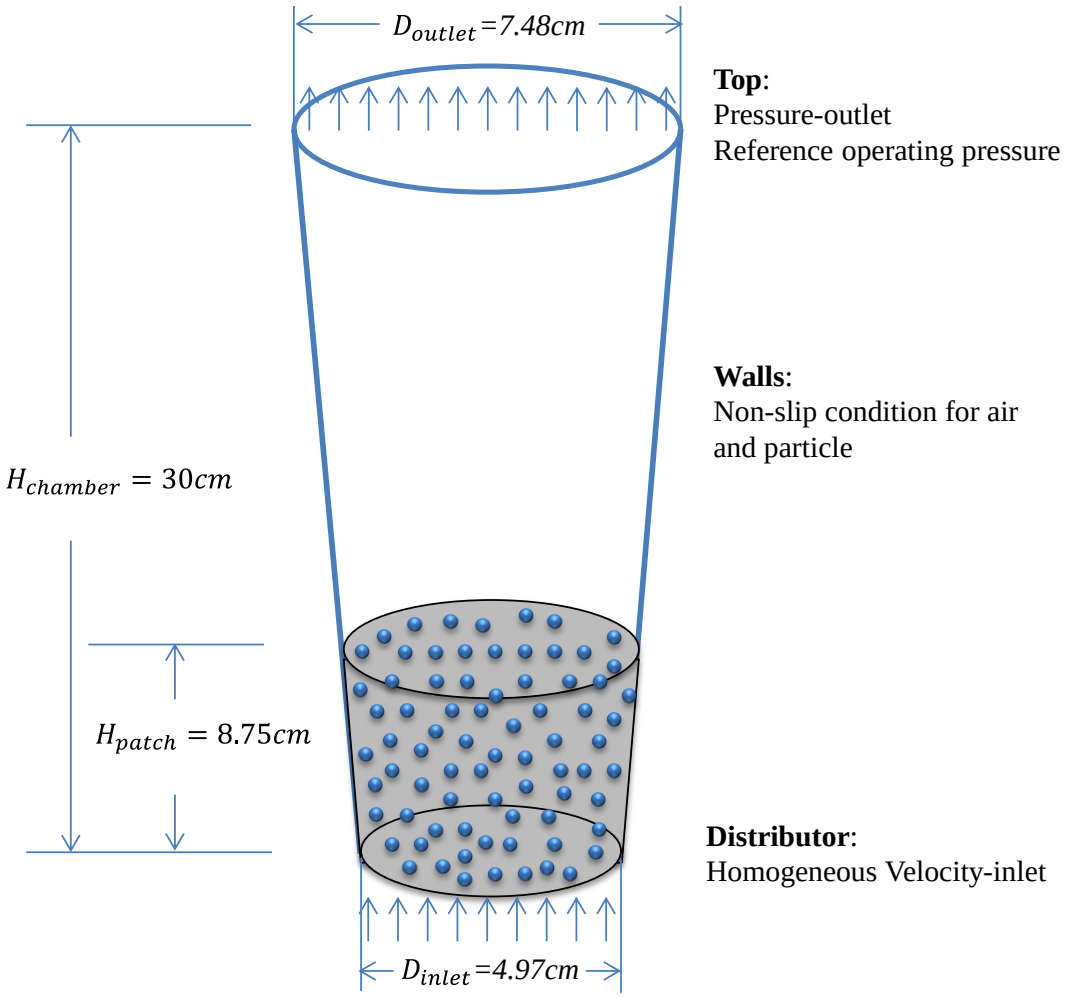

Figure 5.2 The geometry and boundary conditions used in the simulations

The CFD simulations were performed on a 2 GHz Intel Four Core processor desktop computer with 4 GB RAM using a XP platform. Mesh sensitivity studies were carried out at three different grids with total cells of 60000, 101400, and 135000. Three parameters of the bed solid volume fraction, bed pressure drop and bed height were used to monitor the effect of grid density on the simulation results in Figure 5.3, indicating that the grid with a total amount of 101400 cells was adequate to give a grid independent results, which was used in all the simulations.

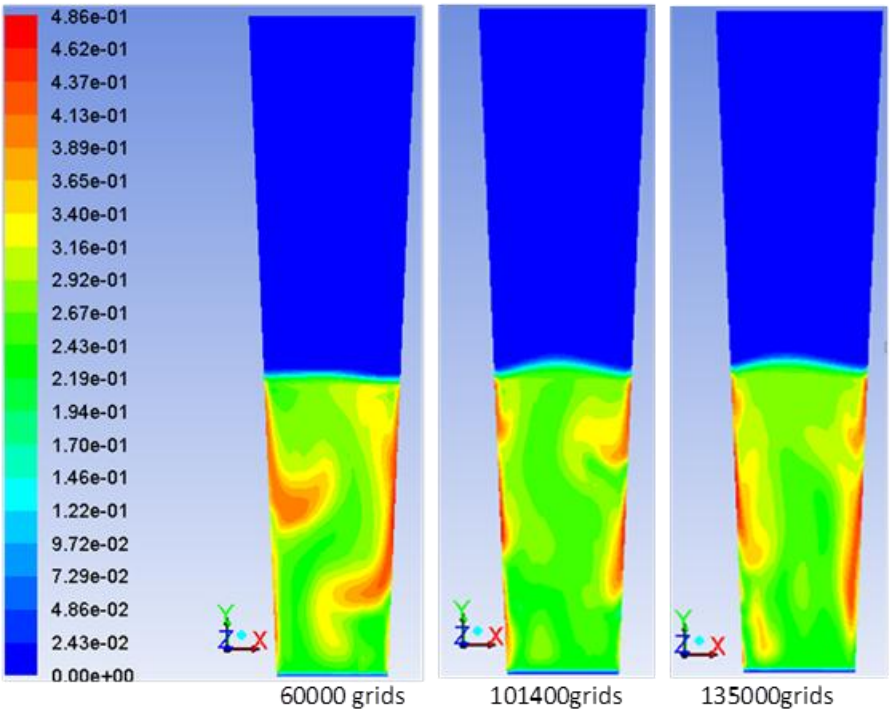
4.86e-01
4.62e-01
4.37e-01
4.13e-01
3.89e-01
3.65e-01
3.40e-01
3.16e-01
2.92e-01
2.67e-01
2.43e-01
2.19e-01
1.94e-01
1.70e-01
1.46e-01
1.22e-01
9.72e-02
7.29e-02
4.86e-02
2.43e-02
0.00e+00
60000 grids
101400grids
135000grids

(a)

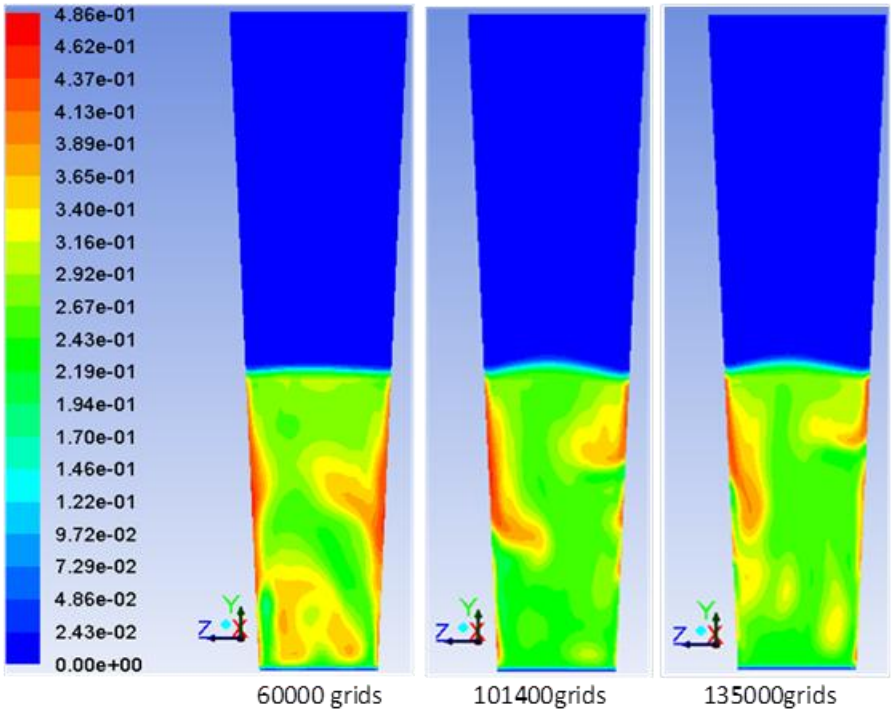
4.86e-01
4.62e-01
4.37e-01
4.13e-01
3.89e-01
3.65e-01
3.40e-01
3.16e-01
2.92e-01
2.67e-01
2.43e-01
2.19e-01
1.94e-01
1.70e-01
1.46e-01
1.22e-01
9.72e-02
7.29e-02
4.86e-02
2.43e-02
0.00e+00
60000 grids
101400grids
135000grids

(b)

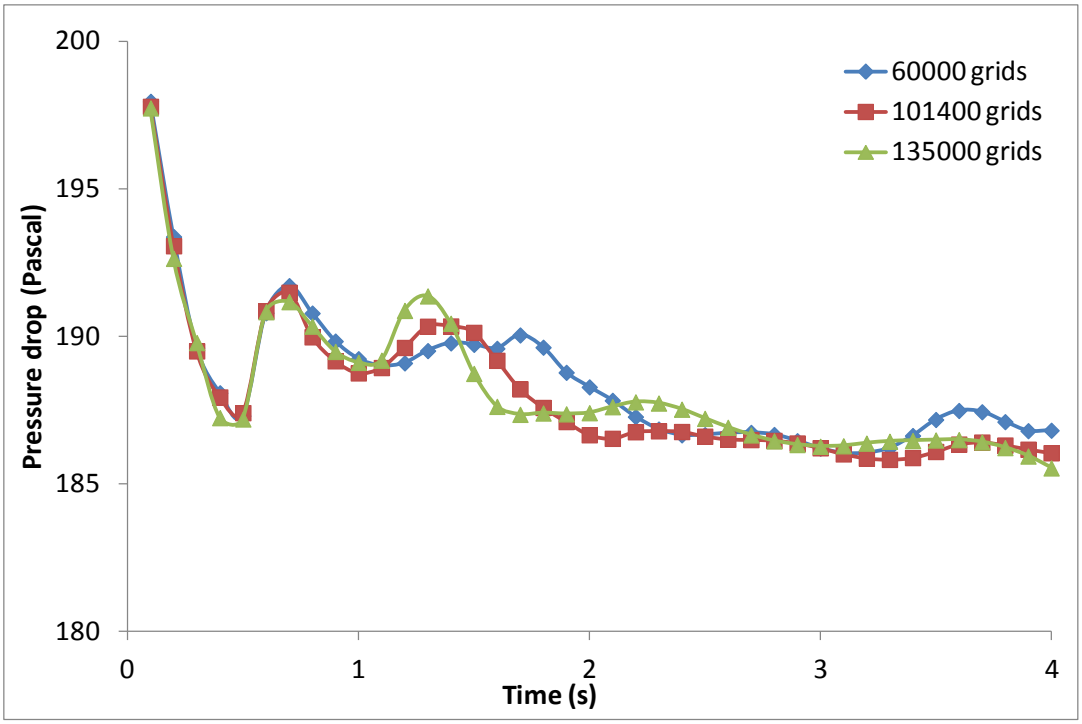

(c)

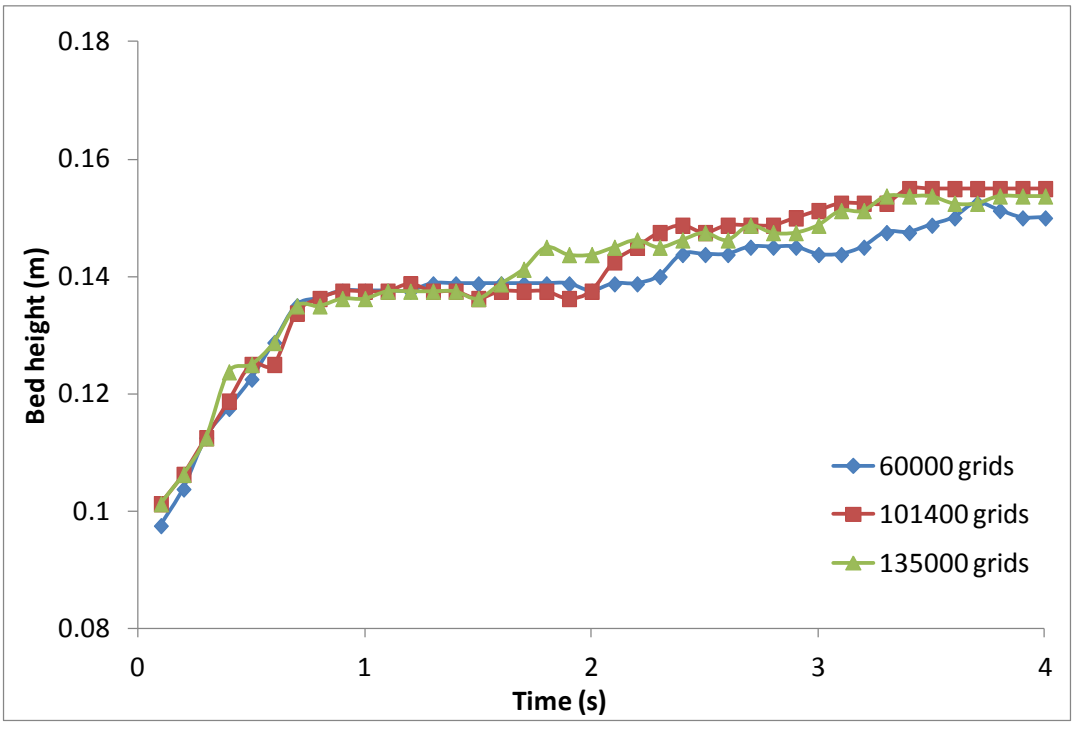

(d)

Figure 5.3 Mesh sensitivity study results; (a) solid volume fraction on cross-sectional plane XY; (b) solid volume fraction on cross-sectional plane YZ; (c) pressure drop with time; (d) bed height with time.

5.4 Design of CFD simulations

In the current study, the solid circulation pattern is represented by the particle circulation time and the granulation process is simulated by increasing the particle size and inlet air velocity. In order to investigate the relationship between the solid circulation pattern with inlet air velocity and the particle size, CFD simulations were designed using JMP 11.0 software (SAS, SAS Institute, Cary, NC, USA). The full factorial experimental design method is selected with air velocity and particle size as factors and each factor has three levels. The low, medium and high levels of each independent factor are determined based on the preliminary experimental study in chapter 3, which represents the beginning, medium and final stages of the granulation experiments, respectively. A total of 9 CFD simulations are designed based on the full factorial experimental design as shown in Table 5.3. A non-linear quadratic model generated by the full-factorial experiment design method is given as:

$$Y = b_0 + b_1 x_1 + b_2 x_2 + b_{12}\left(x_1 - x_{1,midiate}\right)\left(x_2 - x_{1,midiate}\right) \quad (5.1a)$$

$$x_{1,midiate} = \frac{x_{1,min} + x_{1,max}}{2} \quad (5.1b)$$

$$x_{2,midiate} = \frac{x_{2,min} + x_{2,max}}{2} \quad (5.1c)$$

where Y is a measured response associated with each factors combination; b_0 is an intercept; b_1 to b_{12} are regression coefficients calculated from the observed experimental values of Y; x_1 and x_2 are the real values of independent variables and $x_{1,min}$, $x_{1,max}$ and $x_{2,min}$, $x_{2,max}$ are the minimum and maximum value of variable x_1 and x_2, respectively. The term $x_1 x_2$ represents the interaction effect.

Table 5.3 The full factorial experimental design and responses

Run	Independent variables			Dependent variables
	Mode	X_1	X_2	Y_1
1	−−	164	0.6	2.57
2	−0	164	1.2	2.22
3	−+	164	1.8	2.02
4	0−	332	0.6	3.23
5	00	332	1.2	2.37
6	0+	332	1.8	2.22
7	+−	500	0.6	4.61
8	+0	500	1.2	2.56
9	++	500	1.8	2.32

5.5 Results and discussion

5.5.1 Convergence to quasi-steady state and verification of CFD model

The CFD simulation in this study was carried out in transient mode. Although the solid flow in the bed is unsteady with changes of local velocity in both magnitude and direction during fluidization, it is important to ensure that the CFD simulation reaches quasi-steady-state conditions, in which the gas-solid flow dynamics is generally time independent. In order to determine the simulation time to the quasi-steady state, different variables, including the bed steady state pressure drop, the bed height and solid volume fraction on the cross section of X-Y plane, were monitored for simulation 1 shown in Figure 5.4. It is clearly seen that the quasi-steady-state conditions were reached after 5s because all of parameters showed constant values during process. The time needed to reach the quasi-steady state differs between all the simulations. However, study using the same method has shown that all the simulations designed in section 5.4 can reach quasi-steady state after 5 s. Therefore all the results obtained from the CFD simulations are based on the time averaged values from 5s to 10s throughout the thesis.

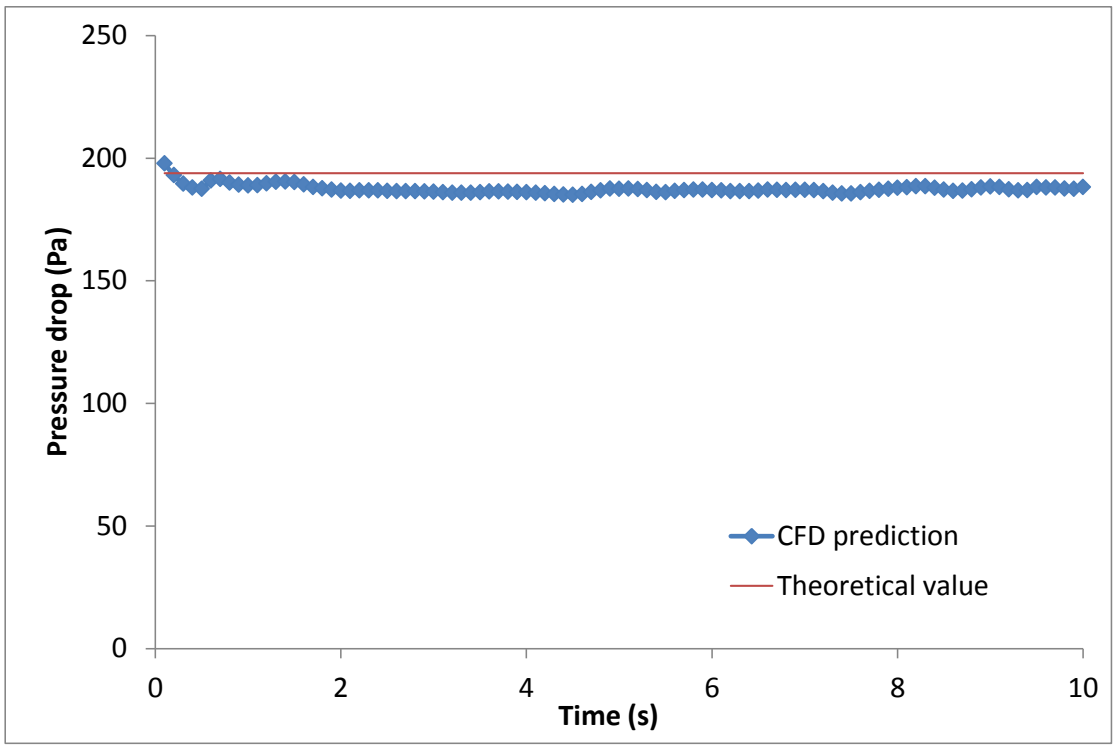
250
200
150
100
50
0
Pressure drop (Pa)
0
2
4
6
8
10
Time (s)
CFD prediction
Theoretical value

(a)

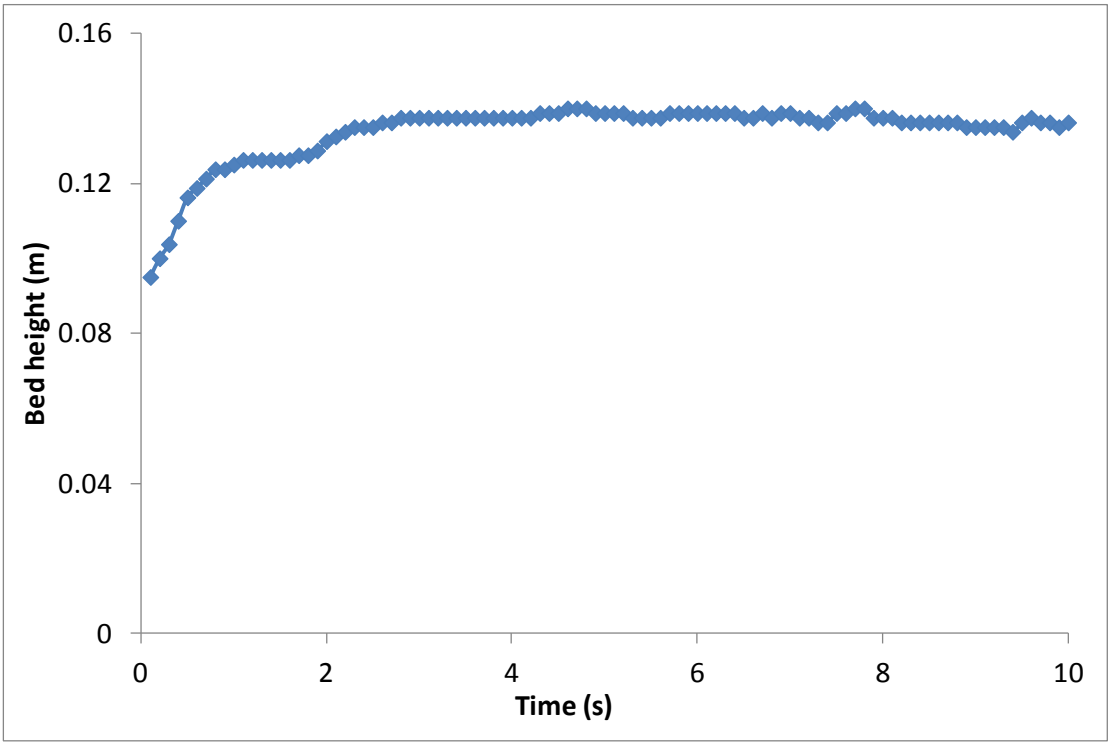
0.16
0.12
0.08
0.04
0
Bed height (m)
0
2
4
6
8
10
Time (s)

(b)

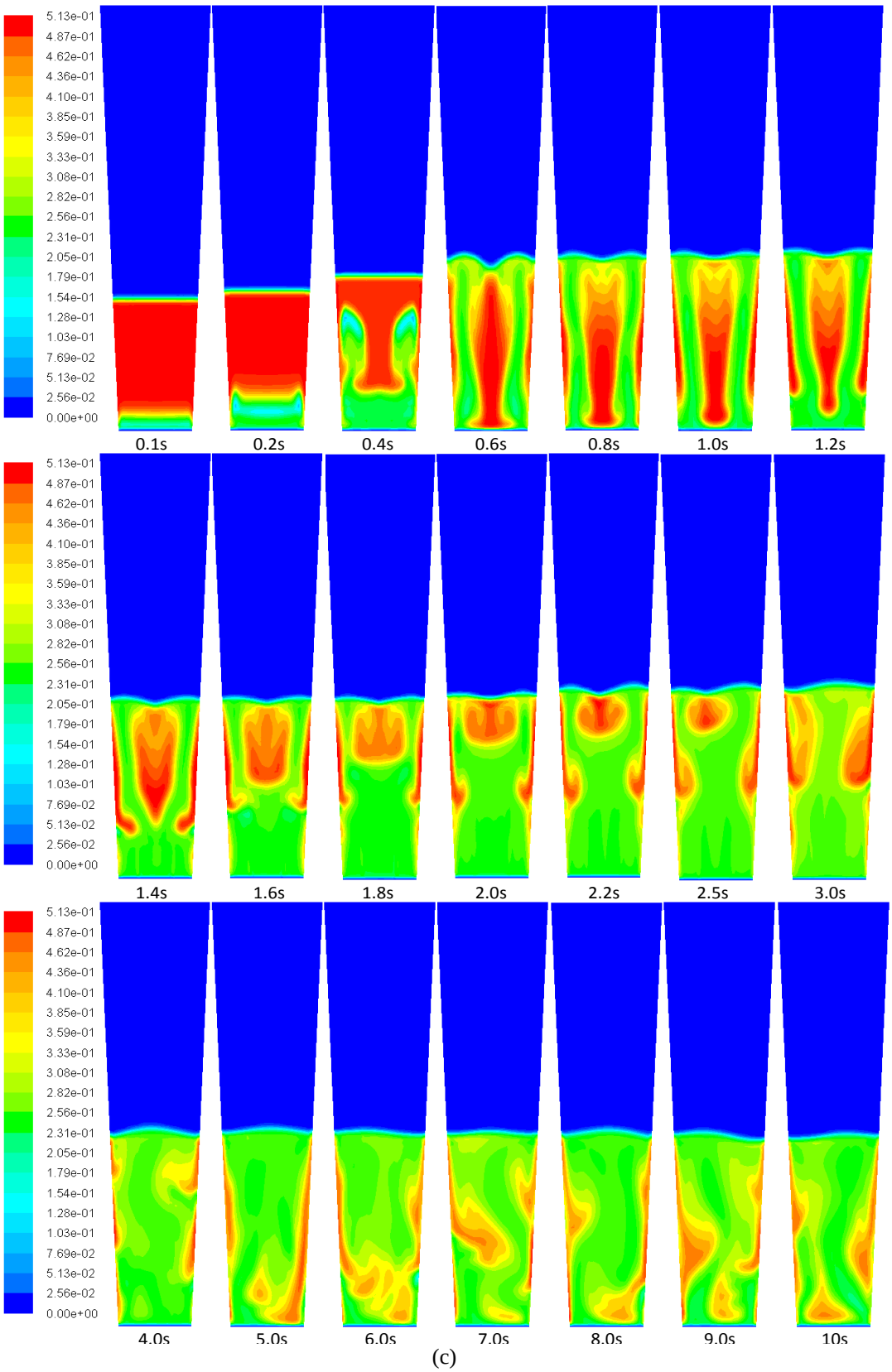

(c)

Figure 5.4 Convergence to quasi-steady state and validation studies for CFD simulation: (a) bed pressure drop; (b) Bed height; (c) distribution of solid volume fraction on the cross section of the XY plane

The effectiveness of the CFD simulation can be validated through comparison of the theoretical prediction and numerical simulation result of the total pressure drop of the bed [226]. It is well known that among all the parameters describing the fluidized bed granulation performance, the pressure drop is one of the most important ones, in particular, in scale-up and design of fluidized bed granulator. In the current study, pressure drop is selected to validate the CFD model by comparing the pressure drop obtained from the CFD simulation with the classical calculated data. At the minimum fluidization conditions, the powder in the bed is fully supported by the upward gas flow. The force generated by the upward gas is proportional with the pressure drop, which is mainly balanced by the weight of the solid bed. Therefore, the pressure drop across the bed is given as [226]:

$$\Delta P = (\rho_s - \rho_g)(1 - \varepsilon_{mb}) g H_{mb} + \varepsilon_{mb} \rho_g g H_{mb} + \rho_g g (H_{chamber} - H_{mb}) \quad (5.2)$$

where, ρ_s and ρ_g are the particle and air densities, H_{mb} and ε_{mf} are the bed height and the bed voidage at the minimum fluidization velocity, and $H_{chamber}$ is the product chamber height. Based on the experiment, it was found that the bed height at the minimum fluidization velocity was 12.7cm and then the bed voidage can be determined as 0.6588. Figure 5.4(a) shows the comparison between the CFD predicted pressure drop and theoretically calculated value as 193.90 *Pa*. It is indicated that at the beginning of fluidization the overall pressure drop decreases significantly and then fluctuates around a steady-state value of 187 *Pa* after 5s. It can be seen that the steady-state value of 193.90 *Pa* obtained by the CFD simulation is in reasonably good agreement with the theatrically calculated value, indicating that the CFD model can be used to predict the performance of a fluidized bed.

5.5.2 Particle flow characteristics

Figure 5.5 shows the time-averaged upward and downward particle velocity at different bed height in the CFD simulation 1. All the other simulations have the similar curve trend and are not given here. It can be seen that both the upward particle flow velocity and downward particle flow velocity increases with bed height from the granulator bottom and starts to decrease with bed height from the middle of the bed until the bed

surface. As we know, the reason why the particles could keep fluidization in the granulator is that the particle weight is balanced by drag force generated from the pressure drop. Figure 5.6 shows the time-averaged static pressure for mixture on different bed heights and the static pressure contour on the vertical plane *XY* from which it can be seen that the pressure decreases significantly with bed height. On the lower bed domain, where the drag force is larger than the particle weight, the particles are accelerated by the drag difference upward, while the particle velocity starts to decrease when the drag force is smaller than particle weight at high bed height. The same theory can be utilized to explain the particle velocity evolution during the downward process.

From Figure 5.6, it can be seen that the pressure drop decreases gradually from the bottom to top of the bed, which can be attributed to the fluidizing air from the bottom distributor. With the same particle size, the pressure drop decreases slowly as the inlet air velocity increases. When the inlet air velocity keeps constant, the pressure drop decreases more quick as the particle diameter increases.

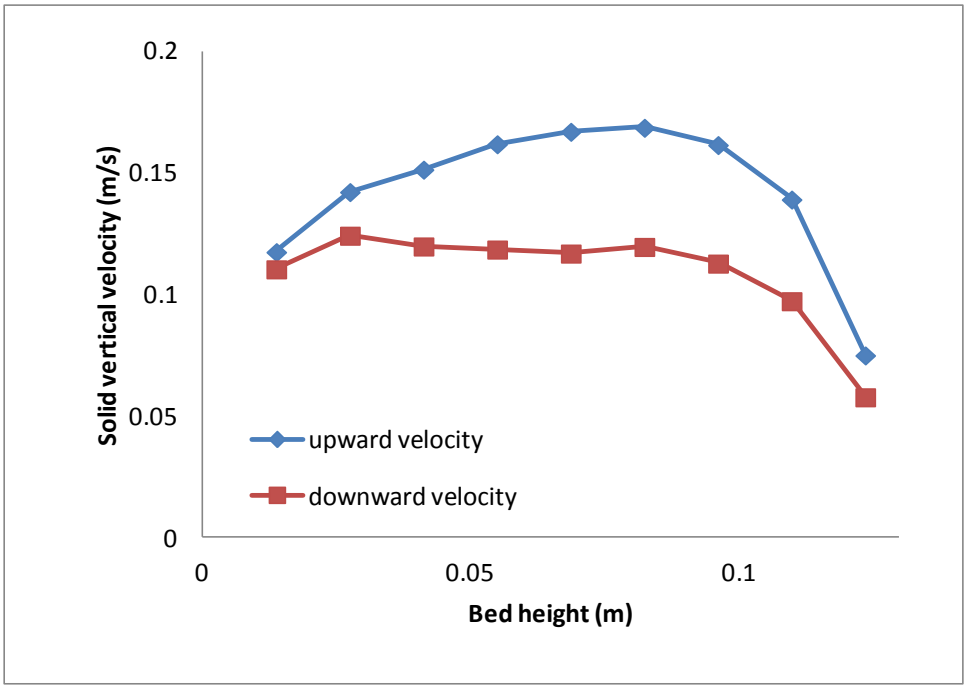

Figure 5.5 The time-averaged upward and downward solid velocity along the bed height

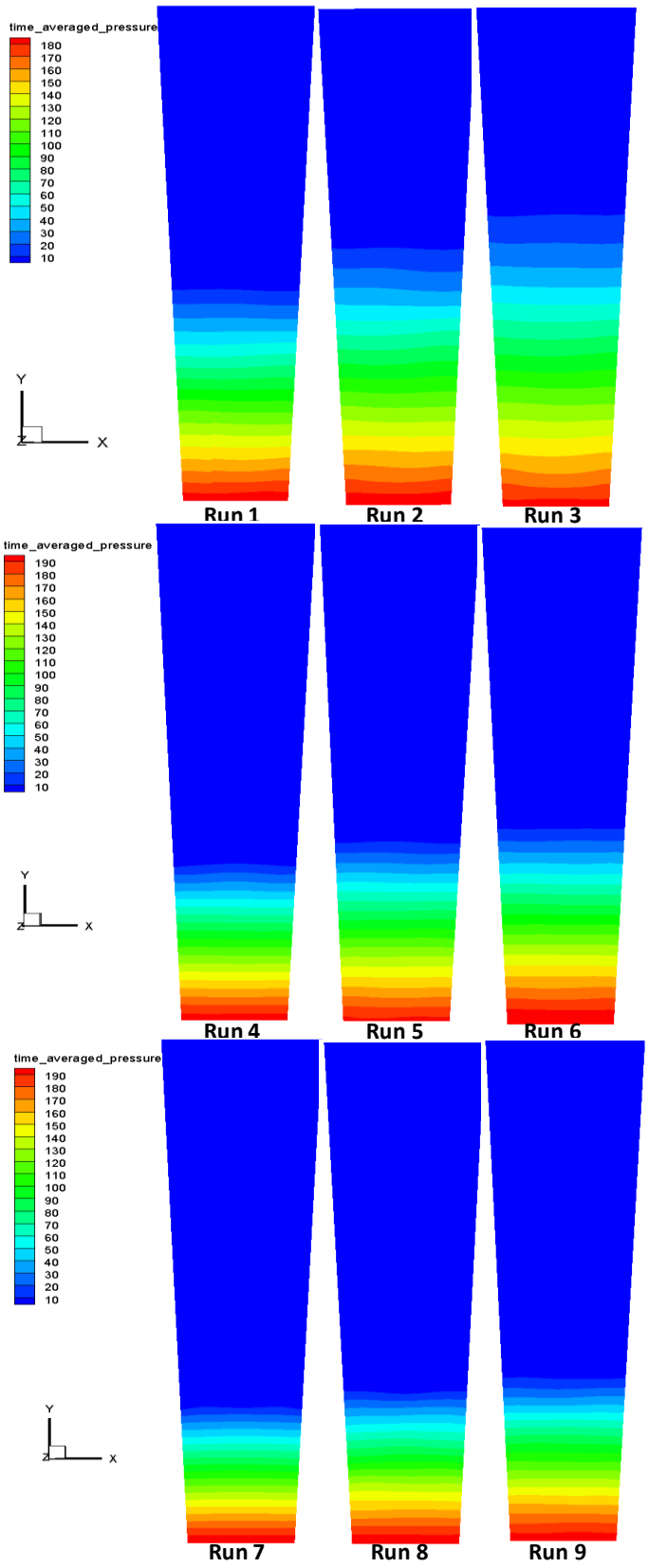

Figure 5.6 Time-averaged static pressure contour of mixture on vertical plane XY

From Figure 5.5, it is clearly indicated that the upward particle velocity is universally larger than the corresponding downward particle velocity at different bed heights, which can be also observed from the CFD results in Figure 5.7. Figure 5.7 shows the time-averaged particle Y velocity vector at different bed heights (0.1, 0.3, 0.5, 0.7, 0.9 times bed height), which has shown that the particles flow upward through the central area and fall downward against the wall through an annulus domain.

Figure 5.8 shows the time-averaged solid concentration contour on the cross-sectional plane at different bed heights for all the nine CFD simulations. In order not to lose generality, the cross-section plane was created at the same ratio of the bed height. It is shown that the downward flow annulus area has an obviously high particle concentration. This phenomenon can well explain the difference between the upward and downward particle velocity, because high particle concentration generates high frictional force between particles and obstructs the increase of downward particle velocity. For each single simulation, it was found that particles are most likely concentrated around the middle bed height but not the bed bottom, which indicated the obvious effect of fluidizing air velocity. During the simulations, when the particle size keeps constant, the solid volume fraction change slightly with the increasing of inlet air velocity, for example simulation 1 to simulation 3, simulation 4 to simulation 6. However, at the same level of inlet air velocity, the particle concentration changed significantly as the particle diameter increased, e.g. from simulation 1 to simulation 4 until simulation 7.

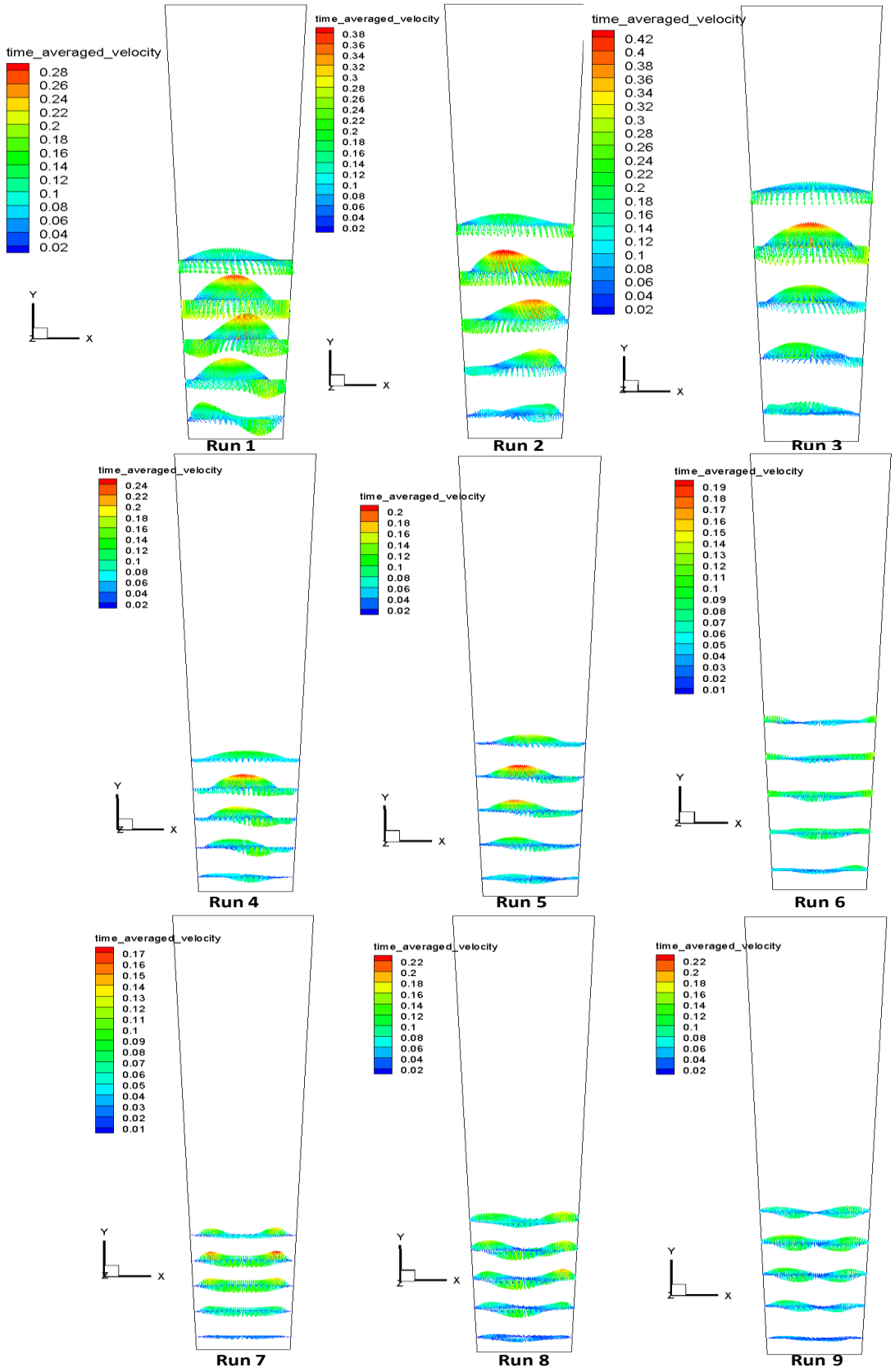

Figure 5.7 The particle *Y* velocity vector on horizontal cross-section plane at different bed heights

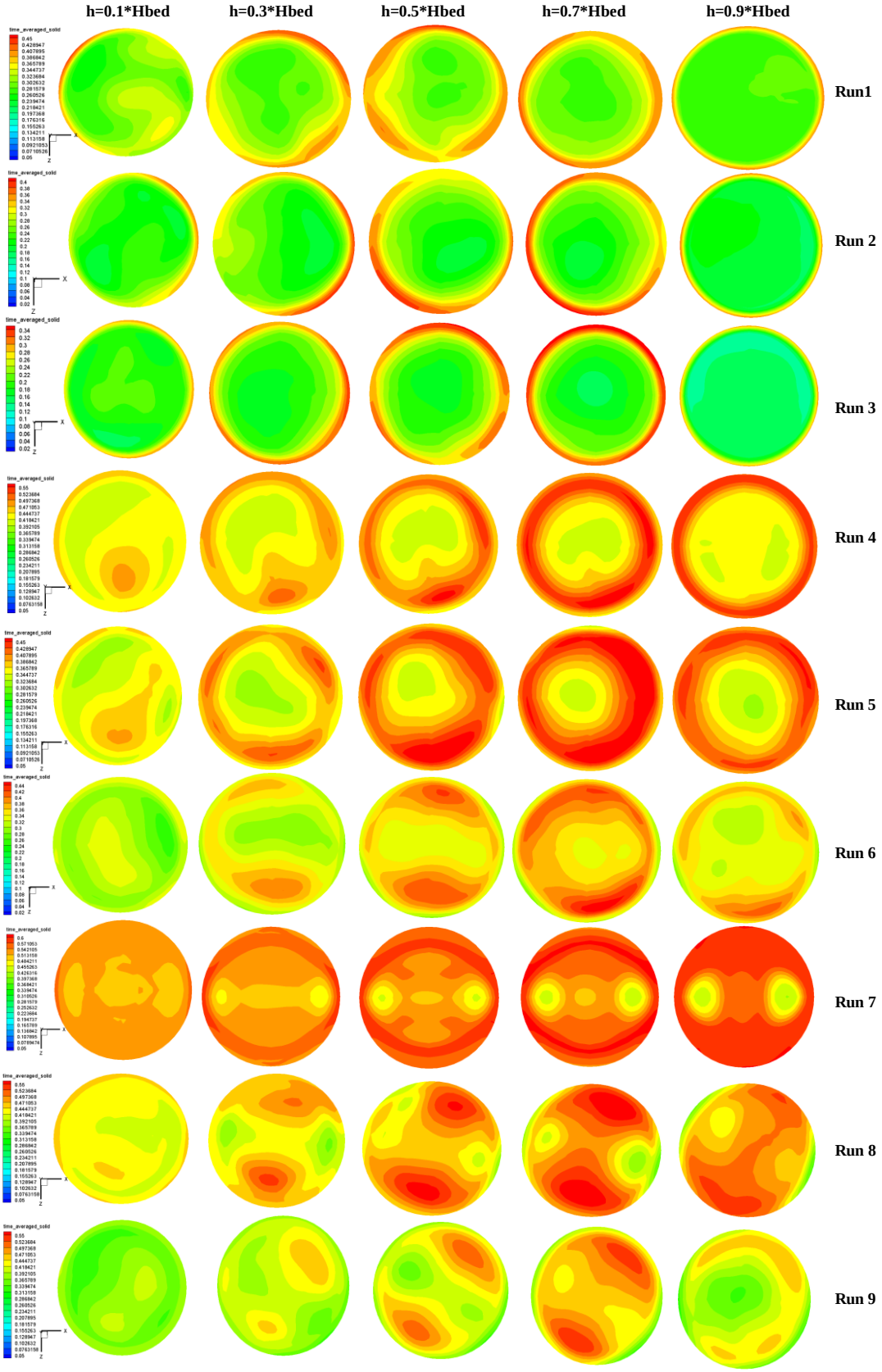

Figure 5.8 Time-averaged solid volume fraction at cross-sectional plane on different bed heights

However, although the upward particle velocity is large than the downward particle velocity, the particle volume exchange flow rate between two adjacent compartments has reached a balance state through any horizontal plane as the particles moves vertically. The volume flow rate (m3/s) through any horizontal plane ($y = h$) was calculated from the Fluent simulation by the following equation in terms of discretized form:

$$R_{downward} = \sum_{s_{vi} \in surface\ y=h} \varepsilon_{s,i} * s_{vi} * \vartheta_{i\_y\_down} \tag{5.3a}$$

$$R_{upward} = \sum_{s_{vi} \in surface\ y=h} \varepsilon_{s,i} * s_{vi} * \vartheta_{i\_y\_up} \tag{5.3b}$$

where, v_i is the cell volume, $\varepsilon_{s,i}$ is the time-averaged solid volume fraction of the cell v_i, s_{vi} is the cross section area of the cell v_i with the horizontal surface, $\vartheta_{i\_y\_up}$ is the particle velocity in cell v_i on the surface through which particle moves upward, $\vartheta_{i\_y\_down}$ is the particle velocity in cell v_i on the surface through which particle moves downward.

Figure 5.9(a), (b), (c) have shown the particle volume flow rate through three horizontal planes which are randomly created at heights of 0.0344m, 0.0688m and 0.1032m in simulation 1, respectively. It is indicated that at the beginning time before 4 seconds the upward particle volume flow rate is larger than the downward volume flow rate, because of the initial particle patching at the bottom of the bed. After 4 seconds, it can be seen that the evolution of the two particle volume flow rates is high consistent with time, because the fluidization basically has reached the quasi-steady state.

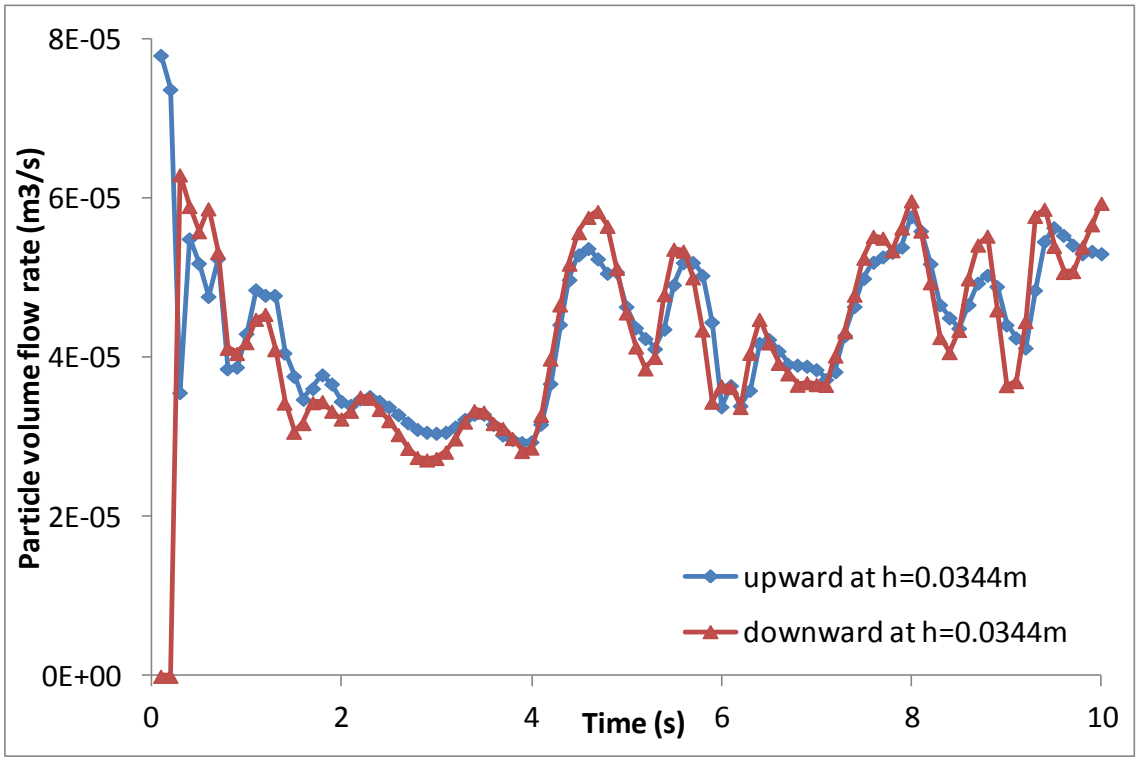
8E-05
6E-05
4E-05
2E-05
0E+00
Particle volume flow rate (m3/s)
0
2
4
6
8
10
Time (s)
upward at h=0.0344m
downward at h=0.0344m

(a)

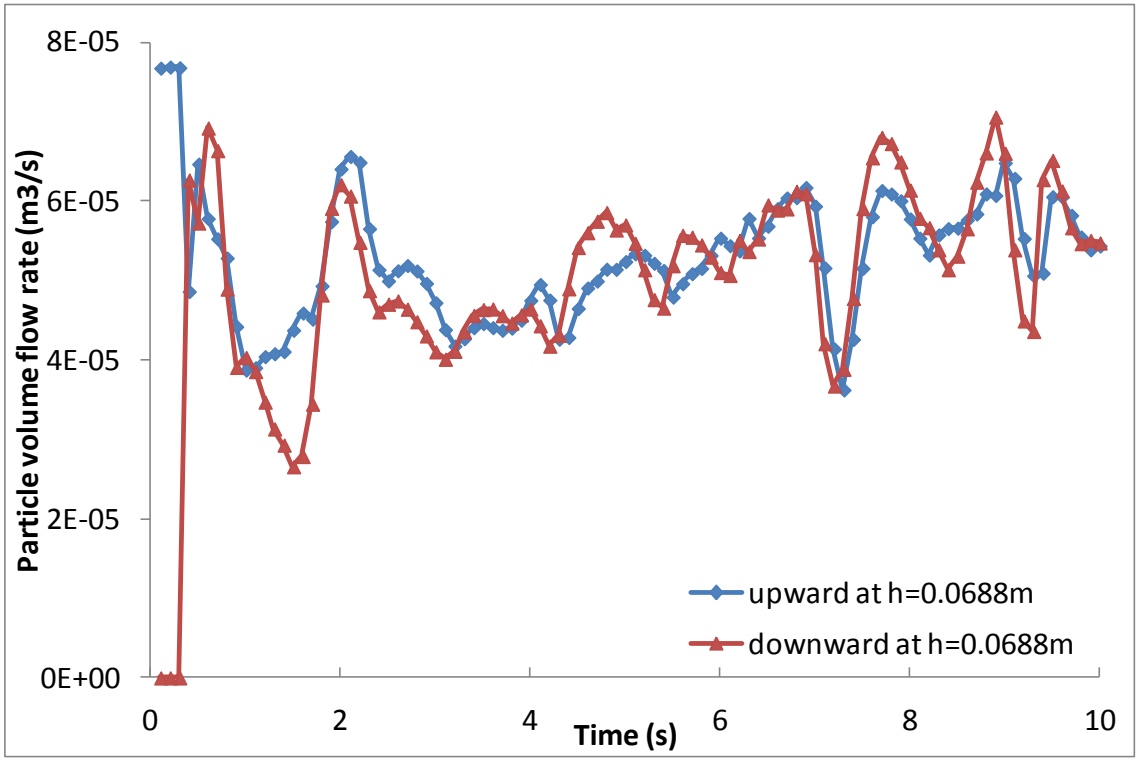
8E-05
6E-05
4E-05
2E-05
0E+00
Particle volume flow rate (m3/s)
0
2
4
6
8
10
Time (s)
upward at h=0.0688m
downward at h=0.0688m

(b)

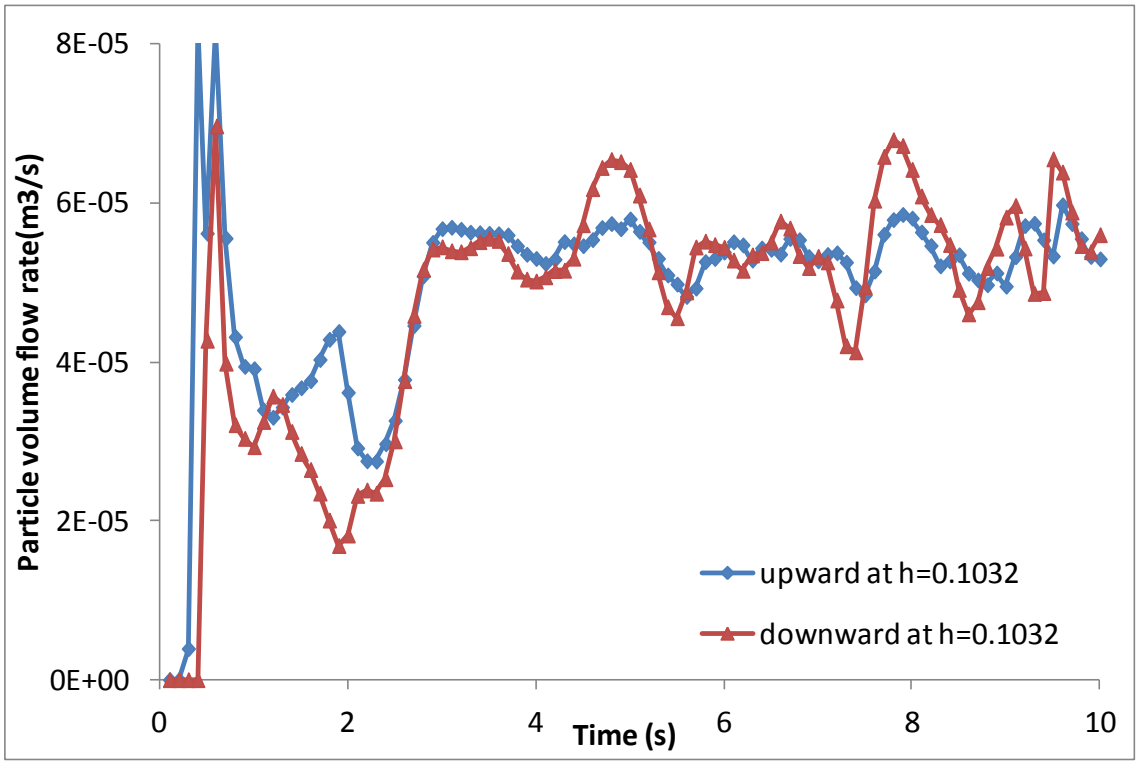

(c)

Figure 5.9 Particle volume flow rate through plane: (a) *h*=0.0344*m*; (b) *h*=0.0688*m*; (c) *h*=0.1032*m*.

The effect of particle size and inlet air velocity on the fluidization is also investigated as shown in Figure 5.10. The particle volume fraction distribution in the granulator at the plane surface XY is plotted for all the simulations with particle from 164*um* to 500*um* and inlet air velocity from 0.6*m3/h* to 1.2*m3/h*. An obvious observation is that the fluidized bed expansion increases with inlet air velocity for all the particle sizes. As the inlet air velocity increases, the bubbles appear initially at the bottom of granulator and increase in both number and size, which is clearly observed for particle size 164*um* and 500*um*. However, the bubbles distorted significantly and merge frequently at high inlet air velocity, which generates long and twisty bubbles as shown in simulation 3 and simulation 9 in Figure 5.10. It can also be seen that the fluidized bed expansion decrease with particle size. Under the same inlet air velocity, more bubbles and a heterogeneous fluidization state are generated by the larger particle size. In particularly, the bed in simulation 7 with velocity 0.6*m3/h* and particle size 500*um* does not even expand, which directly results in a significant high particle circulation time of 4.61*s*.

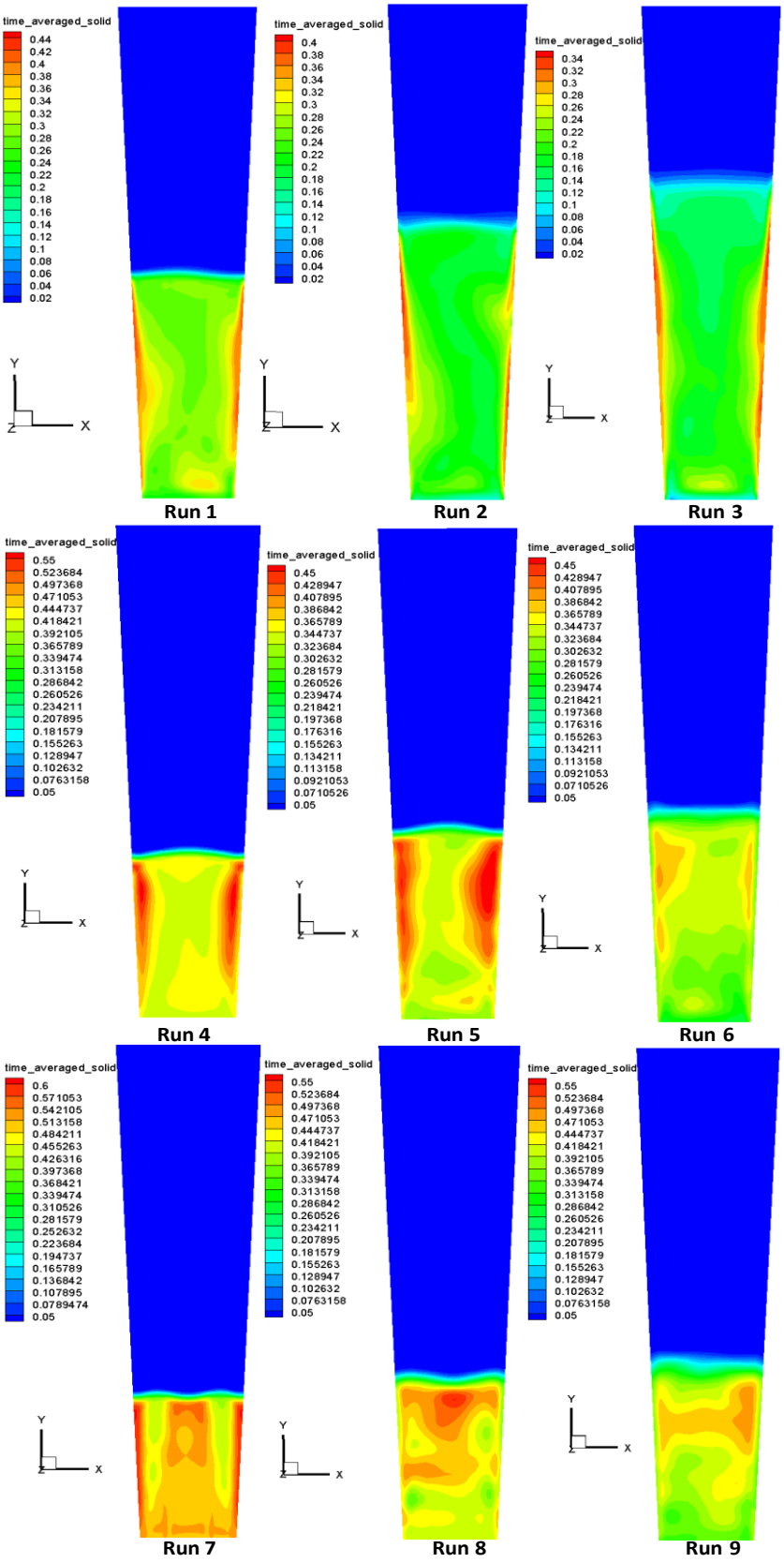

Figure 5.10 Time-averaged particle volume fraction for all the simulations at the plane *XY*.

5.5.3 Particle circulation time

In the fluidized bed granulator, the particle circulation pattern is a very important design attribute of the granulation process, which can be utilized to explain how the aggregation and breakage are happening. As described in chapter 3, the inlet air velocity in the experiments is increased gradually with time to keep the constant flow pattern [227]. In this chapter, the particle circulation time will be considered as an indicator of the particle circulation pattern to investigate the effect of particle size and inlet air velocity on it.

The particle circulation time in the current study is defined as the sum of time required for the particles to reach the bed surface and return back to the air distributor, as described by Rowe [227]:

$$t_c = \frac{V_{upward}}{\bar{v}_{upward}} + \frac{V_{downward}}{\bar{v}_{downward}} \tag{5.4}$$

Where, V_{upward} and $V_{downward}$ are the total upward flowing particle volume and total downward flowing particle volume, respectively. $\bar{v}_{upward}$ and $\bar{v}_{downward}$ are the average upward particle volume flow rate and average downward particle volume flow rate, respectively.

$$V_{upward} = \sum_{v_i>0} \varepsilon_{s,i} * v_i \tag{5.5a}$$

$$V_{downward} = \sum_{v_i<0} \varepsilon_{s,i} * v_i \tag{5.5b}$$

and

$$\bar{v}_{upward} = \sum_{k=1}^{n\_k} \sum_{s_{vi} \in surface\ y=h_k} \varepsilon_{s,i} * s_{vi} * \vartheta_{i\_y\_up} / n\_k \tag{5.6a}$$

$$\bar{v}_{downward} = \sum_{k=1}^{n\_k} \sum_{s_{vi} \in surface\ y=h_k} \varepsilon_{s,i} * s_{vi} * \vartheta_{i\_y\_down} / n\_k \tag{5.6b}$$

$$h_k = (k - 0.5) * H_{chamber}/120 \tag{5.6c}$$

Where, v_i is the cell volume, $\varepsilon_{s,i}$ is the time-averaged solid volume fraction of the cell

v_i, s_{vi} is the cross section area of the cell v_i with the horizontal surface y = h_k, $\vartheta_{i\_y\_up}$ is the particle velocity in cell v_i on the surface through which particle moves upward, $\vartheta_{i\_y\_down}$ is the particle velocity in cell v_i on the surface through which particle moves downward, n_k in the grid number along y-axis, and $H_{chamber}$ is the chamber height.

Using this method, the particle circulation time was calculated for all the nine CFD simulations and filled in the Table 5.3 for later analysis.

Figure 5.11 shows the effect of particle size and inlet air velocity on the particle circulation time in the fluidized bed granulator. It can be seen that the circulation time decreases with inlet air velocity and increase with particle size under the same inlet air velocity. Three CFD simulations run1, run 5 and run 9 with particle size 164*um*, 332*um*, and 500 *um*, respectively, are marked on Figure 5.11. It can be seen that the circulation time can be kept constant by adjusting the inlet air velocity from the observation that the three marked simulations have similar circulation time while particle size increased from 164*um* to 500*um*. For the simulation 7 with condition of particle size 500 *um* and inlet air velocity 0.6 *m3/h*, an apparent high circulation time 4.61*s* is observed, which is caused by the defluidization of the solid bed that will be discussed later. From our previous experimental study [228], it is known that the final particle mean size has a significant range from 290 *um* to 734 *um* among all the experiments. In addition, considering the increasing bed humidity in reality, the inlet air velocity has to be adjusted to keep the solid flow pattern constant.

The process model parameters of b_0, b_1, b_2, and b_{12} in equation (5.1) can be obtained using JMP 11 software (SAS, SAS Institute, Cary, NC, USA). A mathematical model between the particle circulation time and particle size and inlet air velocity is developed by the JMP software is given as follows:

$$t_c = 3.08 + 2.66 \times 10^{-3} * d_{p,m} - 1.07 * v_{a,inlet} - 4.32 \times 10^{-3} * \left(d_{p,m} - 332\right) * \left(v_{a,inlet} - 1.2\right) \quad (5.7)$$

Where, $d_{p,m}$ is the mean particle diameter in um and $v_{a,inlet}$ is the inlet air velocity in *m3/h*. If the particle size distribution can be obtained online, the particle circulation time

can be fixed on T_c by adjusting the inlet air velocity in following algorithm:

$$v_{a,inlet} = \frac{1.359+7.84\times10^{-3}d_{p,m}-T_c}{4.32\times10^{-3}d_{p,m}-0.3642} \tag{5.8}$$

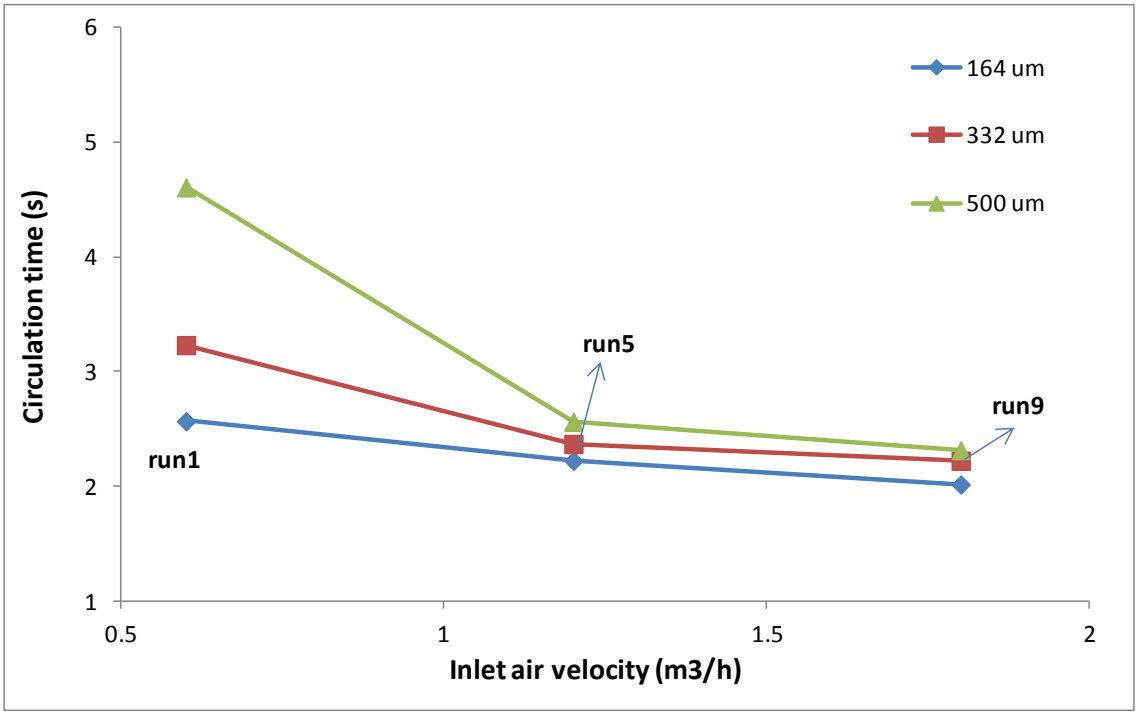

Figure 5.11 Particle circulation time with inlet air velocity under different particle size

5.6 Chapter conclusions

In this chapter, the gas-particle fluid dynamics within the fluidized bed granulator was studied using CFD software ANSYS Fluent 13.0. The influence of particle size and inlet air velocity on the particle circulation pattern was investigated. It was proved that the particle circulation time within the granulator could be kept constant by adjusting the inlet air velocity as the particle size increased. A mathematical model between the particle circulation time and particle size and inlet air velocity was developed, which could work as guidance about how to adjust the inlet air velocity to keep the fluidization in the same level during the experiment. Also the characteristic of granulation, like solid holdup, solid velocity, were also studied by the CFD simulation results.

Chapter 6 Two-compartmental population balance modeling and control of a pulsed spray fluidized bed granulation based on computational fluid dynamics (CFD) analysis

6.1 Chapter overview

In this chapter, the fluidized bed granulator was divided into two compartments, both of which were assumed as homogeneous domain, based on the CFD analysis of gas-solid fluid dynamics in chapter 5. A wetting compartment which contains 30% of the bed size was defined where aggregation happened, while a drying compartment that contains 70% of bed size close to the air distributor where only breakage is considered. A two-compartmental population balance model was developed by combining the one-dimensional PBM and compartments divided by the CFD study. The two-compartmental PBM was validated by the experiment data obtained in chapter 3. The prediction ability on the final particle size distribution was also compared between the two-compartmental PBM and the one-dimensional PBM, which indicated that the two-compartmental PBM did have advantages and had generally shown smaller sum square of error (SSE). Finally, the control strategy proposed in chapter 5 was also applied to control the granulation system based on the two-compartmental PBM, and results showed that the system can be controlled effectively to obtain desired mean size.

6.2 Two-compartmental population balance model (TCPBM)

6.2.1 Two-compartmental modeling strategy

During last decades, a lot of research work on granulation process modeling [210, 229] was based on the one-dimensional discretized population balance model (PBM) of a fluidized bed granulation process in which it is assumed that the fluidized bed is a well-mixed system and the mechanisms of the aggregation and breakage are spatially homogeneous for evolution of granule growth. Obviously it is not true in a real spray fluidized bed granulation process. It is well known that particles in a fluidized bed are not homogeneously distributed and their hydrodynamics and kinetic parameters

regarding the size enlargement process change with the time and position in the bed. Therefore, the PBM based on homogeneity cannot be applied for the whole fluidized bed granulation process.

In a top spray fluidized bed granulator in which the binder liquid solution is sprayed at the top of the bed into the fluidized bed, three regions have been identified with significant temperature gradients and different granulation mechanisms are shown to dominate in each of zones as [56, 230]: 1) the *Wetting-active zone* which is a low temperature and high humidity region near the spraying zone at the topmost part of the bed. The high humidity and temperature gradients are caused by the wetting of the fluidized particles by the liquid binder solution sprayed and the evaporation of the solvent; 2) The *Isothermal zone* which is near the walls and around the wetting-active zone. In this region there is equilibrium between heat and mass transfer and air temperature is homogeneous; 3) the *heat transfer zone* which is situated right above the bottom hot air distributor plate. It has been found that in a top spray fluidized bed granulation process agglomeration of the particles mainly takes place in the wetting active zone because of high humidity and in the isothermal and heat transfer zones granules are dried and solidified. Therefore, it is essential to consider different granulation mechanisms according to different zones in a granulation process model for accurately predicting the evolution of granule growth during granulation. Although multi-compartmental modeling has been effectively used to model the mixing of fluids in reactors, such as granular mixing and bioreactor [231-233], very little research has been carried out for modeling of a spray fluidized bed granulation process by a multi-compartmental model. Very recently the idea of a two-compartmental model has been applied to model a spray fluidized bed granulation process with two well-mixed zones of wetting and drying, in which a one dimension population balance model is only applied to the spray zone for the modeling of aggregation process and the granules communicate between the two zones at a constant flow rate [186, 230]. Obviously more research is required from both fundamental and applied studies on multi-compartmental modeling for fluidized bed granulation processes.

One aim of this chapter is to develop a more advantaged process model considering the

spatially heterogeneous granulation mechanisms of granule growth for a pulsed spray fluidized bed granulation process in comparison with our recent work on the one-dimensional population balance models under assumption of a well-mixed system in which the granulation mechanisms are spatially uniform [229]. The proposed model should be capable to link the key binder solution spray operating factors of the binder spray rate, atomizing air pressure and pulsed frequency to predict granule growth behavior in the system accurately. In this work the developed model was based on two spatial compartments of the wetting and drying zones of a top spray fluidized bed granulator, called the two-compartmental population balance model (TCPBM). It is assumed that each of two compartments is perfectly mixed and can be described by a one-dimensional PBM with different granulation mechanisms to predict the overall granule growth behavior in the granulator, in which the aggregation mechanism is assumed in the wetting compartment and the breakage mechanism is assumed in the drying compartment. Therefore, the proposed TCPBM can predict evolution of the granule size and distribution at different regions within the granulator under different binder spray operating conditions with accuracy.

Two critical issues in the TCPBM modeling of a top spray of fluidized bed granulation process are the sizes of the wetting and drying compartments and particle exchange rate between them. Studies have shown that the size of the wetting compartment can occupy between 14% and 30% of the bed depending on the operating conditions [56, 230]. Without losing generality the fixed sizes of wetting and drying compartments were assumed in this work, i.e., 30% of the bed was the wetting compartment and 70% of the bed was the drying compartment. The exchange rate of particles between the wetting and drying compartments can be determined by the particle residence time in each compartment, which can be characterized by the flow properties and distribution of particles in the bed. In this work, details of the flow properties and distribution of particles were studied by computational fluid dynamics (CFD) techniques as described in chapter 5. It was validated that the particle circulation pattern can be kept constant by adjusting the inlet air velocity, which was selected in our experimental work. Therefore, in this chapter, all the parameters from CFD are based on simulation 1, which represent the initial stage of granulation experiment. The volume fractions of particles in each of

two compartments and particle exchange rate between them were calculated based on the CFD results and then were used in the TCPBM.

6.2.2 Continuous TCPBM

In this work a top-spray granulator is divided into two perfectly mixed compartments: wetting compartment (WC) which is the upper zone of the granulator and drying compartment (DC) which is the low part of the system. In the WC the binder solution is sprayed into the bed to wet particles so that the aggregation of wet particles is carried out. In the DC granules are quickly dried by the inlet hot fluidizing air, therefore only breakage of granules takes place. The particles exchange randomly between the two compartments at certain steady state mass flow rate. The schematic illustration of the two compartments of the system is given in Figure 6.1 in which the following assumptions are made for the model development as

a. Both WC and DC are considered as well-mixed systems.
b. Sizes of the WC and DC are constants during granulation, in which the height of WC is 30% of the bed height as $H_{WC} = 0.3H_b$ and the height of DC is 70% of the bed height as $H_{DC} = 0.7H_b$.
c. Total volumes of particles V_{WC} in WC and V_{DC} in DC remain constant, which are determined by CFD simulations. The volume fraction of particles in the WC is given by $\alpha = \frac{V_{DC}}{V_{WC}+V_{DC}}$ and the volume fraction of particles in the DC is $(1-\alpha)$.
d. The volume exchange rate of particles between two compartments is constant as $R_{DC\to WC} = R_{WC\to DC} = R$, which is determined by CFD simulations. Therefore an average amount of times τ_{WC} and τ_{DC} that a particle spends in the WC and DC can be calculated as

$$\tau_{WC} = \frac{V_{WC}}{R_{WC\to DC}} = \frac{V_{WC}}{R} \tag{6.1}$$

$$\tau_{DC} = \frac{V_{DC}}{R_{DC\to WC}} = \frac{V_{DC}}{R} \tag{6.2}$$

e. Particle aggregation mechanism β_{WC} is considered in the WC while breakage mechanism S_{DC} is considered in the

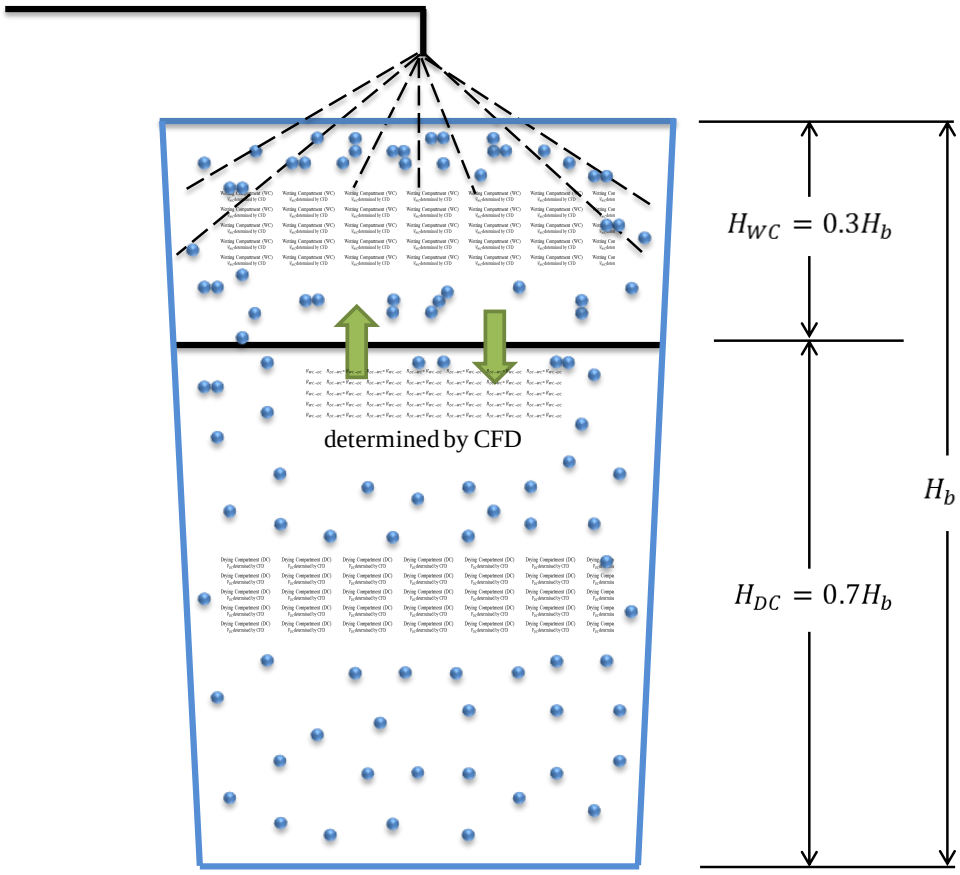

Figure 6.1 Schematic diagram of the TCPBM of a top spray fluidized bed granulation.

If the number density functions in terms of the particle diameter l in the WC and DC are $n_{WC}(t,l)$ and $n_{DC}(t,l)$, based on equation (6.1) the particle flux from the WC to DC $n_{WC\to DC}$ is

$$n_{WC\to DC} = \frac{n_{WC}(t,l)}{\tau_{WC}} \tag{6.3}$$

and based on equation (6.2) the particle flux from DC to WC $n_{DC\to WC}$ is given by

$$n_{DC\to WC} = \frac{n_{DC}(t,l)}{\tau_{DC}} \tag{6.4}$$

Applying a one-dimensional PBM to both of WC and DC, a TCPBM is given by

$$\frac{\partial n_{WC}(t,l)}{\partial t} = \frac{1}{2}\int_0^l \frac{\beta_{WC}\left(t,(l^3-\mu^3)^{\frac{1}{3}},\mu\right) n_{WC}\left(t,(l^3-\mu^3)^{\frac{1}{3}}\right) n_{WC}(t,\mu)}{(l^3-\mu^3)^{\frac{2}{3}}} d\mu - n_{WC}(t,l)\int_0^\infty \beta_{WC}(t,l,\mu) n_{WC}(t,\mu) d\mu - n_{WC\to DC}(t,l) + n_{DC\to WC}(t,l) \tag{6.5a}$$

$$\frac{\partial n_{DC}(t,l)}{\partial t} = \int_l^\infty S_{DC}(t,\mu) b_{DC}(l|\mu) n_{DC}(t,\mu) d\mu - S_{DC}(t,l) n_{DC}(t,l) - n_{DC\to WC}(t,l) + n_{WC\to DC}(t,l) \tag{6.5b}$$

$$n(t,l) = \alpha \cdot n_{WC}(t,l) + (1-\alpha)\cdot n_{DC}(t,l) \tag{6.5c}$$

Where $n(t,l)$ is the number density function of the whole fluidized bed, $\beta_{WC}(t,l,\mu)$ is the length-based aggregation kernel describing the frequency that particles with diameter l and μ collide to form a particle of volume $l^3+\mu^3$, $S_{DC}(t,l)$ is the length-based breakage selection rate constant describing the rate at which particles are selected to break and $b_{DC}(l|\mu)$ is the breakage kernel describing the formation of particles of diameter l from the breakup of particle of diameter μ.

6.2.3 Numerical solution of TCPBM

In order to solve the TCPBM in equation (6.5), the discretized approach proposed by Hounslow et al [107, 234] is employed to determine the change in number of particles $N_{WC,i}$ in the WC by the mechanism of aggregation and $N_{DC,i}$ in the DC by the mechanism of breakage in interval i under the assumption of conservation of the total volume of particles in each compartment. According to particle resident times in equations (6.1) and (6.2), the numbers of particle exchange rate between two compartments are given by

$$N_{WC\to DC}(t,l) = \frac{N_{WC}(t,l)}{\tau_{WC}} = \frac{R}{V_{WC}} N_{WC}(t,l) \tag{6.6}$$

and

$$N_{DC\to WC}(t,l)=\frac{N_{DC}(t,l)}{\tau_{DC}}=\frac{R}{V_{DC}}N_{DC}(t,l) \tag{6.7}$$

Therefore the discretized TCPBM is given by

$$\frac{dN_{WC,i}}{dt}=$$
$$\sum_{j=1}^{i-2}2^{j-i+1}\beta_{WC,i-1,j}N_{WC,i-1}N_{WC,j}+\frac{1}{2}\beta_{WC,i-1,i-1}N_{WC,i-1}^{2}-$$
$$N_{WC,i}\sum_{j=1}^{i-1}2^{j-i}\beta_{WC,i,j}N_{WC,j}-N_{WC,i}\sum_{j=i}^{n_{max}}\beta_{WC,i,j}N_{WC,j}-\frac{R}{V_{WC}}*N_{WC,i}+\frac{R}{V_{DC}}*N_{DC,i} \tag{6.8a}$$

$$\frac{dN_{DC,i}}{dt}=-S_{DC,i}N_{DC,i}+\sum_{j=i}^{n_{max}}b_{DC,i,j}S_{DC,j}N_{DC,j}+\frac{R}{V_{WC}}*N_{WC,i}-\frac{R}{V_{DC}}*N_{DC,i} \tag{6.8b}$$

$$N_i(t)=N_{WC,i}(t)+N_{DC,i}(t) \tag{6.8c}$$

Where $N_{WC,i}$ and $N_{DC,i}$ represent the number of particles in the size range of (L_i, L_{i+1}) for the WC and DC respectively, n_{max} is the total number of size intervals, and $N_i(t)$ is the total number of particle in the bed in the size of (L_i, L_{i+1}). In the discretization scheme, the length domain of particles is divided into geometric interval in the way that the upper and lower limits of each size interval are in a ratio of $r=\frac{L_{i+1}}{L_i}=\sqrt[3]{2}$. The parameters of V_{WC}, V_{DC}, and R in the equations are calculated from the CFD simulations which will be discussed in the next section.

In this work, the group of ordinary differential equations in equations (6.8) was solved by the ode45 solver in MATLAB based on the assumptions: (a) all granules are spherical; (b) the size of granules in particular size class is represented by the left edge of the size interval; and (c) the mechanism of aggregation or breakage is uniform for each particle within the same volume interval [229].

6.2.4 Selection of aggregation model and breakage model

Based on our previous study, it has been found that the aggregation of granules is dependent on the granule volume following the Smoluchowski's shear kernel [229]. Therefore the same aggregation kernel of particles in the WC is selected as [47, 210]

$$\beta_{WC}(t, l, \mu) = \beta_0(t, \Theta, \Psi)(l + u)^3 \tag{6.9}$$

Where $\beta_0(t, \Theta, \Psi)$ is the granulation rate constant, which incorporates various system parameters Θ, such as the binder spray and fluidization operating conditions for a top spray fluidized bed granulator, and nonequipment parameters Ψ, such as physical properties of the powder mixtures.

The same breakage selection function and breakage kernel in the DC are given as [229]:

$$S_{DC}(t, l, \mu) = S_0(t, \Theta, \Psi) \tag{6.10}$$

and

$$b_{DC}(l|\mu) = \frac{6l^2}{\mu^3} \tag{6.11}$$

where $S_0(t, \Theta, \Psi)$ is the breakage selection rate constant, which is a function of the system parameters Θ, such as the binder spray and fluidization operating conditions for a top spray fluidized bed granulator, and nonequipment parameters Ψ, such as physical properties of the powder mixtures.

In order to link the key binder solution spray operating factors of the pulse frequency x_1, binder spray rate x_2 and atomization pressure x_3 in the TCPBM to predict the granule growth behavior in a pulsed spray fluidized bed granulation process, it is assumed that the granulation rate constant $\beta_0(t, \Theta, \Psi)$ in equation (6.9) and breakage selection rate constant $S_0(t, \Theta, \Psi)$ in equation (6.10) can be represented as a non-linear quadratic function of the spray operating factors as [229]

$$\beta_0(x_1, x_2, x_3) = b_0 + b_1x_1 + b_2x_2 + b_3x_3 + b_{12}x_1x_2 + b_{13}x_1x_3 + b_{23}x_2x_3 + b_{11}x_1^2 +$$

$$b_{22}x_2^2 + b_{33}x_3^2 \tag{6.12}$$

and

$$S_0(x_1, x_2, x_3) = c_0 + c_1x_1 + c_2x_2 + c_3x_3 + c_{12}x_1x_2 + c_{13}x_1x_3 + c_{23}x_2x_3 + c_{11}x_1^2 +$$

$$c_{22}x_2^2 + c_{33}x_3^2 \tag{6.13}$$

Where b_0, b_1……, b_{33} and c_0, c_1……, c_{33} are constants.

In order to determine the constants of b_0, b_1……, b_{33} in equation (6.12) and c_0, c_1……, c_{33} in equation (6.13), the same method called a best fit approach used in our previous work is adopted for the best prediction of the experimental data of the granule size distribution in chapter 3 [229]. The detailed method is summarized as:

For each of experimental data set $k = 1,2, \dots, n$, the granulation rate constant $\beta_{0,k}$ and breakage selection rate $S_{0,k}$ are determined by minimizing the following cost function of the sum of square errors (SSE) of the particle size distribution through an iterative optimal algorithm as

$$\min_{\beta_{0,k}, S_{0,k}} \left\{ SSE(\beta_{0,k}, S_{0,k}) = \sum_i \left(V(N_{k,i}) - V\left(\widehat{N}_{k,i}(\beta_{0,k}, S_{0,k})\right)\right)^2 \right\} \tag{6.14}$$

where $N_{k,i}$ is the measured number of granules in the size range of (L_i, L_{i+1}) for the experimental data set k and $V(N_{k,i})$ is the volume of particles $N_{k,i}$, and $\widehat{N}_{k,i}$ is the predicted granule number based on $\beta_{0,k}$ and $S_{0,k}$ and $V(\widehat{N}_{k,i})$ is the volume of particles $\widehat{N}_{k,i}$.

After all the best fit parameters of $\beta_{0,k}$ and $S_{0,k}$ for each of experimental dataset $k = 1,2, \dots, n$ were obtained, the process model parameters of $\beta_0(x_1, x_2, x_3)$ in equation (6.12) and $S_0(x_1, x_2, x_3)$ in equation (6.13) linking the binder solution spray operating parameters of the pulse frequency x_1, binder spray rate x_2 and atomization pressure x_3 can be obtained using JMP 11 software (SAS, SAS Institute, Cary, NC, USA).

6.3 Results and discussion

6.3.1 Determination of the TCPBM parameters based on the CFD simulation

During granulation, the particle size increases due to agglomeration. In order to keep the constant particle flow pattern and fluidized bed height, the inlet air velocity has to be adjusted consistently, which has been described in the chapter 3 and validated in chapter 5. Due to the same particle flow behavior during granulation was adjusted to be constant, the parameters of the volumes of particles in the WC and DC and the exchange rate between them were calculated based on the CFD simulation 1, which corresponds to the beginning stage of granulation.

Figure 6.2 shows the time-averaged particle volume fraction distribution and flow pattern predicted by the CFD simulation. It can be seen that the details of the complex mixing flows and distribution of particles in the bed can be revealed. The distribution of particles in the bed shown in Figures 6.2(a) and (c) is significantly non-homogeneous. A higher density of particles close to the wall is revealed, which is in a good agreement with the real situation in a fluidized bed where the particles intend to attach the wall. The distribution of velocity vectors within the bed indicates that the particles mainly move up to the bed top from the center and fall down close to the wall, showing the existence of the core-annular structure in Figures 6.2(b) and (d). There is a limited radial flow of the particles in the bed shown in Figure 6.2(b).

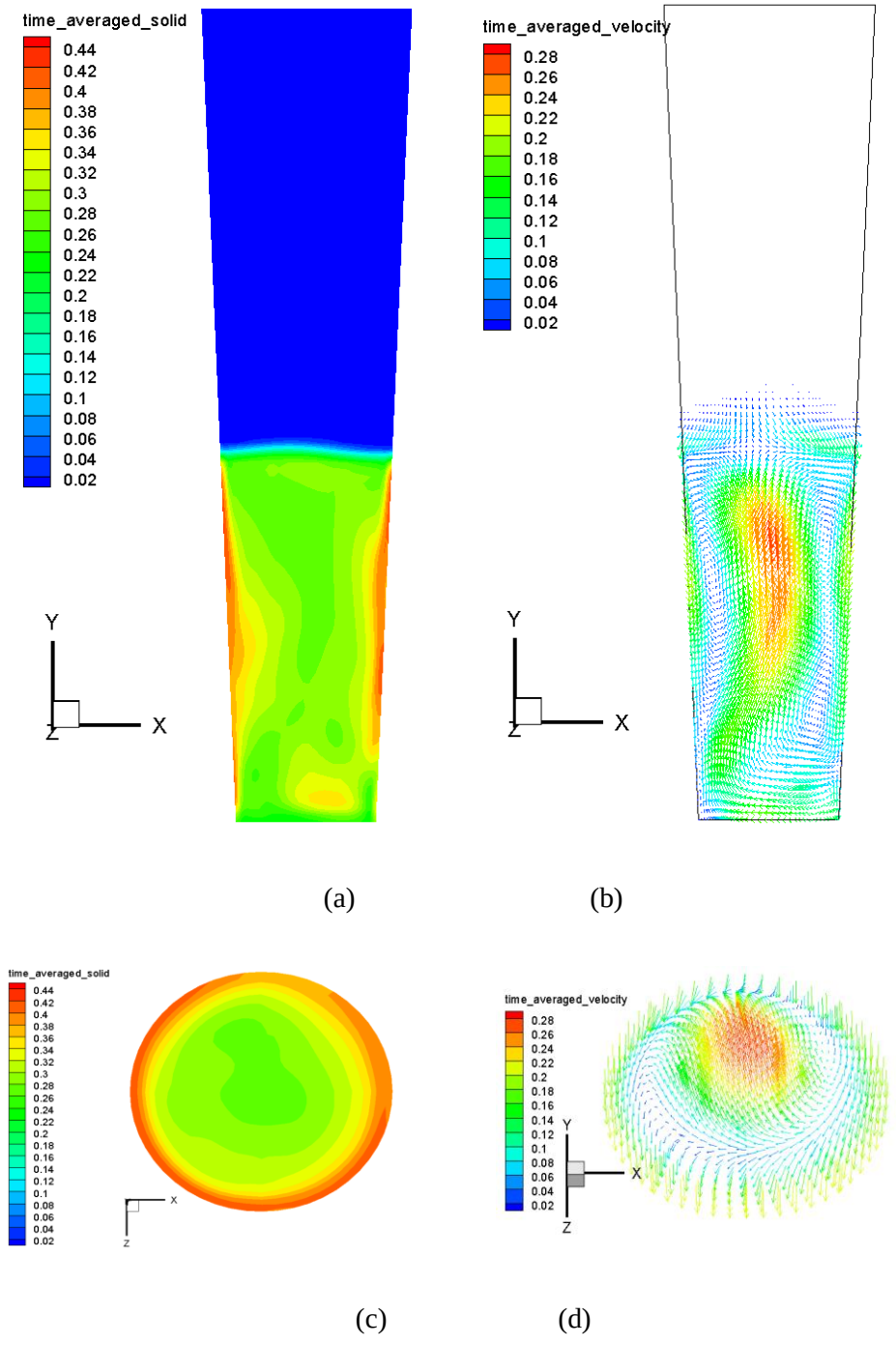

Figure 6.2 CFD simulation results: (a) time-averaged distribution of particle volume fractions at plane XY across the center of the bed; (b) time-averaged particle flow pattern at plane XY across the center of the bed; (c) time-averaged distribution of particle volume fractions on the cross section between wetting and drying compartments; (d) time-average particle flow pattern on the cross section between wetting and drying compartments.

Based on the CFD results, the particle volumes in the two compartments of wetting and

drying and exchange rate can be calculated by

$$V_{WC} = \sum_{v_i \in WC} \varepsilon_{s,i} * v_i \tag{6.15}$$

$$V_{DC} = \sum_{v_i \in DC} \varepsilon_{s,i} * v_i \tag{6.16}$$

and

$$R_{WC \to DC} = \sum_{s_{vi} \in surface\ R} \varepsilon_{s,i} * s_{vi} * \vartheta_{i\_y\_down} \tag{6.17}$$

$$R_{DC \to WC} = \sum_{s_{vi} \in surface\ R} \varepsilon_{s,i} * s_{vi} * \vartheta_{i\_y\_up} \tag{6.18}$$

where, v_i is the cell volume, $\varepsilon_{s,i}$ is the time-averaged solid volume fraction of the cell v_i, s_{vi} is the cross section area of the cell v_i with the surface between the two compartments, $\vartheta_{i\_y\_up}$ is the particle velocity in cell v_i on the surface through which particle moves up from the drying compartment to the wetting compartment, $\vartheta_{i\_y\_down}$ is the particle velocity in cell v_i on the surface through which particle moves down from the wetting compartment to the drying compartment.

The calculated results are shown in Table 6.1.

Table 6.1 Parameters of the TCPBM based on the CFD simulation

Parameters	value
Particle diameter d_s (μm)	164
Superficial inlet velocity v_0 (m/s)	0.086
WC Particle Volume (m^3)	3.43×10^{-5}
DC Particle Volume (m^3)	6.88×10^{-5}
Particle flow rate from WC to DC $R_{WC \to DC}$ (m^3/s)	5.85×10^{-5}
Particle WC resident time τ_{WC} (s)	0.5863
Particle flow rate from DC to WC $R_{DC \to WC}$ (m^3/s)	5.72×10^{-5}
Particle DC resident time τ_{DC} (s)	1.2028

6.3.2 Determination of TCPBM for a pulsed top spray fluidized bed granulation

Using the optimization method proposed in section 6.2.3, a TCPBM can be developed

based on the experimental data in chapter 3. The TCPBM can predict the evolution of granule size in a pulsed spray fluidized bed granulation process at different operating conditions of the binder solution spray. Table 6.2 shows the determined parameters of granulation rate constant $\beta_0(t,\Theta,\Psi)$ in equation (6.12) and the breakage selection rate constant $S_0(t,\Theta,\Psi)$ in equation (6.13). Using a 10% significance level, a factor is considered to affect the response if its *P*-value is less than 0.10 (p<0.10). Therefore the fitted aggregation kernel in the wetting compartment and breakage kernel in drying compartment can be simplified as

$$\beta_0(x_1,x_2,x_3) = 4.97 - 3.00x_1 + 9.73\times10^{-1}x_2 - 8.81\times10^{-1}x_3 + 2.05\times {x_1}^2 \quad (6.19)$$

and

$$S_0(x_1,x_2,x_3) = 2.73\times10^{-3}x_1x_2 \quad (6.20)$$

Firstly, from the Table 6.2, it can be seen that the aggregation model can well fit the original kernel constants according to the R-square of sum of fit and P-value of ANOVA. However, the model for breakage seems not well fitting the original data, which can also explain why only one term is considered significant in the breakage model. From the above equations, it is clearly shown that three binder solution spray factors significantly affect the aggregation kernel in the wetting compartment. The atomization pressure (x_3) has negative effects on the aggregation kernel while the binder spray rate (x_2) has positive effects, all of which have been reported in our previous study [228]. When a pulsed mode is used during granulation, the pulsed frequency has both direct negative and positive quadratic effects on the aggregation kernel shown in equation (6.19), proving that the pulsed spray can be used to control the granulation process [51, 52, 228]. According to the breakage kernel in equation (6.20), it is shown that the breakage in the drying compartment is only affected by the interaction term of the pulsed frequency (x_1) and binder spray rate (x_2) and there is no direct effect from either of three of the binder solution spray operating factors. Actually the coefficient of the term is very small. Therefore it is believed that the breakage kernel is only affected by the mixing conditions.

The comparison of final particle size distributions between experimental data and predictions by the MCPBM is shown in Figure 6.3. It can be seen that the TCPBM can predict the final granule size distributions at different operating conditions with reasonable accuracy except that there are little bit higher prediction errors for experiments 2, 4 and 14, which are similar to those predicted by a one-dimensional PBM in our previous work [229].

Table 6.2 Fitted aggregation kernel in wetting compartment and breakage kernel in drying compartment

	Aggregation model in WC		Breakage model in DC	
	$\beta(x_1, x_2, x_3, l, \mu) = \beta_0(x_1, x_2, x_3)(l + \mu)^3$		$S(x_1, x_2, x_3, l) = S_0(x_1, x_2, x_3)$	
Terms of non-linear quadratic model	$\beta_0(x_1, x_2, x_3)$		$S_0(x_1, x_2, x_3)$	
	Coefficient	P-value	Coefficient	P-value
Constant	4.97	0.0006*	1.01×10^{-3}	0.4779
x_1	-3.00	0.0006*	-1.17×10^{-3}	0.2089
x_2	9.73×10^{-1}	0.0576*	-1.25×10^{-3}	0.1827
x_3	-8.81×10^{-1}	0.0768*	-8.56×10^{-5}	0.9199
$x_1 * x_2$	7.37×10^{-1}	0.2453	2.73×10^{-3}	0.0627*
$x_1 * x_3$	1.68×10^{-1}	0.7763	-3.37×10^{-4}	0.7805
$x_2 * x_3$	1.49×10^{-1}	0.8009	3.84×10^{-5}	0.9746
${x_1}^2$	2.05	0.017*	1.01×10^{-3}	0.4356
${x_2}^2$	-1.08×10^{-1}	0.8599	7.12×10^{-3}	0.5767
${x_3}^2$	-7.51×10^{-1}	0.2543	-1.69×10^{-3}	0.2162
Regression equation	$\beta_0(x_1, x_2, x_3) = 4.97 - 3.00x_1 + 9.73 \times 10^{-1}x_2 - 8.81 \times 10^{-1}x_3 + 2.05 \times {x_1}^2$		$S_0(x_1, x_2, x_3) = 2.73 \times 10^{-3}x_1x_2$	
R-square	0.944176		0.750163	
Prob>F of ANOVA	0.0119		0.2975	

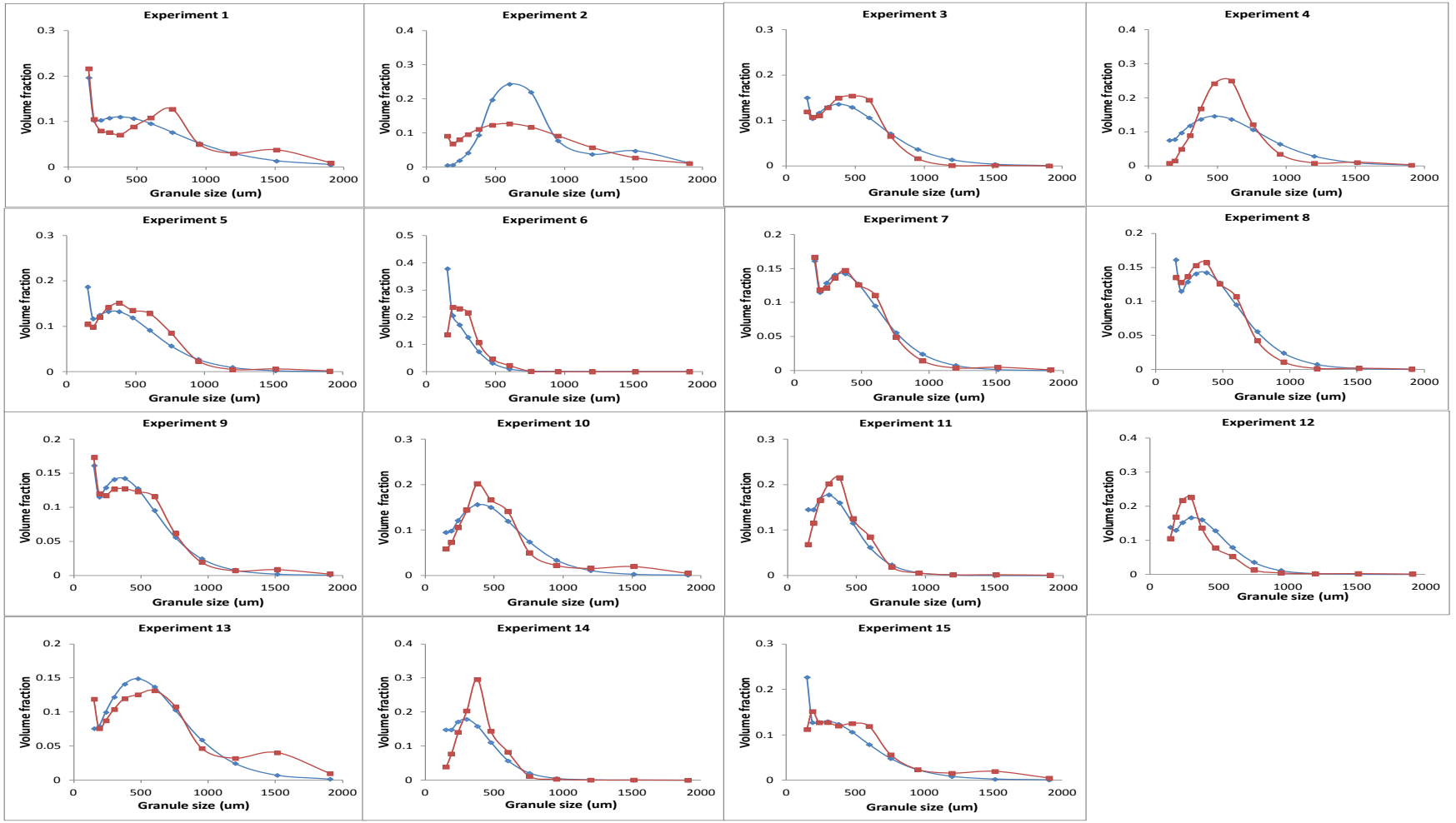

Figure 6.3 Comparison of experimental data with the predictions by the TCPBMs (red square: experimental data; blue diamond: predicted value)

In order to reveal the advantage of the TCPMB, the comparison of the mean size of the end granules between the experiments and predictions by both the TCPBM and single PBM [229] is given in Figure 6.4 (a), indicating that the TCPBM can predict the mean size of final granules more accurate than those by the single PBM. Comparison of each of the sum square of errors (SSEs) between the experiments and predictions by the TCPBM or single PMB is also given in Figure 6.4(b), indicating that the TCPBM generally shows smaller SSEs than those by the single PBM over all the fifteen experiments. It approves that the introduction of the two compartments in a process can improve the ability of PBM on predicting the end granule size distribution. Three replicated experiments 7-9 were carried out at the middle points of the binder spray operating parameters. The final PSD for these three experiments can be predicted accurately by the TCPBM, showing that the model behaves well at the intermediate range of the operating conditions.

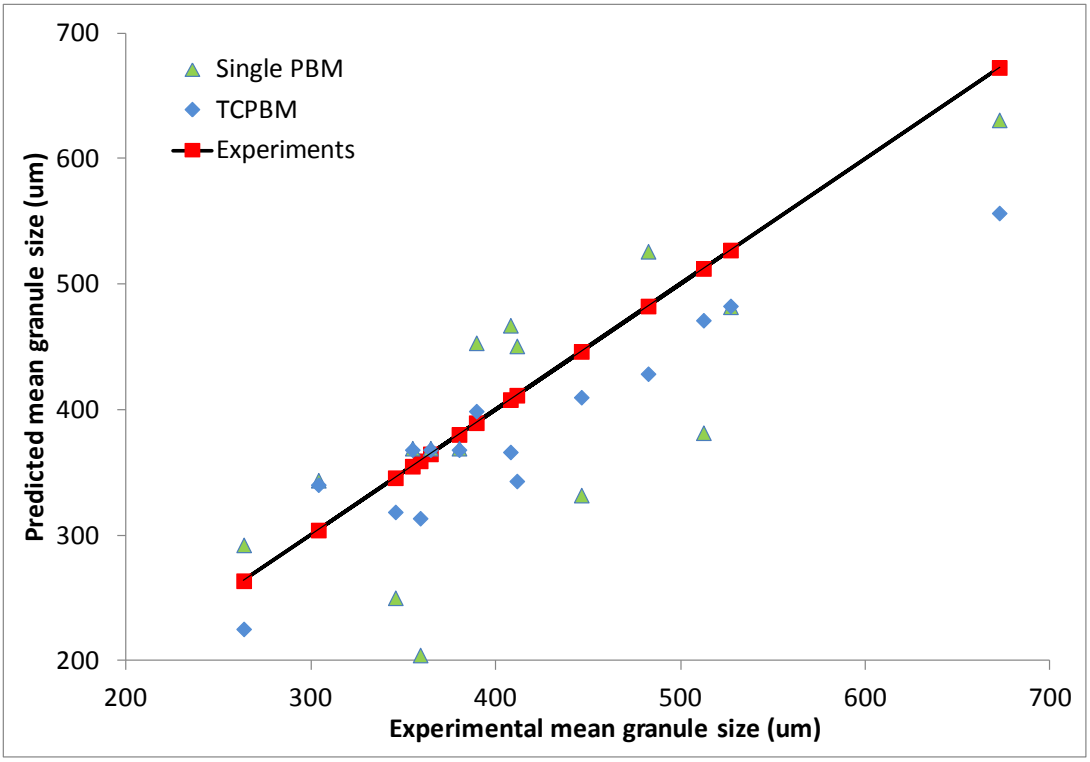

(a)

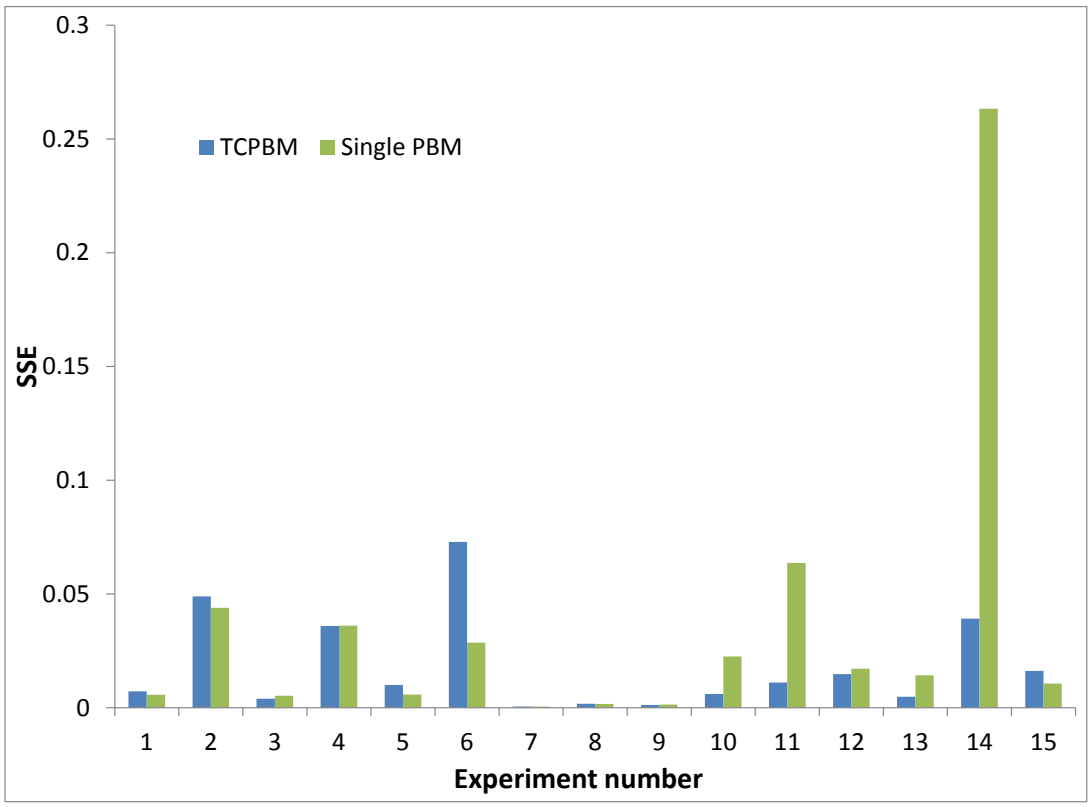

(b)

Figure 6.4 Comparison of the TCPBM and single PBM: (a) mean size; (b) comparison of the sum square of error for each experiment

The effectiveness of the TCPBM has been validated by the experiments. Two experiments which had not been included in the model development were used to validate the developed TCPBM. The comparison of particle size distributions at 30%, 70% and 100% experimental time between experiment data and prediction data by the TCPBM are given in Figures 6.5 and 6.6. Because the process model is fitted based on the end granule size distributions, there are significant prediction errors for the granule size distributions at 30% and 70% of the binder solution sprayed in comparison with the higher accuracy of prediction by the TCPBM for the end granule size distributions. In the future it would be necessary to include more measured granule size distributions during granulation in the TCPBM development.

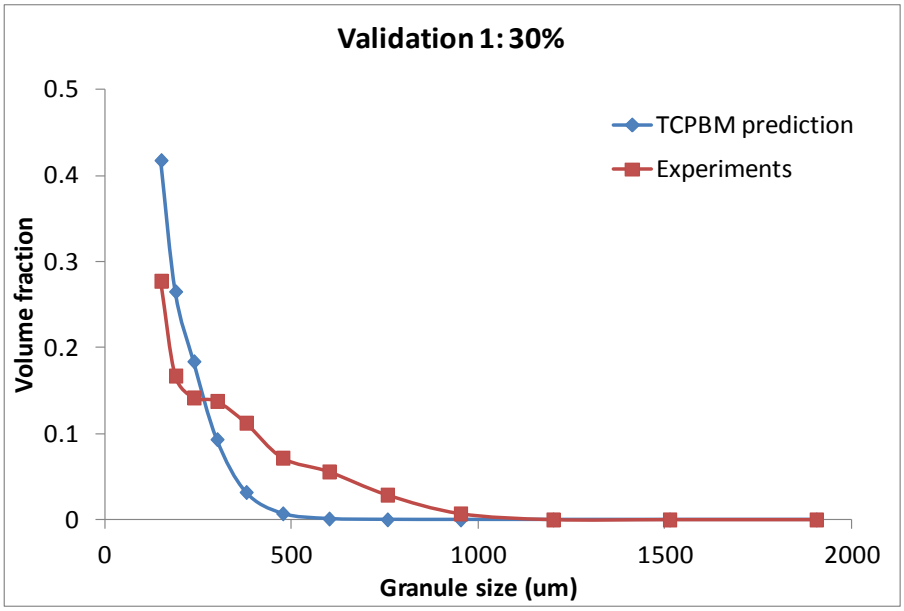
Validation 1: 30%
TCPBM prediction
Experiments
Volume fraction
Granule size (um)
0.5
0.4
0.3
0.2
0.1
0
0
500
1000
1500
2000

(a)

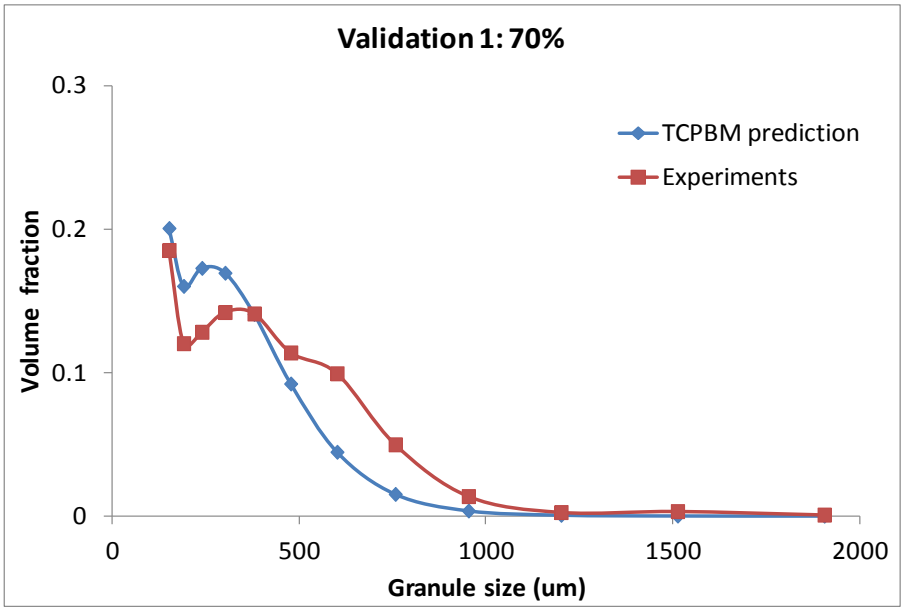
Validation 1: 70%
TCPBM prediction
Experiments
Volume fraction
Granule size (um)
0.3
0.2
0.1
0
0
500
1000
1500
2000

(b)

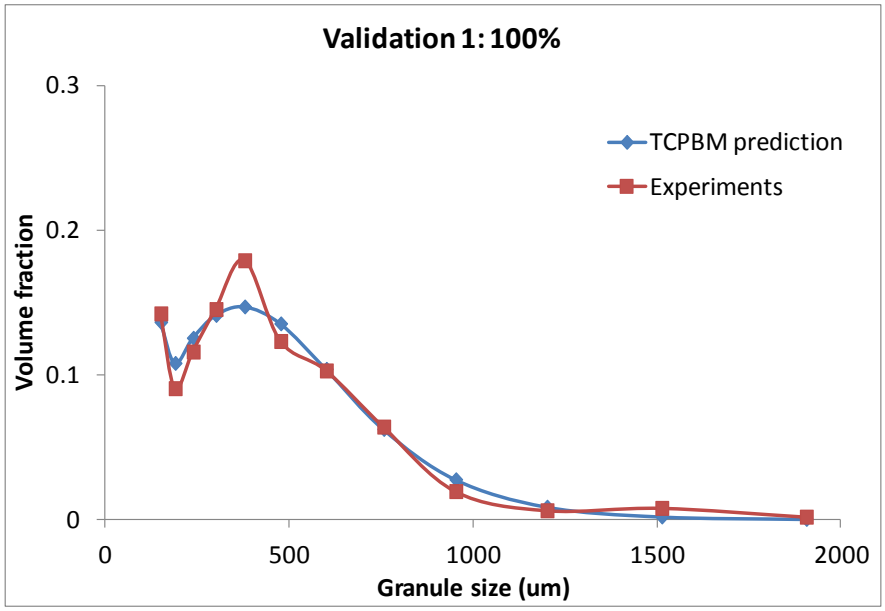

(c)

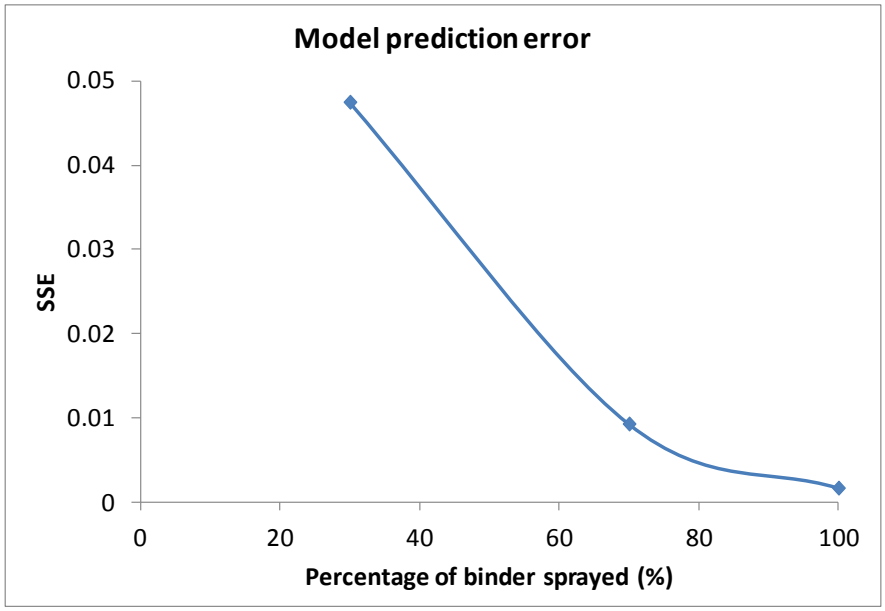

(d)

Figure 6.5 Validation of predictions of granule distribution by the TCPBM at the operating condition of x_1=*0.2;* x_2 = *0.333;* x_3 = *-0.2*: (a) at 30% binder sprayed; (b) at 70% binder sprayed; (c) at 100% binder sprayed.

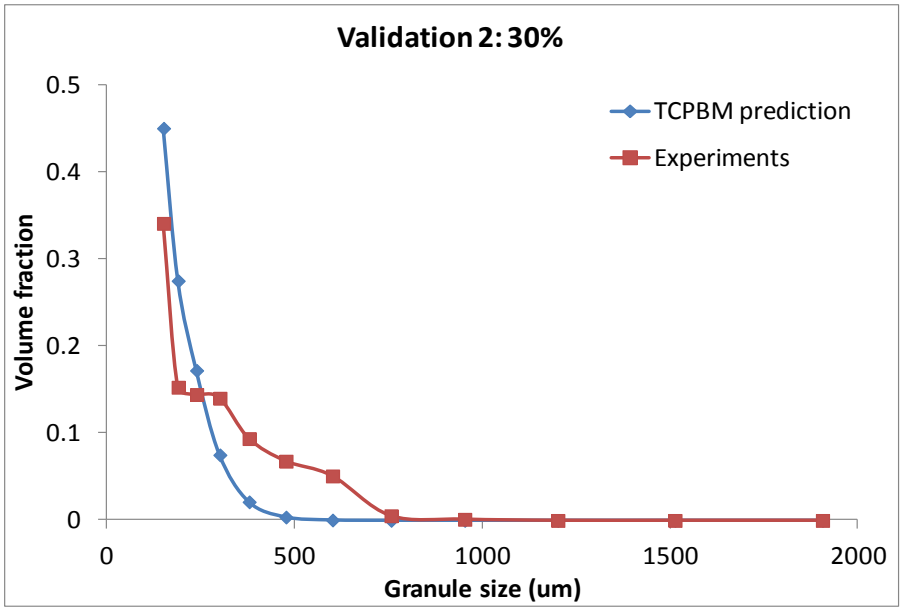
Validation 2: 30%
TCPBM prediction
Experiments
Volume fraction
0.5
0.4
0.3
0.2
0.1
0
0
500
1000
1500
2000
Granule size (um)

(a)

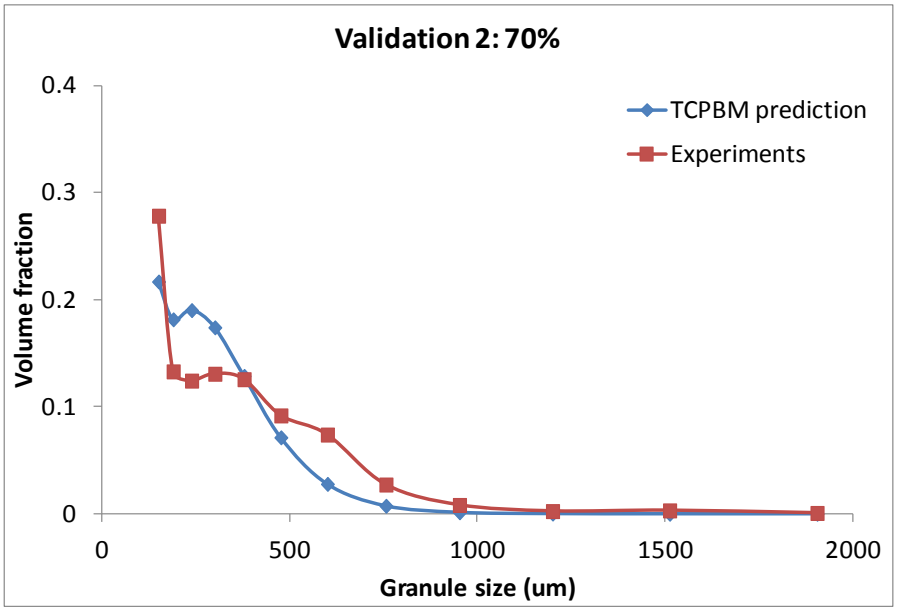
Validation 2: 70%
TCPBM prediction
Experiments
Volume fraction
0.4
0.3
0.2
0.1
0
0
500
1000
1500
2000
Granule size (um)

(b)

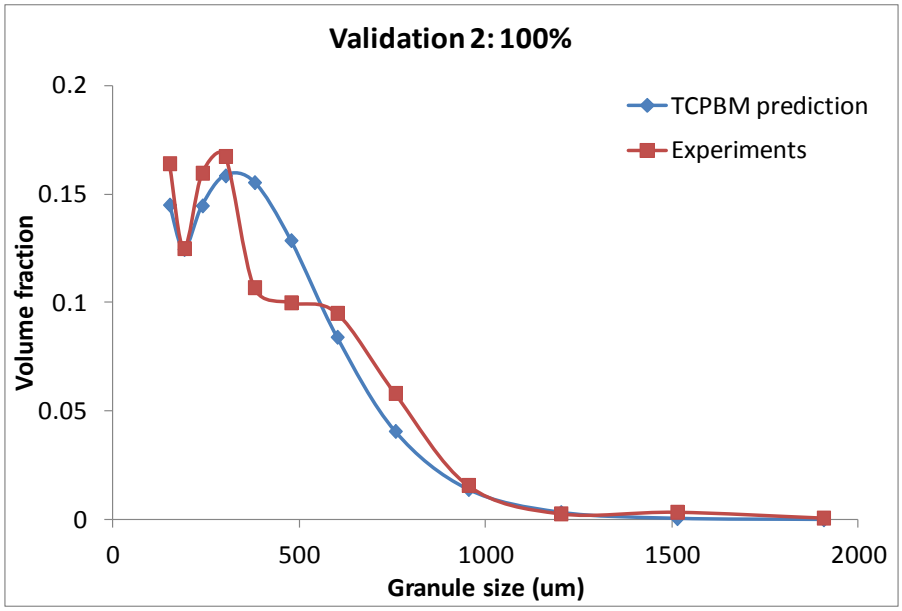

(c)

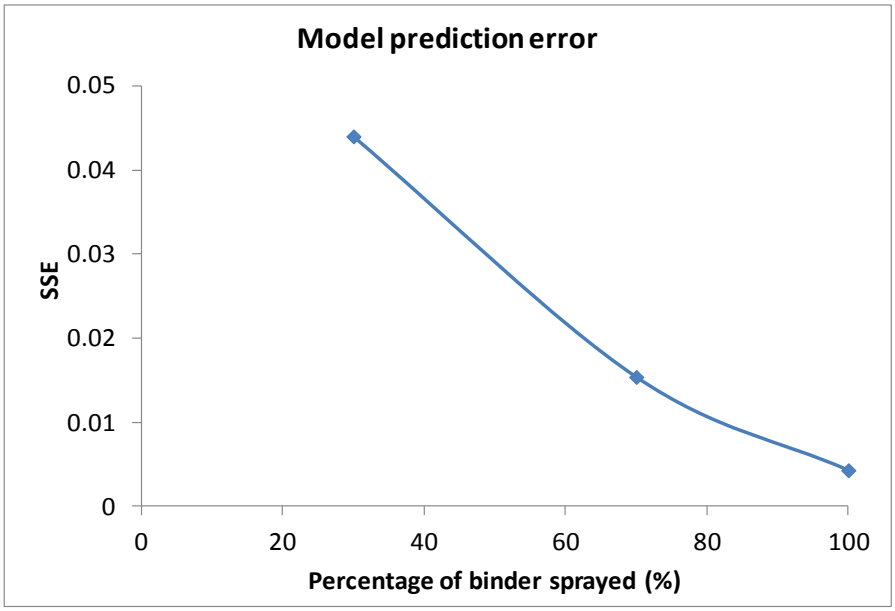

(d)

Figure 6.6 Validation of predictions of granule distribution by the TCPBMs at the operating condition of x_1=0.6; x_2 = 0; x_3 = 0.4: (a) at 30% binder sprayed; (b) at 70% binder sprayed; (c) at 100% binder sprayed.

6.3.3 Multi-stage optimal control of a pulsed top spray fluidized bed granulation based on the TCPBM

In this study, the proposed multi-stage open loop optimal control strategy was applied to control the top spray fluidized bed granulation system using the TCPBM. However, the introduction of two compartments and particle exchange flow between the two compartments significantly increased the complexity of PBM. Hence, the application of proposed multi-stage optimization strategy would be a huge challenge using the TCPBM. The TCPBM determined in last section given in equation (6.19) and equation (6.20) is used for the model-based control strategy implementation.

Comparison of evolution of the granule mean sizes of granulation process and its process model at different operating conditions of binder spray is given in Figure 6.7. It is shown that at the center of each operating variable the process model can predict the granule process accurately in Figure 6.7(a). The significant discrepancy between the outputs of the granulation process and its process model can be found when the operating variables are away from its centers shown in Figures 6.7(b) and 6.7(c).

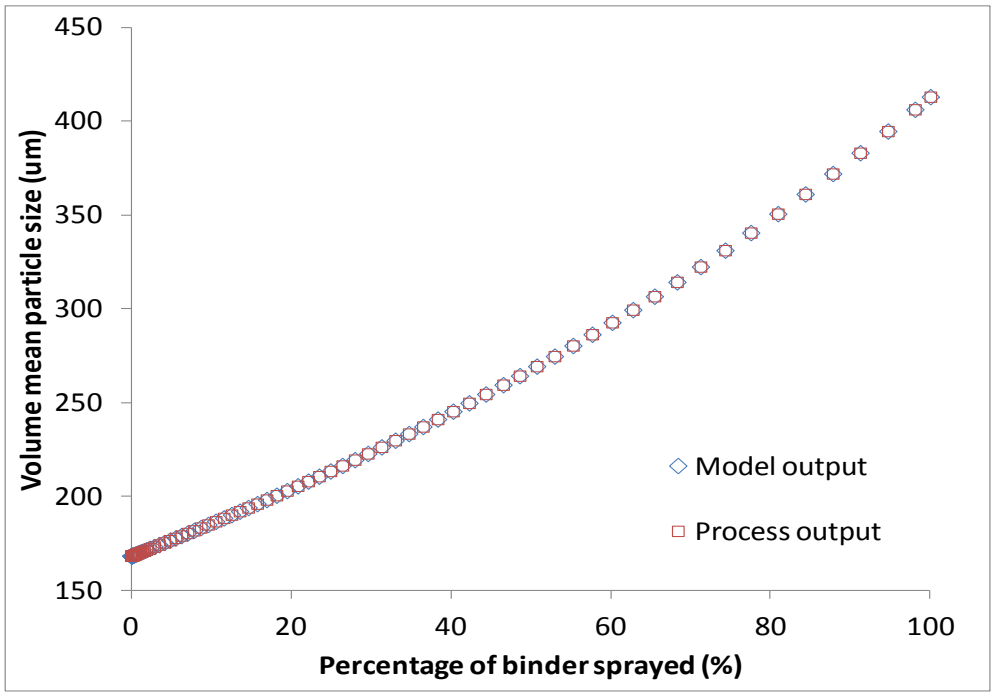

(a)

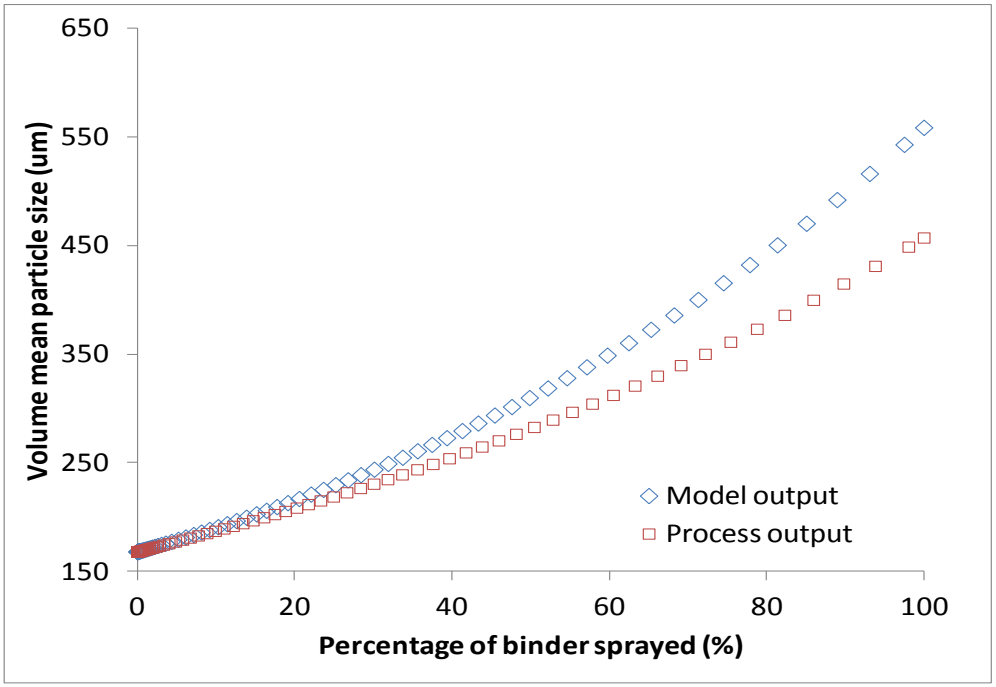

(b)

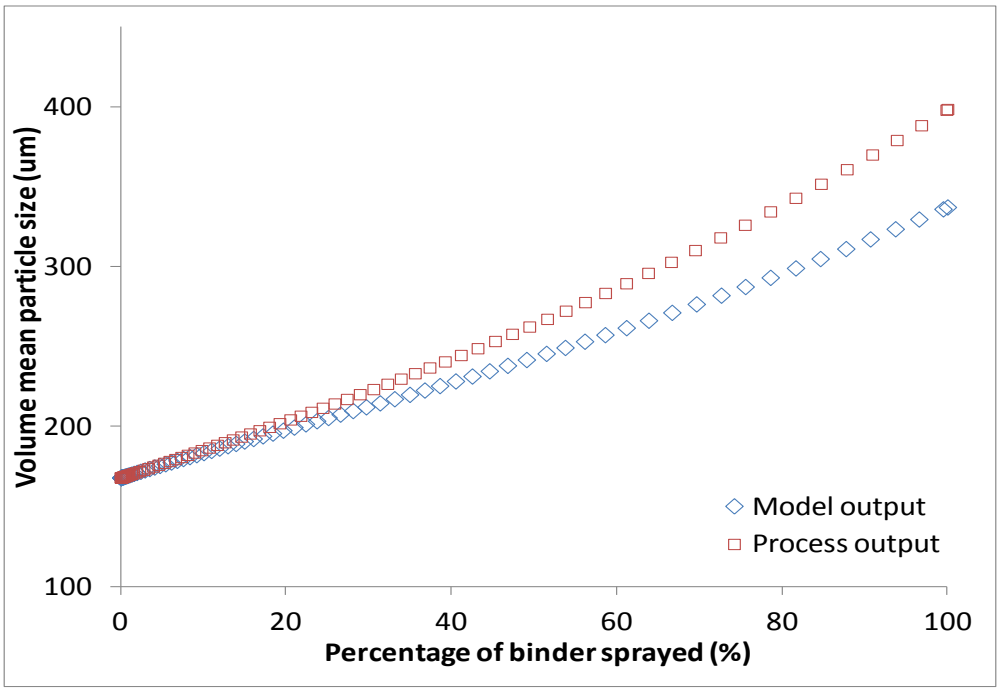

(c)

Figure 6.7 Comparison of evolution of the granule mean sizes of granulation process and its process model at three different random operating conditions: (a) *x1=0, x2=0, x3=0*; (b) *x1=-1, x2=0.1, x3=1*; (c) *x1=0.8, x2=-0.1, x3=0.1*.

In this study, the aim of the granulation control is to increase the powder size from its initial mean size of 150 μm to a desired end mean size of 600 μm. Figure 6.8 shows evolution of mean granule sizes in the simulated granulation process under different operating conditions of binder solution spray obtained by different stages of optimization, including one stage, two stages and three stages. The colored curves in Figures 6.8(a)-(c) show the trajectories of evolution of mean granule size at different stages of optimization obtained by the process model given by equations (6.19) - (6.20). All the black curves in Figure 6.8(a)-(c) show the evolution of actual mean granule sizes under those operating conditions. It can be seen that based on one stage optimization method the end mean granule size of 556 μm is significantly smaller than the desired value of 600μm due to the mismatch of the actual process and the developed process model. Through adjusting the operation conditions of the binder solution spray at 50% of binder spray based on the measured granule size distribution on line, the model mismatch can be compensated through adjusting the desired end mean granule size in the new costing function in equation (4.12) to determine a new trajectory (green color curve) shown in Figure 6.8(b). It is shown that the difference between the end mean granule size and the desired granule size based on two-stage optimization is reduced significantly to 13μm from 44μm based on one-stage optimization. For a three-stage optimization, the end mean granule size is very close to the desired mean size. The operation variables of the binder solution spray obtained by the different stages of optimization are also given in Figure 6.8(a)-(c).

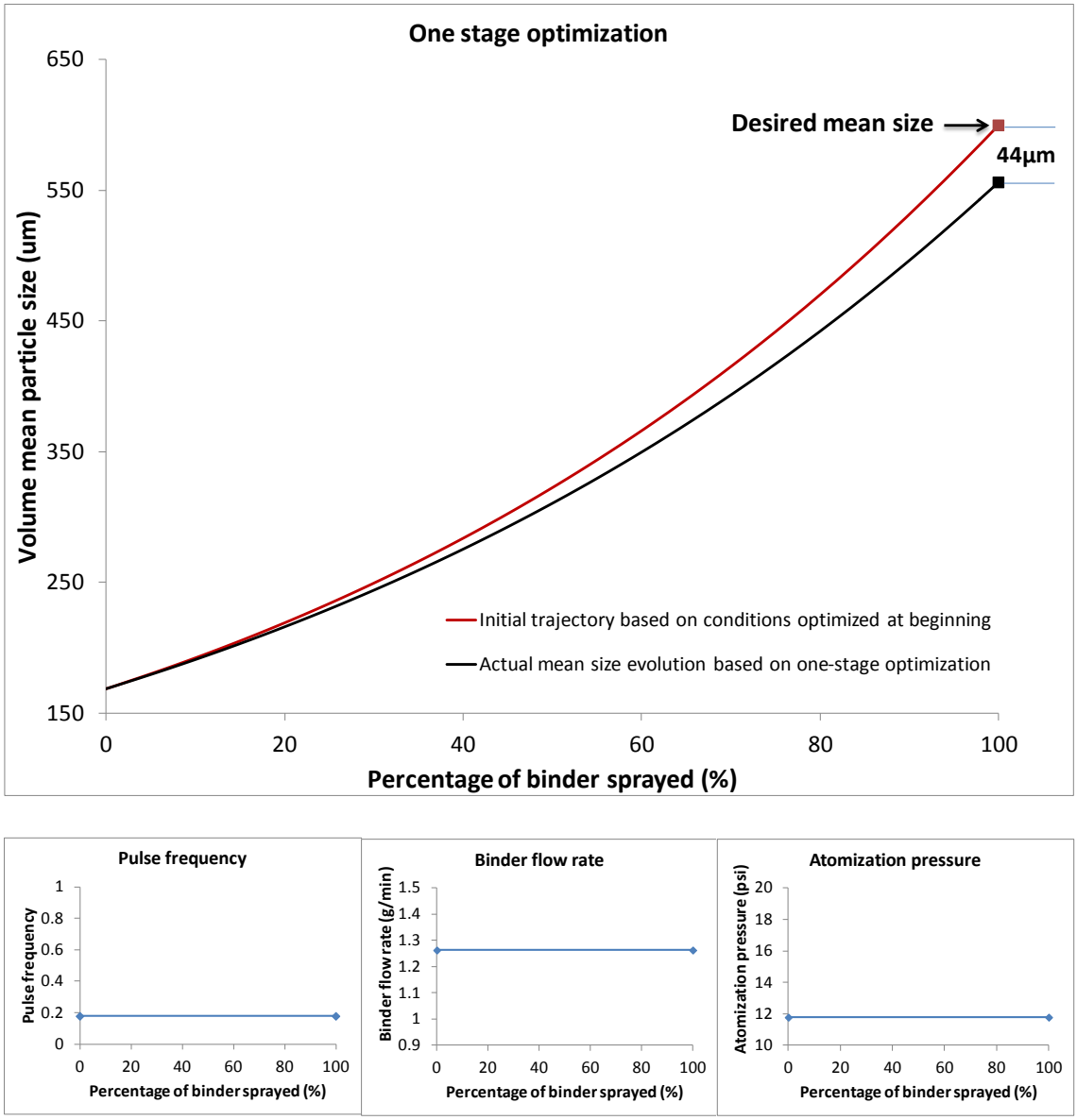
One stage optimization
Volume mean particle size (um)
650
550
450
350
250
150
0
20
40
60
80
100
Percentage of binder sprayed (%)
Desired mean size
44µm
Initial trajectory based on conditions optimized at beginning
Actual mean size evolution based on one-stage optimization
Pulse frequency
Pulse frequency
1
0.8
0.6
0.4
0.2
0
Percentage of binder sprayed (%)
Binder flow rate
Binder flow rate (g/min)
1.5
1.4
1.3
1.2
1.1
1
0.9
Percentage of binder sprayed (%)
Atomization pressure
Atomization pressure (psi)
20
18
16
14
12
10
Percentage of binder sprayed (%)

(a)

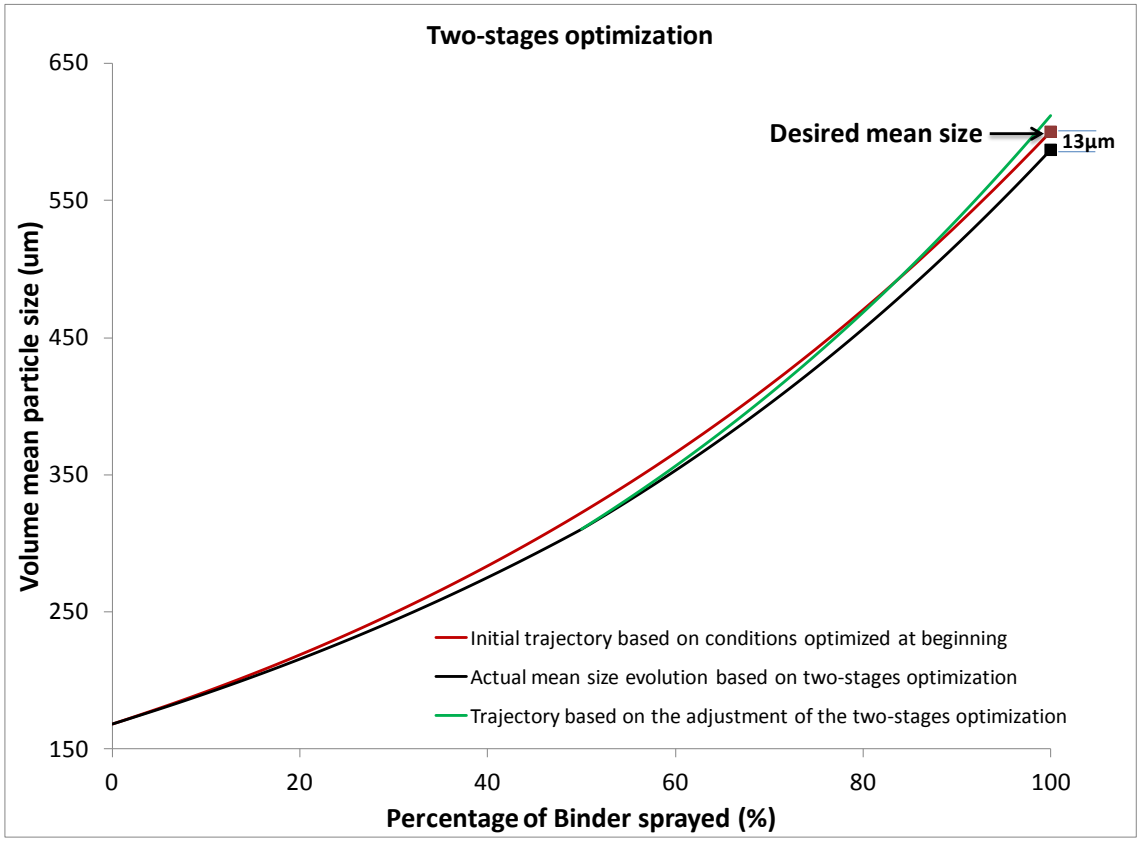
Two-stages optimization
Volume mean particle size (um)
650
550
450
350
250
150
0
20
40
60
80
100
Percentage of Binder sprayed (%)
Desired mean size
13µm
Initial trajectory based on conditions optimized at beginning
Actual mean size evolution based on two-stages optimization
Trajectory based on the adjustment of the two-stages optimization

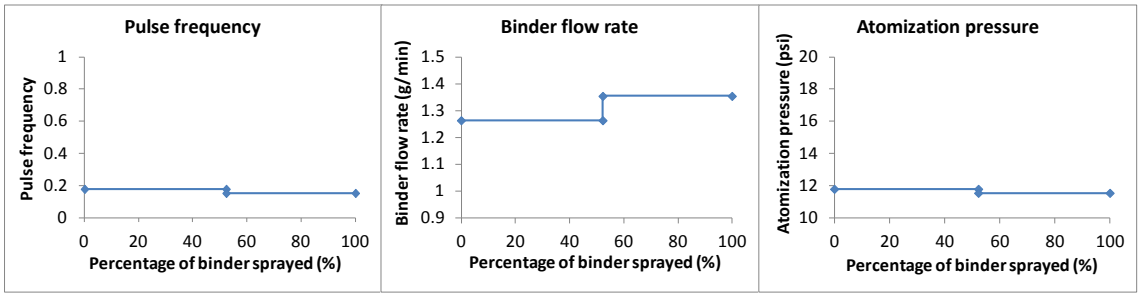
Pulse frequency
Pulse frequency
Percentage of binder sprayed (%)
Binder flow rate
Binder flow rate (g/min)
Percentage of binder sprayed (%)
Atomization pressure
Atomization pressure (psi)
Percentage of binder sprayed (%)

(b)

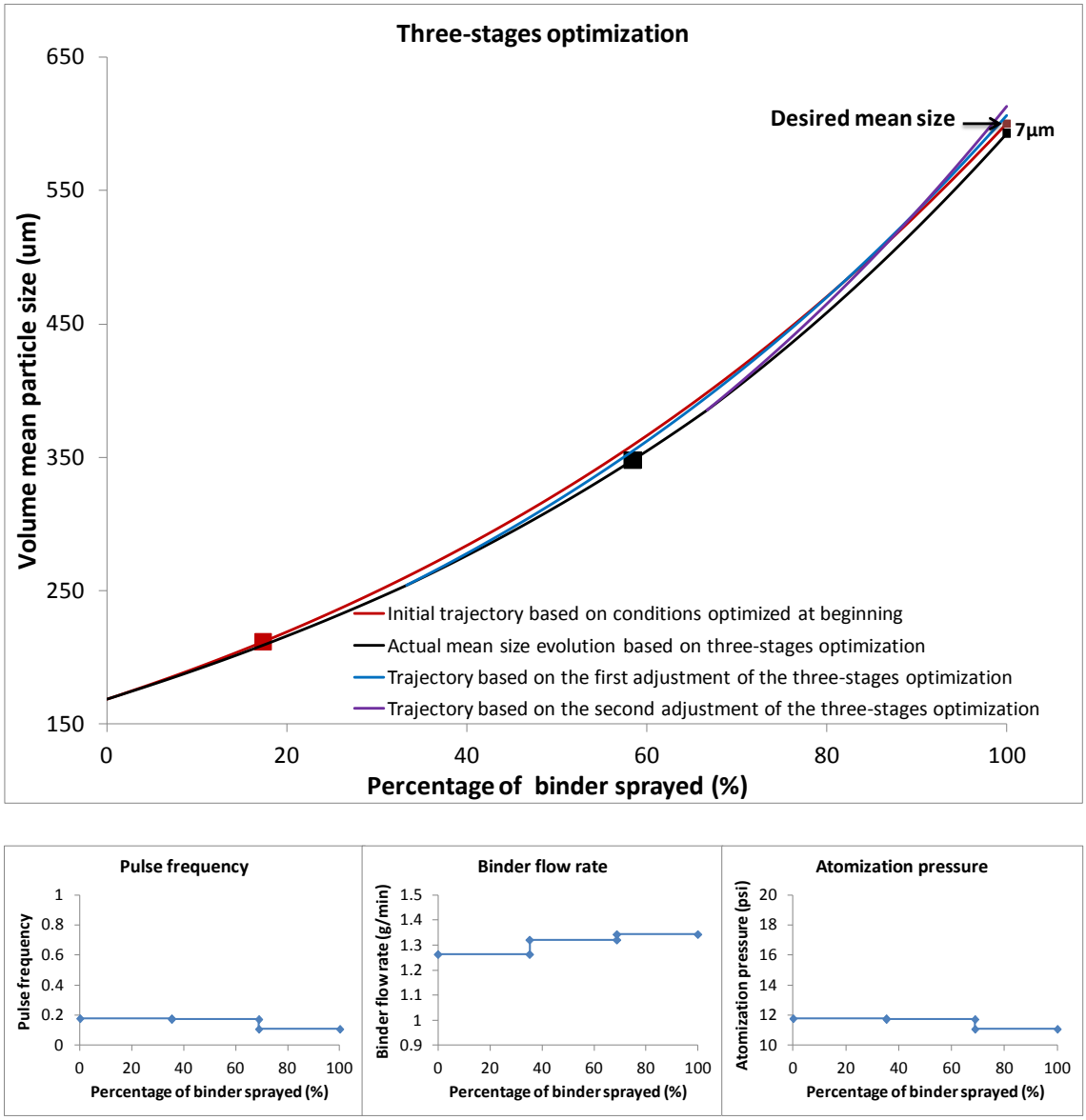

(c)

Figure 6.8 Mean size evolution and size trajectory using different stages of optimization and optimal operating conditions: (a) one-stage optimization results; (b) two-stage optimization results; (c) three-stage optimization results.

6.4 Chapter conclusions

In this chapter, the two-compartmental population balance model (TCPBM) was developed based on the Computational Fluid Dynamics (CFD) analysi. By comparing with experimental particle size distribution (PSD), the TCPBM was proved to be

effective on predicting the particle growth. The prediction ability on end granules particle size distribution was also compared between the TCPBM and one-dimensional PBM, and results indicated that the TCPBM can generally give smaller sum square of error (SSE). Experiments were carried out to validate the TCPBM which proved that the TCPBM can predict final PSD at any random operating conditions accurately. At the end, the control strategy proposed in chapter 4 was successfully applied based on the TCPBM.

Chapter 7 Conclusions and future work

In this chapter, a summary of the present work and main findings are presented. Limitations of the research are also briefly discussed along with potential areas for further research.

7.1 Summary of the presented work

This research mainly focused on the modeling and control of the top-spray fluidized bed granulation system.

The research commenced with a critical literature review about the top-spray fluidized bed granulation, including the detailed granulation mechanisms, experimental study, modeling study and control application recently. The review work presented deep understanding of the current research status of the top-spray fluidized bed granulation, which helps develop the potential research topics to further improve the performance of the spray granulation system. Depending upon the literature review, the primary aim of current work was established, which is to develop a superior population balance model (PBM) based on computational fluid dynamics (CFD) study and to develop control strategy based on the proposed PBM model.

In order to fit parameters in the mathematical model, experiments should be carried out. In this work, the experiments were designed by the Box-Behnken experimental design method. The experiment results were used to investigate the influence of three operating conditions of pulse frequency, binder spray rate and atomization pressure on the final granules properties, and then were used for parameters fitting in the model.

In this work, the particle population within the fluidized bed granulator was modeled using the population balance model (PBM). A one-dimensional PBM was firstly developed and successful applied on predicting final particle size distribution (PSD) comparing with experiment data. In addition, a control strategy was proposed, which is implemented on the granulations system.

The one-dimensional PBM is developed with assumption that the all the particles are homogeneous within the granulator, which is obvious not true in real granulation. The computational fluid dynamics (CFD) software ANSYS Fluent 13.0 was used to study the gas-particle fluid dynamics with the granulator. The particle circulation pattern was investigated and a mathematical model between particle circulation time and inlet air velocity and particle size is developed to give guidance on how to adjust the inlet air velocity as particle size increased during granulation.

Based on the CFD study, a two-compartmental PBM (TCPBM) was developed, in which the particle fluidizing domain was divided into two compartments: spray zone and drying zone. The compartment on the top is wetting zone, where aggregation is considered, and the bottom compartment is drying zone, where only breakage mechanism is considered because of the high speed of hot fluidizing air. This model was also validated by comparing with experiment data. Subsequently, the control strategy proposed for the one-dimensional PBM is applied based on the TCPBM.

7.2 Conclusions

This thesis carried out a comprehensive study of the top-spray fluidized bed granulation, including experimental study, process model development and control strategy design.

The influence factors of pulsed frequency, binder spray rate and atomization pressure of the top-spray fluidized bed granulation process were experimentally studied using the Box-Behnken design method. Different mathematical models were developed to predict the mean size of granules, yield, relative width of granule distribution and final granule moisture content. The experimental study has supported the theory that the granule size can be controlled through the liquid feed pulsing. However, care has to be taken when the pulsed frequency is chosen for controlling the granule size due to the nonlinear quadratic relation in the regression model. The design space of the ranges of operating parameters has been determined based on constraints of the mean size of granules Y_1 ($300 \leq Y_1 \leq 500$) and granule yield Y_2 ($Y_2 \geq 85\%$). High degree of prediction obtained from validation experiments has shown the reliability and effectiveness using the Box-Behnken experimental design method to study the fluidized bed granulation process.

A pulsed top-spray fluidized bed granulation was modeled by one-dimensional population balance models. The developed PBMs have linked the three key binder solution spray operating factors of the binder spray rate, atomizing air pressure and pulsed frequency of spray with the granule properties to predict granule growth behavior in a pulsed spray fluidized bed granulation process at different operating conditions. It has been found that the aggregation of granules was size dependent and breakage of the granules was size independent in a pulsed top-spray fluidized bed granulation process. Experimental validation has shown that the developed PBMs with both the kernel orders of $p=3$ and $q=0$ and the kernel orders of $p=2$ and $q=0$ can predict the evolution of granule size distribution with accuracy.

The developed PBMs have been used to design the control strategies to operate the pulsed spray fluidized bed granulation under more optimal conditions to achieve the desired quality of the end granules. In this work, a multi-stage open optimal control strategy was proposed, in which through adjusting the trajectory of the evolution of the granule size distribution at predefined sample intervals, to determine the optimal operating variables related to the binder spray including the spray rate of binding liquid, atomizing air pressure and pulsed frequency of spray. Simulated results have shown that the proposed multi-stage open optimal control strategy can effectively reduce the effects of the model mismatch and provide an effective tool to determine the optimal operating variables for a pulsed spray fluidized bed granulation process.

The gas-particle fluid dynamics within the fluidized bed granulator was also studied using the computational fluid dynamics (CFD) software ANSYS Fluent 13.0. The influence of particle size and inlet air velocity on the particle flow pattern was investigated. A mathematical model between the particle circulation time and particle size and inlet air velocity was developed, which could work as guidance about how to adjust the inlet air velocity to keep the fluidization in the same level during the experiment. This coincides with the operating method used in our experiments. The study of influence of inlet air velocity on bed characteristics has shown that the bed height increased with inlet air velocity. The bubbles distorted significantly and merge frequently at high inlet air velocity, which generates long and twisty bubbles. Under the

same inlet air velocity, more bubbles and heterogeneous fluidization state are generated by the larger particle size.

Based on the detailed gas-solid fluid dynamics study using the CFD simulation, the two-compartmental population balance model (TCPBM) was developed. By comparing with experimental particle size distribution (PSD), the TCPBM was proved to be effective on predicting the particle growth. The prediction ability on end granules particle size distribution was also compared between the TCPBM and one-dimensional PBM, and results indicated that the TCPBM gave smaller sum square of error (SSE). Experiments were carried out to validate the TCPBM which proved that the TCPBM can predict final PSD at any random operating conditions accurately. At the end, the control strategy proposed in chapter 4 was successfully applied based on the TCPBM.

7.3 Limitations and future work

The further improvement of this project can include the following aspects:

Experiment data set

In this thesis, the experiments were designed by the Box-Behnken experimental design, which is sufficient for the experimental study analysis of the influence of the three operating parameters. However, from the aspect of parameters fitting of the kernel model in the population balance model, fifteen experiments does not seem enough, which can be found from the comparing of final particle size distribution between experiments data and PBM prediction, big mismatch found in several experiments. Therefore, more experiments and accurate measurement should help to contribute to the predicting capability of the kernel models.

Extended application of multi-compartment PBM

The advantages of multi-compartmental PBM lie in describing influence of the local fluid dynamics on the final granule properties. The assumption is that the gas and particle fluid dynamics can be considered as homogeneous in the specified local domain. By the studying in this thesis of the lab-scale spray fluidized bed granulation, it can be

found that the multi-compartmental PBM has already shown some advantages comparing with one-dimensional PBM, while advantages maybe more obvious if applied on large-scale granulator which behaves more heterogeneous and more vortexes generated.

Methods of moment in solving population balance model

In this work, the population balance model is solved by discrete method, which has the advantage of providing the particle size distribution directly. However the discrete method in solving PBM also has the disadvantage of high computation cost, which can avoided by using the method of moment to solve the population balance model. The mth order moment is defined by integrating the population number density function with respect to certain property variable (e.g. particle sizes, particle volumes) weighted with this property raised to its mth power. The lower order moments contain important information about the particle size distribution (e.g. number (0^{th} moment), total diameter (1^{st} moment), total surface area (2^{nd} moment) and total volume of particles (3^{rd} moment)). Therefore, the method of moment could be used in solving the population balance model in further work.

Coupled CFD-PBM model study

Since the gas and particle hydrodynamics and kinetic parameters during the granulation process are changing with time and position within the fluidized bed granulator, the coupled CFD-PBM is actually the most accurate way to describe the particle enlargement process during fluidized bed granulation. However, there are only limited applications of coupled CFD-PBM on the study of fluidized bed granulation due to the high computational cost. In my first year report, actually, the coupled CFD-PBM was already built, which is considered as criterion to validate the compiled MATLAB PBM code, which did not appear in the current thesis. Therefore, the coupled CFD-PBM should be studied further as an important aspect.

References

1. Wurster, D.E., *Preparation of compressed tablet granulations by the air-suspension technique. II.* J Am Pharm Assoc Am Pharm Assoc, 1960. **49**: p. 82-4.
2. Jones, D.M., *Factors to consider in fluid-bed processing.* Pharmaceutical Technology, 1985. **9**(4): p. 50, 55-62.
3. Banks, M. and M.E. Aulton, *Fluidized-bed granulation - A chronology.* Drug Development and Industrial Pharmacy, 1991. **17**(11): p. 1437-1463.
4. Aulton, M. and M. Banks, *Factors affecting fluidized-bed granulation.* Manufacturing Chemist and Aerosol News, 1978. **49**(12): p. 50-56.
5. Scott, M.W., et al., *Continuous production of tablet granulations in a fluidized bed.I. Theory and design considerations.* J Pharm Sci, 1964. **53**: p. 314-20.
6. Khoshtaghaza, M.H. and R.A. Chayjan, *Effect of some physical properties on fluidisation stability of grain products.* Biosystems Engineering, 2007. **98**(2): p. 192-197.
7. Räsänen, E., et al., *The characterization of fluidization behavior using a novel multichamber microscale fluid bed.* Journal of Pharmaceutical Sciences, 2004. **93**(3): p. 780-791.
8. Geldart, D., *Types of gas fluidization.* Powder Technology, 1973. **7**(5): p. 285-292.
9. Lipps, D.M. and A.M. Sakr, *Characterization of wet granulation process parameters using response-surface methodology.1. Top-spray fluidized-bed* Journal of Pharmaceutical Sciences, 1994. **83**(7): p. 937-947.
10. Maronga, S.J. and P. Wnukowski, *Growth kinetics in particle coating by top-spray fluidized bed systems.* Advanced Powder Technology, 2001. **12**(3): p. 371-391.
11. Iveson, S.M., et al., *Nucleation, growth and breakage phenomena in agitated wet granulation processes: a review.* Powder Technology, 2001. **117**(1–2): p. 3-39.
12. Bouffard, J., M. Kaster, and H. Dumont, *Influence of Process Variable and Physicochemical Properties on the Granulation Mechanism of Mannitol in a Fluid Bed Top Spray Granulator.* Drug Development and Industrial Pharmacy, 2005. **31**(9): p. 923-933.
13. Cameron, I.T., et al., *Process systems modelling and applications in granulation: A review.* Chemical Engineering Science, 2005. **60**(14): p. 3723-3750.
14. Ehlers, H., et al., *Granule size control and targeting in pulsed spray fluid bed granulation.* International Journal of Pharmaceutics, 2009. **377**(1&2): p. 9-15.
15. Rajniak, P., et al., *A combined experimental and computational study of wet granulation in a Wurster fluid bed granulator.* Powder Technology, 2009. **189**(2): p. 190-201.
16. Reynolds, G.K., et al., *Breakage in granulation: A review.* Chemical Engineering Science, 2005. **60**(14): p. 3969-3992.
17. Knight, P.C., et al., *An investigation into the kinetics of liquid distribution and growth in high shear mixer agglomeration.* Powder Technology, 1998. **97**(3): p. 246-257.
18. Tardos, et al., *Critical parameters and limiting conditions in binder granulation of fine powders*. 1997, Amsterdam, PAYS-BAS: Elsevier.

19. Schæfer, T. and C. Mathiesen, *Melt pelletization in a high shear mixer. IX. Effects of binder particle size.* International Journal of Pharmaceutics, 1996. **139**(1-2): p. 139-148.
20. Vonk, P., et al., *Growth mechanisms of high-shear pelletisation.* International Journal of Pharmaceutics, 1997. **157**(1): p. 93-102.
21. Le, P.K., et al., *A microscopic study of granulation mechanisms and their effect on granule properties.* Powder Technology, 2011. **206**(1-2): p. 18-24.
22. Hapgood, K.P., J.D. Litster, and R. Smith, *Nucleation regime map for liquid bound granules.* AIChE Journal, 2003. **49**(2): p. 350-361.
23. Paul R, M., *Scale-up of binder agglomeration processes.* Powder Technology, 2005. **150**(2): p. 86-103.
24. Goldschmidt, M.J.V., *Hydrodynamic Modelling of Fluidised Bed Spray Granulation*. 2001: Enschede. p. 303.
25. Ennis, B.J., G. Tardos, and R. Pfeffer, *A microlevel-based characterization of granulation phenomena.* Powder Technology, 1991. **65**(1-3): p. 257-272.
26. Liu, L.X., et al., *Coalescence of deformable granules in wet granulation processes.* AIChE Journal, 2000. **46**(3): p. 529-539.
27. Thornton, C. and Z. Ning, *A theoretical model for the stick/bounce behaviour of adhesive, elastic-plastic spheres.* Powder Technology, 1998. **99**(2): p. 154-162.
28. Rumpf, H., in W.A., Knepper (Ed.), , *The strength of granules and agglomerates. AIME, Agglomeration, interscience.* New York, 1962: p. 379-418.
29. Iveson, S.M. and J.D. Litster, *Fundamental studies of granule consolidation part 2: Quantifying the effects of particle and binder properties.* Powder Technology, 1998b. **99**(3): p. 243-250.
30. Iveson, S.M., J.D. Litster, and B.J. Ennis, *Fundamental studies of granule consolidation Part 1: Effects of binder content and binder viscosity.* Powder Technology, 1996. **88**(1): p. 15-20.
31. Naito, M., et al., *Microscopic analysis on the consolidation process of granule beds.* Powder Technology, 1998. **95**(3): p. 214-219.
32. Kristensen, H.G., P. Holm, and T. Schaefer, *Granulation in high-speed mixers Part VI. Effects of process conditions on power consumption and granule growth.* Powder Technology, 1985. **43**(3): p. 225-233.
33. Ouchiyama, N. and T. Tanaka, *Stochastic Model for Compaction of Pellets in Granulation.* Industrial & Engineering Chemistry Process Design and Development, 1980. **19**(4): p. 555-560.
34. Ritala, M., et al., *A Comparison Between Binders in the Wet Phase of Granulation in a High Shear Mixer.* Drug Development and Industrial Pharmacy, 1986. **12**(11-13): p. 1685-1700.
35. van den Dries, K., et al., *Granule breakage phenomena in a high shear mixer; influence of process and formulation variables and consequences on granule homogeneity.* Powder Technology, 2003. **133**(1–3): p. 228-236.
36. Pearson, J.M.K., M.J. Hounslow, and T. Instone, *Tracer studies of high-shear granulation: I. Experimental results.* AIChE Journal, 2001. **47**(9): p. 1978-1983.
37. Knight, P.C., et al., *An investigation of the effects on agglomeration of changing the speed of a mechanical mixer.* Powder Technology, 2000. **110**(3): p. 204-209.

38. Liu, L.X., R. Smith, and J.D. Litster, *Wet granule breakage in a breakage only high-hear mixer: Effect of formulation properties on breakage behaviour.* Powder Technology, 2009. **189**(2): p. 158-164.
39. Tan, H.S., A.D. Salman, and M.J. Hounslow, *Kinetics of fluidised bed melt granulation III: Tracer studies.* Chemical Engineering Science, 2005a. **60**(14): p. 3835-3845.
40. Biggs, C.A., et al., *Fluidised bed granulation: modelling the growth and breakage kinetics using population balances.* Proceedings of World Congress on Particle Technology, Sydney,, 2002: p. 629-636.
41. Ramachandran, R., et al., *A mechanistic model for breakage in population balances of granulation: Theoretical kernel development and experimental validation.* Chemical Engineering Research and Design, 2009. **87**(4): p. 598-614.
42. Iveson, S.M., J.A. Beathe, and N.W. Page, *The dynamic strength of partially saturated powder compacts: the effect of liquid properties.* Powder Technology, 2002. **127**(2): p. 149-161.
43. Iveson, S.M. and J.D. Litster, *Liquid-bound granule impact deformation and coefficient of restitution.* Powder Technology, 1998a. **99**(3): p. 234-242.
44. Salman, A.D., et al., *Impact breakage of fertiliser granules.* Powder Technology, 2003. **130**(1-3): p. 359-366.
45. Salman, A.D., et al., *An experimental investigation of particle fragmentation using single particle impact studies.* Powder Technology, 2002. **128**(1): p. 36-46.
46. Salman, A.D. and D.A. Gorham, *The fracture of glass spheres.* Powder Technology, 2000. **107**(1-2): p. 179-185.
47. Fu, J., et al., *An experimental study of the impact breakage of wet granules.* Chemical Engineering Science, 2005. **60**(14): p. 4005-4018.
48. Verkoeijen, D., et al., *Determining granule strength as a function of moisture content.* Powder Technology, 2002. **124**(3): p. 195-200.
49. Niskanen, T. and J. Yliruusi, *Attrition of theophylline granules during drying in a fluidised bed granulator.* Pharm. Ind., 1994(56): p. 282-285.
50. Schaafsma, S.H., et al., *Effects and control of humidity and particle mixing in fluid-bad granulation.* AIChE Journal, 1999. **45**(6): p. 1202-1210.
51. Ehlers, H., et al., *Granule size control and targeting in pulsed spray fluid bed granulation.* International Journal of Pharmaceutics, 2009. **377**(1–2): p. 9-15.
52. Närvänen, T., et al., *Controlling granule size by granulation liquid feed pulsing.* International Journal of Pharmaceutics, 2008. **357**(1–2): p. 132-138.
53. Rambali, B., L. Baert, and D.L. Massart, *Using experimental design to optimize the process parameters in fluidized bed granulation on a semi-full scale.* International Journal of Pharmaceutics, 2001. **220**(1–2): p. 149-160.
54. Hemati, M., et al., *Fluidized bed coating and granulation: influence of process-related variables and physicochemical properties on the growth kinetics.* Powder Technology, 2003. **130**(1–3): p. 18-34.
55. Tan, H.S., A.D. Salman, and M.J. Hounslow, *Kinetics of fluidised bed melt granulation I: The effect of process variables.* Chemical Engineering Science, 2006. **61**(5): p. 1585-1601.
56. Jiménez, T., C. Turchiuli, and E. Dumoulin, *Particles agglomeration in a conical*

fluidized bed in relation with air temperature profiles. Chemical Engineering Science, 2006. **61**(18): p. 5954-5961.

57. Faure, A., P. York, and R.C. Rowe, *Process control and scale-up of pharmaceutical wet granulation processes: a review.* European Journal of Pharmaceutics and Biopharmaceutics, 2001. **52**(3): p. 269-277.
58. Crooks, M.J. and H.W. Schade, *Fluidized bed granulation of a microdose pharmaceutical powder.* Powder Technology, 1978. **19**(1): p. 103-108.
59. Liu, H. and M.C. Altan, *Science and Engineering of Droplets: Fundamentals and Applications.* Applied Mechanics Reviews, 2002. **55**(1): p. B16-B17.
60. Davies, W.L. and W.T. Gloor, *Batch production of pharmaceutical granulations in a fluidized bed I: Effects of process variables on physical properties of final granulation.* Journal of Pharmaceutical Sciences, 1971. **60**(12): p. 1869-1874.
61. Abberger, T., A. Seo, and T. Schæfer, *The effect of droplet size and powder particle size on the mechanisms of nucleation and growth in fluid bed melt agglomeration.* International Journal of Pharmaceutics, 2002. **249**(1–2): p. 185-197.
62. Zhai, H., et al., *Nucleation and growth in fluidised hot melt granulation.* Powder Technology, 2009. **189**(2): p. 230-237.
63. Ansari, M.A. and F. Stepanek, *Formation of hollow core granules by fluid bed in situ melt granulation: Modelling and experiments.* International Journal of Pharmaceutics, 2006. **321**(1–2): p. 108-116.
64. Seo, A., P. Holm, and T. Schæfer, *Effects of droplet size and type of binder on the agglomerate growth mechanisms by melt agglomeration in a fluidised bed.* European Journal of Pharmaceutical Sciences, 2002. **16**(3): p. 95-105.
65. Lipsanen, T., et al., *Novel description of a design space for fluidised bed granulation.* International Journal of Pharmaceutics, 2007. **345**(1–2): p. 101-107.
66. Lipsanen, T., et al., *Effect of fluidisation activity on end-point detection of a fluid bed drying process.* International Journal of Pharmaceutics, 2008. **357**(1–2): p. 37-43.
67. Tan, H.S., A.D. Salman, and M.J. Hounslow, *Kinetics of fluidised bed melt granulation V: Simultaneous modelling of aggregation and breakage.* Chemical Engineering Science, 2005c. **60**(14): p. 3847-3866.
68. Hu, X., J. Cunningham, and D. Winstead, *Understanding and predicting bed humidity in fluidized bed granulation.* Journal of Pharmaceutical Sciences, 2008a. **97**(4): p. 1564-1577.
69. Walker, G.M., G. Andrews, and D. Jones, *Effect of process parameters on the melt granulation of pharmaceutical powders.* Powder Technology, 2006. **165**(3): p. 161-166.
70. Ormos, Z. and K. Pataki, *Studies on granulation in a fluidised-bed .VII. effect of raw-material upon the granule formation.* Hungarian Journal of Industrial Chemistry, 1979. **7**(1): p. 89-103.
71. Rajniak, P., et al., *Experimental study of wet granulation in fluidized bed: Impact of the binder properties on the granule morphology.* International Journal of Pharmaceutics, 2007. **334**(1–2): p. 92-102.
72. Abberger, T., *The effect of powder type, free moisture and deformation behaviour of granules on the kinetics of fluid-bed granulation.* European Journal of

Pharmaceutics and Biopharmaceutics, 2001. **52**(3): p. 327-336.
73. Pont, V., et al., *Influence of the physicochemical properties on the growth of solid particles by granulation in fluidized bed.* Powder Technology, 2001. **120**(1–2): p. 97-104.
74. Walker, G.M., et al., *Influence of process parameters on fluidised hot-melt granulation and tablet pressing of pharmaceutical powders.* Chemical Engineering Science, 2005. **60**(14): p. 3867-3877.
75. Tan, H.S., et al., *Population Balance Modelling of Fluidized Bed Melt Granulation: An Overview.* Chemical Engineering Research and Design, 2005b. **83**(7): p. 871-880.
76. Adetayo, A.A., et al., *Population balance modelling of drum granulation of materials with wide size distribution.* Powder Technology, 1995. **82**(1): p. 37-49.
77. Peglow, M., et al., *A generic population balance model for simultaneous agglomeration and drying in fluidized beds.* Chemical Engineering Science, 2007. **62**(1-2): p. 513-532.
78. X. Liu, L. and J. D. Litster, *Population balance modelling of granulation with a physically based coalescence kernel.* Chemical Engineering Science, 2002. **57**(12): p. 2183-2191.
79. Liu, Y. and I.T. Cameron, *A new wavelet-based method for the solution of the population balance equation.* Chemical Engineering Science, 2001. **56**(18): p. 5283-5294.
80. Cryer, S.A., *Modeling agglomeration processes in fluid-bed granulation.* AIChE Journal, 1999. **45**(10): p. 2069-2078.
81. Tan, H.S., A.D. Salman, and M.J. Hounslow, *Kinetics of fluidised bed melt granulation: IV. Selecting the breakage model.* Powder Technology, 2004. **143-144**(0): p. 65-83.
82. Vreman, A.W., C.E. van Lare, and M.J. Hounslow, *A basic population balance model for fluid bed spray granulation.* Chemical Engineering Science, 2009. **64**(21): p. 4389-4398.
83. Heinrich, S., et al., *Analysis of the start-up process in continuous fluidized bed spray granulation by population balance modelling.* Chemical Engineering Science, 2002. **57**(20): p. 4369-4390.
84. Drechsler, J., et al., *Investigating the dynamic behaviour of fluidized bed spray granulation processes applying numerical simulation tools.* Chemical Engineering Science, 2005. **60**(14): p. 3817-3833.
85. Radichkov, R., et al., *A numerical bifurcation analysis of continuous fluidized bed spray granulation with external product classification.* Chemical Engineering and Processing: Process Intensification, 2006. **45**(10): p. 826-837.
86. Landgrebe, J.D. and S.E. Pratsinis, *Gas-phase manufacture of particulates: interplay of chemical reaction and aerosol coagulation in the free-molecular regime.* Industrial & Engineering Chemistry Research, 1989. **28**(10): p. 1474-1481.
87. Randolph, A.D. and M.A. Larson, *Theory of particulate processes : analysis and techniques of continuous crystallization*. 1988, San Diego: Academic Press.
88. Ramkrishna, D., *Population Balances. Theory and applications to particulate systems in engineering.* . 2000, New York: Academic Press.

89. Hounslow, M.J., J.M.K. Pearson, and T. Instone, *Tracer studies of high-shear granulation: II. Population balance modeling.* AIChE Journal, 2001b. **47**(9): p. 1984-1999.
90. Marchisio, D.L., R.D. Vigil, and R.O. Fox, *Quadrature method of moments for aggregation–breakage processes.* Journal of Colloid and Interface Science, 2003b. **258**(2): p. 322-334.
91. Poon, J.M.H., et al., *Experimental validation studies on a multi-dimensional and multi-scale population balance model of batch granulation.* Chemical Engineering Science, 2009. **64**(4): p. 775-786.
92. Poon, J.M.H., et al., *A three-dimensional population balance model of granulation with a mechanistic representation of the nucleation and aggregation phenomena.* Chemical Engineering Science, 2008. **63**(5): p. 1315-1329.
93. Darelius, A., et al., *High shear wet granulation modelling—a mechanistic approach using population balances.* Powder Technology, 2005. **160**(3): p. 209-218.
94. Kapur, P.C., *Kinetics of granulation by non-random coalescence mechanism.* Chemical Engineering Science, 1972. **27**(10): p. 1863-1869.
95. Kapur, P.C. and D.W. Fuerstenau, *Coalescence Model for Granulation.* Industrial & Engineering Chemistry Process Design and Development, 1969. **8**(1): p. 56-62.
96. Sastry, K.V.S., *Similarity size distribution of agglomerates during their growth by coalescence in granulation or green pelletization.* International Journal of Mineral Processing, 1975. **2**(2): p. 187-203.
97. Adetayo, A.A. and B.J. Ennis, *Unifying approach to modeling granule coalescence mechanisms.* AIChE Journal, 1997. **43**(4): p. 927-934.
98. Friedlander, S.K., *Smoke, dust and haze. Fundamentals of aerosol behavior: John Wiley, New York, London, Sydney, Toronto. 1977. Pp. xvii + 317.* Environmental Pollution (1970), 1977. **15**(4): p. 315-315.
99. Golovin, A.M., *The solution of the coagulating equation for cloud droplets in a rising air current.* B. Acad. Sci. USSR, Ser. Geophys., 1963. **5**: p. 482-487.
100. Kumar, J., et al., *An efficient numerical technique for solving population balance equation involving aggregation, breakage, growth and nucleation.* Powder Technology, 2008. **182**(1): p. 81-104.
101. Roy, P., et al., *Size-dependent coalescence kernel in fertilizer granulation-A comparative study.* Particuology, 2009. **7**(6): p. 445-450.
102. Friedlander, S.K., *Smoke, dust and haze. Fundamentals of aerosol behavior. John Wiley, New York, 1977; second ed. Oxford University Press, NY.* 2000.
103. Soos, M., J. Sefcik, and M. Morbidelli, *Investigation of aggregation, breakage and restructuring kinetics of colloidal dispersions in turbulent flows by population balance modeling and static light scattering.* Chemical Engineering Science, 2006. **61**(8): p. 2349-2363.
104. Dhanarajan, A. and R. Bandyopadhyay, *An energy-based population-balance approach to model granule growth and breakage in high-shear wet granulation processes.* AAPS PharmSciTech, 2007. **8**(3): p. E118-E125.
105. Attarakih, M.M., H.J.H.-J. Bart, and N.M. Faqir, *Numerical solution of the spatially distributed population balance equation describing the hydrodynamics of*

interacting liquid-liquid dispersions. Chemical Engineering Science, 2004. **59**(12): p. 2567-2592.
106. Vanni, M., *Approximate Population Balance Equations for Aggregation-Breakage Processes.* Journal of Colloid and Interface Science, 2000. **221**(2): p. 143-160.
107. Hounslow, M.J., R.L. Ryall, and V.R. Marshall, *A discretized population balance for nucleation, growth, and aggregation.* AIChE Journal, 1988. **34**(11): p. 1821-1832.
108. Lister, J.D., D.J. Smit, and M.J. Hounslow, *Adjustable discretized population balance for growth and aggregation.* AIChE Journal, 1995. **41**(3): p. 591-603.
109. Kumar, S. and D. Ramkrishna, *On the solution of population balance equations by discretization--I. A fixed pivot technique.* Chemical Engineering Science, 1996a. **51**(8): p. 1311-1332.
110. Kumar, S. and D. Ramkrishna, *On the solution of population balance equations by discretization--II. A moving pivot technique.* Chemical Engineering Science, 1996b. **51**(8): p. 1333-1342.
111. Batterham, R.J., J.S. Hall, and G. Barton, *Proceedings, 3rd International Symposium on Agglomeration, Nürnberg (1981) p. A136 .* 1981.
112. Hulburt, H.M. and S. Katz, *Some problems in particle technology: A statistical mechanical formulation.* Chemical Engineering Science, 1964. **19**(8): p. 555-574.
113. Wan, B. and T.A. Ring, *Verification of SMOM and QMOM population balance modeling in CFD code using analytical solutions for batch particulate processes.* China Particuology, 2006. **4**(5): p. 243-249.
114. Frenklach, M. and S.J. Harris, *Aerosol dynamics modeling using the method of moments.* Journal of Colloid and Interface Science, 1987. **118**(1): p. 252-261.
115. Pratsinis, S.E., S.K. Friedlander, and A.J. Pearlstein, *Aerosol reactor theory: Stability and dynamics of a continuous stirred tank aerosol reactor.* AIChE Journal, 1986. **32**(2): p. 177-185.
116. Kruis, F.E., et al., *A Simple Model for the Evolution of the Characteristics of Aggregate Particles Undergoing Coagulation and Sintering.* Aerosol Science and Technology, 1993. **19**(4): p. 514-526.
117. Lee, K.W., *Change of particle size distribution during Brownian coagulation.* Journal of Colloid and Interface Science, 1983. **92**(2): p. 315-325.
118. McGraw, R., *Description of Aerosol Dynamics by the Quadrature Method of Moments.* Aerosol Science and Technology, 1997. **27**(2): p. 255-265.
119. Marchisio, D.L., R. Dennis Vigil, and R. O. Fox, *Implementation of the quadrature method of moments in CFD codes for aggregation-breakage problems.* Chemical Engineering Science, 2003c. **58**(15): p. 3337-3351.
120. Marchisio, D.L. and R.O. Fox, *Solution of population balance equations using the direct quadrature method of moments.* Journal of Aerosol Science, 2005. **36**(1): p. 43-73.
121. Marchisio, D.L., et al., *Quadrature method of moments for population-balance equations.* AIChE Journal, 2003a. **49**(5): p. 1266-1276.
122. Upadhyay, R.R. and O.A. Ezekoye, *Evaluation of the 1-point quadrature approximation in QMOM for combined aerosol growth laws.* Journal of Aerosol Science, 2003. **34**(12): p. 1665-1683.
123. Piskunov, V.N. and A.I. Golubev, *The generalized approximation method for*

modeling coagulation kinetics--Part 1: justification and implementation of the method. Journal of Aerosol Science, 2002a. **33**(1): p. 51-63.

124. Piskunov, V.N., et al., *The generalized approximation method for modeling coagulation kinetics--Part 2: comparison with other methods.* Journal of Aerosol Science, 2002b. **33**(1): p. 65-75.
125. Attarakih, M.M., et al., *Solution of the population balance equation using the sectional quadrature method of moments (SQMOM)*, in *Computer Aided Chemical Engineering*. 2006, Elsevier. p. 209-214.
126. Mishra, B.K., *Monte Carlo simulation of particle breakage process during grinding.* Powder Technology, 2000. **110**(3): p. 246-252.
127. Shah, B.H., D. Ramkrishna, and J.D. Borwanker, *Simulation of particulate systems using the concept of the interval of quiescence.* AIChE Journal, 1977. **23**(6): p. 897-904.
128. van Peborgh Gooch, J.R. and M.J. Hounslow, *Monte Carlo simulation of size-enlargement mechanisms in crystallization.* AIChE Journal, 1996. **42**(7): p. 1864-1874.
129. Liffman, K., *A direct simulation Monte-Carlo method for cluster coagulation.* Journal of Computational Physics, 1992. **100**(1): p. 116-127.
130. Debry, E., B. Sportisse, and B. Jourdain, *A stochastic approach for the numerical simulation of the general dynamics equation for aerosols.* Journal of Computational Physics, 2003. **184**(2): p. 649-669.
131. Maisels, A., F. Einar Kruis, and H. Fissan, *Direct simulation Monte Carlo for simultaneous nucleation, coagulation, and surface growth in dispersed systems.* Chemical Engineering Science, 2004. **59**(11): p. 2231-2239.
132. Kruis, F.E., A. Maisels, and H. Fissan, *Direct simulation Monte Carlo method for particle coagulation and aggregation.* AIChE Journal, 2000. **46**(9): p. 1735-1742.
133. Maisels, A., et al., *A Study of Nanoparticle Aerosol Charging by Monte Carlo Simulations.* Journal of Nanoparticle Research, 2003. **5**(3): p. 225-235.
134. Lin, Y., K. Lee, and T. Matsoukas, *Solution of the population balance equation using constant-number Monte Carlo.* Chemical Engineering Science, 2002. **57**(12): p. 2241-2252.
135. Lee, K. and T. Matsoukas, *Simultaneous coagulation and break-up using constant-N Monte Carlo.* Powder Technology, 2000. **110**(1-2): p. 82-89.
136. Smith, M. and T. Matsoukas, *Constant-number Monte Carlo simulation of population balances.* Chemical Engineering Science, 1998. **53**(9): p. 1777-1786.
137. Utikar, R.P. and V.V. Ranade, *Single jet fluidized beds: Experiments and CFD simulations with glass and polypropylene particles.* Chemical Engineering Science, 2007. **62**(1-2): p. 167-183.
138. Vaishali, S., S. Roy, and P.L. Mills, *Hydrodynamic simulation of gas-solids downflow reactors.* Chemical Engineering Science, 2008. **63**(21): p. 5107-5119.
139. Zhong, W.Q., et al., *Discrete Element Method Simulation of Cylinder-Shaped Particle Flow in a Gas-Solid Fluidized Bed.* Chemical Engineering & Technology, 2009. **32**(3): p. 386-391.
140. Taghipour, F., N. Ellis, and C. Wong, *Experimental and computational study of gas - solid fluidized bed hydrodynamics.* Chemical Engineering Science, 2005. **60**(24):

p. 6857-6867.
141. Ahuja, G.N. and A.W. Patwardhan, *CFD and experimental studies of solids hold-up distribution and circulation patterns in gas - solid fluidized beds.* Chemical Engineering Journal, 2008. **143**(1-3): p. 147-160.
142. Wang, J., M.A. van der Hoef, and J.A.M. Kuipers, *CFD study of the minimum bubbling velocity of Geldart A particles in gas-fluidized beds.* Chemical Engineering Science. **65**(12): p. 3772-3785.
143. Hosseini, S.H., et al., *CFD studies of solids hold-up distribution and circulation patterns in gas - solid fluidized beds.* Powder Technology, 2010. **200**(3): p. 202-215.
144. Papadikis, K., A.V. Bridgwater, and S. Gu, *CFD modelling of the fast pyrolysis of biomass in fluidised bed reactors, Part A: Eulerian computation of momentum transport in bubbling fluidised beds.* Chemical Engineering Science, 2008. **63**(16): p. 4218-4227.
145. Armstrong, L.M., S. Gu, and K.H. Luo, *Study of wall-to-bed heat transfer in a bubbling fluidised bed using the kinetic theory of granular flow.* International Journal of Heat and Mass Transfer, 2010. **53**(21-22): p. 4949-4959.
146. Yu, L., et al., *Numerical simulation of the bubbling fluidized bed coal gasification by the kinetic theory of granular flow (KTGF).* Fuel, 2007. **86**(5-6): p. 722-734.
147. Yusuf, R., B. Halvorsen, and M.C. Melaaen, *An experimental and computational study of wall to bed heat transfer in a bubbling gas-solid fluidized bed.* International Journal of Multiphase Flow, 2012. **42**(0): p. 9-23.
148. Ahmadi, G. and M. Shahinpoor, *A kinetic model for rapid flows of granular materials.* International Journal of Non-Linear Mechanics, 1984. **19**(2): p. 177-186.
149. Lun, C.K.K. and S.B. Savage, *A Simple Kinetic Theory for Granular Flow of Rough, Inelastic, Spherical Particles.* Journal of Applied Mechanics, 1987. **54**(1): p. 47-53.
150. Gidaspow, D., *Multiphase flow and fluidization: Continuum and kinetic theory descriptions.* Academic Press, San Diego, 1994.
151. Kafui, K.D., C. Thornton, and M.J. Adams, *Discrete particle-continuum fluid modelling of gas-solid fluidised beds.* Chemical Engineering Science, 2002. **57**(13): p. 2395-2410.
152. Link, J.M., et al., *Comparison of fibre optical measurements and discrete element simulations for the study of granulation in a spout fluidized bed.* Powder Technology, 2009. **189**(2): p. 202-217.
153. Fries, L., et al., *DEM-CFD modeling of a fluidized bed spray granulator.* Chemical Engineering Science, 2011. **66**(11): p. 2340-2355.
154. Goldschmidt, M.J.V., et al., *Discrete element modelling of fluidised bed spray granulation.* Powder Technology, 2003. **138**(1): p. 39-45.
155. van Buijtenen, M.S., et al., *A discrete element study of wet particle–particle interaction during granulation in a spout fluidized bed.* The Canadian Journal of Chemical Engineering, 2009. **87**(2): p. 308-317.
156. Kafui, D.K. and C. Thornton, *Fully-3D DEM simulation of fluidised bed spray granulation using an exploratory surface energy-based spray zone concept.* Powder Technology, 2008. **184**(2): p. 177-188.
157. Radeke, C.A., B.J. Glasser, and J.G. Khinast, *Large-scale powder mixer simulations*

using massively parallel GPUarchitectures. Chemical Engineering Science, 2010. **65**(24): p. 6435-6442.
158. Gidaspow, D., *Multiphase flow and fluidization: Continuum and kinetic theory descriptions.* San Diego, USA: Academic Press, 1994.
159. Ding, J. and D. Gidaspow, *A bubbling fluidization model using kinetic theory of granular flow.* AIChE Journal, 1990. **36**(4): p. 523-538.
160. M. Syamlal, W. Rogers, and O.Brien T. J, *MFIX Documentation: Volume1, Theory Guide>. National Technical Information Service, Springfield, VA. DOE/METC-9411004, NTIS/DE94000871993.*
161. Gidaspow, D., R.B. , and J.D. , *Hydrodynamics of Circulating Fluidized Beds, Kinetic Theory Approach.* In Fluidization VII, Proceeding of the 7th Engineering Foundation Conference on Fluidization, 1992: p. 75-82.
162. Lun, C.K.K., et al., *Kinetic Theories for Granular Flow: Inelastic Particles in Couette Flow and Slightly Inelastic Particles in a General Flow Field.* Journal of Fluid Mechanics 1984. **140**: p. 223-256.
163. Ma, D. and G. Ahmadi, *A thermodynamical formulation for dispersed multiphase turbulent flows II: Simple shear flows for dense mixtures.* International Journal of Multiphase Flow, 1990. **16**(2): p. 341-351.
164. Ogawa, S., A. Umemura, and N. Oshima, *On the equations of fully fluidized granular materials.* Zeitschrift fÃ¼r angewandte Mathematik und Physik ZAMP, 1980. **31**(4): p. 483-493.
165. Iddir, H. and H. Arastoopour, *Modeling of multitype particle flow using the kinetic theory approach.* AIChE Journal, 2005. **51**(6): p. 1620-1632.
166. Teaters, L., *A Computational Study of the Hydrodynamics of Gas-Solid Fluidized Beds* Msc thesis, Virginia Polytechnic Institute and State University, 2012.
167. Richardson, J.R. and W.N. Zaki, *Sedimentation and Fluidization: Part I.* Transactions of the Institute of Chemical Engineering, 1954. **32**(1): p. 35-53.
168. Wen, C.Y. and Y.H. Yu, *A generalized method for predicting the minimum fluidization velocity.* AIChE Journal, 1966. **12**(3): p. 610-612.
169. Gibilaro, L.G., et al., *Generalized friction factor and drag coefficient correlations for fluid-particle interactions.* Chemical Engineering Science, 1985. **40**(10): p. 1817-1823.
170. Syamlal, M. and T.J. O'Brien, *Computer Simulation of Bubbles in a Fluidized Bed.* American Institute of Chemical Engineers Symposium Series, 1989. **85**: p. 22-31.
171. Arastoopour, H., P. Pakdel, and M. Adewumi, *Hydrodynamic analysis of dilute gas-solids flow in a vertical pipe.* Powder Technology, 1990. **62**(2): p. 163-170.
172. Di Felice, R., *The voidage function for fluid-particle interaction systems.* International Journal of Multiphase Flow, 1994. **20**(1): p. 153-159.
173. Koch, D.L. and R.J. Hill, *Inertial Effects in Suspension and Porous-Media Flows.* Annual Review of Fluid Mechanics, 2001. **33**(1): p. 619-647.
174. Zhang, Y. and J.M. Reese, *The Drag Force in Two Fluid Models of Gas-Solid Flows.* Chemical Engineering Science, 2003. **58**(8): p. 1641-1644.
175. Maronga, S.J. and P. Wnukowski, *Establishing temperature and humidity profiles in fluidized bed particulate coating.* Powder Technology, 1997. **94**(2): p. 181-185.
176. Heinrich, S., et al., *Study of dynamic multi-dimensional temperature and*

concentration distributions in liquid-sprayed fluidized beds. Chemical Engineering Science, 2003. **58**(23-24): p. 5135-5160.

177. Chen, X.-Z., et al., *Three-dimensional CFD-PBM coupled model of the temperature fields in fluidized-bed polymerization reactors.* AIChE Journal, 2011. **57**(12): p. 3351-3366.
178. A. Öncül, A.A., et al., *CFD modelling of BaSO4 precipitation inside microemulsion droplets in a semi-batch reactor.* Chemical Engineering Journal, 2008. **138**(1-3): p. 498-509.
179. Venneker, B.C.H., J.J. Derksen, and H.E.A. Van den Akker, *Population balance modeling of aerated stirred vessels based on CFD.* AIChE Journal, 2002. **48**(4): p. 673-685.
180. Fan, R., D.L. Marchisio, and R.O. Fox, *Application of the direct quadrature method of moments to polydisperse gas-solid fluidized beds.* Powder Technology, 2004. **139**(1): p. 7-20.
181. Fan, R. and R.O. Fox, *Segregation in polydisperse fluidized beds: Validation of a multi-fluid model.* Chemical Engineering Science, 2008. **63**(1): p. 272-285.
182. Ahmadzadeh, A., et al., *Population balance equations' application in rotating fluidized bed polymerization reactor.* Chemical Engineering Research and Design, 2008. **86**(4): p. 329-343.
183. Balaji, S., et al., *Multi-scale modeling and control of fluidized beds for the production of solar grade silicon.* Powder Technology, 2010. **199**(1): p. 23-31.
184. Börner, M., M. Peglow, and E. Tsotsas, *Derivation of parameters for a two compartment population balance model of Wurster fluidised bed granulation.* Powder Technology, 2013. **238**(0): p. 122-131.
185. Turchiuli, C., T. Jimenèz, and E. Dumoulin, *Identification of thermal zones and population balance modelling of fluidized bed spray granulation.* Powder Technology, 2011. **208**(2): p. 542-552.
186. Hussain, M., et al., *On two-compartment population balance modeling of spray fluidized bed agglomeration.* Computers & Chemical Engineering, 2014. **61**(0): p. 185-202.
187. Zhang, J., et al., *Evaluation of control strategies for fertiliser granulation circuits using dynamic simulation.* Powder Technology, 2000. **108**(2–3): p. 122-129.
188. Watano, S., Y. Sato, and K. Miyanami, *Application of fuzzy-logic to moisture control in fluidized-bed granulation.* Journal of Chemical Engineering of Japan, 1995. **28**(3): p. 282-287.
189. Watano, S., K. Terashita, and K. Miyanami, *Moisture feedback control and process automation in fluidized bed granulation.* Advanced Powder Technology, 1992. **3**(4): p. 255-265.
190. Watano, S., Y. Sato, and K. Miyanami, *Control of granule growth in fluidized bed granulation by an image processing system.* Chemical & pharmaceutical bulletin, 1996. **44**(8): p. 1556-1560.
191. Watano, S., *Direct control of wet granulation processes by image processing system.* Powder Technology, 2001. **117**(1-2): p. 163-172.
192. Gatzke, E.P. and F.J. Doyle, *Model predictive control of a granulation system using soft output constraints and prioritized control objectives.* Powder Technology,

2001. **121**(2-3): p. 149-158.
193. Pottmann, M., et al., *Model-based control of a granulation system.* Powder Technology, 2000. **108**(2-3): p. 192-201.
194. Sanders, C.F.W., M.J. Hounslow, and F.J. Doyle Iii, *Identification of models for control of wet granulation.* Powder Technology, 2009. **188**(3): p. 255-263.
195. Long, C.E., J.A. Gantt, and E.R. Gatzke. *Batch granulation control using a simplified population balance and nonlinear model predictive control*. in *American Control Conference, 2005. Proceedings of the 2005*. 2005.
196. Mort, P.R., S.W. Capeci, and J.W. Holder, *Control of agglomerate attributes in a continuous binder-agglomeration process.* Powder Technology, 2001. **117**(1-2): p. 173-176.
197. Lourenço, V., et al., *A quality by design study applied to an industrial pharmaceutical fluid bed granulation.* European Journal of Pharmaceutics and Biopharmaceutics, 2012. **81**(2): p. 438-447.
198. Liu, H., et al., *Using the Box–Behnken experimental design to optimise operating parameters in pulsed spray fluidised bed granulation.* International Journal of Pharmaceutics, 2013. **448**(2): p. 329-338.
199. Närvänen, T., et al., *Controlling granule size by granulation liquid feed pulsing.* International Journal of Pharmaceutics, 2008. **357**(1&2): p. 132-138.
200. Liu, H. and M. Li, *Population balance modelling and multi-stage optimal control of a pulsed spray fluidized bed granulation.* International Journal of Pharmaceutics, 2014(0).
201. CDER, F.a.D.A., *Guidance for Industry Q8 Pharmaceutical Development.* May 2006.
202. CDER, F.a.D.A., *Guidance for Industry Q8(R2) Pharmaceutical Development.* November 2009.
203. Tomba, E., et al., *Latent variable modeling to assist the implementation of Quality-by-Design paradigms in pharmaceutical development and manufacturing: A review.* International Journal of Pharmaceutics, 2013. **457**(1): p. 283-297.
204. Rambali, B., et al., *Using Experimental Design to Optimize the Process Parameters in Fluidized Bed Granulation.* Drug Development and Industrial Pharmacy, 2001. **27**(1): p. 47-55.
205. Montgomery, D.C., *Design and analysis of experiments*. Third Edition ed. 1991: John wiley & sons.
206. Zidan, A.S., et al., *Quality by design: Understanding the formulation variables of a cyclosporine A self-nanoemulsified drug delivery systems by Box-Behnken design and desirability function.* International Journal of Pharmaceutics, 2007. **332**(1&2): p. 55-63.
207. Govender, S., et al., *Optimisation and characterisation of bioadhesive controlled release tetracycline microspheres.* International Journal of Pharmaceutics, 2005. **306**(1&2): p. 24-40.
208. Aulton, M.E., *Pharmaceutics: the Science of Dosage Form Design*. Second ed. 2002: Churchill Livingstone.
209. Schaafsma, S.H., et al., *Effects and control of humidity and particle mixing in fluid-bed granulation.* AIChE Journal, 1999. **45**(6): p. 1202-1210.
210. Iveson, S.M., *Limitations of one-dimensional population balance models of wet*

granulation processes. Powder Technology, 2002. **124**(3): p. 219-229.
211. Ding, A., M.J. Hounslow, and C.A. Biggs, *Population balance modelling of activated sludge flocculation: Investigating the size dependence of aggregation, breakage and collision efficiency.* Chemical Engineering Science, 2006. **61**(1): p. 63-74.
212. Glaser, T., et al., *Model predictive control of continuous drum granulation.* Journal of Process Control, 2009. **19**(4): p. 615-622.
213. Ramachandran, R. and A. Chaudhury, *Model-based design and control of a continuous drum granulation process.* Chemical Engineering Research and Design, 2012. **90**(8): p. 1063-1073.
214. Gatzke, E.P. and F.J. Doyle Iii, *Model predictive control of a granulation system using soft output constraints and prioritized control objectives.* Powder Technology, 2001. **121**(2–3): p. 149-158.
215. Burggraeve, A., et al., *Process analytical tools for monitoring, understanding, and control of pharmaceutical fluidized bed granulation: A review.* European Journal of Pharmaceutics and Biopharmaceutics, 2013. **83**(1): p. 2-15.
216. Wang, J., M.A. van der Hoef, and J.A.M. Kuipers, *CFD study of the minimum bubbling velocity of Geldart A particles in gas-fluidized beds.* Chemical Engineering Science, 2010. **65**(12): p. 3772-3785.
217. Depypere, F.d.r., J.G. Pieters, and K. Dewettinck, *CFD analysis of air distribution in fluidised bed equipment.* Powder Technology, 2004. **145**(3): p. 176-189.
218. Armstrong, L.M., K.H. Luo, and S. Gu, *Two-dimensional and three-dimensional computational studies of hydrodynamics in the transition from bubbling to circulating fluidised bed.* Chemical Engineering Journal, 2010. **160**(1): p. 239-248.
219. Feng, Y., et al., *CFD modeling of gas-solid flow in an internally circulating fluidized bed.* Powder Technology, 2012. **219**(0): p. 78-85.
220. Taghipour, F., N. Ellis, and C. Wong, *Experimental and computational study of gas-solid fluidized bed hydrodynamics.* Chemical Engineering Science, 2005. **60**(24): p. 6857-6867.
221. van Wachem, B.G.M. and A.E. Almstedt, *Methods for multiphase computational fluid dynamics.* Chemical Engineering Journal, 2003. **96**(1–3): p. 81-98.
222. Gidaspow, D., R. Bezburuah, and J. Ding, *Hydrodynamics of circulating fluidized beds: Kinetic theory approach*. 1991. Medium: ED; Size: Pages: (8 p).
223. Lun, C.K.K., et al., *Kinetic theories for granular flow: inelastic particles in Couette flow and slightly inelastic particles in a general flow field.* Journal of Fluid Mechanics, 1984. **vol. 140**: p. p.223-256.
224. Syamal M, Rogers W, and O.B. TJ., *Theory Guide. Springfield: National Technical Information Service.* MIFX Documentation 1993. **Vol. 1**.
225. Schaeffer, D.G., *Instability in the evolution equations describing incompressible granular flow.* Journal of Differential Equations, 1987. **66**(1): p. 19-50.
226. Lettieri, P., et al., *CFD modelling of liquid fluidized beds in slugging mode.* Powder Technology, 2006. **167**(2): p. 94-103.
227. Ronsse, F., J. Depelchin, and J.G. Pieters, *Particle surface moisture content estimation using population balance modelling in fluidised bed agglomeration.* Journal of Food Engineering. **109**(3): p. 347-357.

228. Liu, H., et al., *Using the Box-Behnken experimental design to optimise operating parameters in pulsed spray fluidised bed granulation.* International Journal of Pharmaceutics, 2013. **448**(2): p. 329-338.
229. Liu, H. and M. Li, *Population balance modelling and multi-stage optimal control of a pulsed spray fluidized bed granulation.* International Journal of Pharmaceutics, 2014. **468**(1-2): p. 223-233.
230. Turchiuli, C., T. Jimenez, and E. Dumoulin, *Identification of thermal zones and population balance modelling of fluidized bed spray granulation.* Powder Technology, 2011. **208**(2): p. 542-552.
231. Bezzo, F., S. Macchietto, and C.C. Pantelides, *General hybrid multizonal/CFD approach for bioreactor modeling.* AIChE Journal, 2003. **49**(8): p. 2133-2148.
232. Bezzo, F., S. Macchietto, and C.C. Pantelides, *Computational issues in hybrid multizonal/computational fluid dynamics models.* AIChE Journal, 2005. **51**(4): p. 1169-1177.
233. Portillo, P.M., F.J. Muzzio, and M.G. Ierapetritou, *Hybrid DEM-compartment modeling approach for granular mixing.* AIChE Journal, 2007. **53**(1): p. 119-128.
234. Hounslow, M.J., J.M.K. Pearson, and T. Instone, *Tracer studies of high-shear granulation: II. Population balance modeling.* AIChE Journal, 2001. **47**(9): p. 1984-1999.

Appendixes

A1 Figures for chapter 3

A1.1 Figures of 15 experiments

A1.1.1 Particle size distribution in mass fraction at 30%, 70% and 100% binder sprayed of experiment 1

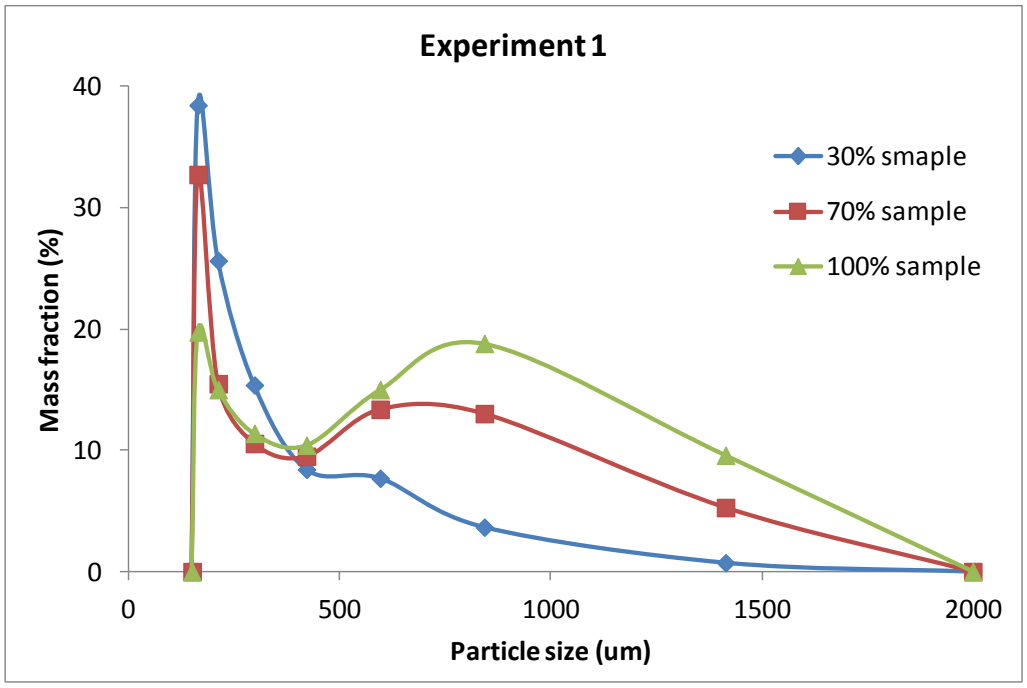

A1.1.2 Particle size distribution in mass fraction at 30%, 70% and 100% binder sprayed of experiment 2

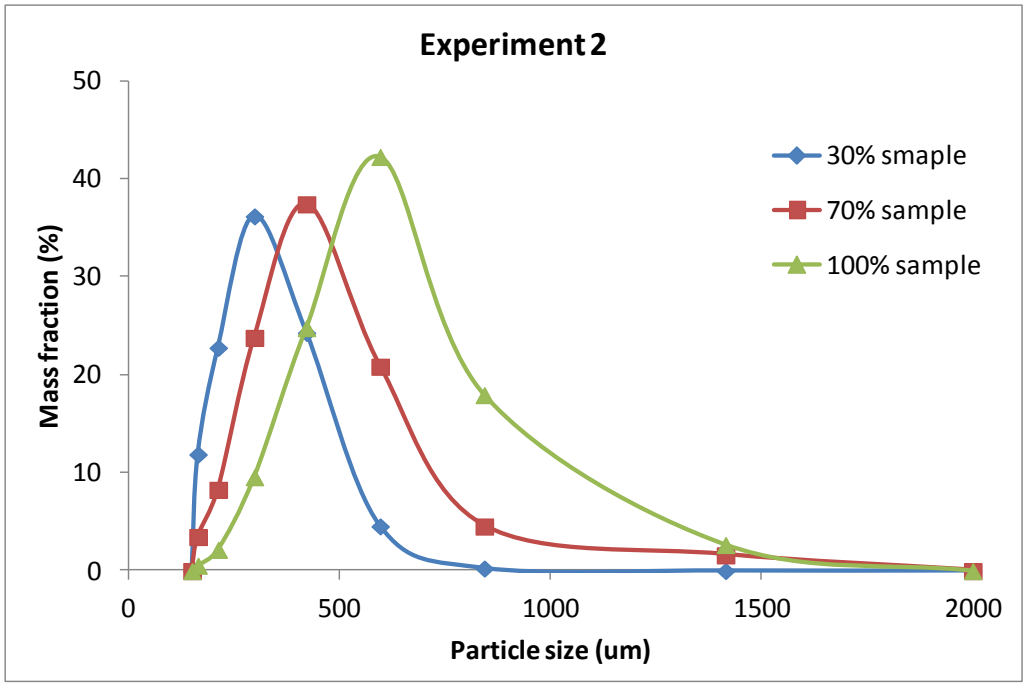

A1.1.3 Particle size distribution in mass fraction at 30%, 70% and 100% binder sprayed of experiment 3

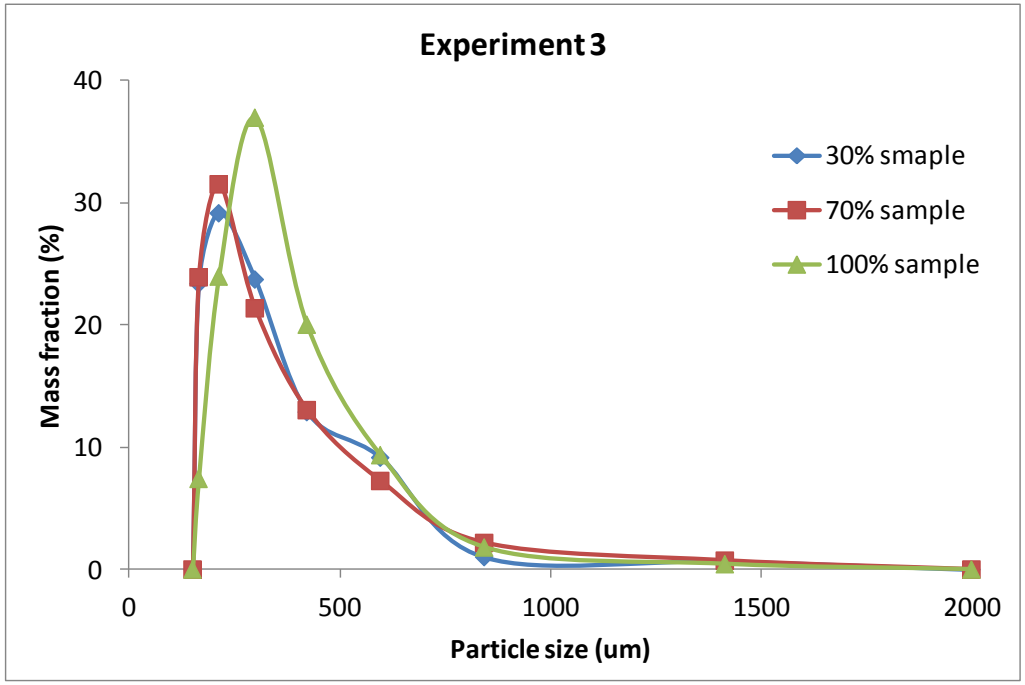

A1.1.4 Particle size distribution in mass fraction at 30%, 70% and 100% binder sprayed of experiment 4

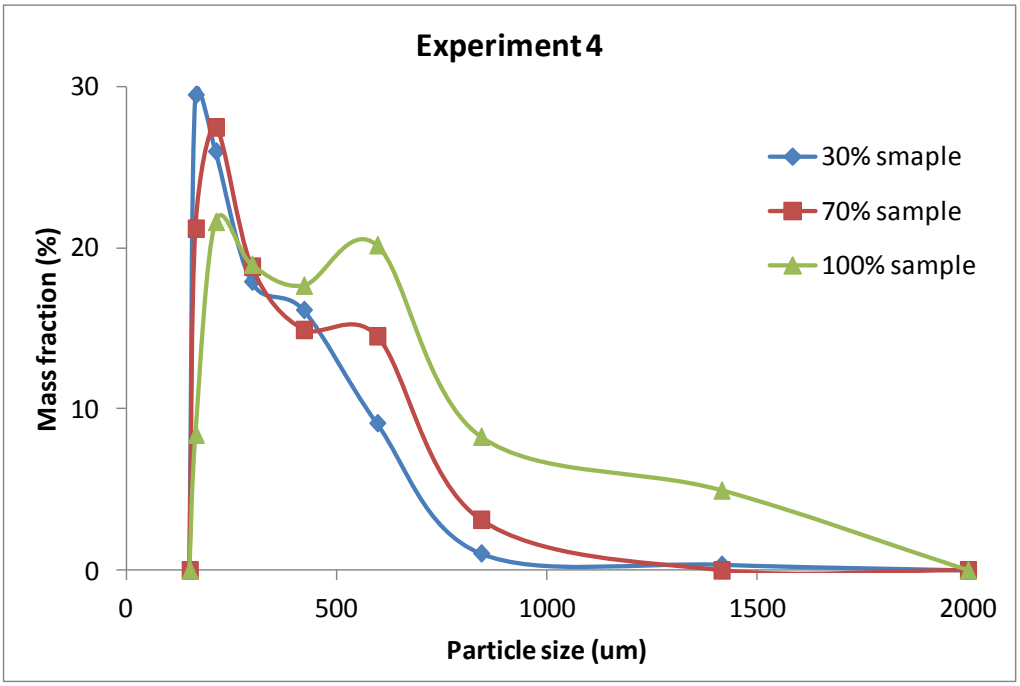

A1.1.5 Particle size distribution in mass fraction at 30%, 70% and 100% binder sprayed of experiment 5

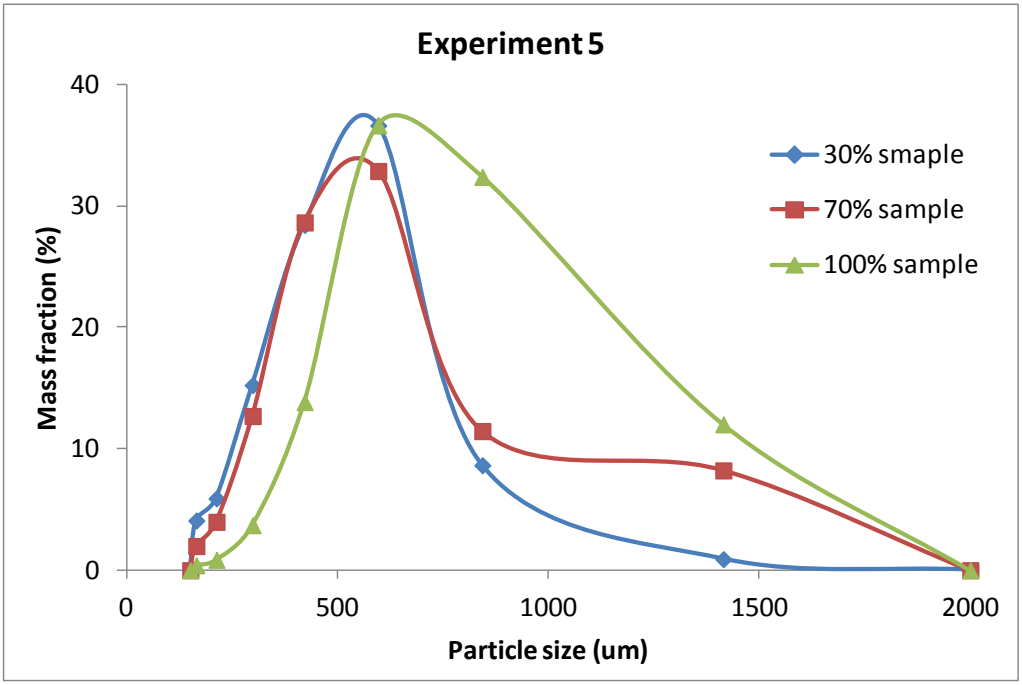

A1.1.6 Particle size distribution in mass fraction at 30%, 70% and 100% binder sprayed of experiment 6

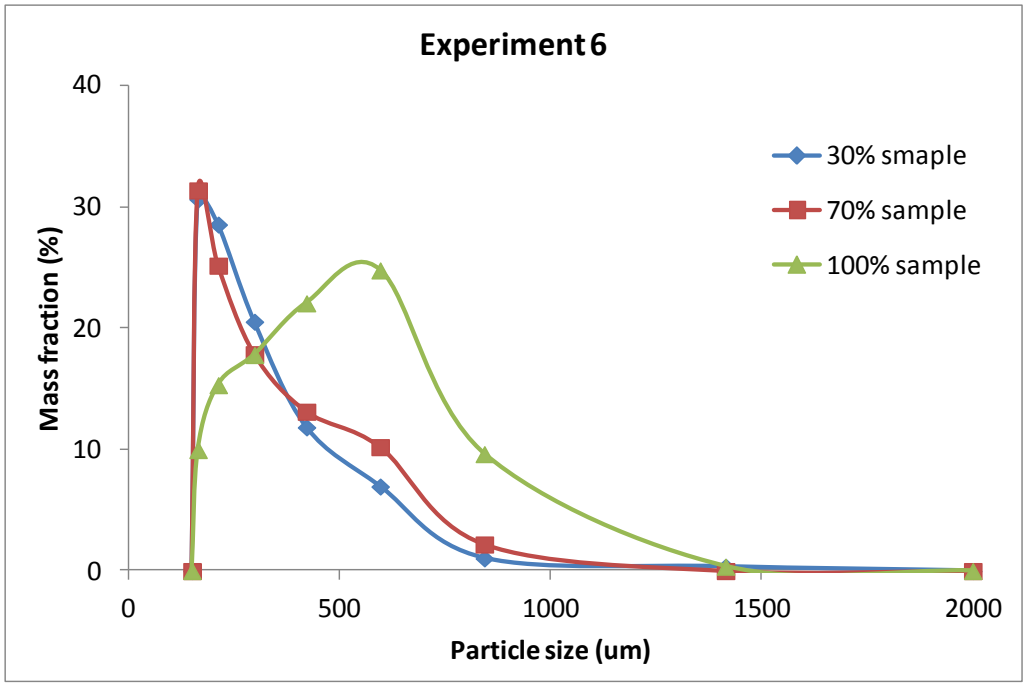

A1.1.7 Particle size distribution in mass fraction at 30%, 70% and 100% binder sprayed of experiment 7

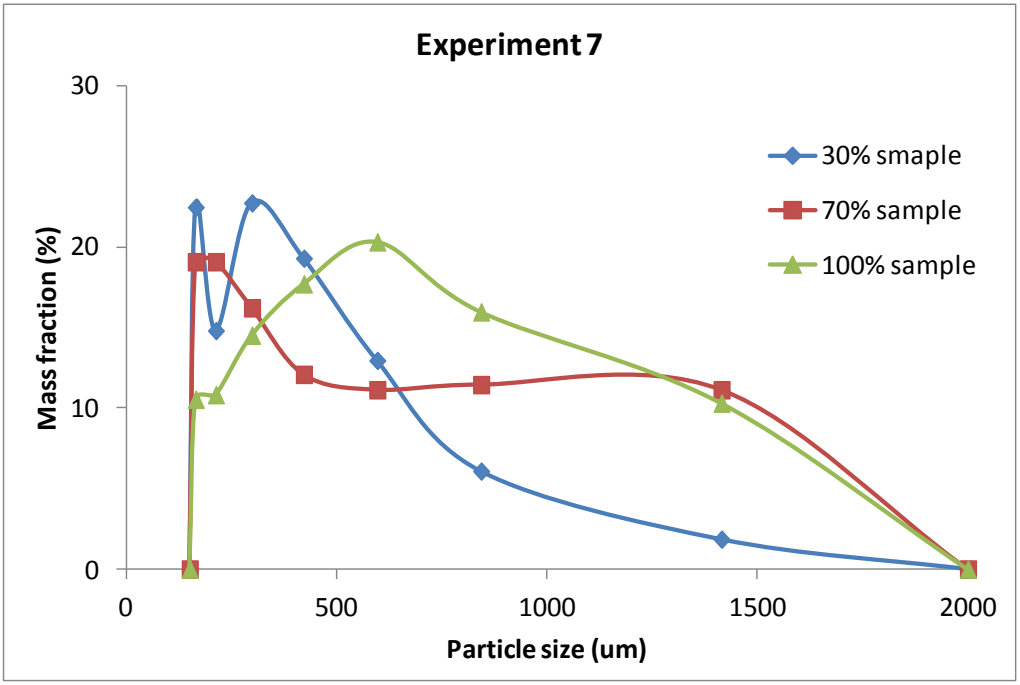

A1.1.8 Particle size distribution in mass fraction at 30%, 70% and 100% binder sprayed of experiment 8

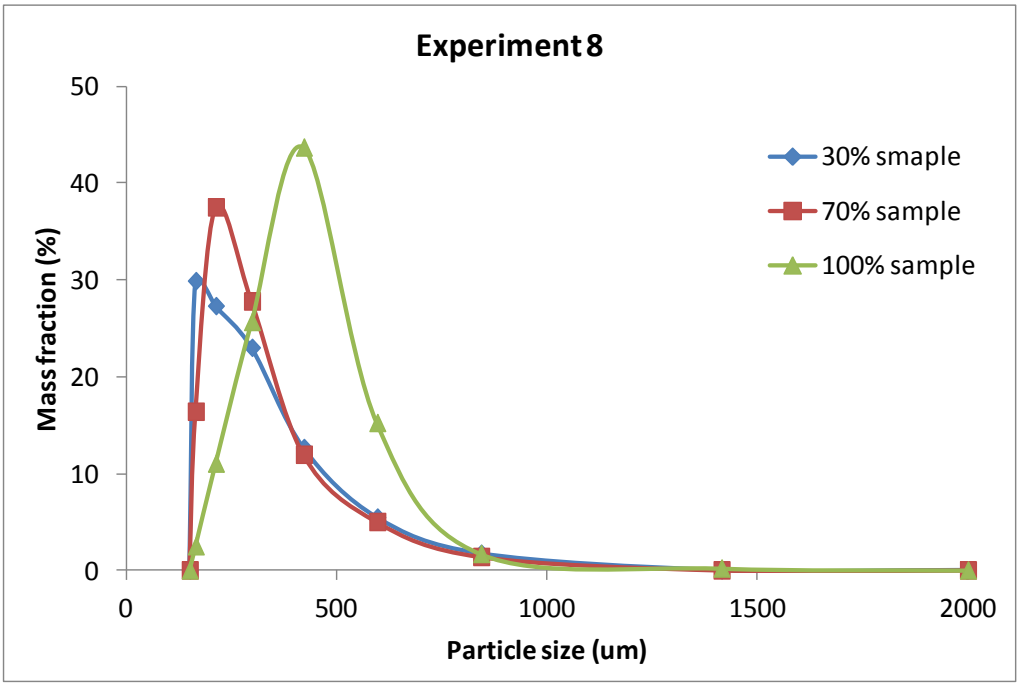

A1.1.9 Particle size distribution in mass fraction at 30%, 70% and 100% binder sprayed of experiment 9

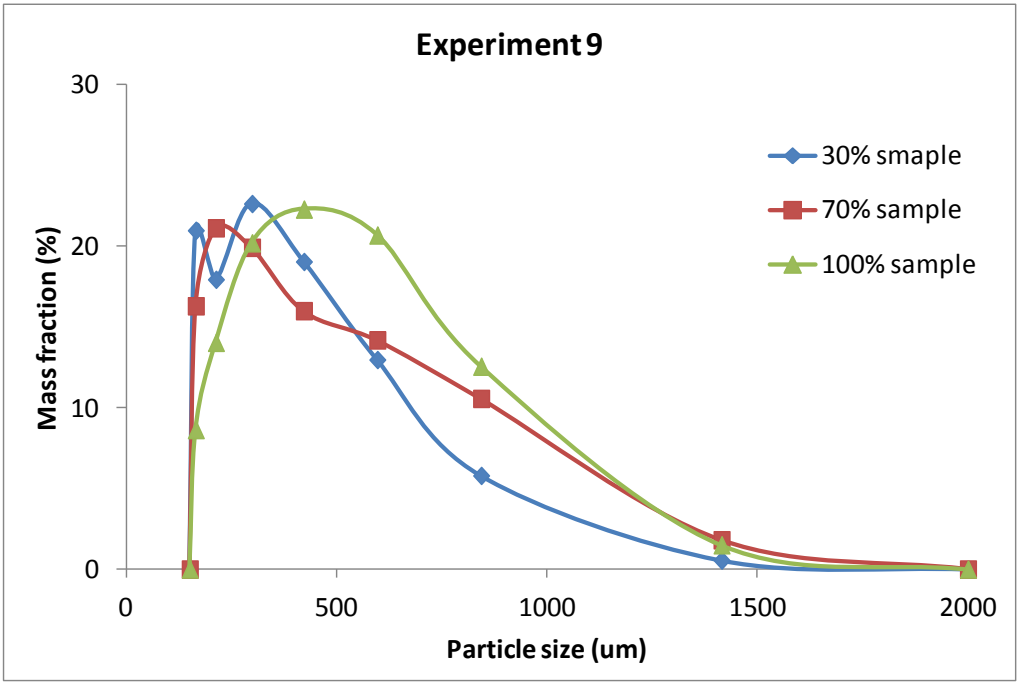

A1.1.10 Particle size distribution in mass fraction at 30%, 70% and 100% binder sprayed of experiment 10

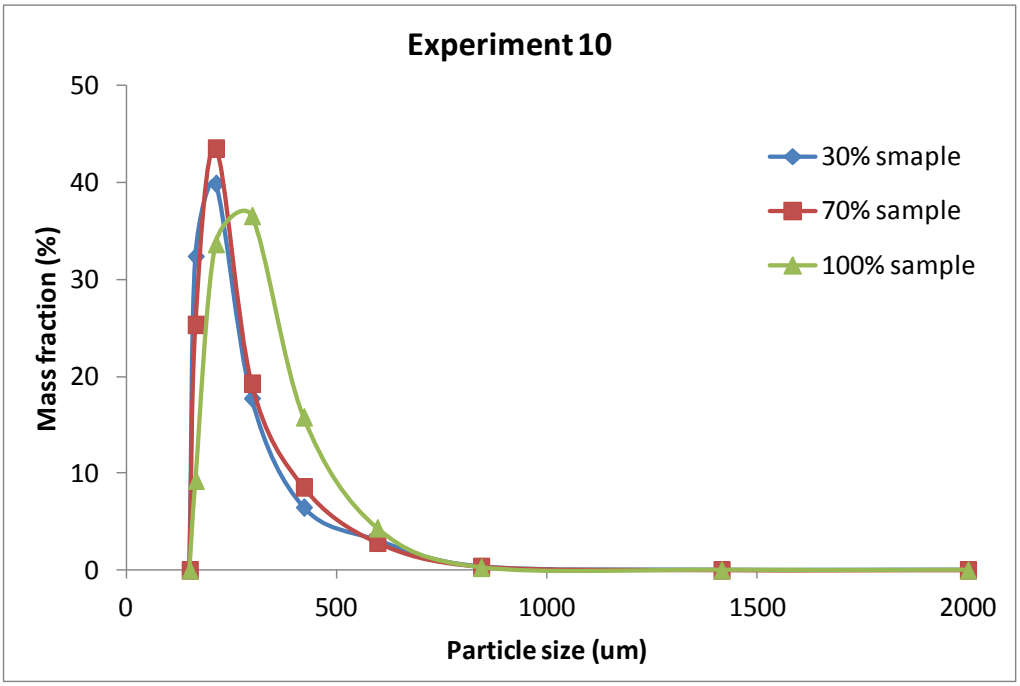

A1.1.11 Particle size distribution in mass fraction at 30%, 70% and 100% binder sprayed of experiment 11

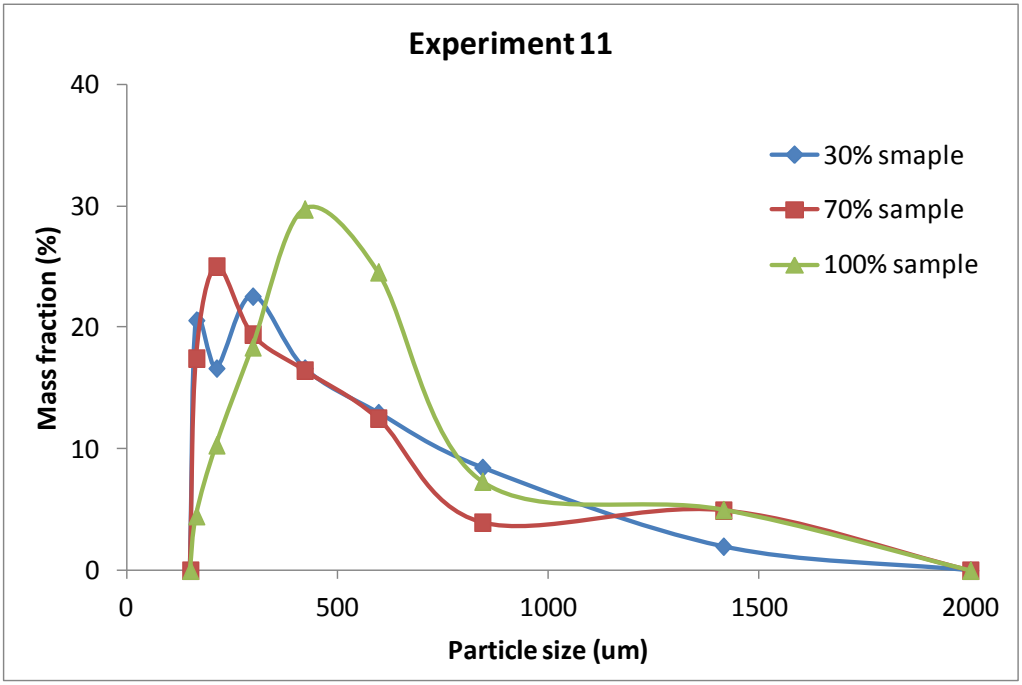

A1.1.12 Particle size distribution in mass fraction at 30%, 70% and 100% binder sprayed of experiment 12

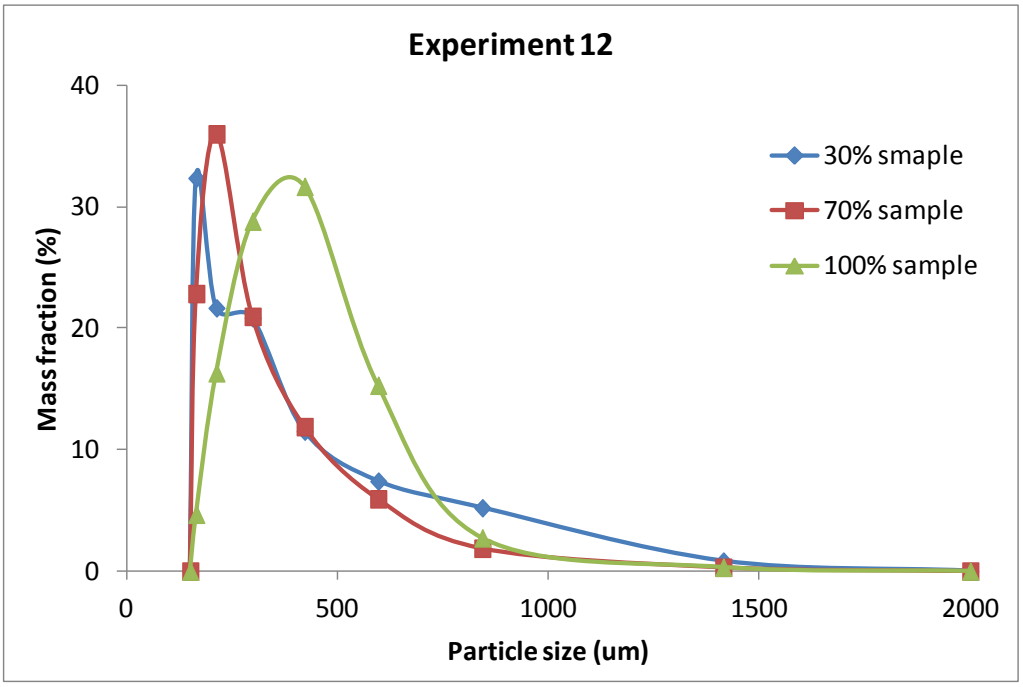

A1.1.13 Particle size distribution in mass fraction at 30%, 70% and 100% binder sprayed of experiment 13

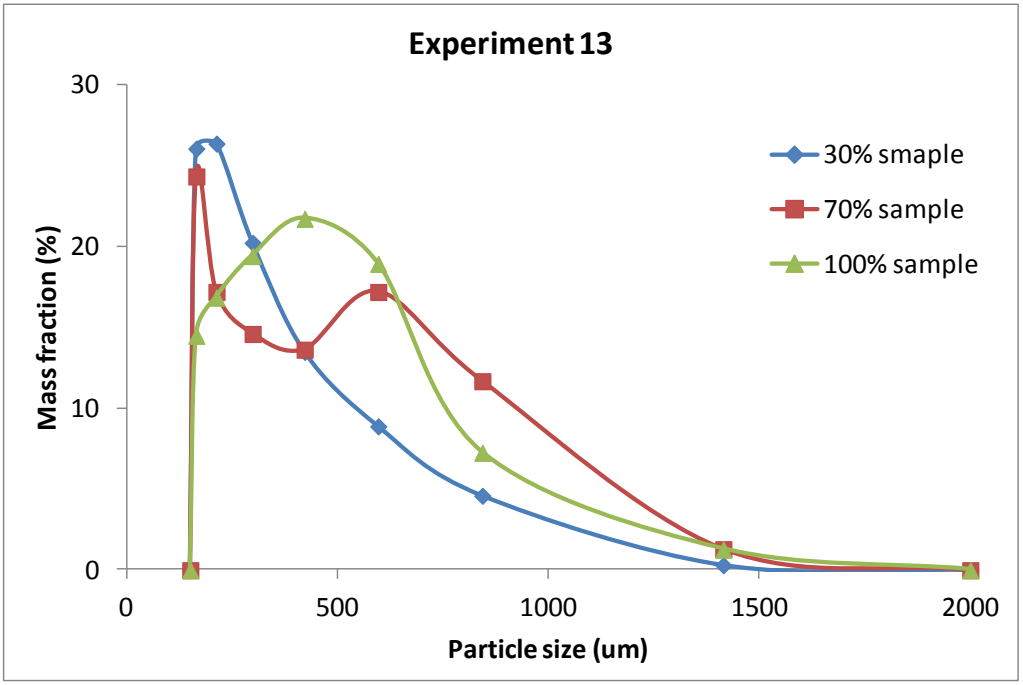

A1.1.14 Particle size distribution in mass fraction at 30%, 70% and 100% binder sprayed of experiment 14

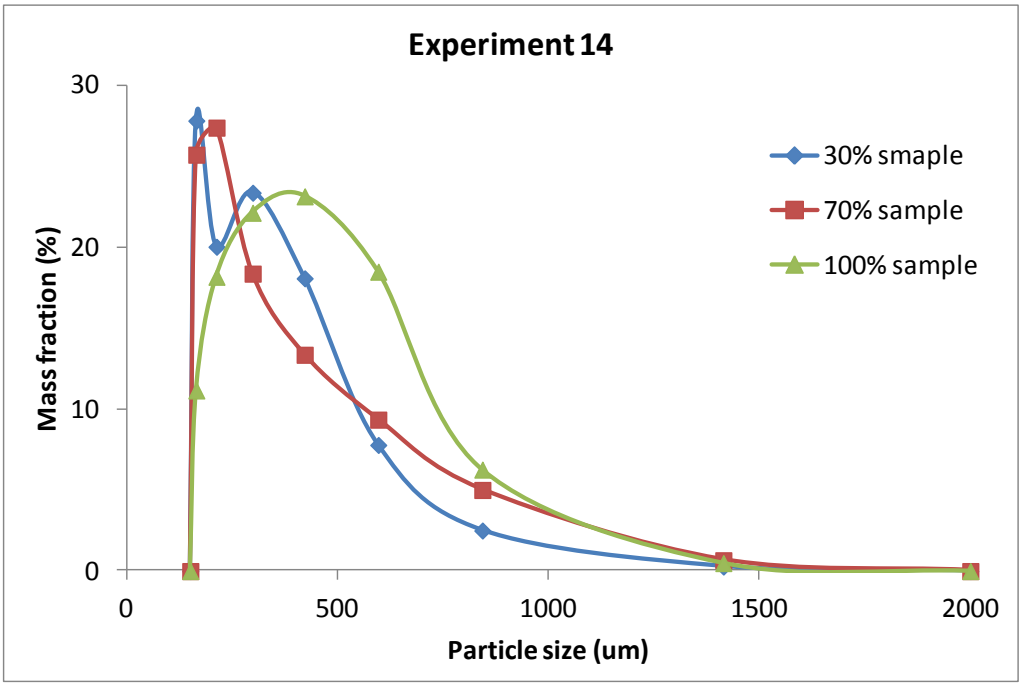

A1.1.15 Particle size distribution in mass fraction at 30%, 70% and 100% binder sprayed of experiment 15

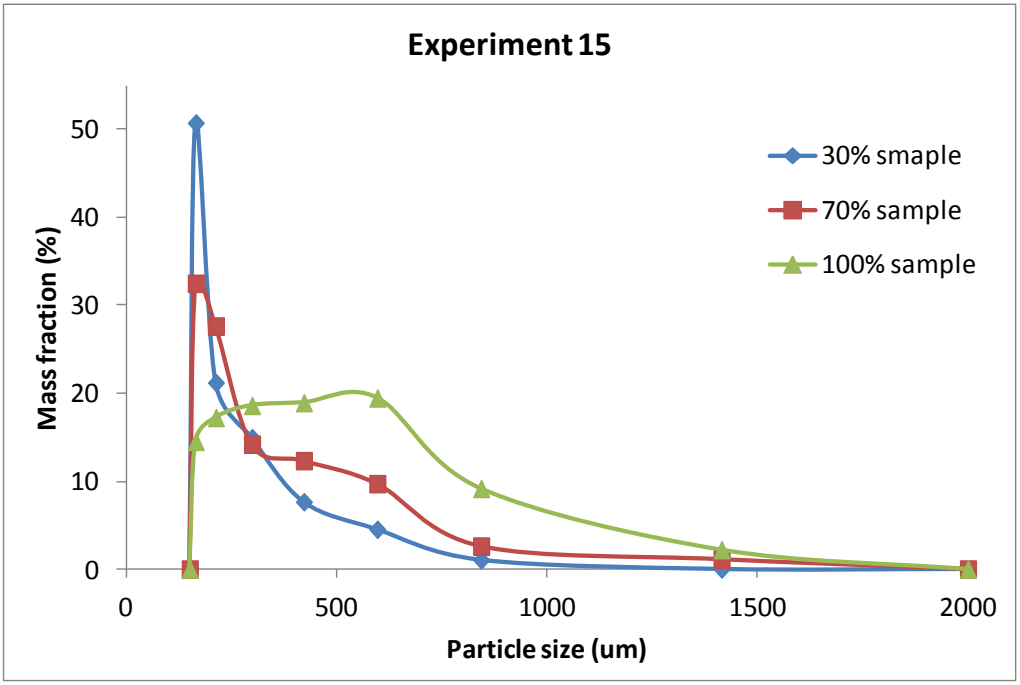

A1.2 Figures of validation experiments

A1.2.1 Particle size distribution in mass fraction at 30%, 70% and 100% binder sprayed

of validation experiment 1

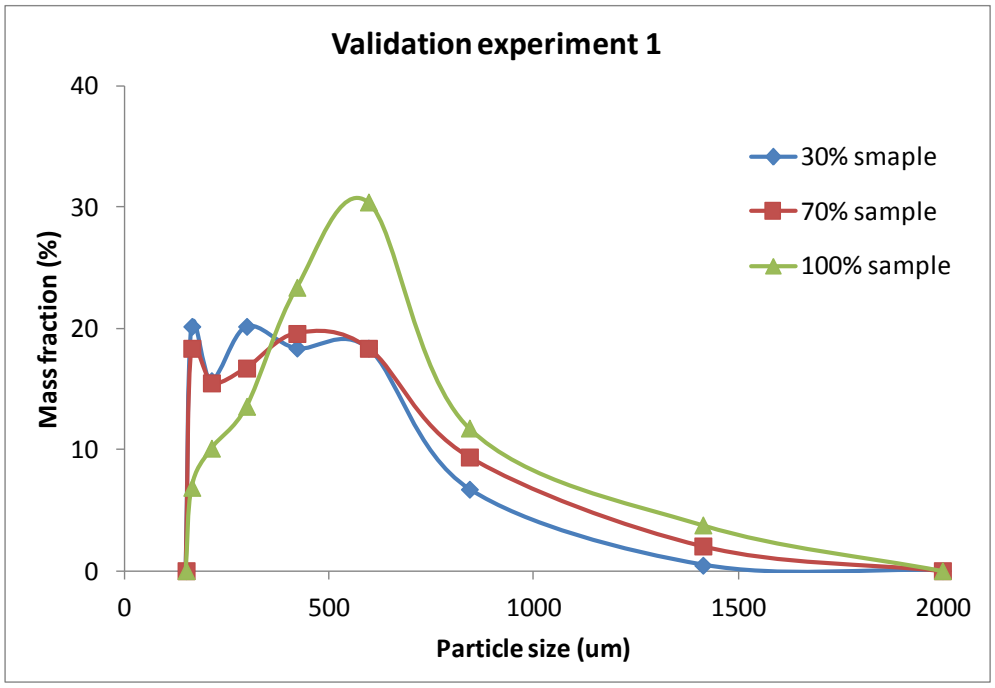

A1.2.2 Particle size distribution in mass fraction at 30%, 70% and 100% binder sprayed of validation experiment 2

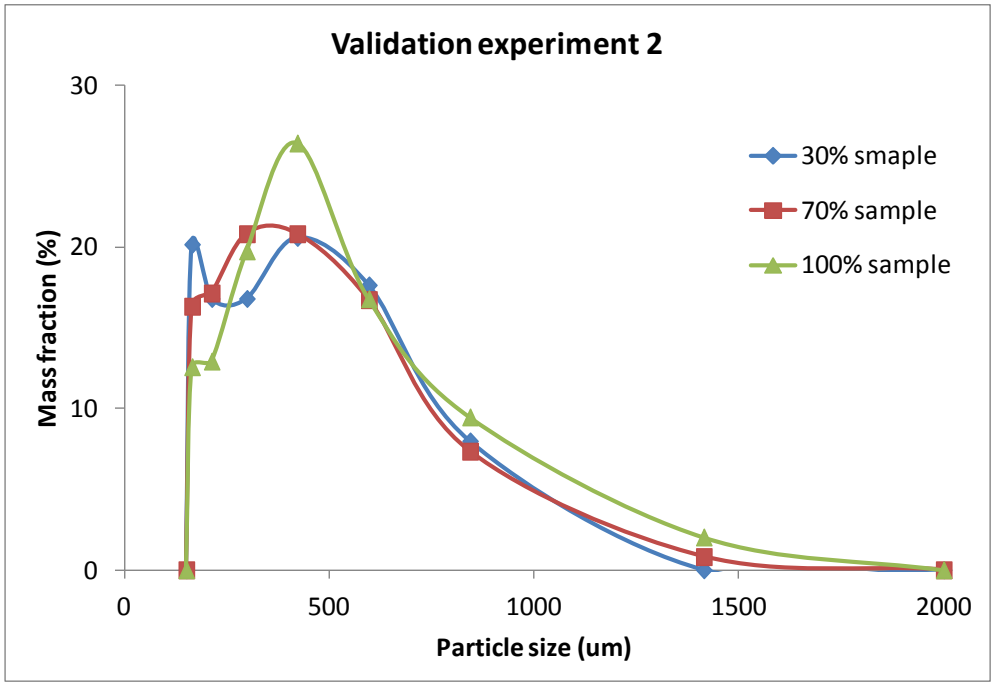

A1.2.3 Particle size distribution in mass fraction at 30%, 70% and 100% binder sprayed

of validation experiment 3

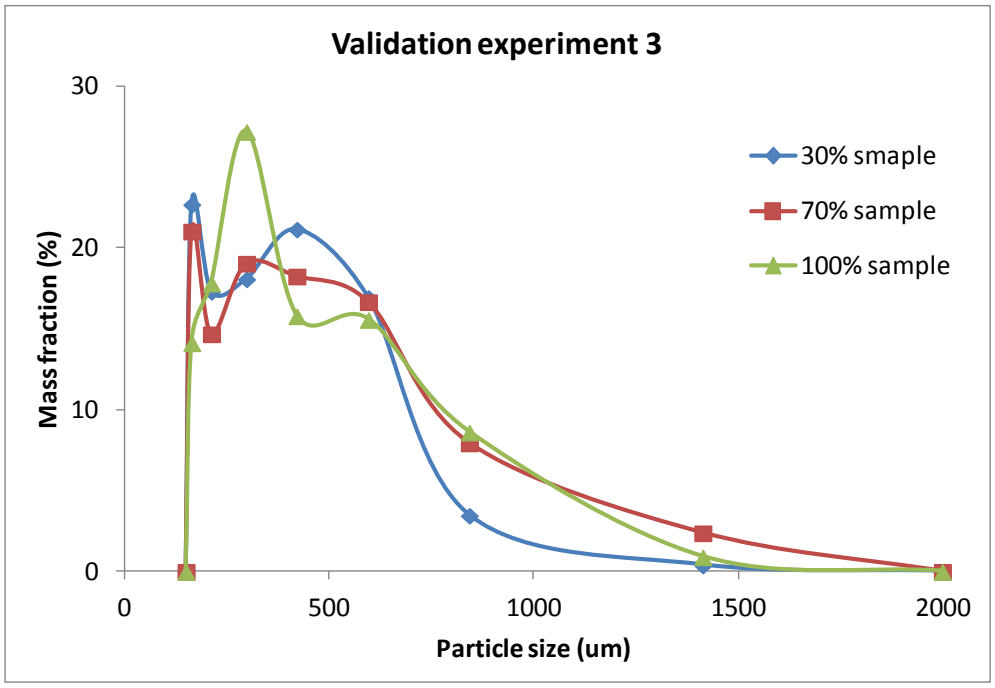

A1.2.4 Particle size distribution in mass fraction at 30%, 70% and 100% binder sprayed of validation experiment 4

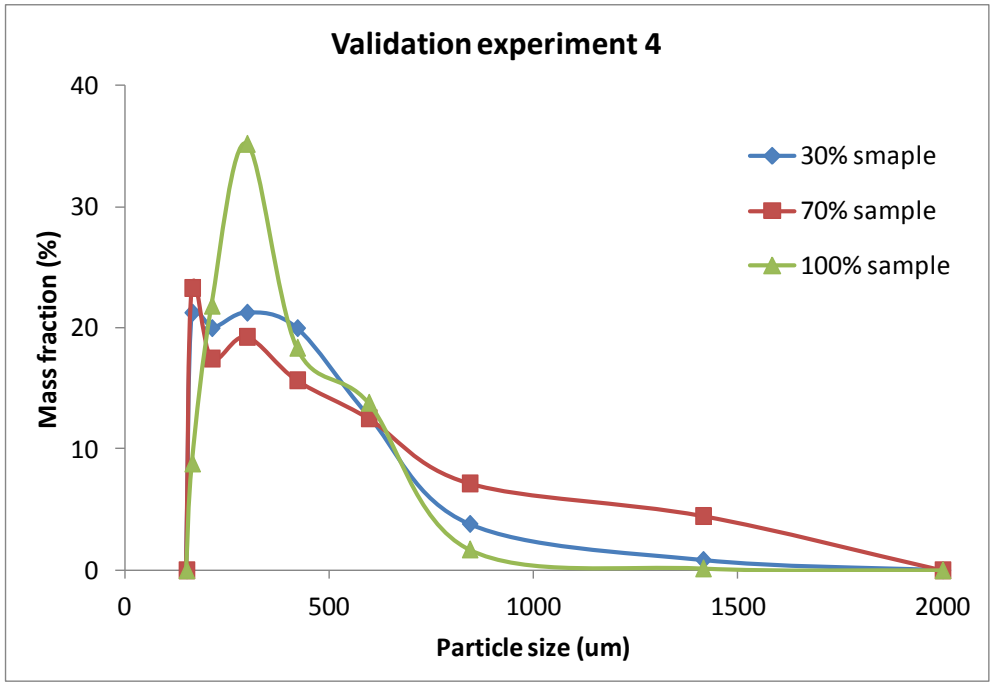

A2 Figures for chapter 4

A2.1 Figures of 15 experiments

A2.1.1 Final (100% binder sprayed) particle size distribution in volume fraction after transformation of experiment 1

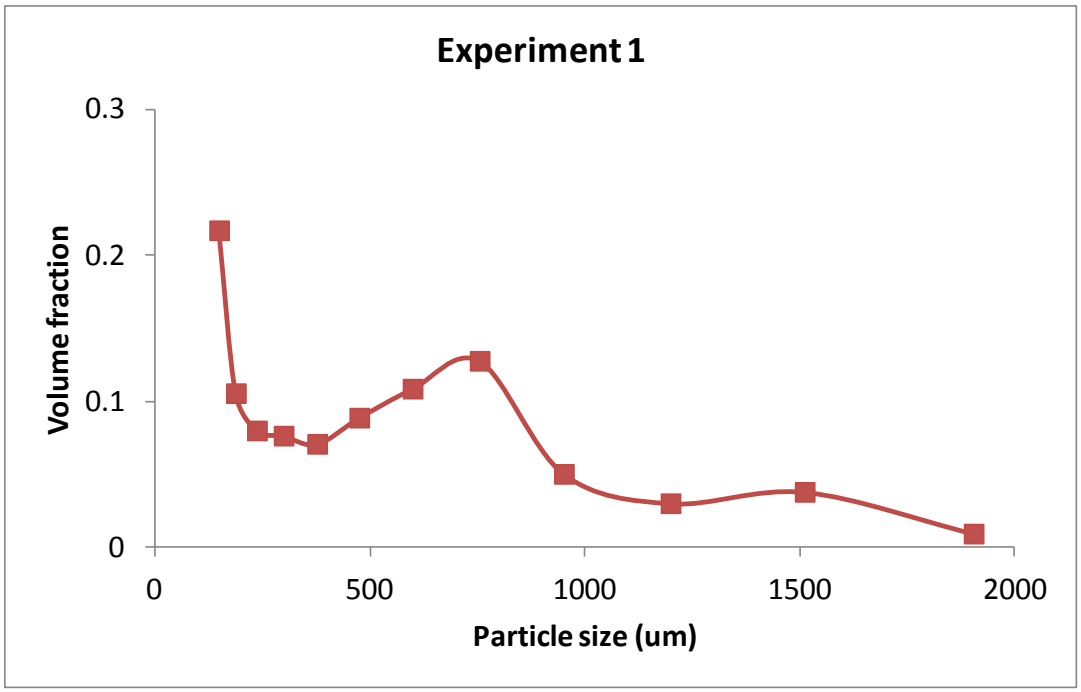

A2.1.2 Final (100% binder sprayed) particle size distribution in volume fraction after transformation of experiment 2

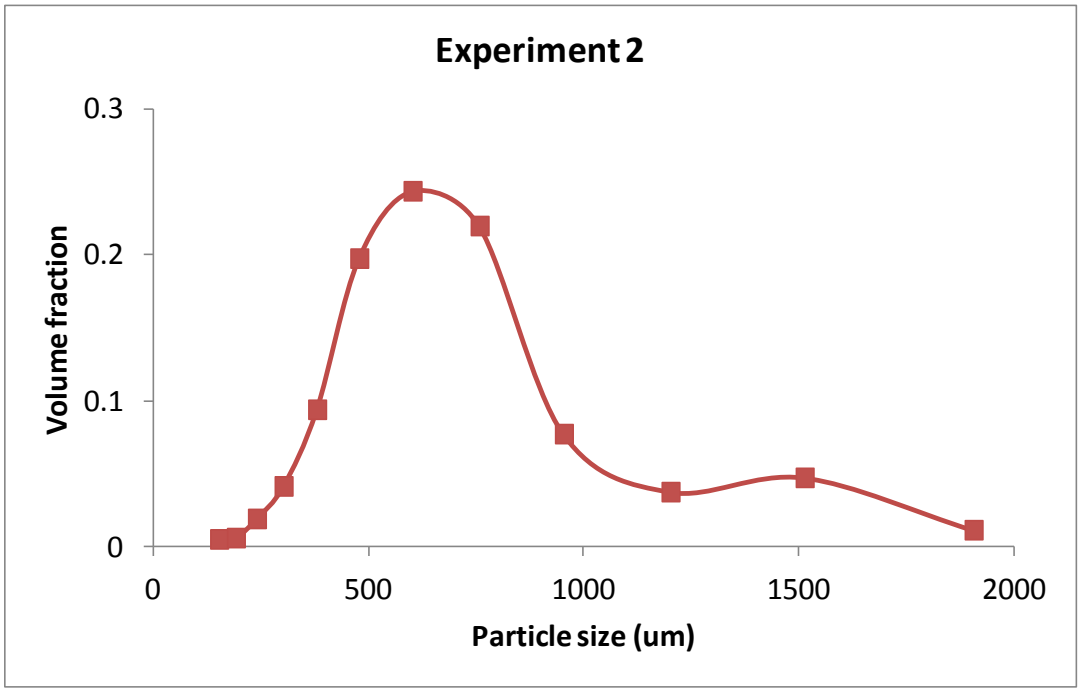

A2.1.3 Final (100% binder sprayed) particle size distribution in volume fraction after transformation of experiment 3

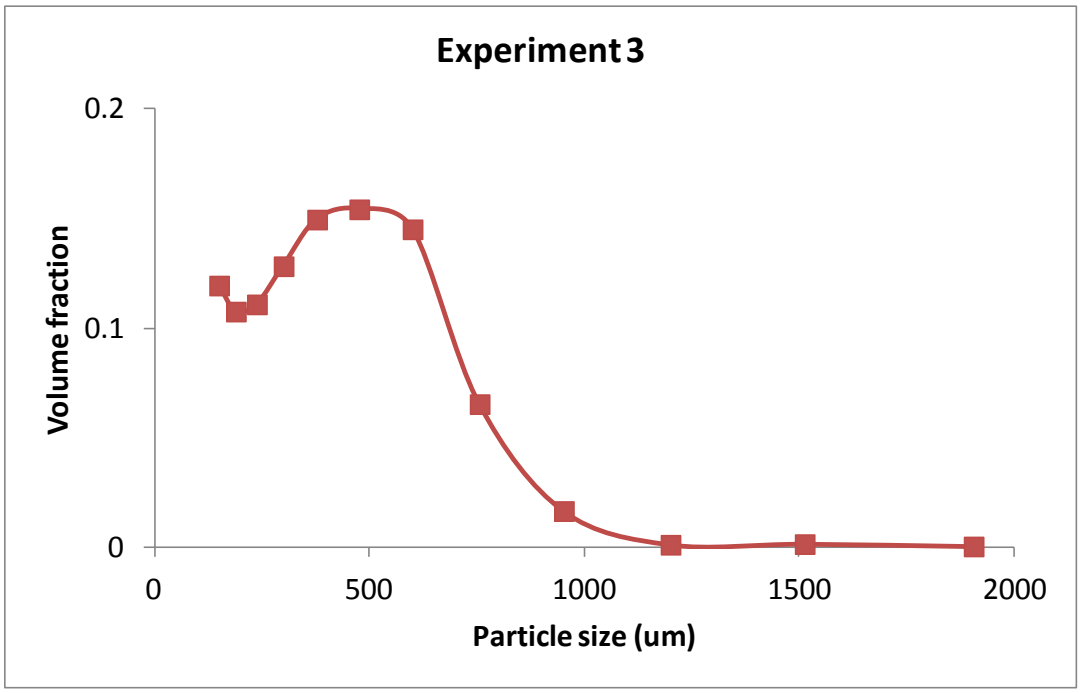

A2.1.4 Final (100% binder sprayed) particle size distribution in volume fraction after transformation of experiment 4

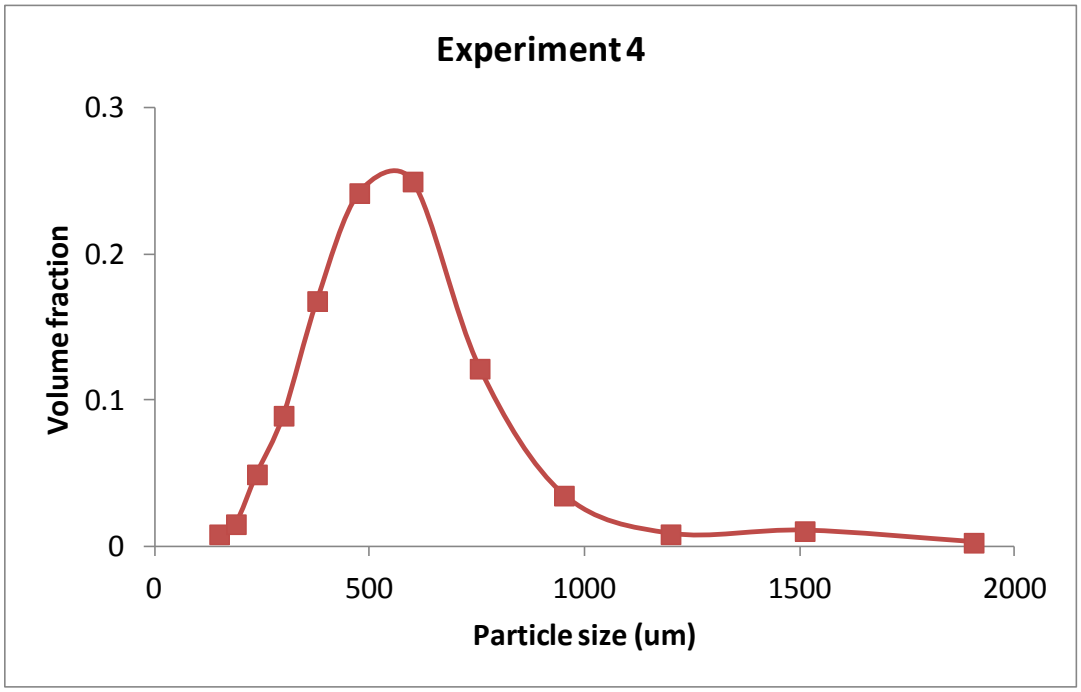

A2.1.5 Final (100% binder sprayed) particle size distribution in volume fraction after transformation of experiment 5

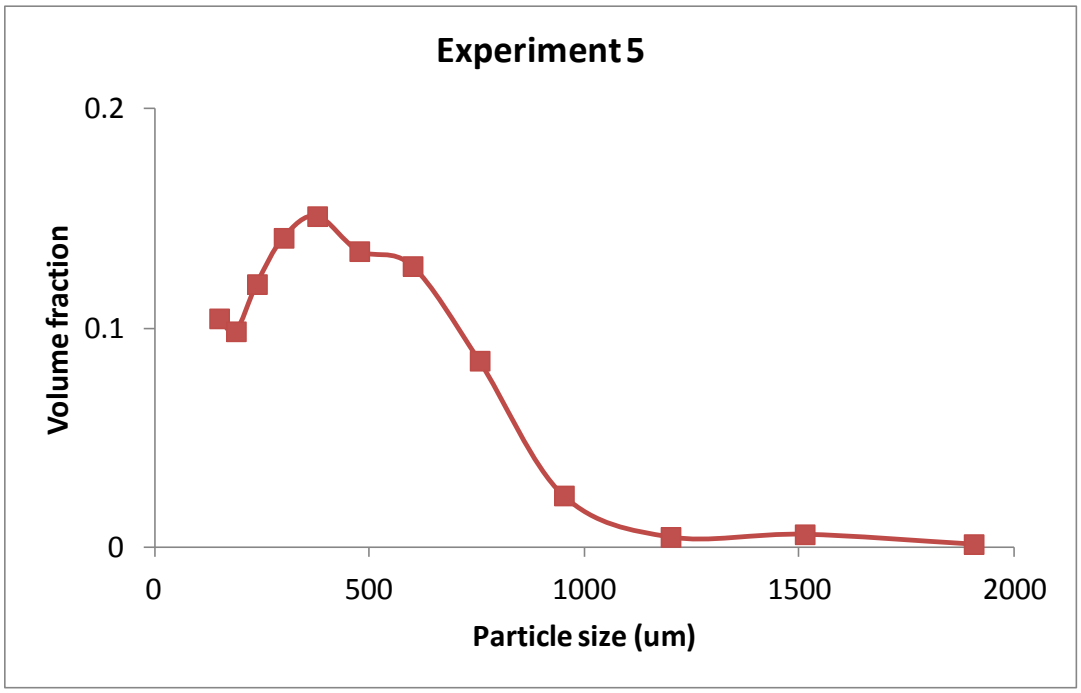

A2.1.6 Final (100% binder sprayed) particle size distribution in volume fraction after transformation of experiment 6

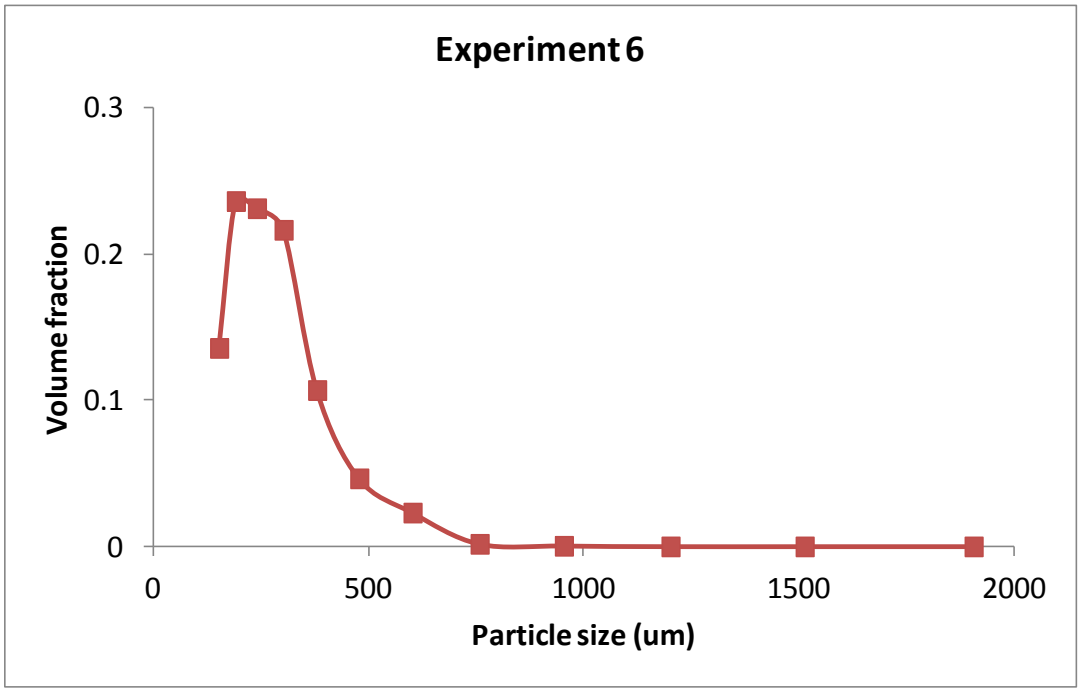

A2.1.7 Final (100% binder sprayed) particle size distribution in volume fraction after transformation of experiment 7

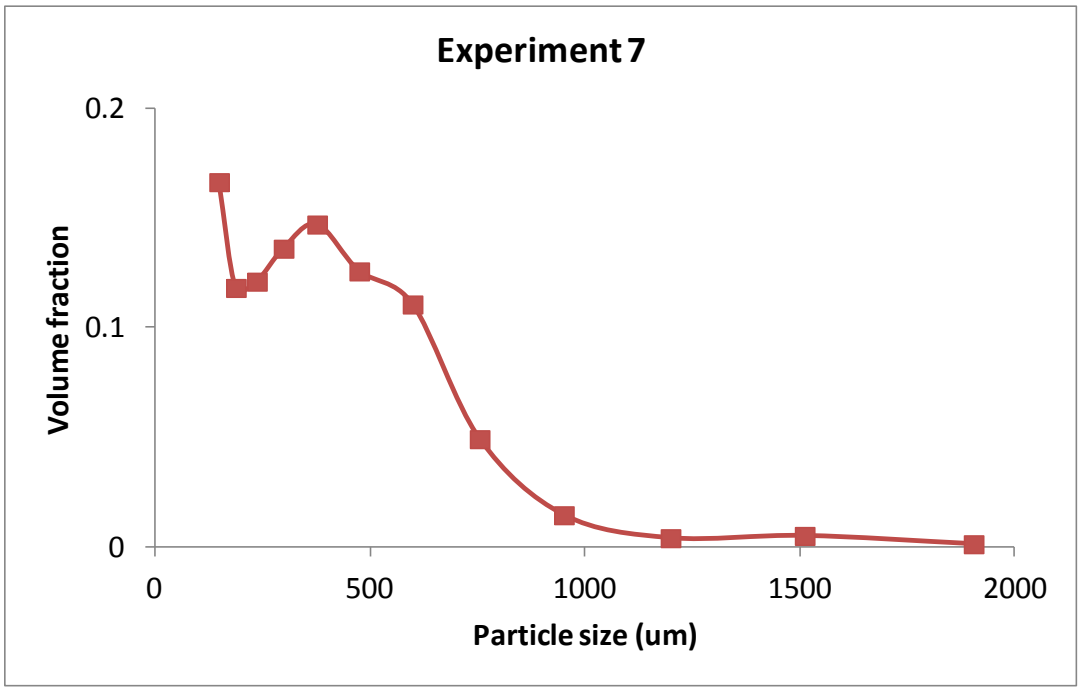

A2.1.8 Final (100% binder sprayed) particle size distribution in volume fraction after transformation of experiment 8

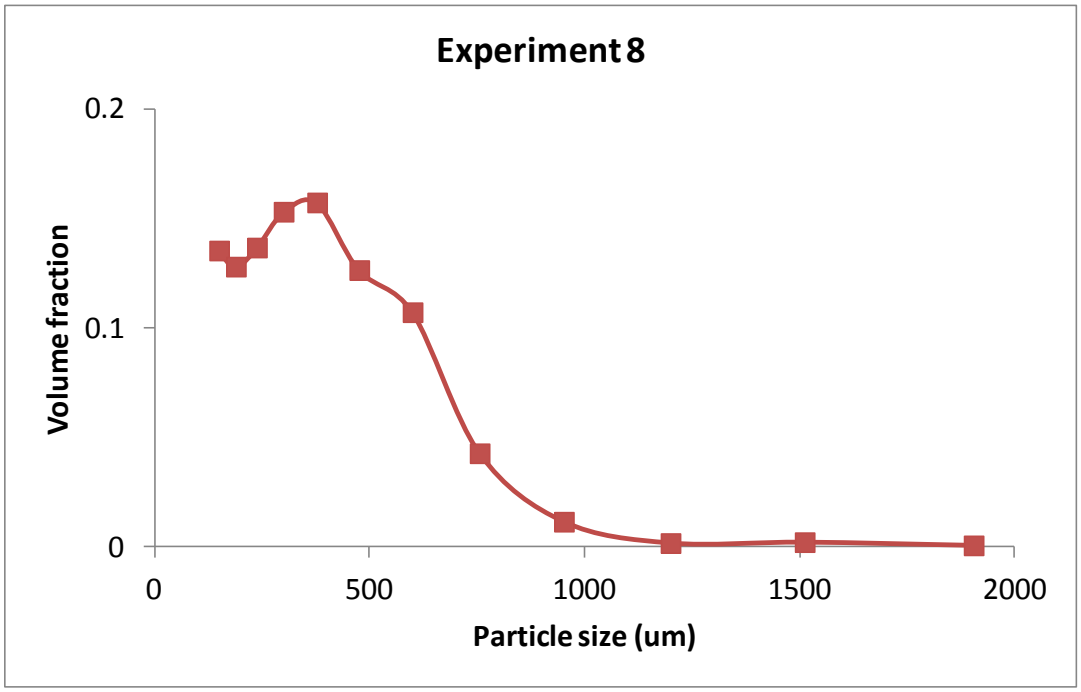

A2.1.9 Final (100% binder sprayed) particle size distribution in volume fraction after transformation of experiment 9

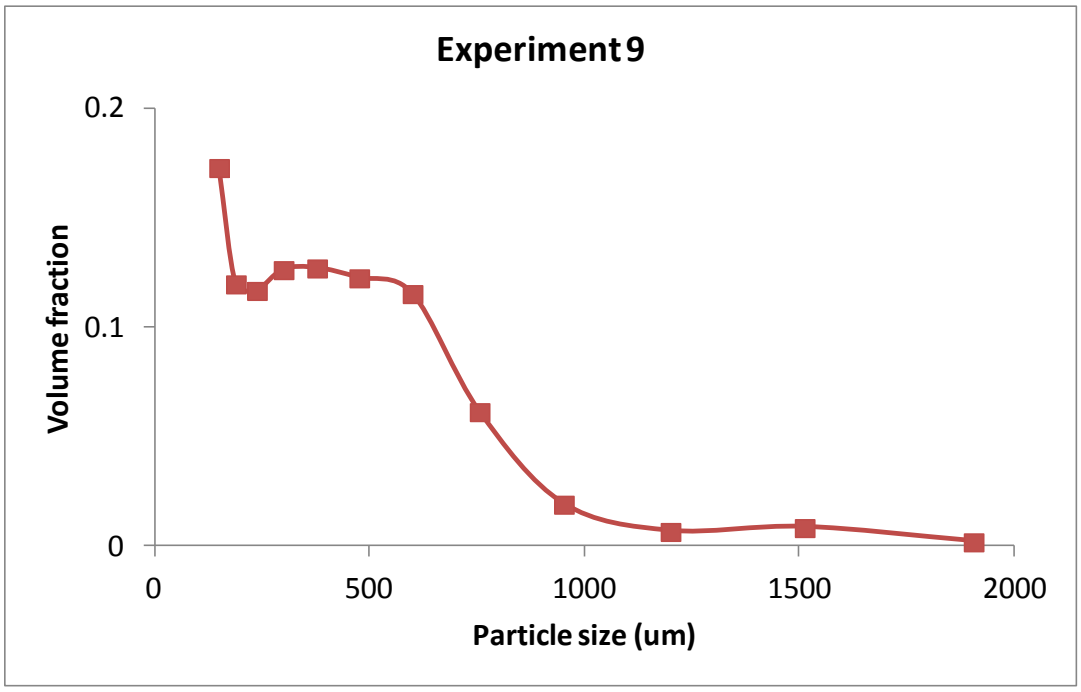

A2.1.10 Final (100% binder sprayed) particle size distribution in volume fraction after transformation of experiment 10

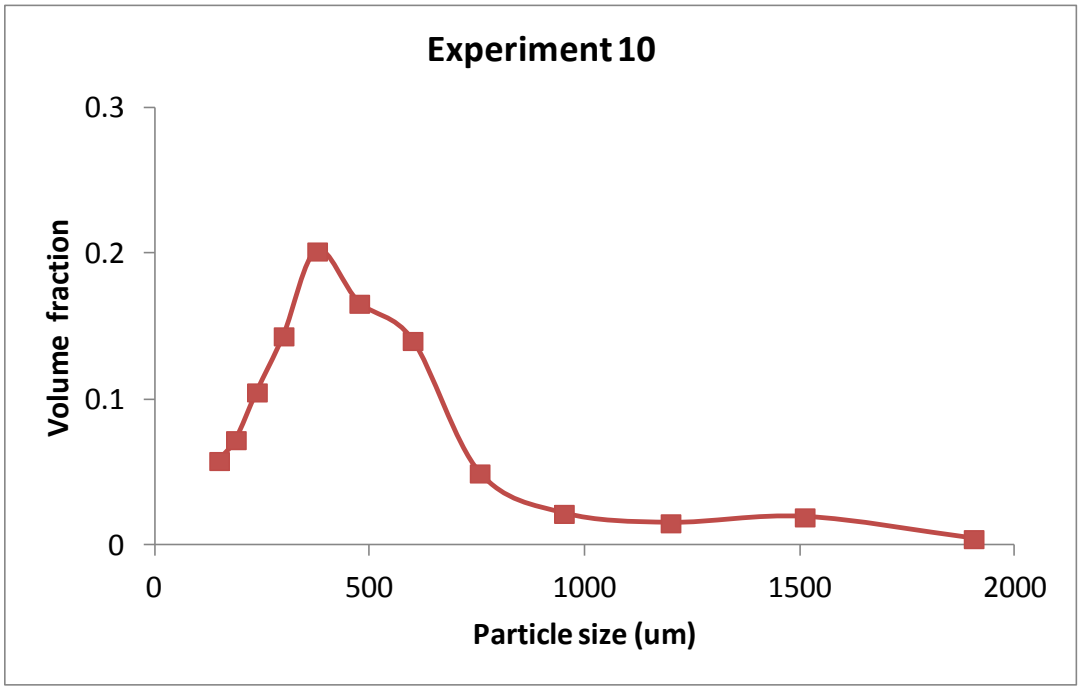

A2.1.11 Final (100% binder sprayed) particle size distribution in volume fraction after transformation of experiment 11

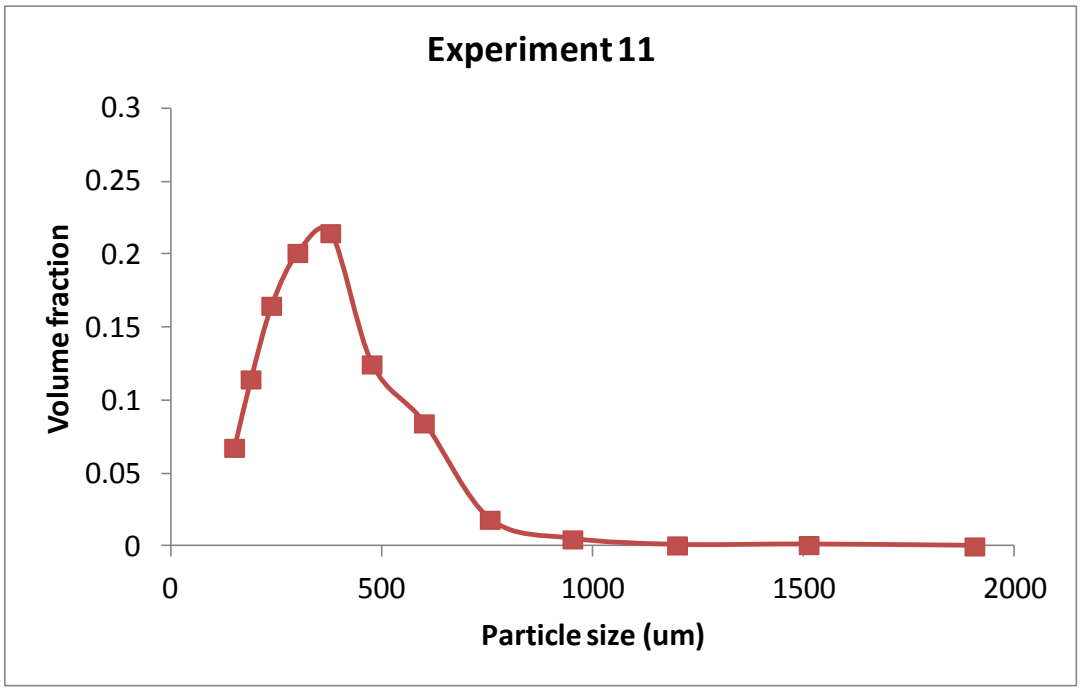

A2.1.12 Final (100% binder sprayed) particle size distribution in volume fraction after transformation of experiment 12

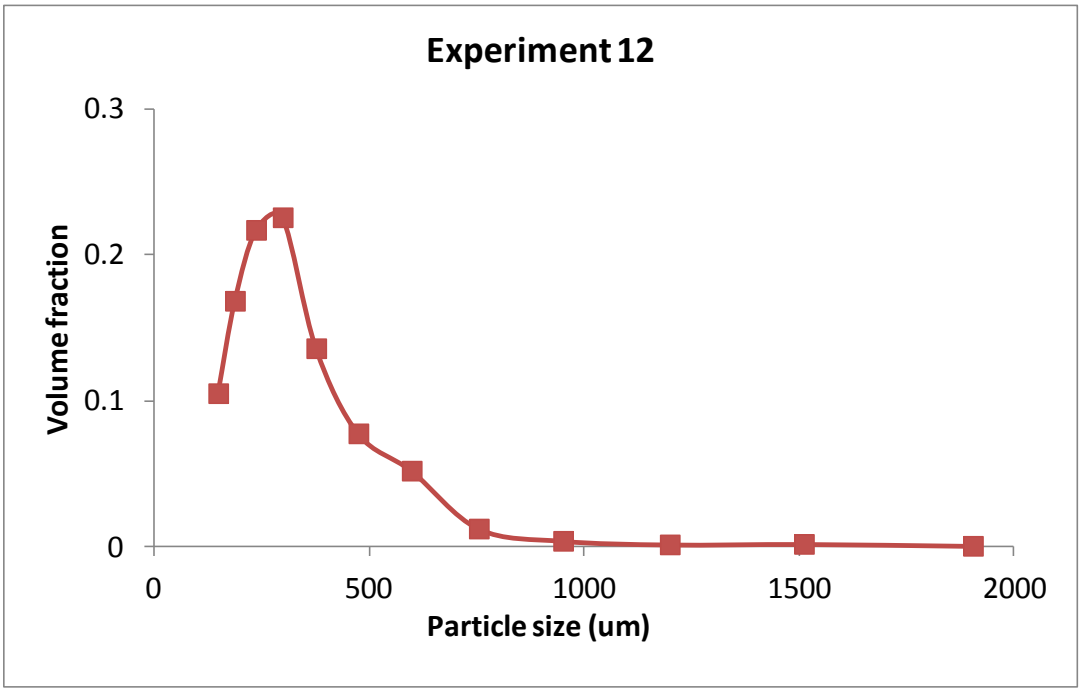

A2.1.13 Final (100% binder sprayed) particle size distribution in volume fraction after transformation of experiment 13

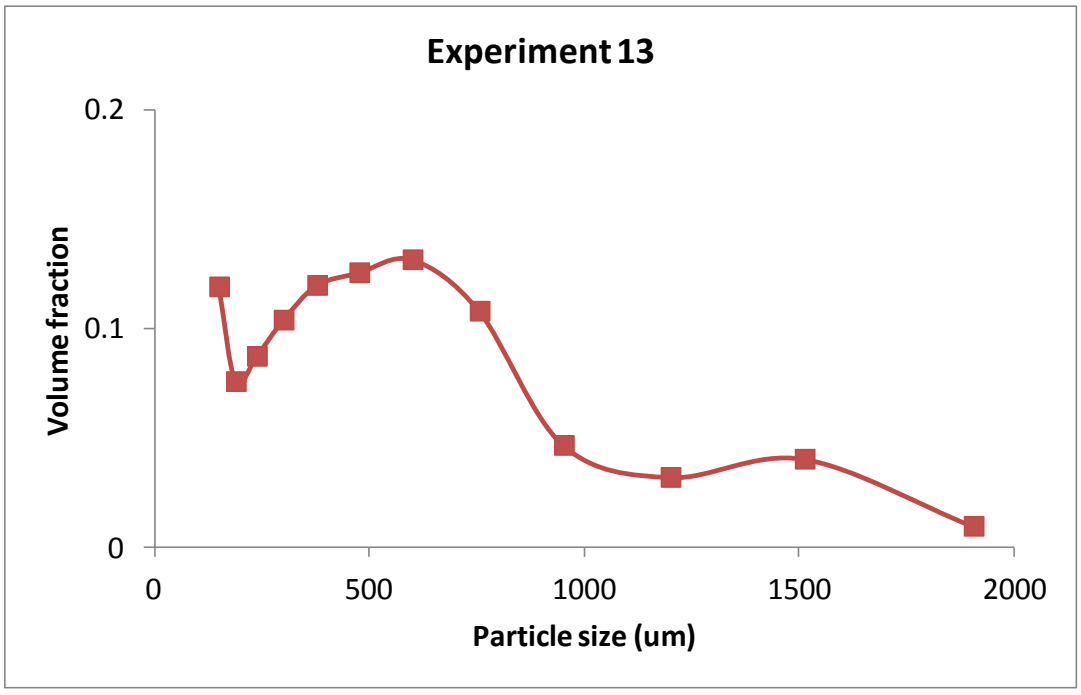

A2.1.14 Final (100% binder sprayed) particle size distribution in volume fraction after transformation of experiment 14

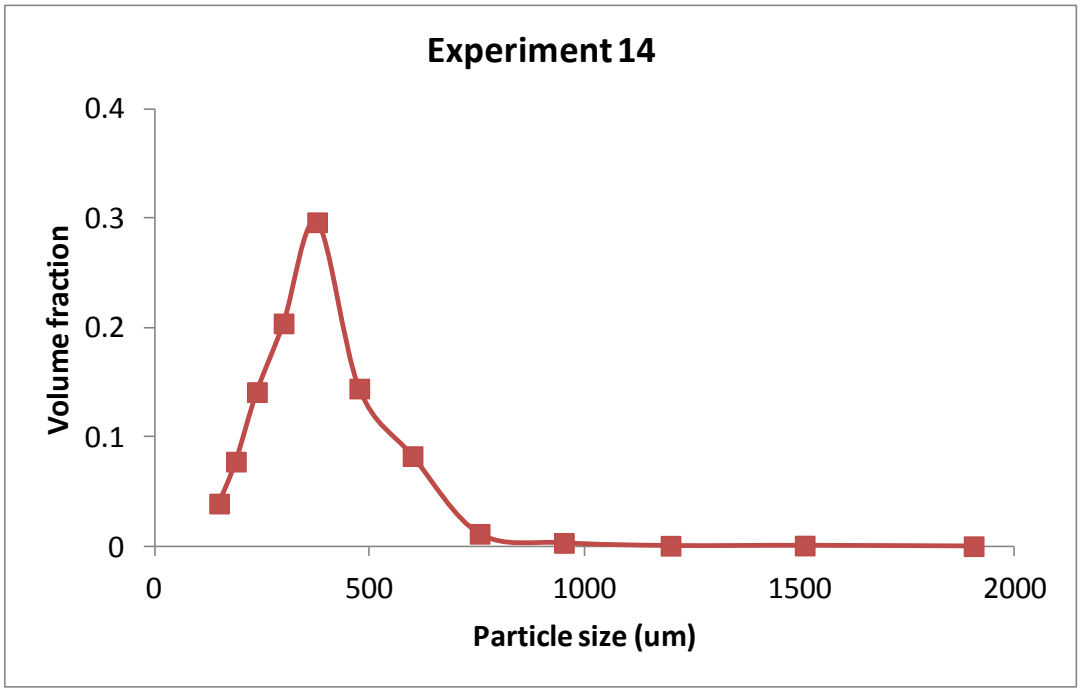

A2.1.15 Final (100% binder sprayed) particle size distribution in volume fraction after transformation of experiment 15

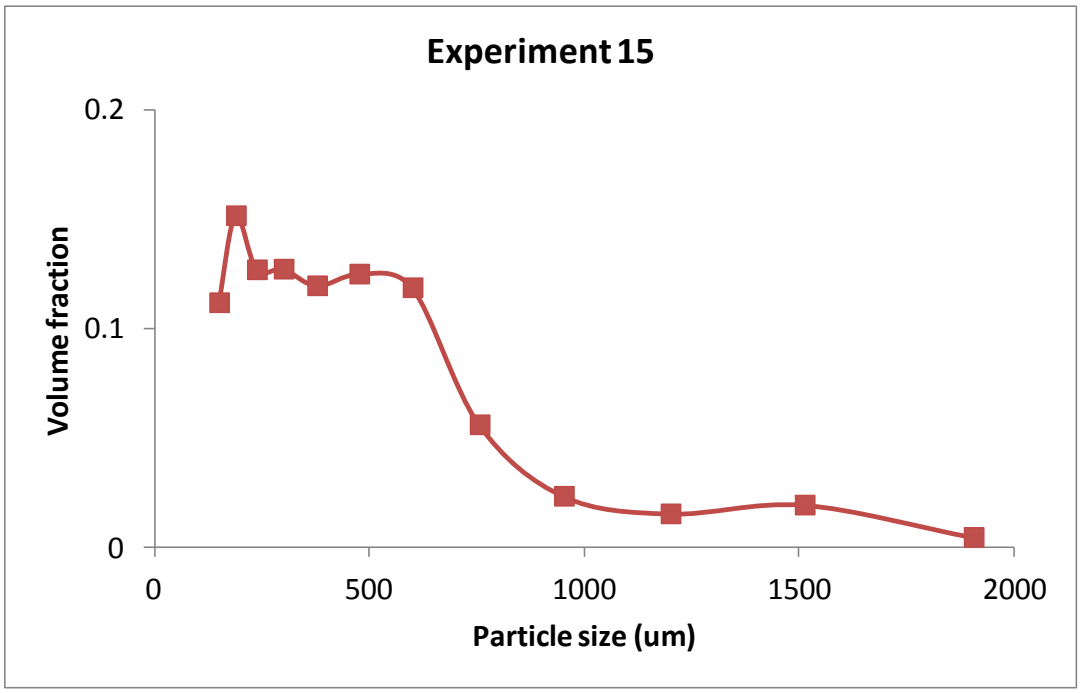

A2.2 Figures of validation experiments

A2.2.1 Particle size distribution in volume fraction after transformation at 30%, 70%

and 100% binder sprayed of validation experiment 2

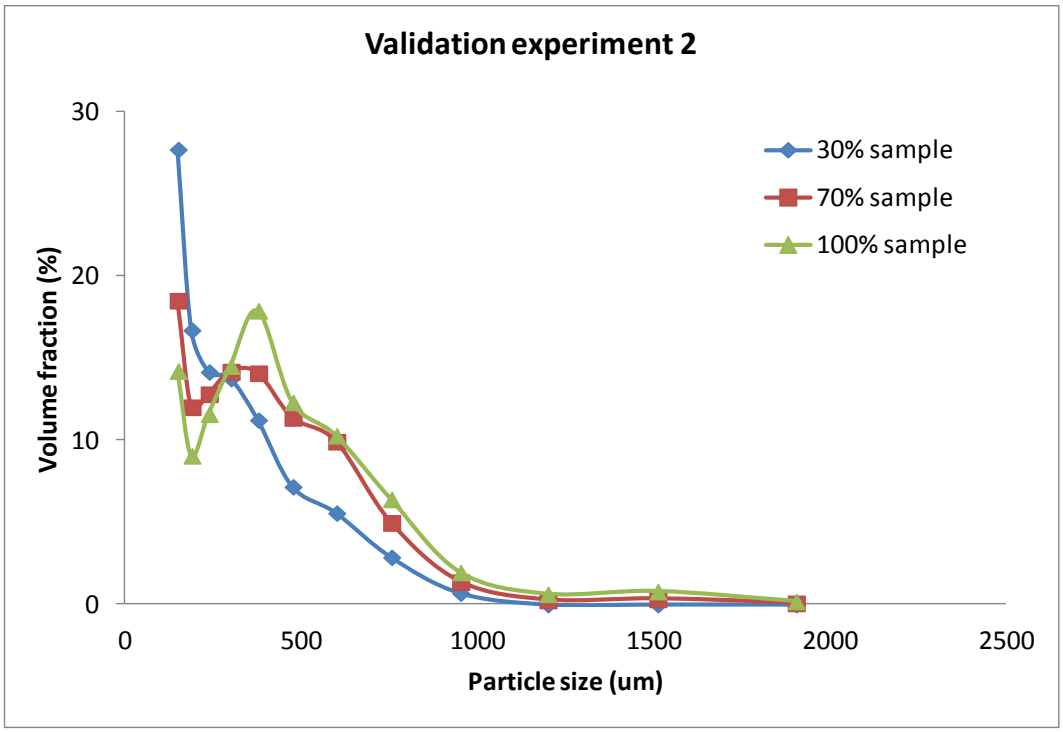

A2.2.2 Particle size distribution in volume fraction after transformation at 30%, 70% and 100% binder sprayed of validation experiment 3